

## *Comptonatus chasei*, a new iguanodontian dinosaur from the Lower Cretaceous Wessex Formation of the Isle of Wight, southern England

Jeremy A. F. Lockwood, David M. Martill & Susannah C. R. Maidment

To cite this article: Jeremy A. F. Lockwood, David M. Martill & Susannah C. R. Maidment (2024) *Comptonatus chasei*, a new iguanodontian dinosaur from the Lower Cretaceous Wessex Formation of the Isle of Wight, southern England, Journal of Systematic Palaeontology, 22:1, 2346573, DOI: [10.1080/14772019.2024.2346573](https://doi.org/10.1080/14772019.2024.2346573)

To link to this article: <https://doi.org/10.1080/14772019.2024.2346573>



© 2024 The Author(s). Published by Informa UK Limited, trading as Taylor & Francis Group.



[View supplementary material](#)



Published online: 09 Jul 2024.



[Submit your article to this journal](#)



[View related articles](#)



[View Crossmark data](#)

# *Comptonatus chasei*, a new iguanodontian dinosaur from the Lower Cretaceous Wessex Formation of the Isle of Wight, southern England

Jeremy A. F. Lockwood<sup>a,b,\*</sup> , David M. Martill<sup>a</sup>  and Susannah C. R. Maidment<sup>b</sup> 

<sup>a</sup>School of the Environment, Geography and Geosciences, University of Portsmouth PO1 2DT, UK; <sup>b</sup>Fossil Reptiles, Amphibians and Birds Section, Natural History Museum, London SW7 5BD, UK

(Received 2 November 2023; accepted 26 March 2024)

A new iguanodontian dinosaur, *Comptonatus chasei* gen. et sp. nov., is described from the Lower Cretaceous Wessex Formation of the Isle of Wight. These strata provide an important record of a critical time in the development of iguanodontian diversity. The specimen, which is described here for the first time, was found and excavated in 2013 and represents the most complete iguanodontian skeleton discovered in the Wealden Group for a century. A new taxon is diagnosed by several autapomorphies found in the neurocranium, teeth, coracoid and other parts of the body, together with a unique suite of characters. These include a dentary with a straight ventral border, and a markedly expanded prepubic blade. These features set it apart from the sympatric *Mantellisaurus atherfieldensis*, *Brighstoneus simmondsi* and *Iguanodon* cf. *bernissartensis*, increasing the known diversity of this clade in the Barremian–early Aptian of England.

<http://zoobank.org/urn:lsid:zoobank.org:pub:2F3125A5-BDEF-4835-8829-92104752A86F>

**Keywords:** Barremian; Wealden Group; supraoccipital; vomer; diversity

## Introduction

Iguanodontia was a highly successful clade of ornithischian dinosaurs, probably originating during the late Middle Jurassic, the earliest member being *Callovosaurus leedsi* Galton, 1980a (Lydekker, 1889) from the Oxford Clay Formation of eastern England (Ruiz-Omeñaca *et al.*, 2007), while the youngest include the duck-billed hadrosaurids that survived to the end Maastrichtian (Horner *et al.*, 2004). The clade also includes iconic dinosaurs such as *Iguanodon bernissartensis* Boulenger (in Van Beneden, 1881), *Ouranosaurus nigeriensis* Taquet, 1976, and *Parasaurolophus walkeri* Parks, 1922. Iguanodontians are historically important because teeth from an indeterminate member of the clade were the first fossils found that would become recognized as ornithischian (Mantell, 1825), and an iguanodontian sacrum recovered from the Barremian of the Isle of Wight gave Richard Owen the crucial osteological evidence he needed to ‘invent’ the Dinosauria (Owen, 1842; Torrens, 2014). Iguanodontian diversity appears to have remained low during the Late Jurassic and earliest part of the Cretaceous but increased rapidly during the Aptian and Albian (Barrett, McGowan, *et al.*, 2009; Weishampel *et al.*, 2004). The highly fossiliferous Wealden Group exposures of the Isle of Wight (Wessex and Vectis formations), which probably extend from the Late

Hauterivian (Jacobs *et al.*, 2023), through the Barremian and into the early Aptian, represent an estimated time span of at least 6 Ma (Cohen *et al.*, 2013 updated 2023; Gale *et al.*, 2020), and were deposited during the early stages of this radiation. They are, therefore, critical in elucidating the early development of iguanodontian diversification. The larger iguanodontians from these deposits have generally been assigned to either the very large *Iguanodon bernissartensis* or the medium-large and more gracile *Mantellisaurus atherfieldensis* (Hooley, 1925), a taxonomic practice that has effectively remained unchanged for nearly a century (Bonsor *et al.*, 2023; Martill & Naish, 2001). Several other iguanodontian taxa have been erected during this time, including: *Vectisaurus valdensis* Hulke, 1879; *Iguanodon seelyi* Hulke, 1882; *Sphenospondylus gracilis* Lydekker, 1888; *Dollodon seelyi* Carpenter & Ishida, 2010; *Proplanicoxa galtoni* Carpenter & Ishida, 2010; and *Brighstoneus simmondsi* Lockwood *et al.*, 2021. However, the validity of all but *Brighstoneus simmondsi* has been challenged (Norman, 1990, 2011a, 2012, 2013; McDonald, 2012a) and most have now been subsumed into synonymy or are considered *nomina dubia*.

In large part, difficulties in assessing iguanodontian diversity in the Wealden Group of the Isle of Wight relate to the condition of the available material, much of which consists of isolated bones, or very incomplete

\*Corresponding author. Email: [jlockwood156@aol.com](mailto:jlockwood156@aol.com)

partial skeletons. Despite a wealth of postcranial elements eroding from the cliffs, very little character-rich cranial material survives. This is not just a recent problem and was documented by John Whitaker Hulke (1871, p. 199), who over a hundred and fifty years ago was compelled to write, “It is remarkable that so little is known of the skulls of the Wealden Dinosauria, the more so as their other remains have been procured in some abundance in the south-east of England and the Isle of Wight during the fifty years which have elapsed since Dr Mantell’s discovery of an Iguanodon’s tooth in the quarry near Cuckfield”. Much of the evidence for disparity in dinosaurs is expressed in cranial material, and given its rarity on the Isle of Wight, combined with the somewhat conservative iguanodontian postcrania, a greater degree of diversity in the Wealden Group could easily have been overlooked. Recent years have also seen a steady increase in non-iguanodontian dinosaur taxa recognized from specimens collected from the Wealden Group exposures on the Isle of Wight. These represent Ornithischia with the ankylosaurian *Vectipelta barretti* (Pond *et al.*, 2023) and the hypsilophodontid *Vectidromeus insularis* (Longrich *et al.*, 2023) and Theropoda with the dromaeosaurid *Vectiraptor greeni* (Longrich *et al.*, 2022), the spinosaurids *Ceratosuchops inferodios* and *Riparovenator milnerae* (Barker *et al.*, 2021), and a possible spinosaurine (Barker *et al.*, 2022).

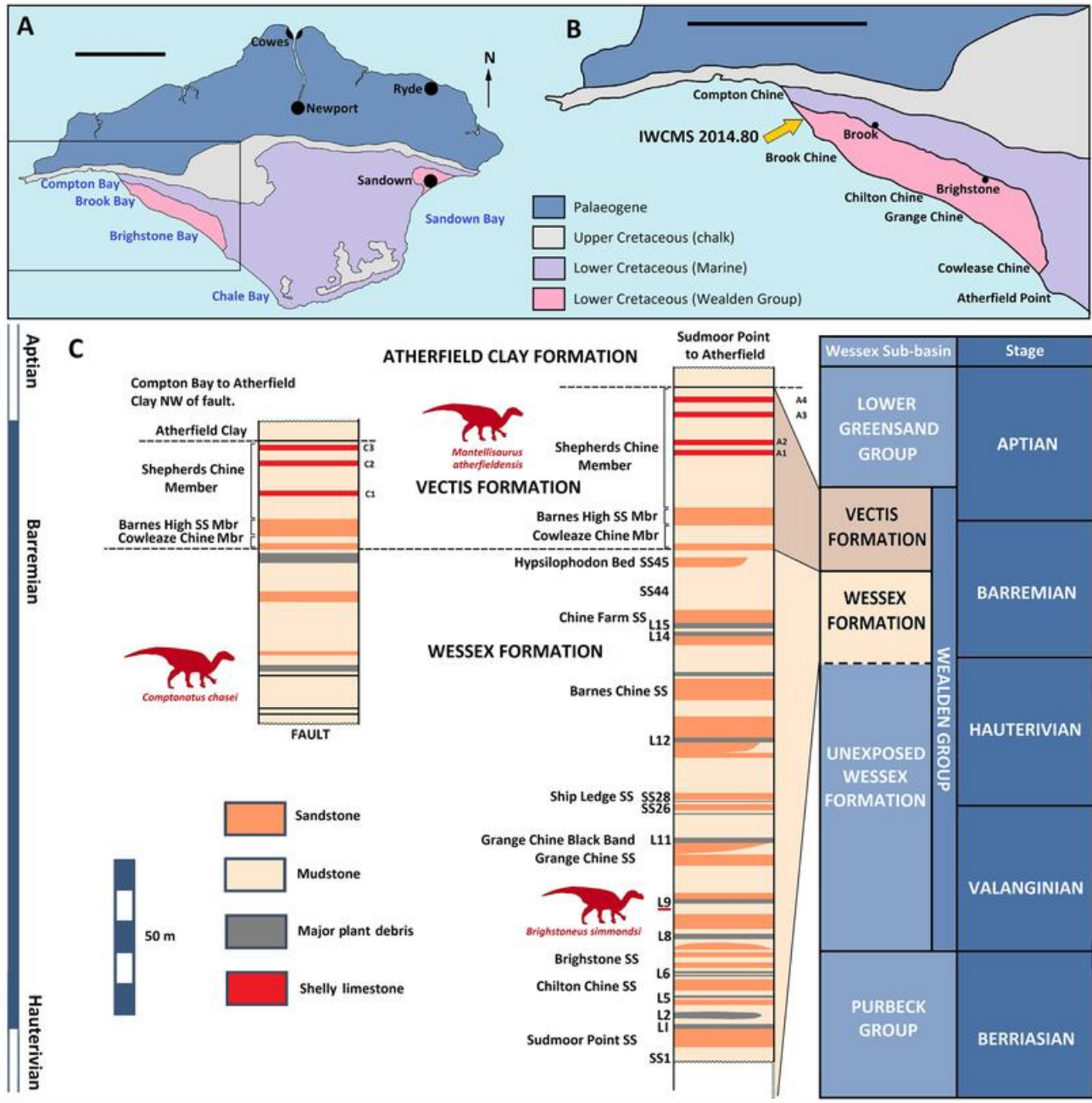
Here we report the detailed osteology of the most complete iguanodontian skeleton found in the Wealden Group of the Wessex sub-basin since the discovery of the holotype of *Mantellisaurus atherfieldensis* by Reginald Hooley (1917, 1925) in 1914. The exceptional specimen described herein, which includes cranial material and most of the postcranium, was excavated from the cliffs of Compton Bay in 2013 after being discovered by the late Mr Nick Chase. Based on a unique combination of characters and several autapomorphies, we propose this as a novel taxon. Specimen IWCMS 2014.80 joins the recently described *Brighstoneus simmondsi* (Lockwood *et al.*, 2021) in adding to the known iguanodontians from the Wealden Group exposures of the Isle of Wight and provides further support for an ecosystem in the Wessex Sub-basin that sustained a highly diverse and evolving iguanodontian population through the Barremian and early Aptian.

## Geological setting

The term ‘Wealden’ has been used to describe several non-marine sedimentary successions from the Early Cretaceous, which span the north-west of Europe including Belgium, England, France, Germany, and the

Iberian Peninsula. In southern England, these non-marine strata are represented by the Wealden Group, whose sequence can be divided into those occupying the more easterly Weald Sub-basin and those occupying the more southerly Wessex Sub-basin, the northern part of which outcrops on the Isle of Wight (Batten & Austin, 2011; Gale, 2019; Radley, 2006; Sweetman, 2011). The oldest rocks exposed on the Isle of Wight are from the Wealden Group of the Wessex Sub-basin and are found principally along the south-west coast with a smaller exposure to the east near Sandown (Fig. 1). The Wealden Group of the Isle of Wight is further divided into the older Wessex Formation and the younger Vectis Formation (Gale, 2019). The 180 m thick exposure of the Wessex Formation is largely composed of variegated overbank mudstones and siltstones, with interbedded fluvial sandstones deposited in a fluvio-lacustrine setting (Gale, 2019). The overlying Vectis Formation is represented by approximately 40 m of clays and shales, with occasional interbedded sandstones and shelly limestones containing the bivalve *Filosina gregaria* and small oysters, deposited predominantly in a shallow coastal lagoon of varying salinity (Radley & Barker, 1998, 2000; Radley *et al.*, 1998). The Wessex Formation is well known for its fossil-rich plant debris beds (*sensu* Oldham, 1976), which form grey units of limited lateral extent, that were interpreted by Sweetman and Insole (2010, p. 409) as representing a “locally generated sheet flood, which was then transformed on the floodplain into a debris flow by the acquisition of surface material”. Despite only contributing a small volume to the overall succession (Fig. 1C), plant debris beds provide the main source of dinosaur and other vertebrate fossils on the Isle of Wight.

The strata to the south-east of Hanover Point represent the oldest units of the exposed Wealden Group (Fig. 1C), although borehole data shows that the Wealden Group on the Isle of Wight extends to a total thickness of 592 m in the subsurface (Falcon & Kent, 1960). The lack of biostratigraphically informative fossils and volcanic elements has hindered precise dating; however, palynological evidence suggests that the exposed Wessex Formation on the Isle of Wight is entirely Barremian (Allen & Wimbledon, 1991; Hughes & McDougall, 1990), while carbon-isotope stratigraphy has placed the ‘Pine Raft’ (an accumulation of fossilized *Pseudofrenelopsis parceramosa* Watson, 1977 pine trees at Hanover Point) within magnetocron M3r (Ogg, 2020; Robinson & Hesselbo, 2004), which crosses the Hauterivian–Barremian boundary (Ogg, 2020). This is in agreement with recent work using U–Pb geochronology on diagenetic calcite, which suggests an age of  $127.3 \pm 2.7$  Ma (Hauterivian to earliest Barremian) for



the earliest rocks exposed on the island (Jacobs et al., 2023). The overlying Vectis Formation has been shown to contain the Barremian–Aptian boundary within the Shepherds Chine Member, which forms the youngest unit of the formation (Kerth & Hailwood, 1988;

Robinson & Hesselbo, 2004). A fault has resulted in two exposures of the Wessex and Vectis formations at Compton Bay (Radley, 1994), with IWCMS 2014.80 being discovered high in the cliff in a major plant debris bed within the Wessex Formation, north-west of the

fault (Fig. 1). Dinosaur fossils are less common in the Vectis Formation, but discoveries have been made, famously including the *Mantellisaurus atherfieldensis* holotype (NHMUK PV R 5764), probably originating in the early Aptian (Bonsor *et al.*, 2023). Correlation of the different exposures of the Wessex Formation on the Isle of Wight can be difficult, but if the sedimentation rate is broadly assumed to be uniform and continuous, then *Mantellisaurus atherfieldensis*, *Brighstoneus simmondsi* and IWCMS 2014.80 could be distanced from each other by several million years.

Overall, the Wessex Formation represents a fluvio-lacustrine meander plain, which supported a rich riparian ecosystem (Austen & Batten, 2018; Batten, 2011; Sweetman *et al.*, 2014; Sweetman, 2016). Palaeontological studies on macro and microvertebrate fossils has resulted in the Wessex Formation being shown to yield one of the world's most taxonomically diverse, non-marine, Early Cretaceous vertebrate assemblages (Penn & Sweetman, 2022).

## Material and methods

### Material

The material consists of a single, largely complete iguanodontian skeleton (holotype), collected from Compton Bay on the Isle of Wight. It was accessioned to Dinosaur Isle Museum, Sandown, Isle of Wight, England in 2014, where it was prepared and is currently stored under the collection number IWCMS 2014.80.

### Phylogenetic analysis

Phylogenetic relationships were assessed using the matrix of Lockwood *et al.* (2021) with the addition of *Comptonatus chasei* and some minor updates (see Supplemental material S4, p. 153). This matrix was a modified version of the matrix of Xu *et al.* (2018), which itself was modified from Norman (2015) and McDonald (2012b). The matrix was chosen as it covers early diverging iguanodontians without being overly focused on hadrosaurids. The modifications from the original Xu *et al.* (2018) matrix were the rescoring of *Mantellisaurus atherfieldensis* based solely on holotype material (NHMUK PV R 5764), the addition of *Brighstoneus simmondsi* (Lockwood *et al.*, 2021) and *Comptonatus chasei*, giving a total of 42 taxa, and the inclusion of two extra characters (124 and 125), giving a total of 125 (see Lockwood *et al.*, 2021). The matrix was compiled in Mesquite v. 3.61 (Maddison & Maddison, 2015) and analysed in TNT v. 1.6 (Goloboff & Morales, 2023), using a traditional search under the tree bisection reconnection (TBR) swapping algorithm, saving 1000 trees per replication. *Lesothosaurus diagnosticus* was set as the outgroup. Consistency index, rescaled

consistency index and retention index were calculated using the TNT script STAT.RUN and clade support using the TNT script BREMER.RUN and TNT bootstrap, set to 1000 replicates, reporting groupings found in >50% of pseudoreplicate datasets.

### Histology

Thin sections of bone for histological examination were made from two fragments of dorsal rib shaft. Rib sections were selected largely pragmatically. The samples were cut using a Buehler IsoMet saw. They were bonded using EpoThin II low viscosity resin by Buehler to glass slides that had been prefrosted with a diamond cupwheel. The samples were trimmed to a thickness of 0.7 mm using a PetroThin thin sectioning machine by Buehler and the upper surface ground flat with a cupwheel. The upper surfaces were then finished by grinding with 600 grade silicon carbide on a glass plate. The slices were then bonded with EpoThin II to a glass slide prefrosted with 600 grade silicon carbide. They were then ground down to 30 µm using a PetroThin cupwheel and 600 grade silicon carbide for the final 5 µm. The coverslips were affixed using UV activated Norland Optical Adhesive 61. Slides were examined using a Leica DM750 P microscope and photographed with a Leica MC 120 HD 2.5-megapixel camera.

### Institutional abbreviations

**CEUM**, College of Eastern Utah Prehistoric Museum, Price, UT, USA; **FMNH**, The Field Museum, Chicago, IL, USA; **GDF**, Musee National du Niger, Niamey, Niger; **IWCMS**, Isle of Wight County Museum Service (MIWG, Museum of Isle of Wight Geology, was also used for accessions prior to 1994), Dinosaur Isle Museum, Isle of Wight, UK; **LACM**, Natural History Museum of Los Angeles County, Los Angeles, CA, USA; **MOR**, Museum of the Rockies, Bozeman, MT, USA; **MSNVE**, Museo di Storia Naturale di Venezia, Venice, Italy; **NHMUK**, The Natural History Museum, London, UK; **RBINS**, Royal Belgian Institute of Natural Sciences, Brussels, Belgium; **SM**, Senckenberg Museum, Frankfurt, Germany; **USNM**, United States National Museum (National Museum of Natural History), Washington DC, USA; **YPM**, Peabody Museum of Natural History, Yale University, New Haven, CT, USA.

### Systematic palaeontology

**Dinosauria** Owen, 1842  
**Ornithischia** Seeley, 1887  
**Ornithopoda** Marsh, 1881

**Iguanodontia** Baur, 1891  
**Ankylopollexia** Sereno, 1986  
**Styracosterna** Sereno, 1986  
**Hadrosauriformes** Sereno, 1997  
**Comptonatus** gen. nov.

**Etymology.** *Comptonatus* ('the Compton thunderer') is a contraction of the words 'Compton' on the Isle of Wight and 'tonatus', the Latin for thundered, and reflects the place of discovery and the large size of the animal.

**Type species.** *Comptonatus chasei* gen. et sp. nov.

**Diagnosis.** As for type and only species (see below).

**Location and horizon.** The Wessex Formation, 'middle' Barremian, Lower Cretaceous. IWCMS 2014.80 was excavated during September–October 2013, from a plant debris bed on National Trust property to the west of the fault in Compton Bay, and close (c. 50 m) to where IWCMS 2013.175, a skeleton of *Valdosaurus canaliculatus* Galton, 1977 (Barrett, 2016) was excavated the previous year. The excavation was conducted under the supervision of Dinosaur Isle Museum (IWCMS) and site records and drawings were collected by Mr Stephen Hutt, the then curator. The site exposes a deep (c. 3 m) plant debris bed that occasionally yields articulated dinosaur remains, but frequently produces the trunks of large conifers, usually attributed to *Pseudofrenelopsis parceramosa* (Francis, 1987). Other vertebrate remains uncovered from the excavation site include ganoid fish scales (cf. *Scheenstia* sp.), an indeterminate crocodylian tooth and several very large, but fragmentary iguanodontian remains, including three pedal phalanges, a neural arch, and some rib sections.

*Comptonatus chasei* gen. et sp. nov.  
 (Figs 2–40, 42–45)

**Etymology.** The specific name honours the late Mr Nick Chase, winner of the Palaeontological Association's Mary Anning Award in 2018, who made the initial discovery and through his lifetime contributed enormously to the collections at Dinosaur Isle Museum, Isle of Wight, and the Natural History Museum, London (Lockwood et al., 2019).

**Holotype.** IWCMS 2014.80, an almost complete skeleton composed of the following elements: right maxilla, right nasal fragment, both vomers, both quadrates, both squamosals, both prefrontals, both frontals, both postorbitals, neurocranium, right dentary, left dentary

fragments, left surangular, one loose dentary tooth, eight opisthocoeleous presacral vertebrae, cervical rib fragment, 15 dorsal vertebrae including the sacrodorsal, dorsal rib fragments, sacrum, 40 caudal vertebrae, 15 chevrons, both scapulae, both coracoids, both sternal bones, right humerus, left radius, left ulna, left carpus, left metacarpals III and IV, right metacarpals II and V, both pollices, left digit II manual phalanx 1, unisided digit II manual phalanx 2, right digit IV manual phalanx 1, both ilia, both pubes, both ischia, left femur, both tibiae, both fibulae, both astragali, right metatarsal II, left metatarsals II, III and IV, digit II: right pedal phalanx 1, left pedal phalanges 1 and 2, digit III: right pedal phalanx 4, left pedal phalanges 1–4, and digit IV: left pedal phalanges 1–4.

### Diagnosis.

*Comptonatus chasei* differs from all other iguanodontians by possessing the following autapomorphies and unique combination of characters (autapomorphies indicated with an asterisk): (1) parietal 'tubercle' and step, dorsolateral to ascending process of supraoccipital\*; (2) exoccipital bar/bridge overhangs the exoccipital pillar\*; (3) basioccipital with thin median ridge in ventral sulcus; (4) dentary is straight across the entire ventral margin in lateral view; (5) dentary and maxillary crowns both have grooved primary ridges\*; (6) tall neural spines on proximal caudal vertebrae (neural spine > three times height of centrum and c. four times the height in Cd1); (7) excluding Cd1 and Cd2, both proximal and middle caudal vertebrae have a deep ventral sulcus; (8) supraglenoid fossa of the scapula absent; (9) coracoid boss on dorsolateral medial surface\*; (10) coracoid has medial cavity buttressed by cornuate ridge\*; (11) prepubic blade markedly dorsoventrally expanded with (reconstructed) ratio of maximum to minimum depth of the prepubic blade c. 2.5; (12) boss on medial surface of tibia near dorsal margin\*.

### Differential diagnosis of diagnostic characters.

(3) Also present in *Cumnoria prestwichii* (Maidment et al., 2022) and *Jintasaurus meniscus* (You & Li, 2009). (4) Also present in *Kukufeldia tilgatensis* (McDonald, Barrett, et al., 2010). (6) Also seen in *Hypselospinus* cf. *fittoni* NHMUK PV R 604 (c. 4.4). (7) Also present in *Valdosaurus canaliculatus* (Barrett, 2016), *Magnamanus soriaensis* (Fuentes Vidarte et al., 2016), *Brightstoneus simmondsi* (Lockwood et al., 2021) and variable in *Zalmoxes robustus* (Weishampel et al., 2003). (8) Also as in *Iguanodon bernissartensis* (RBINS R51), '*Dollodon bampingi*' (Norman, 1986) and in later diverging hadrosauriforms. (11) The ratio of c. 2.5 is greater than in other non-hadrosaurid iguanodontians.

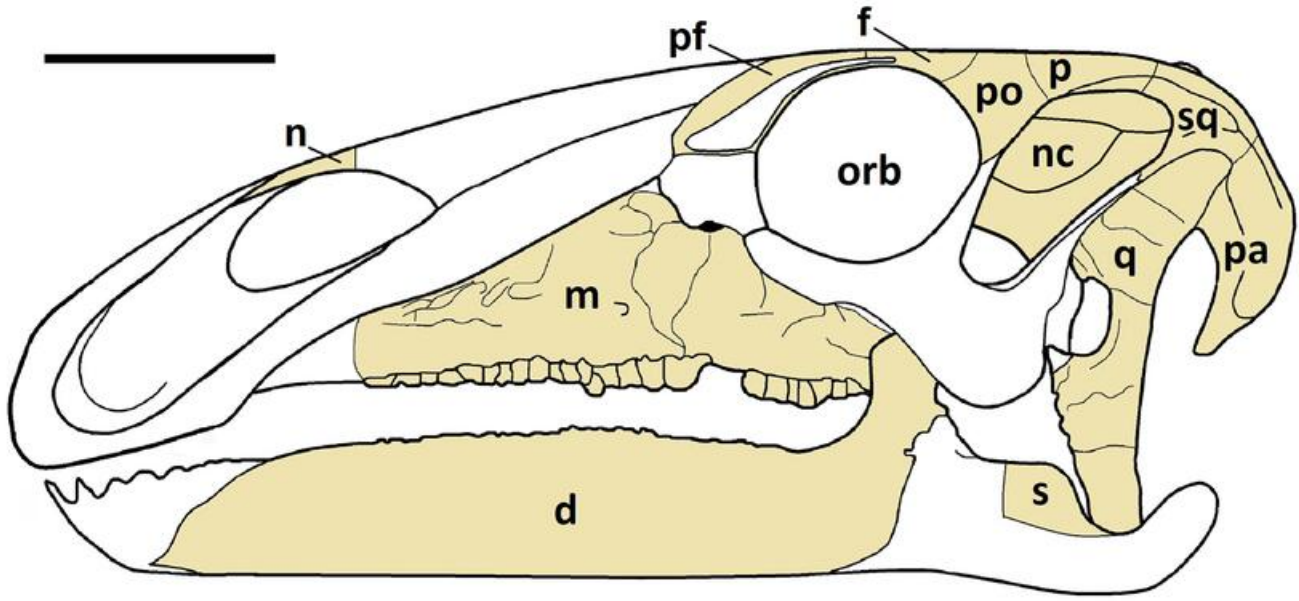


**Figure 2.** *Comptonatus chasei* gen. et sp. nov. (IWCMS 2014.80). Preliminary reconstruction of the skull. Shaded areas represent material present in the holotype. **Abbreviations:** **d**, dentary; **f**, frontal; **m**, maxilla; **n**, nasal; **nc**, neurocranium; **orb**, orbit; **p**, parietal; **pa**, paroccipital process; **pf**, prefrontal; **po**, postorbital; **q**, quadrate; **s**, surangular; **sq**, squamosal. Scale bar represents 100 mm.

## Osteological description

*Comptonatus chasei* represents one of the most complete iguanodontians, including cranial elements (Fig. 2), found in Britain. The bones have undergone some crushing, are heavily pyritized and some of the cortical surfaces have a roughened texture, so that fine detail such as muscle scars are often hard to discern. References to *Mantellisaurus atherfieldensis* in this paper, unless otherwise stated, refer to the holotype (NHMUK PV R 5764), which was examined at first hand (JAFL & SCRUM). Detailed photographs and measurements of all elements can be found in [Supplemental material](#) (pp. 33–150).

### Maxilla

The right maxilla is preserved (Figs 2, 3) but with anterior losses to the anterodorsal and anteroventral processes, the jugal process and the ascending process. It is robust and in lateral view forms an anteroposteriorly elongate triangle with the apex orientated dorsally forming the ascending process. In lateral view the ventral margin is shallowly concave, being almost straight in the middle section. There are 26 tooth positions present (confirmed by the number of ‘special foramina’ *sensu* Edmund, 1957), although the anteroventral process is missing and the tooth row extends to the fracture line. Assuming the occlusal surface was the same length as in the dentary, the tooth count was originally likely to

be *c.* 27. The alveoli are largely empty or contain the fractured bases of crowns, although one functional crown and one emergent crown are visible (see below). In ventral view the tooth row is straight in its mid-section, but posteriorly it curves laterally. The lateral surface of the maxilla has eight recognizable foramina of 2–5 mm diameter, situated dorsal to and broadly parallel with the tooth row, the larger examples being more centrally placed with anteriorly orientated exit grooves. Although the anteroventral process of the maxilla is missing, assuming it had a similar morphology to *Mantellisaurus atherfieldensis*, the ratio of the length of the maxilla anterior to the midpoint of the ascending process, to the overall length is *c.* 0.56. In *Mantellisaurus atherfieldensis* the ratio is 0.61 and in *Brighstoneus simmondsi*, which has an unusually long rostrum, it is 0.76. The anterior and posterior dorsal margins of the lateral wall of the maxilla slope dorsally and meet to form the apex of the ascending process. The apex of the ascending process is incomplete but still retains the floor of a narrow groove, for articulation with the maxillary process of the premaxilla. This groove widens considerably in a medial direction as it extends anteriorly, maintaining a thin, vertically orientated medial wall, while the lateral wall becomes a stouter, rounded ridge. This is also seen in *Sirindhorna koratensis* (Shibata *et al.*, 2015) and *Zhanghenglong yangchengensis* (Xing *et al.*, 2014), where the stouter lateral ridge continues as the anteroventral process and the medial ridge as the anterodorsal process. At its

anterior end the lateral ridge has a 'D'-shaped indentation on its dorsal surface (Fig. 3D), the straight edge of the 'D' being where it is cut short by the fractured distal end of the maxilla. This is in a similar position to an elongate oval depression found in *Jinzhouosaurus yangi* (see Barrett, Butler, et al., 2009 for a full description), located at the junction of the dorsal maxilla with the maxillary process of the premaxilla. It is absent in *Mantellisaurus atherfieldensis*. On the lateral surface of the maxilla, only the base of the jugal process is preserved. Medial to this is a narrow trough, that flattens out and expands over the posterior maxilla to form the convex dorsal surface of the ectopterygoid shelf. This supports an ectopterygoid ridge laterally, as occurs in many iguanodontians, for example, *Mantellisaurus atherfieldensis*, *Eolambia caroljonesa* (McDonald, Bird, et al., 2012), *Bactrosaurus johnsoni* (Prieto-Marquez, 2011) and *Amurosaurus riabinini* (Godefroit et al., 2004).

In medial view the maxilla is broadly triangular. Above the tooth row it displays a gently curved, ventrally concave, arcade of 'special foramina'. The 'special foramina' are larger and circular in the central area of the maxillae and become smaller and elliptical (long axis anteroposterior) at both extremities. Between these foramina and the tooth row the cortical bone is thin with a textured surface, forming the alveolar parapet. The shape of the 'special foramina' differ from those of *Mantellisaurus atherfieldensis*, which, although damaged, mainly resemble letter-box-like slits (axis anteroposterior), although some are elliptical. In *Brighstoneus simmondsi* (MIWG 6344) they are all almost perfectly circular.

The medial shelf of the maxilla begins at the level of the ascending process and extends anteriorly. The proximal section of the dorsal surface of the shelf is transversely flat with no everted margin, unlike the condition in *Mantellisaurus atherfieldensis* (Bonsor et al. 2023) and *Brighstoneus simmondsi* (Lockwood et al. 2021), where the surface is slightly concave transversely. Anteriorly, the surface twists slightly to face dorsomedially. The medial surface of the maxilla below the shelf is dorsoventrally convex and shallows anteriorly.

### Nasal

A rather incomplete fragment of thin bone probably represents a section of the right nasal (Figs 2, 4), with part of the process which formed the posterior margin of the naris. The margins are damaged with no evidence of any sutural structure. If correctly identified, it is curved transversely.

### Quadrate

Both quadrates are preserved although the right is highly abraded and provides little useful data, while the left is

in good condition (Figs 2, 5) and forms the basis of this description. There are losses to the medial pterygoid wing and the tip of the flange forming the anteroventral border of the paraquadratic notch.

In lateral profile the quadrate is crescent-shaped with the posterior border forming a gently concave curve that is more pronounced in its dorsal half. Although the dentary of *Comptonatus chasei* is 14% longer than the *Mantellisaurus atherfieldensis* holotype, the dorsoventral height of the quadrate, which is critical to the height of the skull, is 3% smaller. A posterior buttress ('quadrate buttress' *sensu* Gates et al., 2018) supporting the dorsal condyle is present in *Comptonatus chasei* but is considerably less prominent than in *Mantellisaurus atherfieldensis*. This buttress is present in other non-hadrosaurid iguanodontians such as *Iguanodon bernissartensis* (Norman, 1980); *Jinzhouosaurus yangi* (Barrett, Butler, et al., 2009); *Equijubus normani* (McDonald et al., 2014); *Gilmoresaurus mongoliensis* (Prieto-Marquez & Norell, 2010); *Bactrosaurus johnsoni* (Godefroit et al., 1998) and *Telmatosaurus transsylvanicus* (Weishampel et al., 1993), but is frequently absent in hadrosaurids (Prieto-Marquez & Norell, 2010).

In lateral view the quadrate is divided into dorsal and ventral flanges by the paraquadratic notch, an anteriorly placed, deeply curved embayment occupying the central area of the bone. The paraquadratic notch of *Comptonatus chasei* is centred close to the midpoint of the dorsoventral height of the quadrate. This is also the case in *Dryosaurus altus* (Galton, 1983); *Dysalotosaurus lettowvorbecki* (Janensch, 1955); *Xuwulong yueluni* (You et al., 2011); *Mantellisaurus atherfieldensis*; *Jeyawati rugoculus* (McDonald, Wolfe, et al., 2010); *Altirhinus kurzanovi* (Norman, 1998); *Choyrodon barsboldi* (Gates et al., 2018) and *Probactrosaurus gobiensis* (Norman, 2002). However, the paraquadratic notch in many iguanodontians is situated more ventrally, for example in *Iguanodon bernissartensis* (Norman, 1980); *Equijubus normani* (McDonald et al., 2014); *Ouranosaurus nigeriensis* (Taquet, 1976); *Proa valdearinnensis* (McDonald, Espilez, et al., 2012); *Protohadros byrdi* (Head, 1998); *Gilmoresaurus mongoliensis* (Prieto-Marquez & Norell, 2010); *Bactrosaurus johnsoni* (Godefroit et al., 1998); *Gobihadros mongoliensis* (Tsogtbaatar et al., 2019); *Edmontosaurus regalis* (Xing et al., 2017) and *Brachylophosaurus canadensis* (Prieto-Marquez, 2001).

In lateral view, the dorsal flange has a convex anterior margin. It narrows dorsally in shoulder-like fashion to form a 'D'-shaped condyle in dorsal view, with the straight margin facing laterally. The condyle inserts into the quadrate cotylus, a deep socket in the squamosal. Extending ventrally from the paraquadratic notch, the ventral flange narrows slightly in lateral view but

remains stout, terminating as the lateral border of the ventral articular condyle. In posterior view the quadrate is seen as a robust shaft of bone with articular condyles at both ends. Dorsally the shaft is relatively narrow,

while ventrally it expands transversely to form the ventral condyle, which is slightly angled, extending further ventrally on its lateral side. In anterior and posterior views, the medial and lateral margins of the distal

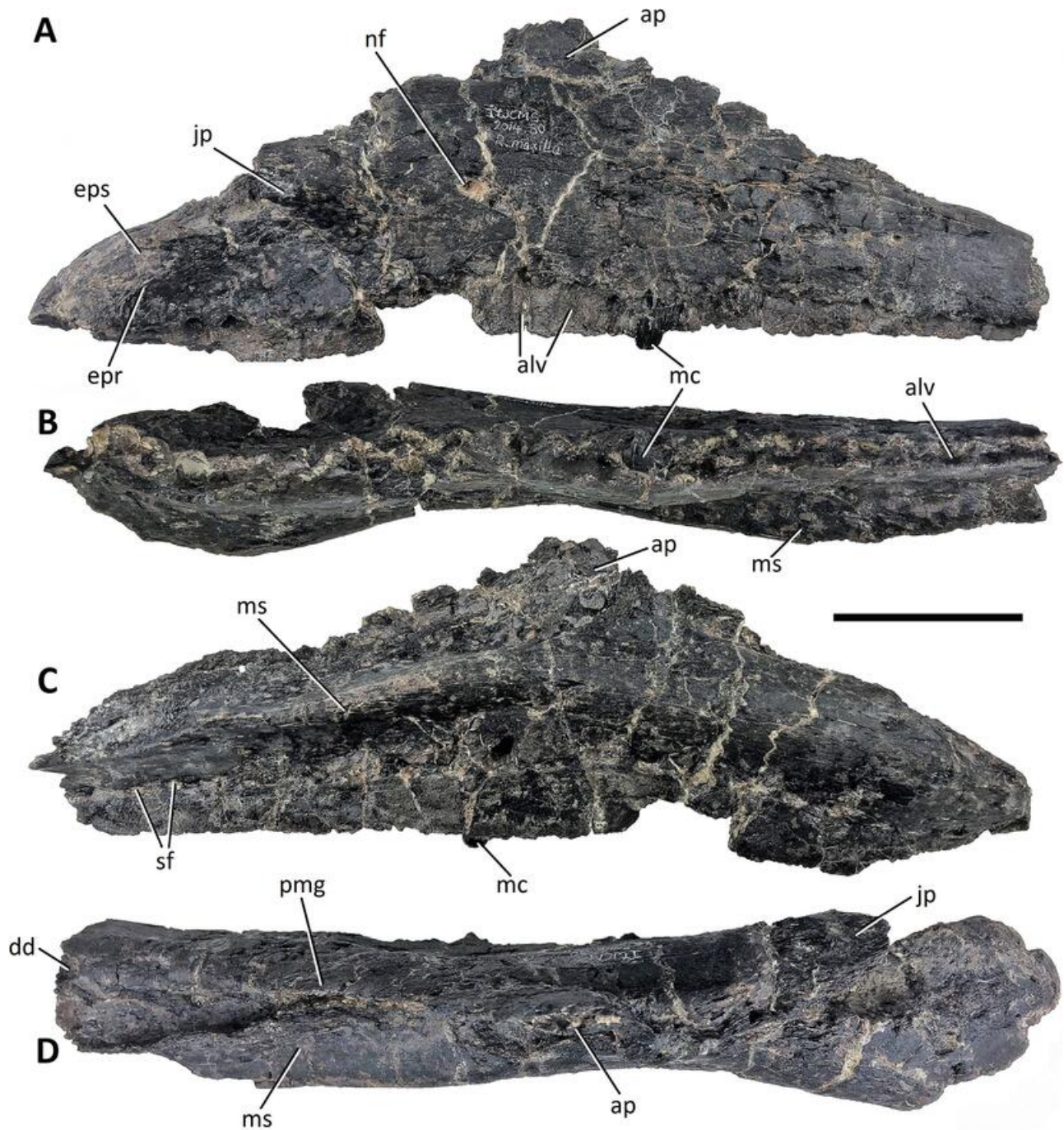


**Figure 3.** *Comptonatus chasei* gen. et sp. nov. (IWCMS 2014.80). Right maxilla in **A**, lateral, **B**, ventral, **C**, medial and **D**, dorsal views. **Abbreviations:** **ap**, ascending process; **alv**, alveolar socket; **dd**, D-shaped depression; **epr**, ectopterygoid ridge; **eps**, ectopterygoid shelf; **jp**, jugal process; **mc**, maxillary crown; **ms**, medial shelf; **nf**, nutrient foramen; **pmg**, premaxillary groove; **sf**, special foramina. Scale bar represents 50 mm.

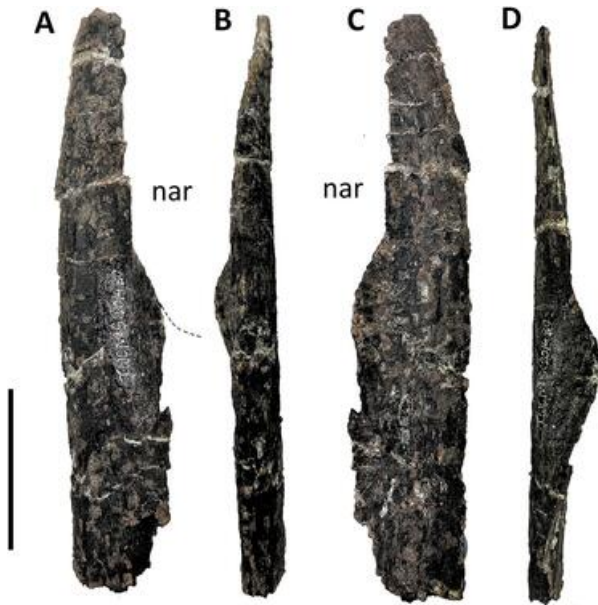


**Figure 4.** *Comptonatus chasei* gen. et sp. nov. (IWCMS 2014.80). Assumed right nasal fragment in **A**, lateral, **B**, dorsal, **C**, medial and **D**, ventral views. **Abbreviations:** nar, naris. Scale bar represents 30 mm.

quadrate shaft and condyle are not symmetrical, having a smoothly rounded ventrolateral corner and a concave medial margin with a protruding, more angular ventromedial corner. The latter is suggestive of an osteological correlate for a ligament or tendon. To varying degrees this morphology is observed in iguanodontian quadrates, but is particularly pronounced in *Ouranosaurus nigeriensis* (Taquet, 1976) and *Jeyawati rugoculus* (McDonald, Wolfe, et al., 2010). In ventral view the anteroposterior depth of the condyle is greatest laterally and tapers slightly medially. The articular surface is smooth and convex laterally and slightly depressed anteromedially (see surangular for a description of the quadrate-surangular articulation). In anterior view the medial or pterygoid wing can be seen to arise from most of the anteromedial border of the main quadrate shaft, starting just below the dorsal condyle and ending approximately 45 mm above the ventral condyle. The ventral margin of the wing is still largely intact and is initially concave as it extends anteriorly from the main quadrate shaft. The margin then becomes straighter and horizontal, and the wing curves anteromedially. Although only partial, the preserved marginal angles suggest that the pterygoid wing was subtriangular, as in *Bactrosaurus johnsoni* (Godefroit et al., 1998) and *Gobihadros mongoliensis* (Tsogtbaatar et al., 2019). Anteriorly there is a shallow dorsoventrally orientated depression in the shaft separating the medial pterygoid wing from the laterally placed dorsal and ventral flanges.

### Prefrontal

The left prefrontal has anterior and posterior losses, while the right (Figs 2, 6) is better preserved, having some anterior losses but an intact prefrontal-frontal suture and provides the basis of this description. In lateral view the prefrontal has a gently convex dorsal margin which medially would have sutured to the nasal and a concave ventral margin which contributed to the orbital fenestra. The bone can be divided into a posterior section that is dorsoventrally compressed and an anterior section that is transversely compressed. The tip of the posterior section is irregular and slotted into a cuboidal excavation in the anterior frontal, lateral to the nasal sutural surface (see frontal). The anterior section is incomplete anteriorly, leaving no evidence of a sutural surface for the lacrimal. Laterally is a slightly depressed area anterior to the orbital margin which may have been the facet for a palpebral. In medial view a shallow but dorsoventrally wide groove extends just below the dorsal margin of the prefrontal, perhaps connected with the paranasal airspaces. The dorsal margin is constructed of thin bone that would have sutured against the nasal. Ventral to the groove the prefrontal is irregularly excavated and contributed to the lateral wall of the nasal cavity.

### Frontal

Both frontals (Figs 6, 7) are well preserved except for slight damage to the sutural surfaces for the nasals and the parietals. The right is isolated, but the left has the postorbital attached, although it has been flattened by dorsoventral crushing, and the suture has slipped slightly, so was presumably not fused antemortem.

In dorsal view each frontal has a quadrilateral outline. The widest transverse diameter is the anterior margin (right 72 mm, left 78 mm) and the medial margin is the longest anteroposteriorly (right 91 mm, left 96 mm), so they are longer than wide. This shows similarities to the frontals of *Iguanodon bernissartensis* (Norman, 1980) and *Ouranosaurus nigeriensis* (Taquet, 1976) but differs from the reconstruction of the skull of ‘*Dollodon bampingi*’ (Norman, 1986, fig. 4), where they are wider than long. The dorsal surface is smooth and slightly depressed medially, rising towards the lateral margins. The medial margins form the sagittally placed interfrontal suture. This is not straight but slightly sinusoidal, being gently convex posteriorly on the left frontal and concave on the right and is generally similar to the suture in *Tenontosaurus tilletti* (Thomas, 2015). The sutural surface has a little damage but shows a longitudinal ridge and some vague evidence of slight interdigitation. The interfrontal sutural surface is deepest between the anterior third and the posterior two-thirds,

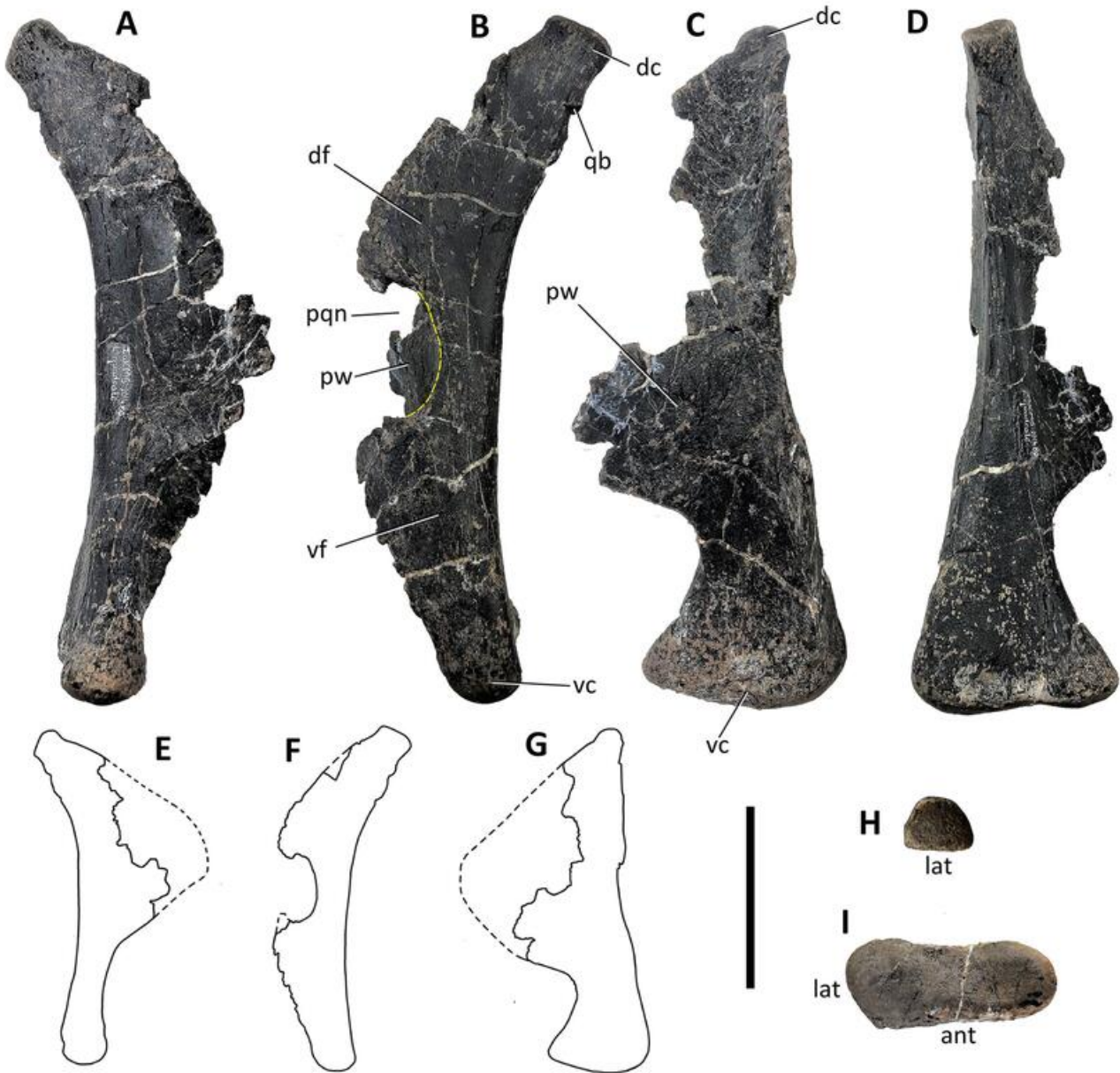


**Figure 5.** *Comptonatus chasei* gen. et sp. nov. (IWCMS 2014.80). Left quadrate in **A**, medial; **B**, lateral (yellow dashed line indicates border of paraquadratic notch); **C**, anterior; **D**, posterior; **E**, medial surface; **F**, lateral surface; **G**, anterior surface; **H**, dorsal (articular surface) and **I**, ventral (articular surface). **Abbreviations:** ant, anterior; dc, dorsal condyle; df, dorsal flange; lat, lateral; pqn, paraquadratic notch; pw, pterygoid wing; qb, quadrate buttress; vc, ventral condyle; vf, ventral flange. Scale bar represents 50 mm.

with a straight dorsal margin and a convex ventral margin. The anterior surface of the frontal provides articular surfaces for the nasals medially and the prefrontals laterally. There has been damage medially and the shape of the nasofrontal articulation in dorsal view is not clear. Laterally the anterior surface of the frontal has a subrectangular opening, extending into a cuboidal excavation, which forms a socket for insertion of the prefrontal

(Figs 6, 7). This is roofed by relatively thick bone dorsally, which has a roughened internal surface, but the socket is open ventrally apart from a small cavity posteriorly, enclosed ventrally by thin bone. It appears that when articulated a short, roughened posterior section of the prefrontal slotted into the cavity, but the prefrontal formed most of the ventral surface of this socket. This ventral surface was continuous with the smooth surface

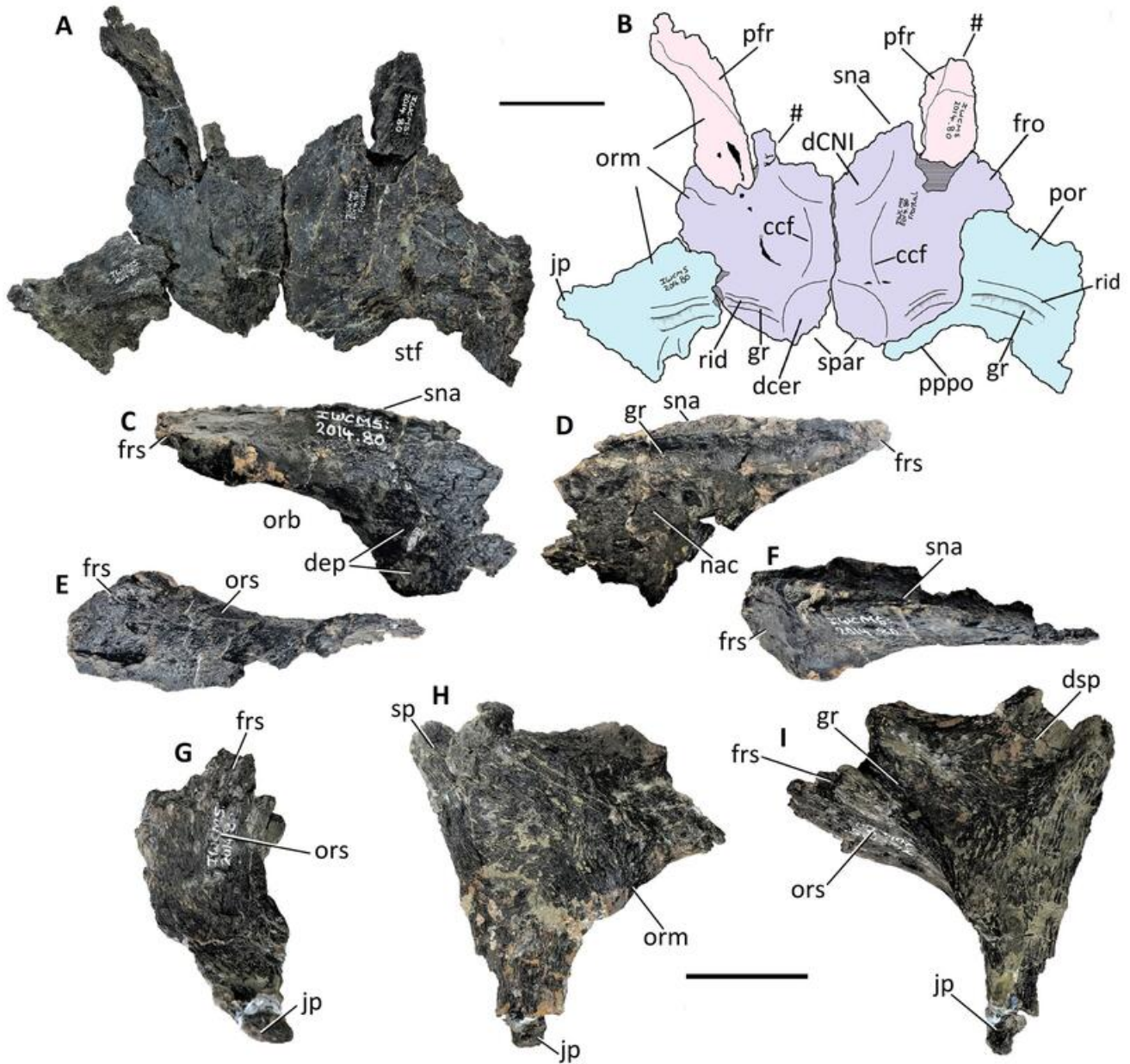


**Figure 6.** *Comptonatus chasei* gen. et sp. nov. (IWCMS 2014.80). Skull roof, right prefrontal and right postorbital. Skull roof in **A**, ventral view and **B**, schematic of ventral view. Right prefrontal in **C**, lateral, **D**, medial, **E**, ventral and **F**, dorsal views. Right postorbital in **G**, anterior, **H**, lateral and **I**, medial views. **Abbreviations:** **ccf**, crista cranii frontalis; **dcer**, depression for cerebrum; **dCNI**, depression for olfactory bulb; **dep**, depression, possibly palpebral facet; **dsp**, depressed area in squamosal process; **fro**, frontal (purple); **frs**, frontal suture; **gr**, groove; **jp**, jugal process (the base of); **nac**, nasal cavity; **orb**, dorsal orbital fenestra; **orm**, orbital margin; **ors**, orbital surface; **pppo**, parietal process of postorbital; **pfr**, prefrontal (pink); **por**, postorbital (blue); **rid**, ridge; **spar**, suture for parietal; **sna**, suture for nasal; **sp**, squamosal process; **stf**, supratemporal fenestra; #, fracture surface. Scale bar for **A** and **B** represents 50 mm, for **C**–**I**, 30 mm.

of the ventral side of the frontal, both contributing to the anterodorsal orbital surface adjacent to the margin of the orbital fenestra. The anterior section of the lateral surface of the frontal contributes to the orbital margin, while posteriorly is a surface with two longitudinal

ridges and several shorter dorsoventral ridges for articulation with the main body of the postorbital (see postorbital). A process from the postorbital extended posteromedially towards the parietal, along the lateral two-thirds of the posterior margin of the frontal. This is

the deepest and most robust area of the frontal and has a rugose surface. The frontal is excluded from the margin of the supratemporal fenestra by the postorbital. Medially the posterior surface of the frontal is slightly damaged but with its antimere probably formed an anteriorly pointing ‘V’-shaped notch for insertion of the interparietal process (*sensu* Lull & Wright, 1942). The ventral surface of each frontal is divided longitudinally by a curved ridge, the crista cranii frontalis, which is convex medially. When the frontals are articulated the cristae form an hourglass shape with semicircular depressions anteriorly and posteriorly. The anterior depression housed the olfactory bulbs and the posterior depression the anterior cerebrum. Slightly anterior to the posterolateral margin of the frontal is a ridge extending anterolaterally, with a shallow groove lying between the ridge and the posterior margin. This groove (Fig. 6B) continues as a deeper and wider structure on the internal surface of the postorbital.

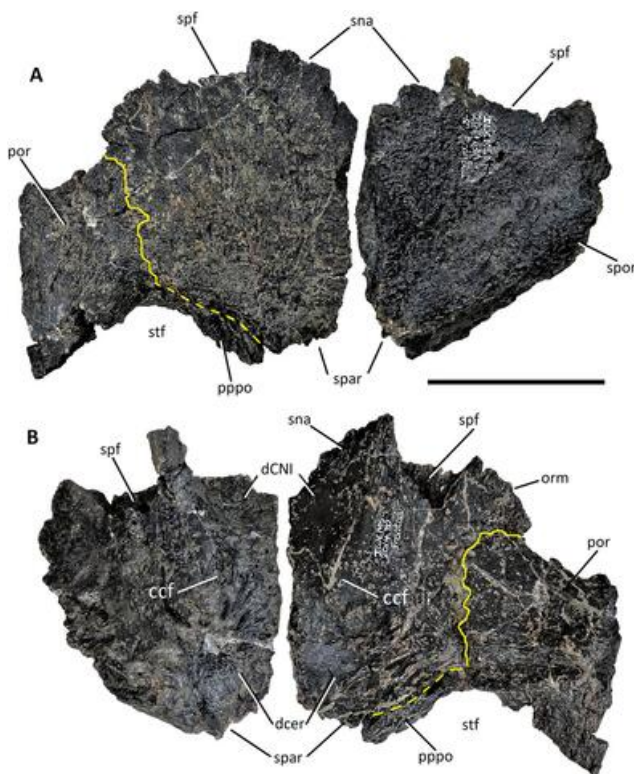


**Figure 7.** *Comptonatus chasei* gen. et sp. nov. (IWCMS 2014.80). Frontals and left partial postorbital in **A**, dorsal and **B**, ventral views. **Abbreviations.** **ccf**, crista cranii frontalis; **dcer**, depression for cerebrum; **dcNI**, depression for olfactory lobes; **orm**, orbital margin; **por**, postorbital, **pppo**, parietal process of the postorbital; **sna**, suture for the nasal; **spar**, suture for the parietal; **spf**, suture for the prefrontal, **spor**, suture for the postorbital; **stf**, supratemporal fenestra. Suture line between the frontal and postorbital marked in yellow. Scale bar represents 50 mm.

### Postorbital

The right and left postorbitals (Figs 2, 6, 7) are preserved but both are incomplete with losses to the processes to the jugal, squamosal and on the right to the parietal. The left remains articulated with the frontal. In dorsolateral view the postorbital is a triradiate bone with a triangular body. The apex of the body is orientated ventrally and would have continued as the jugal process. Two other processes originated from the posterodorsal angle. One, if complete, would have extended posteriorly to suture with the squamosal, and another which extends posteromedially along the posterior border of the frontal would have presumably articulated with a process from the parietal. The parietal process of the postorbital is preserved on the left and separates the lateral two thirds of the posterior margin of the frontal from the supratemporal fenestra. The postorbital articulates with the posterior section of the lateral margin of the frontal by means of a complex ridge and groove joint, the groove being in the postorbital, as is usual in iguanodontians (Weishampel, 1984). The edges of the suture are crenulate, and the dorsal margin of the suture is situated further medially than the ventral margin. The anteroventral surface of the postorbital contributes to the orbital surface and is transversely flat, being wide dorsally and tapering ventrally to become the jugal process (Fig. 6G, jp). In lateral view, this surface is concave and contributes to the majority of the posterodorsal margin of the orbit. Medially the internal surface of the postorbital has a posteroventrally directed ridge and groove (Fig. 6I, gr), which is continuous with the less pronounced ridge and groove on the lateral aspect of the ventral surface of the frontal. These presumably were for articulation with the laterosphenoid. At the base of the squamosal process in both postorbitals is a depressed area (Fig. 6I, dsp), although its extent is unknown due to fractures.

### Squamosal

The left squamosal (Figs 2, 8, 9) is almost complete, lacking only the anterior section of the postorbital process. It is incompletely fused to the parietal, and antemortem was probably not fused to the paroccipital process. The squamosal consists of a body with three prominent processes, articulating with the postorbital, the paroccipital process and the parietal, and a smaller, freestanding, precotyloid process (Fig. 8A). In lateral view the postorbital process extends anteriorly. The base of this process is approximately triangular in cross-section, having a ventromedial surface which is very slightly dorsoventrally concave and faces the neurocranium, a dorsal surface which is smooth and almost flat, and a lateral surface which is bounded dorsally by a

ridge, which extends posteriorly to form the dorsal margin of the subtriangular precotyloid fossa (*sensu* Gates et al., 2018) (Fig. 8A). The anteroventral border of the precotyloid fossa forms the posterodorsal margin of the lateral temporal fenestra and the posteroventral border forms the anterodorsal margin of the quadrate cotylus. The precotyloid fossa was interpreted by Ostrom (1961) as the origin of the adductor mandibulae externus superficialis muscle and is moderately well developed in *Comptonatus chasei*. It is also prominent in *Iguanodon bernissartensis* (Norman, 1980); *Mantellisaurus atherfieldensis*; *Jinzhousaurus yangi* (Barrett, Butler, et al., 2009); *Altirhinus kurzanovi* (Norman, 1998); *Equijubus normani* (McDonald et al., 2014) and *Choyrodon barsboldi* (Gates et al., 2018). Prieto-Marquez and Norell (2010) found the fossa absent in the more deeply nested *Bactrosaurus johnsoni* and *Tanius sinensis*, and only weakly developed in *Lophorhothon atopus*.

Ventral to the precotyloid fossa, the precotyloid process extends ventrally and slightly anteriorly and tapers to a point. The posterior surface of the precotyloid process is flat and would have braced the dorsal condyle of the quadrate against forward rotation (Norman, 1986). The precotyloid process in *Mantellisaurus atherfieldensis*; *Equijubus normani* (McDonald et al., 2014) and *Choyrodon barsboldi* (Gates et al., 2018) has a more prominent ridge along the posterolateral margin, and the posterior surface is twisted to face slightly posterolaterally compared to *Comptonatus chasei*. The anterior margin of the precotyloid process, with the precotyloid fossa and ventral border of the postorbital process, defines the posterodorsal extent of the lateral temporal fenestra.

The precotyloid process is separated from the postcotyloid process by the quadrate cotylus, a deep, anteroposteriorly orientated oval socket into which the dorsal condyle of the quadrate inserted. Posterior to the cotylus, the well-developed postcotyloid process extends ventrolaterally from the posterior margin of the squamosal. It forms a dorsoventrally elongate rectangle with somewhat crenulate margins, which is strongly anterolaterally–posteromedially compressed and is slightly rounded distally. The posteromedial surface articulates with the exoccipital-opisthotic complex, and has slipped slightly from its antemortem position, suggesting it was unfused.

The dorsomedial process extends from the posteromedial surface of the squamosal. Its ventral surface articulates with, and is partially fused to, the parietal but it is unclear whether it contacted the supraoccipital. Throughout its length it remains distinct from the supraoccipital. However, in a slightly damaged area lateral to the lateral process of the supraoccipital, the possibility

that a very small section of the ventromedial edge of the squamosal was in direct contact with the supraoccipital cannot be excluded. In *Choyrodon barsboldi* (Gates et al., 2018) and *Jintasaurus meniscus* (You & Li, 2009) the squamosal is excluded from contact with the supraoccipital by the parietal dorsally and the exoccipital-opisthotic complex ventrally. However, in many iguanodontians, the middle section of the lateral margin of the supraoccipital articulates directly with the squamosal, as in *Dysalotosaurus lettowvorbecki* (Galton, 1983); *Tenontosaurus dossi* (Winkler et al., 1997); probably *Dakotadon lakatoensis* (Boyd & Pagnac, 2015); *Iguanodon bernissartensis* (Norman, 1980); *Bactrosaurus johnsoni* (Godefroit et al., 1998) and *Brachylophosaurus canadensis* (Prieto-Marquez, 2001). It is probable that in some specimens the squamosal and parietal may be solidly fused with obliteration of the suture, thus making it difficult to know the true relationships of the individual bones. The distal end of the dorsomedial process is probably anteroposteriorly expanded although no definite suture is visible. The anterior border of the dorsomedial process and the medial border of the postorbital process form the posterolateral margin of the supratemporal fenestra.

### Parietal

A transversely compressed dorsal ridge is present along the anteroposterior midline of the fused parietals (Figs 8, 9), forming a shallow sagittal crest. The crest extends almost to the posterior margin of the parietal, but anteriorly it bifurcates to produce two straight ridges that extend anterolaterally, delineating a triangular, but incompletely preserved anteromedian plate. This plate probably extended anteriorly as the interparietal process (*sensu* Lull & Wright, 1942), which articulated with a small recess in the posterior margin of the frontals. The sagittal crest provides the medial margins of the supratemporal fenestrae. The anterior articular surface of the parietal is damaged, but still shows evidence of a transverse interdigitate suture with the frontal, and losses are probably not extensive. The anterolateral processes of the parietal that would have extended along the posterior margin of the frontal to articulate with the parietal process of the postorbital are missing. In lateral view the sagittal crest is slightly depressed anteriorly due to the taphonomic crushing of the anterior parietals but was probably horizontal in life. A relatively long and straight sagittal crest is seen in ‘*Dollodon bampingi*’ RBINS R57; *Proa valdearinnensis* (McDonald, Espilez, et al., 2012) and *Probactrosaurus gobiensis* (Norman, 2002), but in some iguanodontians the crest is shorter and splits into two posteriorly as well as anteriorly, notably in *Camptosaurus dispar* (Gilmore, 1909); *Bactrosaurus johnsoni* (Godefroit et al., 1998) and *Gobihadros mongoliensis* (Tsogbaatar

*et al.*, 2019). The posterior margin of the parietal of *Comptonatus chasei* is unfused with the squamosal (Fig. 9A). The posterior dorsal apex of the parietal separates the dorsomedial processes of the two squamosals by *c.* 3 mm. Physical contact between the dorsomedial processes of the squamosals is present in all lambeosaurines and the saurolophines *Maiasaura* and *Saurolophus* (Horner *et al.*, 2004), while in other saurolophines the squamosals are separated by the intervening parietal, for example in *Edmontosaurus regalis* (Xing *et al.*, 2017). In earlier-diverging iguanodontians, the majority of squamosals are separated by a narrow strip of parietal; for example, *Tenontosaurus tilletti* (Thomas, 2015); *Jinzhouosaurus yangi* (Barrett, Butler, *et al.*, 2009); *Proa valdearinnensis* (McDonald, Espilez, *et al.*, 2012); *Sirindhorna khoratensis* (Shibata *et al.*, 2015); *Probactrosaurus gobiensis* (Norman, 2002); *Jintasaurus meniscus* (You & Li, 2009); *Levnesovia transoxiana* (Sues & Averianov, 2009); *Bactrosaurus johnsoni* (Godefroit *et al.*, 1998) and *Gobihadros mongoliensis* (Tsogbaatar *et al.*, 2019), while in some they are relatively widely separated, for example, *Zalmoxes robustus* (Weishampel *et al.*, 2003); *Camptosaurus dispar* (Gilmore, 1909); *Iguanodon bernissartensis* (Norman, 1980); ‘*Dollodon bampingi*’ (Norman, 1986); *Ouranosaurus nigeriensis* (Taquet, 1976) and *Telmatosaurus transsylvanicus* (Horner *et al.*, 2004). It appears that the dorsomedial process of the squamosal forms a lap joint with a depressed area on the posterolateral surface of the parietal, although despite there being no fusion of the two bones posteriorly it is difficult to identify the anterior suture line with certainty, suggesting partial fusion. In posterior view, the posterior margins (occipital processes) of the parietal extend ventrolaterally from the apex to at least the level of the exoccipital-opisthotic complex and the lateral supraoccipital boss. On either side of the dorsal boss of the ascending process of the supraoccipital, the posterior margin of the parietal expands a little transversely and turns sharply anteriorly to produce a short step before continuing posterolaterally. This results in a slightly rounded and expanded surface (tuberosity), presumably for tendon or ligament insertion (Fig. 9B, tub). This feature is undescribed in other non-hadrosaurid iguanodontians and is considered autapomorphic. The step is situated adjacent to the suggested attachment sites on the ascending process of the supraoccipital for the rectus capitis posterior muscles (Langstone, 1960; Tsuihiji, 2010). Extending ventrally the parietal is medially expanded to follow the contour of the embayment between the ascending and lateral processes of the supraoccipital. Examples of this area of anatomy in iguanodontians are scarce, but similar morphology can be observed in *Ouranosaurus nigeriensis* (Taquet, 1976, fig. 13) and in a fragmentary hadrosaurian cranium (USNM 11893) with a posteriorly incomplete parietal (Ostrom, 1961, fig. 73), collected in the

Campanian aged Two Medicine Formation of Montana (Gilmore, 1937). In the space between this medial expansion of the parietal and the ascending process of the supraoccipital is a foramen, regarded as the posterior temporal foramen by Norman (1980) and Langstone (1960), and as the portal for the vena capitis dorsalis in *Iguanodon bernissartensis* (Norman, 1980). The foramen appears to be sited in the same place as the ‘external opening’ (*sensu* Sobral *et al.*, 2012) for the vena capitis dorsalis in *Dysalotosaurus lettowvorbecki*. A fine groove extends ventrally from this foramen (possibly as a channel for the vena capitis dorsalis) and curves concavely laterally to a possible second foramen (Fig. 9, for?), although this is pyrite filled and difficult to interpret. In lateral view there is an obvious suture line between the ventral margin of the parietal and the lateral wall of the brain case. This is particularly marked between the parietal and the laterosphenoid but continues between the parietal and proötic and presumably the opisthotic, although the latter two bones are fused together with obliteration of the suture and cannot be differentiated.

**Comment on posttemporal foramen terminology.** Terminology surrounding the posttemporal foramen or fenestra is not well defined and used by some authors (e.g. Norman 1980) for the foramen situated between the supraoccipital and the parietal, and by others for the more laterally placed foramen which lies between the paroccipital process ventrally and the squamosal dorsally (e.g. Langer, 2004). Averianov *et al.* (2007) described the two openings as medial and lateral posttemporal foramina in a stegosaurian braincase, with the medial providing the channel for the vena capitis dorsalis. Herein we describe the lateral foramen as the posttemporal foramen and the medial as the external opening of the vena capitis dorsalis.

### Supraoccipital

The supraoccipital (Fig. 9A) is exceptionally well preserved in *Comptonatus chasei* and demonstrates its articulation with the surrounding bones well. In posterior view it is a triradiate structure having an ascending process dorsally in the sagittal plane and right and left lateral processes ventrally. Its ventral border is solidly fused to the transverse exoccipital bar or bridge (*sensu* Langstone, 1960), with no suture line visible, although a posterodorsal facing step on the posterior surface could be explained as the exoccipital extending further posteriorly than the supraoccipital. Dorsally the supraoccipital articulates with the parietals, the posterior margins of which form a lambda-shaped roof over the ascending process, which extends to the dorsal margins of the lateral processes (Fig. 9A). The body of the ascending process is roughened by several longitudinal grooves, is transversely convex and

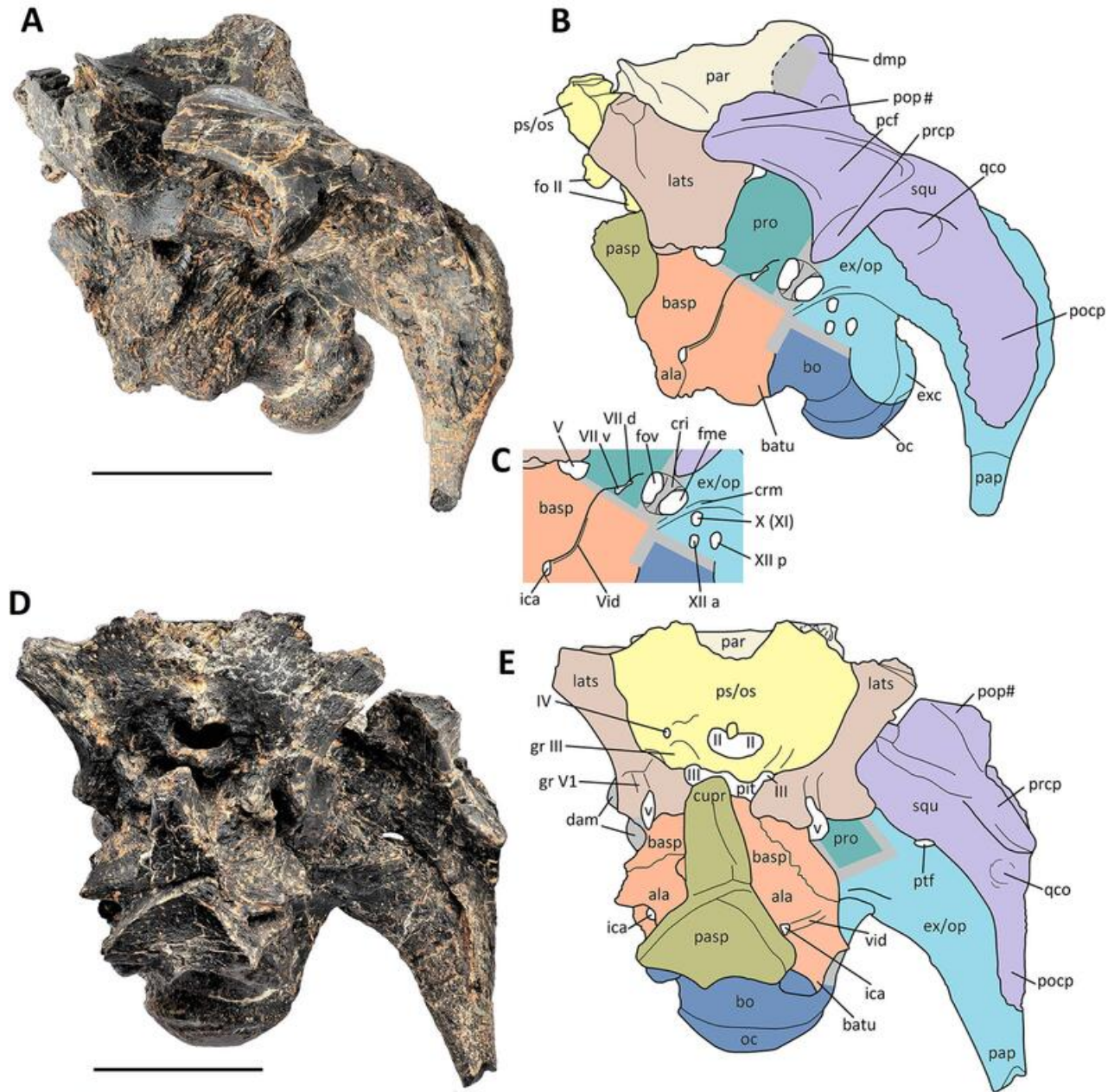


**Figure 8.** *Comptonatus chasei* gen. et sp. nov. (IWCMS 2014.80). Neurocranium in **A**, left lateral view, **B**, labelled schematic of left lateral view and **C**, labelled schematic of area surrounding auditory recess in left lateral view. Neurocranium in **D**, anterior view and **E**, labelled schematic of anterior view. **Abbreviations**; ala, alar process of basisphenoid; basp, basisphenoid (pale orange); batu, basal tubera; bo, basioccipital (dark blue); cri, crista interfenestralis; crm, crista metotica; cupr, cultriform process of parasphenoid; dam, damaged bone; dmp, dorsomedial process; exc, exoccipital condyloid; ex/op, exoccipital-opisthotic complex (light blue); fme, fenestra metotica; fo II, borders of the foramen for CN II; fov, fenestra ovalis; gr III, groove for CN III; gr V1, groove for ophthalmic division of CN V; ica, foramen for internal carotid artery; lats, laterosphenoid (light brown); oc, occipital condyle; pap, paroccipital process; par, parietal (beige); pasp, parasphenoid (olive green); pcf, precotyloid fossa; pit, fractured base of pituitary fossa; pocp, postcotyloid process; pop#, fractured postorbital process; prcp, precotyloid process; pro, proötic (sea green); ps/os, presphenoid-orbitosphenoid complex (yellow); ptf, posttemporal (lateral) foramen; qco, quadrate cotylus; squ, squamosal (lilac); Vid, Vidian canal; VII d, dorsal ramus of CN VII; VII v, ventral ramus of CN VII; XII a, anterior ramus of CN XII; XII p, posterior ramus of CN XII. Roman numerals indicate cranial nerves. Grey areas are unknown due to obliteration of sutures or damage. Scale bars represent 50 mm.

slightly depressed near its lateral margins, the latter feature suggested as osteological correlates for attachment of the paired rectus capitis posterior muscles (Langstone, 1960; Tsuihiji, 2010). It is capped dorsally by a rounded boss, above which is the nuchal shelf, a depression that was thought to have provided an area for the attachment of the ligamentum nuchae (Lull & Wright, 1942; Ostrom, 1961), although more recent work using extant phylogenetic bracketing suggests the ligamentum nuchae

(‘supraspinous ligament’) was more likely to be attached to the dorsoventrally ridged sagittal part of the ascending process of the supraoccipital (Bertozzo *et al.*, 2021; Tsuihiji, 2010). In the angle between the ascending and lateral processes, a medial expansion of the parietal divides the space into a dorsal foramen and ventrolateral area connected by a groove (Fig. 9A, see parietal). The ventral half of the lateral articulation of the supraoccipital is harder to define because the paroccipital process is

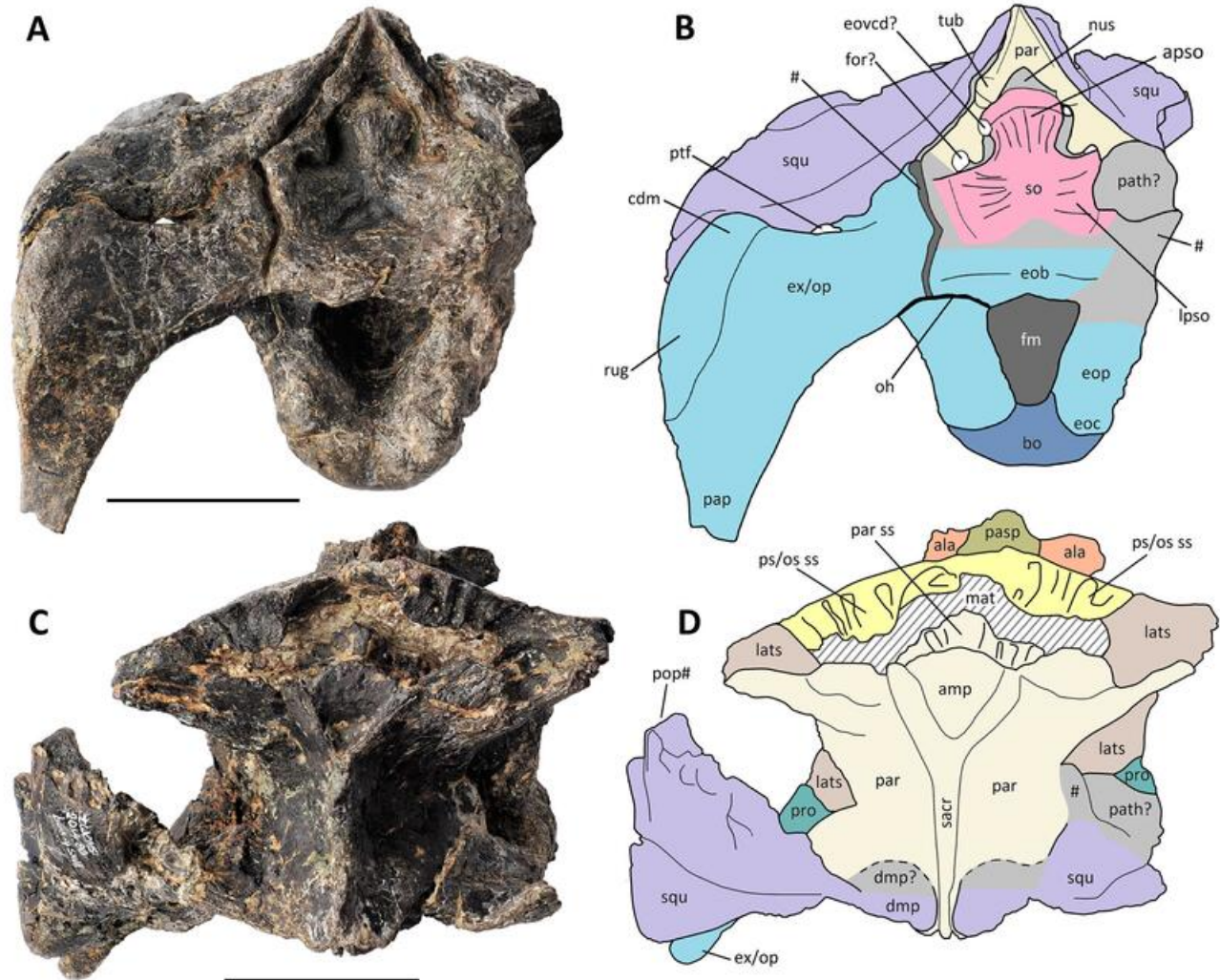


**Figure 9.** *Comptonatus chasei* gen. et sp. nov. (IWCMS 2014.80). Neurocranium in **A**, posterior view with **B**, labelled schematic of posterior view, and **C**, dorsal view with **D**, labelled schematic of dorsal view. **Abbreviations:** ala, alar wing of basisphenoid (orange); amp, anteromedian plate of parietal; apso, ascending process of supraoccipital; bo, basioccipital (dark blue); cdm, convex dorsal margin of paroccipital process; dmp, dorsomedial process of squamosal; dmp?, possible dorsomedial process of squamosal; ex/op, exoccipital-opisthotic complex (light blue); eovcd?, possible external opening for vena capitis dorsalis; eob, exoccipital bar/bridge; eoc, exoccipital condyloid; eop, exoccipital pillar; fm, foramen magnum; for?, possible foramen; lats, laterosphenoid (light brown); lps, lateral process of supraoccipital; mat, matrix; nus, nuchal shelf; oh, overhang of exoccipital bar; pap, paroccipital process; par, parietal (beige); par ss, parietal sutural surface; pasp, parasphenoid (olive green); path, possible pathological bone growth; pop#, postorbital process of squamosal (fracture surface); pro, proötic (sea green); ps/os ss, presphenoid-orbitosphenoid sutural surface (yellow); ptf, posttemporal (lateral) foramen; rug, rugosity; so, supraoccipital (pink); sacr, sagittal crest; squ, squamosal (lilac); tub, parietal tuberosity, and step; #, fracture surface. Grey areas are unknown due to obliteration of sutures or damage. Scale bars represent 50 mm.

missing on the right and there is a fracture line on the left. The lateral processes become slightly widened dorsoventrally as they extend laterally and appear to end in a boss-like structure (squamosal boss *sensu* Norman, 1980, fig. 7), less marked but similar to that seen in the ascending process. This boss appears to articulate with the exoccipital-opisthotic. Longitudinal striations are also present on the lateral processes, being more pronounced than on the ascending process and may also have provided an insertion point for the rectus capitis posterior muscles (Tsuihiji, 2010). There appears to be a postmortem fracture line between the supraoccipital and the exoccipital-opisthotic, extending ventrally to also divide the exoccipital.

The posterior surface of the supraoccipital faces slightly posterodorsally, although it is difficult to estimate the angle accurately without a more complete skull.

### Exoccipital-opisthotic

The exoccipitals form a bridge which is fused to the ventral margin of the supraoccipital with obliteration of all sutures. This provides the roof of the foramen magnum and as in most iguanodontians totally excludes the supraoccipital from contributing, although the supraoccipital does roof the foramen magnum in the early diverging *Dysalotosaurus lettowvorbecki* (Sobral et al., 2012), *Camptosaurus dispar* (Gilmore, 1909) and *Cumnoria prestwichii* (Maidment et al., 2022). The paroccipital process of the exoccipital-opisthotic is missing on the right side but is present on the left. It extends posterolaterally while expanding dorsoventrally, then curves ventrally and tapers towards a point, although the tip is not preserved. In posterior view the medial part of the dorsal margin of the paroccipital process is fairly straight, horizontal and articulates with the squamosal, although an elliptical foramen (long axis transverse) is present between the process and the squamosal (posttemporal foramen). Similarly placed foramina are evident in *Camptosaurus dispar* (USNM 5473; Gilmore, 1909, fig. 4), *Tenontosaurus tilletti* and *Tenontosaurus dossi* (Thomas, 2015). As the process extends laterally it develops a wide convex tab on its dorsal margin (Fig. 9B, cdm) that articulates with a concave depression in the squamosal. The lateral border as it curves ventrally is thickened and everted with a rugose surface. The articulation between the paroccipital process and the squamosal was unfused and has slipped slightly in the specimen. The tapered ventral section of the paroccipital process is convex anteriorly and flat posteriorly in cross-section. In lateral view, the ventral section of the proximal base of the paroccipital process bifurcates, one part continuing in an anteromedial direction as the crista

metotica (see below) and the other extending posteromedially to blend with the exoccipital bridge, but also overhanging the dorsal origin of the exoccipital pillar, resulting in the formation of a small fossa between them (see below and Fig. 9B, oh). This fossa is possibly homologous with a shallow depression in the same area, seen in *Camptosaurus dispar* (Gilmore, 1909); *Jintasaurus meniscus* (You & Li, 2009) and *Edmontosaurus regalis* (Xing et al., 2017), but we consider the appearance of an overhang and fossa, extending across the whole of the exoccipital pillar, to be autapomorphic for *Comptonatus chasei*.

The lateral walls of the foramen magnum are formed by the exoccipital pillars which are expanded ventrally to produce lateral condyloids (*sensu* Weishampel & Bjork, 1989), that form the dorsolateral part of the occipital condyle. The dorsal junction between the exoccipital pillar and the exoccipital bridge which forms the roof of the foramen magnum, is damaged on the right by recent fracture loss but appears to show confluent bone. Above this damaged area the bone is generally expanded with an irregular texture that may be indicative of pathology. The exoccipital condyloids do not contact each other, and the floor of the foramen magnum is provided by the basioccipital. This is also the case in iguanodontians such as *Zalmoxes robustus* (Weishampel et al., 2003); *Dysalotosaurus lettowvorbecki* (Galton, 1983); *Tenontosaurus tilletti* (Thomas, 2015); *Camptosaurus dispar* (Gilmore, 1909); *Probactrosaurus gobiensis* (Norman, 2002); *Eolambia caroljonesa* (McDonald, Bird, et al., 2012) and all hadrosaurids (Prieto-Marquez, 2010). The basioccipital is excluded from the foramen magnum by the exoccipitals in *Iguanodon bernissartensis* (Norman, 1980); *Equijubus normani* (McDonald et al., 2014) and *Proa valdearinnensis* (McDonald, Espilez, et al., 2012).

In lateral view of the braincase, the opisthotic is sutured anteriorly to the proötic, although the suture is fully fused and not visible. A pronounced crest of bone, the crista metotica (*sensu* Thomas, 2015) or metotic strut (*sensu* Godefroit, Bolotsky, et al., 2012), extends posterodorsally from the anteroventral margin of the opisthotic-proötic suture and flattens out dorsally before joining the medial border of the paroccipital process (Fig. 8C, crm). Posterior to the crista metotica are three foramina. The large posterior foramen, which is close to the exoccipital pillar, probably provided the exit for the posterior ramus of the hypoglossal nerve (CN XII), the anteroventral foramen for the anterior ramus of the hypoglossal nerve (CN XII), and the anterodorsal foramen for the vagus (CN X) and possibly the spinal accessory (CN XI) nerves (e.g. Norman, 1986, 2021; Thomas, 2015; Tsogtbaatar et al., 2019; Weishampel et al., 1993; Winkler et al., 1997). Anterior to the crista

metotica are two foramina separated by the crista interfenestralis and lying in a subcircular auditory recess. The larger fenestra ovalis is anterior to the crista interfenestralis and the fenestra metotica posterior.

### Proötic

The proötic (Figs 8, 9) forms the lateral wall of the braincase and articulates with the opisthotic posteriorly, the basisphenoid ventrally, the laterosphenoid anteriorly, and the parietal dorsally. Due to damage and probably complete fusion and obliteration of the suture, it is not possible to identify the articulation between the opisthotic and the proötic. By contrast, the suture between the proötic and the laterosphenoid is visible, the latter being slightly raised, suggesting that the laterosphenoid overlapped the proötic. The suture terminates ventrally at the midpoint of the dorsal margin of the large exit foramen and cavity for the Gasserian ganglion of the trigeminal nerve (CN V). The dorsal margin of this foramen is therefore contributed to by both the proötic and the laterosphenoid. From the foramen for the trigeminal nerve the ophthalmic branch ( $V_1$ ) is directed anteriorly, forming a deep but short groove in the posteroventral corner of the laterosphenoid, before emerging onto the ventral surface between the laterosphenoid and the orbitosphenoid-presphenoid complex. Between the trigeminal foramen and the auditory foramen is a narrow elongate foramen for the facial nerve (CN VII), with its long axis directed posterodorsally. The foramen is slightly constricted at its midpoint, giving it an hourglass appearance with slight grooves extending dorsally and ventrally. This suggests that the facial nerve had divided prior to exiting the braincase into a dorsal branch, the ramus hyomandibularis, and a ventral branch, the ramus palatinus (Lauters *et al.*, 2013).

### Laterosphenoid

The laterosphenoid (Figs 8, 9) is a large, stout bone which participates in the anterior part of the lateral wall of the braincase. Posteriorly it overlaps the anterior margin of the lateral surface of the proötic, being anterior to the trigeminal foramen and contributing to the anterodorsal margin of the foramen. It is limited ventrally by the basisphenoid, anteriorly by the orbitosphenoid and dorsally by the parietal. It extends anterolaterally, the posterior margin curving concavely, towards articulation with the postorbital, and forms part of the structure separating the orbit from the supratemporal fenestra. The medial margin of the laterosphenoid provides the lateral margin of a foramen for the oculomotor nerve (CN III), (Fig. 8E, III).

### Orbitosphenoid and presphenoid

The orbitosphenoid and presphenoid (Figs 8, 9) are completely fused and are indistinguishable. This is also the case in *Corythosaurus casuarius* (Ostrom, 1961) and *Edmontosaurus regalis* (Xing *et al.*, 2017), but they are seen as separate bones in *Batyrosaurus rhozhdestvenskyi* (Godefroit, Bolotsky, *et al.*, 2012) and *Brachylophosaurus canadensis* (Prieto-Marquez, 2005). There is no evidence of a presphenoid element preserved in *Tenontosaurus tillitti*, *Tenontosaurus dossi* (Thomas, 2015) or *Iguanodon bernissartensis* (Norman, 1980), possibly because it failed to ossify. The two orbitosphenoid-presphenoid complexes articulate with each other producing, in ventral view, a 'V'-shaped opening situated anteriorly in the sagittal plane, for the exit of the olfactory tracts leading to the olfactory bulbs. The margins of this opening are provided by the more medially placed presphenoids. Contact with the frontals was by a digitate suture, the dorsoventral ridges of which are still present, suggesting it was unfused. Posteriorly is an elliptical opening (long axis transverse), with a small nubbin of bone anterior to it in the sagittal plane, presumably to separate the emerging optic nerves (CN II). On the right side, lateral to the optic foramen is a much smaller elliptical foramen (long axis anteroposterior) for the trochlear nerve (CN IV) with a short exit groove anteriorly. This is not visible on the left, probably obscured by damage to the surface. Laterally the orbitosphenoid contacts the laterosphenoid. The posterior margin of the orbitosphenoid provides the anterior border of a large foramen also bounded laterally by the laterosphenoids. This foramen lies dorsal to the parasphenoid, and forms a sagittally placed triangular opening, with the apex directed posteriorly and the two anterior corners rounded, with a broad but shallow exit groove for the oculomotor nerve (CN III), extending anteriorly along the sides of the optic foramen. A large part of this opening represents damage to the dorsal part of the parasphenoid, exposing the hypophysal fossa.

### Basioccipital

The basioccipital is well preserved, although the surface of the basal tubera are irregular due to taphonomic distortion. The basioccipital (Figs 8, 9) is the major contributor to the occipital condyle, apart from the dorsolateral areas which are formed by the exoccipital condyloids (see above). In posterior view the occipital condyle has a smooth surface and is reniform, with a shallow groove dorsally where it contributes to the foramen magnum. The smooth surface continues a considerable way onto the ventral surface. Its depth in the sagittal plane is 29 mm and its maximum width is 51 mm. The neck of the basioccipital is separated from the smooth articular surface by a step that is most

prominent ventrally. Extending anteriorly in ventral view the basioccipital is divided by a deep median sulcus, producing two short, stout pillars which support the basal tubera. There is evidence of the very slight remnants of a thin medial crest along the floor of the sulcus as described in *Jintasaurus meniscus* (You & Li, 2009), although a more robust crest is present in *Cumnoria prestwichii* (Hulke, 1880; Maidment et al., 2022). Although the surfaces of the basal tubera are irregular due to taphonomy, there is a faint suture showing that the basioccipital probably provided a small portion of the posterior surface of the tubera while the basisphenoid was the major contributor.

### Basisphenoid and parasphenoid

The basisphenoid (Fig. 8) forms the middle section of the floor of the braincase and provides most of the ventral surfaces of the basal tubera. The margins that articulate with the laterosphenoids, proötics and the parasphenoid cannot be defined. The basisphenoid lies ventral to the proötic, the laterosphenoid, and the foramen for the trigeminal nerve (CN V), the ventral margin of which forms a gently concave depression in the dorsal margin of the basisphenoid. The basipterygoid processes are broken on both sides. Anterodorsal to the bases of the basipterygoid processes are well formed alar processes. The Vidian canal is a deep groove between the posterior margin of the alar process and the anterior part of the basal tubera. The groove is orientated dorsoventrally, and merges ventrally with the foramen for the internal carotid artery, which is directed anteromedially towards the pituitary fossa. Dorsally the canal blends with the ventral groove from the foramen for the facial nerve (CN VII). The parasphenoid is fused to the basisphenoid although no suture is visible. The process is incomplete but tapers anteriorly in ventral view becoming increasingly transversely compressed to form an incomplete cultriform process. The ventral surfaces of the basisphenoid and the parasphenoid are smooth and are angled steeply anterodorsally in lateral view.

### Vomer

Two thin blades of bone were recovered, interpreted here as partial vomers (Fig. 10). One is better preserved than the other, being more complete at both ends, but morphologically the two are almost mirror images of each other. The description of the better-preserved element assumes the orientation in Fig. 10K, L. Both ends are fractured. In lateral profile the ventral margin is almost straight while the dorsal margin is maximally convex at the junction of the posterior and middle

thirds. At this point the vomer is maximally deep dorsoventrally, but thereafter tapers as the margin descends anteroventrally. The ventral margin in ventral view is grooved in its posterior two thirds and is straight anteriorly but posteriorly curves posterolaterally. The anterodorsal section of the bone is very thin and forms a smooth sided blade. The bladed area is transversely compressed, and delineated ventrally by a slight step as it joins the more thickly transversely expanded ventral region of the vomer. The ventral margin of the blade extends posteriorly, following the ventral margin of the vomer closely, before curving dorsally to join the dorsal margin (Fig. 10G, I). On the medial side is a similarly depressed area, although it does not extend as far posteriorly. It is assumed that the anterior sections were appressed together to form part of the septum between the internarial cavities and choanae and would have extended anteriorly to articulate with the premaxilla. The groove possibly represents the articulation with either the palatine and/or pterygoid. The vomer is exceptionally well preserved and is described in *Tenontosaurus tilletti* (Thomas, 2015), but also informative in some hadrosaurids, notably *Brachylophosaurus canadensis* (Heaton, 1972). Among non-hadrosaurid styracosternans, it is generally unpreserved, fragmentary, or inaccessible, leading to scant descriptions. Heaton (1972) describes the vomers in *Brachylophosaurus canadensis* as heavily crushed but having a wedge-shaped body in medial view consisting of a transversely thin sheet of bone which tapers down to a point where it expands transversely, articulates with its antimere and after a short distance both are inserted between the premaxillae. Viewed dorsally as the vomers extend posteriorly from this articulation, they splay away from each other. The ventral margin is straight and articulated with the medial surface of the maxilla. Posteriorly they articulate with the palatine. This is compatible with the interpretation in *Comptonatus chasei*. Thomas (2015) describes the vomer in *Tenontosaurus tilletti* as the longest element in the skull and also (as in *Comptonatus chasei*) as a probably paired element fused to its antimere anteriorly. As it extends posteriorly a median ventral ridge develops that continues posteriorly and splits into two posterior processes. The vomer also switches at this point from being dorsoventrally to transversely thin. Possibly the preserved material in *Comptonatus chasei* represents similarly placed transversely thin sections of the vomer.

### Dentary

Two small sections of the left dentary are preserved but the right dentary (Figs 2, 11) is almost complete with a few fragments of the splenial attached. The sutural

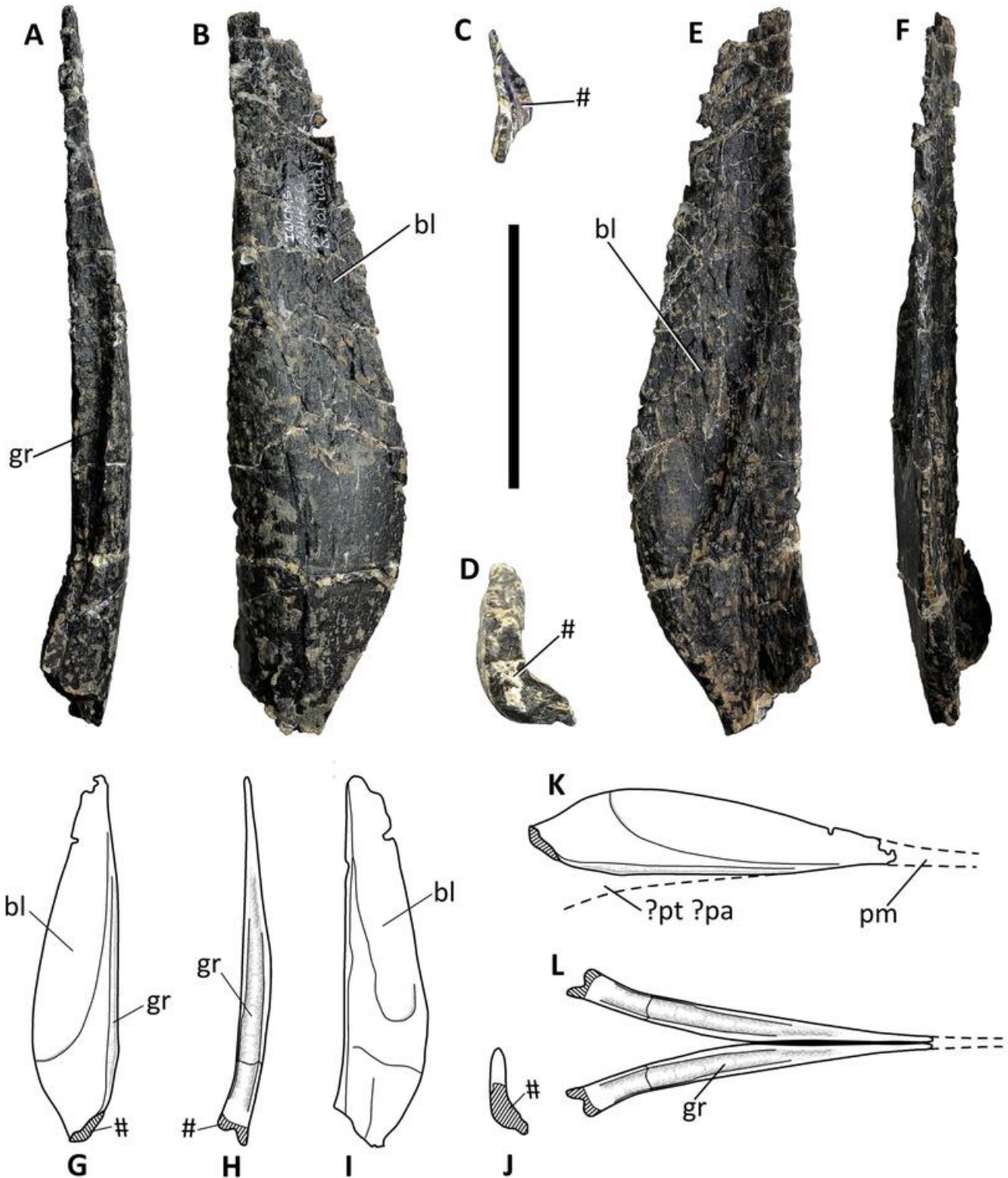


**Figure 10.** *Comptonatus chasei* gen. et sp. nov. (IWCMS 2014.80). Possible vomer (orientation presumes right vomer positioned as in **K**, and **L**) in **A**, ventral, **B**, medial, **C**, anterior, **D**, posterior, **E**, lateral, **F**, dorsal, **Drawings: G**, lateral, **H**, ventral, **I**, medial and **J**, posterior views. **K**, presumed position of vomer in lateral view. **L**, possible reconstruction of ventral view of vomer and antimere, **Abbreviations: bl**, blade; **gr**, groove; **?pt?pa**, possible articulation with pterygoid and/or palatine; **pm**, continuation towards premaxilla; **#** fracture surface. Scale bar represents 50 mm.

surface for the surangular has been damaged and is incomplete, especially ventrally. The dentary has been transversely compressed posteriorly, resulting in collapse of the ventromedial wall that covered the Meckelian canal, with partial closure of the adductor fossa. There is some damage to the anterior quarter of the dentary, with some localized lateral crushing; however, inspection of the ventral cortical surface shows it to be intact, smoothly contoured, and undistorted, although the distal end of the dentary and symphysis has been angled slightly laterally.

In lateral view, the dentary forms an elongate rectangle which anteriorly lacks the ventral deflection commonly observed in many iguanodontians. The dorsal edge is crenulate due to empty alveoli and is very slightly convex, apart from anteriorly where the convexity increases as it curves ventrally towards the symphysis. In lateral view the ventral margin of the dentary is completely straight throughout its length (Fig. 11). This contrasts with *Mantellisaurus atherfieldensis* and *Brighstoneus simmondsi* (Lockwood et al., 2021), where the dentary is ventrally deflected anteriorly, and the ventral margin is gently concave along its whole length so that the mid-section is the least deep (see discussion section for a full account of this character). The tooth row is composed of at least 23 and probably 24 alveolar positions. It describes a shallow sigmoid curve when viewed dorsally, posteriorly curving laterally to meet the base of the coronoid process, and anteriorly curving slightly medially. Most of the teeth are lost, although five fragmentary and damaged crowns are retained (see below). The alveolar septa are not parallel and have been shaped by the teeth. This is the usual morphology found in *Iguanodon bernissartensis* (Norman, 1980); *Mantellisaurus atherfieldensis* (Norman, 1986); *Brighstoneus simmondsi* (Lockwood et al., 2021) and *Ouranosaurus nigeriensis* (Taquet, 1976), but in more deeply nested taxa such as *Probactrosaurus gobiensis* (Norman, 2002), *Eolambia caroljonesa* (McDonald, Bird, et al., 2012), *Bactrosaurus johnsoni* (Godefroit et al., 1998) and all hadrosaurids (Horner et al., 2004) the alveolar walls are parallel. Based on the alveolar sizes, the tooth sizes are maximal in the mid-section and become progressively smaller at both ends, more markedly so anteriorly. In dorsal view the tooth row is situated medially while laterally there is a moderately developed buccal shelf which is widest posteriorly. The shelf deflects ventrally to form the lateral wall which is dorsoventrally convex throughout the length of the alveolar row. Approximately 12 foramina (2–5 mm diameter), with exit grooves that extend anteriorly, are located along the line of this drop off on the lateral

side of the dentary. At the junction of the posterior third and anterior two-thirds of the dentary, one of these foramina is represented by two smaller foramina arranged dorsoventrally. In dorsal view, the middle section of the lateral wall is weakly concave. Anteriorly the dentary twists so that the medial wall faces dorsally and curves medially to meet its antimere at the mandibular symphysis. A small, longitudinally grooved section is present at the posterior end of the symphysis, which represents part of the attachment area of the prementary. The ventral surface of the symphysis has an oval depression (long axis anteroposterior), which suggests an articulation site for a prementary possessing a bilobed ventral process, similar to *Bayannurosaurus perfectus* (Xu et al., 2018); *Brighstoneus simmondsi* (Lockwood et al., 2021) and *Proa valdearinoensis* (McDonald, Espilez, et al., 2012). In dorsal view, the medial margin of the symphysis and the lateral margin of the dentary diverge posteriorly.

Anteriorly the tooth row gives way to a thin edentulous area or diastema. This almost immediately begins to descend anteroventrally without a horizontal element, forming a convex arc before broadening transversely to form the articular surface for the prementary.

On the medial surface of the dentary, there is a line of ‘special foramina’, above which the alveolar parapet is almost completely lost. Ventrally the Meckelian canal is exposed, extending anteriorly from the adductor fossa, and gradually tapering to terminate in line with the fourth alveolus.

The coronoid process is placed laterally and in lateral view its axis is almost at right angles but a little posterodorsal to the main body of the dentary. This is similar to *Mantellisaurus atherfieldensis* and *Brighstoneus simmondsi* (MIWG 6344) but the process in *Iguanodon bernissartensis* (RBINS R52, R56) tends to be angled slightly anterodorsally. An anterodorsally orientated coronoid process is often seen in hadrosaurids, for example *Brachylophosaurus canadensis* (Prieto-Marquez, 2001); *Gryposaurus latidens* (Prieto-Marquez, 2012) and *Edmontosaurus regalis* (Xing et al., 2017). Dorsally, the coronoid process is slightly expanded anteroposteriorly, and the vertical plane of the process is aligned parasagittally. The lateral surface of the coronoid process is anteroposteriorly convex, while the medial surface is flatter. The surface topography of the coronoid process is indistinct although there are some striae on the anterodorsal quadrant of the lateral surface. The posterior alveoli lie directly medial to the base of the coronoid process with no intervening buccal platform and extend posteriorly as far as the midpoint of the base of the coronoid process.

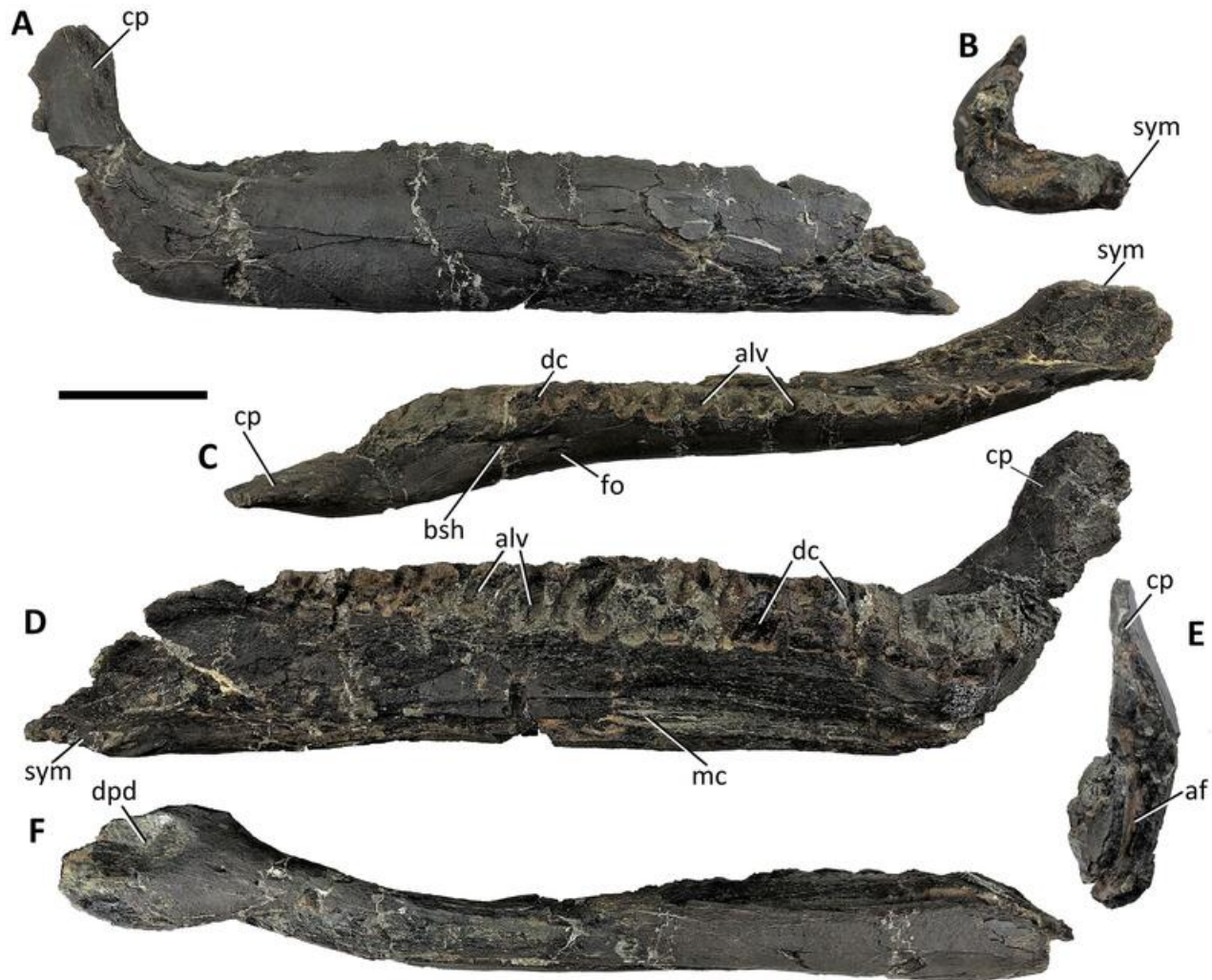


**Figure 11.** *Comptonatus chasei* gen. et sp. nov. (IWCMS 2014.80). Right dentary in **A**, lateral, **B**, anterior, **C**, dorsal, **D**, medial, **E**, posterior and **F**, ventral views. **Abbreviations:** **af**, adductor fossa; **alv**, alveoli; **bsh**, buccal shelf; **cp**, coronoid process; **dc**, dentary crown; **dpd**, depression for ventromedian process of the predentary; **fo**, nutrient foramen; **mc**, Meckelian canal; **sym**, mandibular symphysis. Scale bar represents 50 mm.

### Surangular

Only the posterior part of the surangular (Fig. 12) is preserved, and it has also lost the posterior end of the articular process. The lateral wall is very slightly convex anteroposteriorly and dorsoventrally, and in lateral view has a convex dorsal margin (the lateral flange of the glenoid *sensu* McDonald, Bird, et al., 2012) and a straight ventral margin. On the ventral surface there is a deep longitudinal groove for articulation with the angular. Dorsally, the surangular supplies the lateral part of the mandibular glenoid for articulation with the lateral part of the ventral quadrate condyle. The dorsal surface of the surangular is divided into anterior and posterior depressed areas by a transverse ridge. The posterior

depression is deeper than the anterior and acted as the lateral articular surface of the glenoid, while the anterior surface was presumably continuous with the floor of the adductor fossa. In dorsal view, the surface of the glenoid projects medially as a thin horizontal plate, and the articular process extends posteriorly. Medially, the surangular would have articulated with the articular, which provided the medial section of the mandibular glenoid. No surangular foramen is visible on the fragment from *Comptonatus chasei*.

### Comment on the quadrate-surangular articulation.

Although the lateral part of the quadrate condyle is more expanded anteroposteriorly than the medial part, it

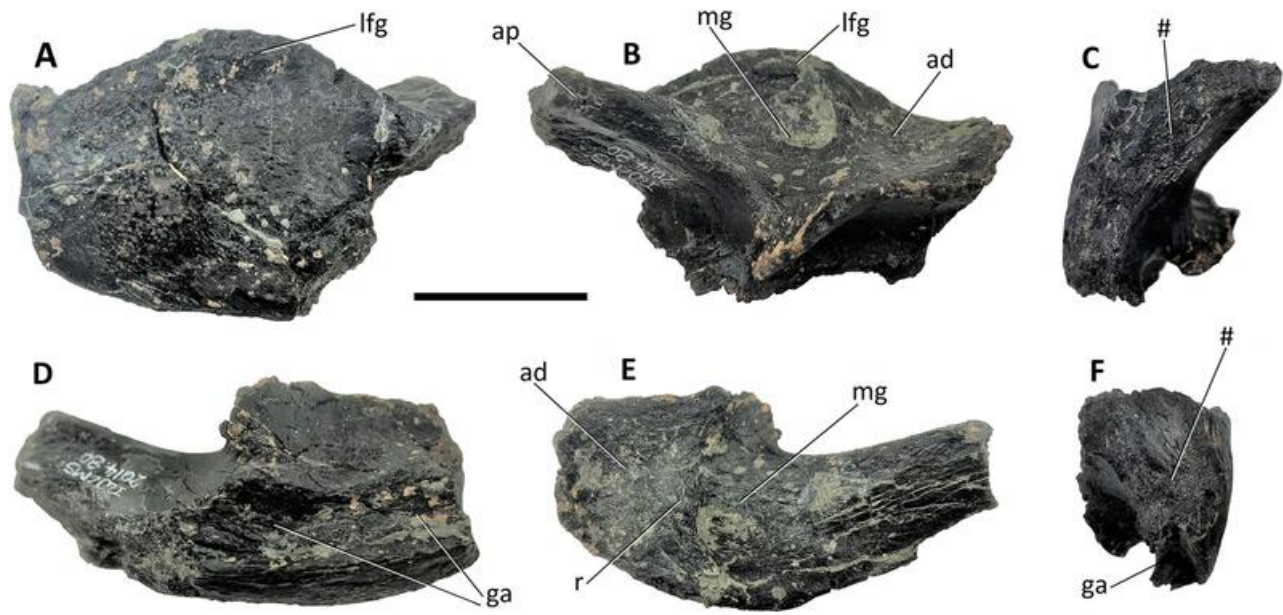


**Figure 12.** *Comptonatus chasei* gen. et sp. nov. (IWCMS 2014.80). Fragment of left surangular in **A**, lateral, **B**, medial, **C**, posterior, **D**, ventral, **E**, dorsal and **F**, anterior views. **Abbreviations:** **ad**, anterior depression; **ap**, articular process; **ga**, groove for angular; **lfg**, lateral flange of glenoid; **mg**, mandibular glenoid; **r**, ridge; **#**, fracture surface. Scale bar represents 20 mm.

is obvious that the surangular component of the mandibular glenoid provided less than half of the width of the condyle. This is at variance with Norman's (1986) description of '*Dollodon bampingi*' where the surangular makes a greater contribution to the glenoid than the articular (only a fragment of the surangular and articular are preserved in *Mantellisaurus atherfieldensis*). To accommodate the whole condyle, either the width of the articular must have been considerably greater than the surangular, or the articular was expanded medially by fibrocartilage. In NHMUK PV R 11521, a specimen referred to *Mantellisaurus atherfieldensis* (Barrett, Butler, et al., 2009; McDonald, 2012a; Norman, 2012) and found in the Wessex Formation of the Isle of Wight, the mandibular glenoid is completely preserved and the distal condyle of the quadrate overlaps the medial margin. In *Alligator mississippiensis* the quadrate forms a synovial joint, principally with the articular. Sections through the joint show that a cartilaginous lip is present medially (Bailleul & Holliday, 2017), and this may have been the case in *Comptonatus chasei*.

## Dentition

**Maxillary dentition.** Two maxillary crowns are preserved *in situ*, one functional and one partially erupted. The functional crown is better preserved and used in this description, although the apical section of the mesial margin is missing (Fig. 13G). The maxillary crown is narrower and more rectangular, with a greater

height to width ratio than the dentary crowns. The labial surface has a thicker coating of enamel than the lingual surface and bears ornamentation. This consists of a distally situated, prominent primary ridge extending from the base of the crown to the occlusal surface, so that the labial surface is divided approximately into a distal quarter and a mesial three quarters. A primary ridge, set distally to this degree, is also seen in *Cumnoria prestwichii* (Maidment et al., 2022); *Brighstoneus simmondsi* (Lockwood et al., 2021); *Ouranosaurus nigeriensis* (Taquet, 1976) and *Bolong yixianensis* (Wu & Godefroit, 2012). No maxillary crowns are completely preserved in *Mantellisaurus atherfieldensis*, although some fractured cross-sections of their bases are visible and suggest a more centrally placed, albeit still posteriorly displaced primary ridge, as is also the case in *Iguanodon bernissartensis* (Norman, 1980). Maxillary teeth from the earlier diverging *Dysalotosaurus lettowvorbecki* (Janensch, 1955) and *Dryosaurus altus* (Galton, 1983) have a marked central or very minimally distally offset primary ridge. The primary ridge in *Comptonatus chasei* also appears to have a groove running apicobasally along its length (see dentary dentition below for comparative anatomy). This is best-preserved as it approaches the occlusal surface, although basally taphonomic damage has cracked the enamel layer, making evaluation more difficult. There are three thin, but distinct accessory ridges present in the functional crown of *Comptonatus chasei*, situated mesial to the primary ridge. Basally, the first accessory ridge curves and joins

the second accessory ridge. The second and third ridges extend a good distance basally, although damage to the basal crown makes it unclear where they terminated. The appearance is similar to *Cumnoria prestwichii*, which possesses up to five secondary ridges (Maidment *et al.*, 2022), and *Bolong yixianensis* which has up to four (Wu & Godefroit, 2012). *Brighstoneus simmondsi* has up to six mesial accessory ridges (Lockwood *et al.*, 2021) and some much shorter ridges situated apicomediaally. No accessory ridges are present in *Eolambia caroljonesa* (McDonald, Bird, *et al.*, 2012), *Lophorhynchon atopus* (Gates & Lamb, 2021; Langstone, 1960), *Protohadros byrdi* (Head, 1998), *Shuangmiaosaurus gilmorei* (You *et al.*, 2003) and hadrosaurids (Horner *et al.*, 2004). Wedge-shaped marginal denticles are situated mesially and distally. The mesial border is incomplete but probably supported more denticles than the distal border, both possibly reaching the high teens in number. The marginal denticles bear up to three

mammillae, *c.* 150  $\mu\text{m}$  in diameter. The lingual surface is largely obscured by the maxilla and matrix although a small section of an apicobasally orientated ridge is visible. However, the mesial facet of this ridge could be secondary to damage.

**Dentary dentition.** Most of the alveolar sockets in the right dentary are empty, although the remains of five shattered and incomplete crowns are still in place posteriorly. A loose left sided dentary tooth of commensurate size, with a partially preserved root, was found associated with the specimen. The tooth has the typical shield-shaped crown and tapering root seen in iguanodontian dentary teeth. The enamel is thicker on the lingual side, which is also ornamented. There are two ridges extending apicobasally from the occlusal surface to the root. The primary distal ridge is slightly broader than the secondary mesial ridge, but both are prominent. The primary ridge also has a very fine groove running

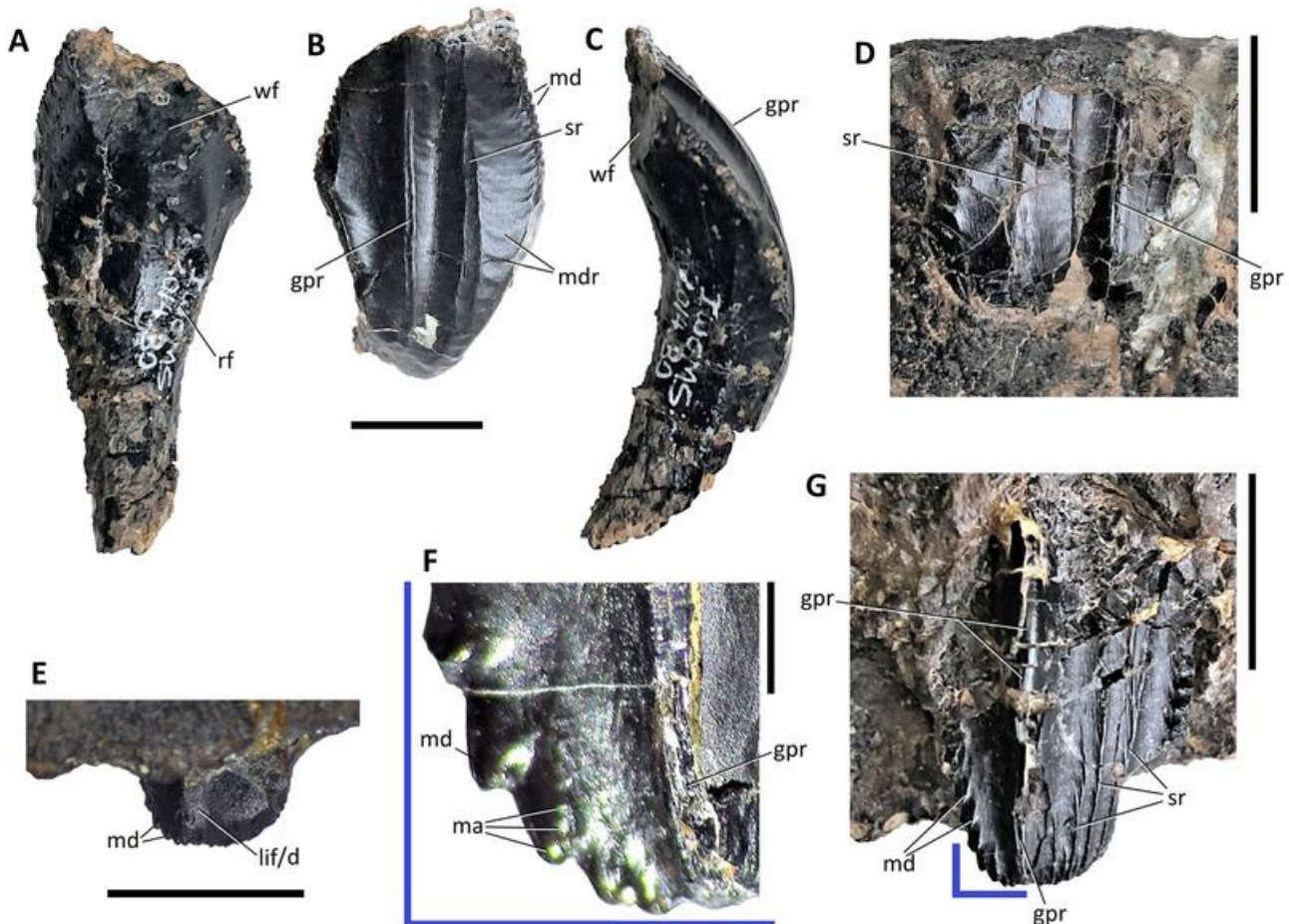


**Figure 13.** *Comptonatus chasei* gen. et sp. nov. (IWCMS 2014.80). Dentary and maxillary crowns. Isolated left dentary crown in **A**, labial, **B**, lingual and **C**, distal views; **D**, *in situ* right dentary crown in lingual view; *in situ* right maxillary crown in **E**, lingual, **F**, magnified section of apicodistal section and **G**, labial view. **Abbreviations:** **gpr**, grooved primary ridge; **lif/d**, lingual facet/damage; **ma**, mammillae; **md**, marginal denticle; **mdr**, mesiodistal ridges; **rf**, replacement facet; **sr**, secondary ridge; **wf**, wear facet. Scale bar represents 1 mm (F) and 10 mm (A–E, G).

along its whole length, which appears to be a feature of the primary ridge and not close alignment with a distal accessory ridge (Fig. 13, gpr). Between the ridges is a broad, moderately pronounced groove. Primary ridges which are grooved are not found in other iguanodontians, and as far as we are aware *Comptonatus chasei* is the only taxon with a grooved primary ridge recorded in the dentary and maxillary crowns. The mesial and distal margins are worn, but marginal denticles are visible in the apical half. The denticles possess two or three small mammillae arranged labiolingually. Basally the marginal denticles give way to facets, which extend onto the root and would have accommodated emergent replacement crowns on either side. The dentary crown is not ornamented labially, but the apex has an occlusal wear facet. The root extends basolabially. Two reasonably complete crowns on the dentary appear to have the same morphology and all lack tertiary ridges. The primary ridge surface in one is damaged but the other also shows a groove. The isolated tooth also shows mesiodistally orientated ridges, concave apically, extending from the distal margin to the secondary ridge. These appear to be loosely associated with the marginal denticles but vary, being hardly or not represented by some marginal denticles. There are much finer and more numerous mesiodistally orientated ridges, that are less concave, between the distal margin and the primary ridge and also between the primary and secondary ridges. These are not apparent in the poorly preserved in situ dentary crowns. The more pronounced ridges between the mesial margin and the secondary ridge are also seen in *Mantellisaurus atherfieldensis*, the holotype of *Owenodon hoggii* (Galton, 2009) and *Penelopognathus weishampeli* (Godefroit et al., 2005).

### Axial skeleton

Detailed photographs and measurements of all vertebrae can be found in the [Supplemental material \(S1, figs S23–66; S2, tables S7–10\)](#).

**Cervical vertebrae.** Eight opisthocoelous vertebrae with a convex anterior articular surface are preserved (Fig. 14). The surface texture is roughened, making interpretation difficult, but it appears that the neurocentral synchondroses are only partially visible. The atlas and axis were not preserved, giving a minimum vertebral count of 10, but at least one cervical appears to be missing from the series and two show transitional features (see below). In non-hadrosaurid iguanodontians, cervical vertebral number varies between nine and 12, e.g. *Tenontosaurus tilletti* 12 (Forster, 1990); *Camptosaurus dispar* 9 (Gilmore, 1909); *Uteodon aphanocetes* 9 (Carpenter & Wilson, 2008, *Camptosaurus aphanocetes* therein);

*Iguanodon bernissartensis* 11 (Norman, 1980); *Bayannurosaurus perfectus* 11 (Xu et al., 2018); *Ouranosaurus nigeriensis* 11 (Bertozzo, Della Vecchia, et al., 2017); *Mantellisaurus atherfieldensis* 11 (Norman, 1986); *Jinzhouosaurus yangi* 11 (Wang et al., 2010); *Bolong yixianensis* 11 (Wu & Godefroit, 2012); *Equijubus normani* 11 (McDonald et al., 2014) and *Gobihadros mongoliensis* 11 (Tsogtbaatar et al., 2019).

Common trends are observable in more complete articulated specimens of iguanodontians such as *Tenontosaurus tilletti* (Forster, 1990); *Camptosaurus dispar* (Carpenter & Wilson, 2008); *Iguanodon bernissartensis* (Norman, 1980) and *Mantellisaurus atherfieldensis*, enabling anterior and posterior cervical vertebrae to be distinguished. The posterior articular surface of the centrum in anterior cervical vertebrae is slightly dorsoventrally compressed but it expands and becomes deeper in more posterior vertebrae, developing more of a heart shape as it approaches the dorsal series, e.g. *Iguanodon bernissartensis* (Norman, 1980), *Ouranosaurus nigeriensis* (Bertozzo, Della Vecchia, et al., 2017), *Mantellisaurus atherfieldensis*. The anterior centra, especially Cv3–5, are shorter ventrally than dorsally due to the ventrally concave arc of the neck anteriorly, the condition being reversed posteriorly, e.g. as in *Mantellisaurus atherfieldensis*, suggesting a sigmoidal-shaped neck as proposed by Norman (1986). The parapophyses become larger and closer to the neurocentral synchondrosis posteriorly, e.g. *Mantellisaurus atherfieldensis*. In *Ouranosaurus nigeriensis* the parapophysis is on a relatively long pedestal anteriorly (Cv3) but becomes nearly flush with the lateral wall of the centrum posteriorly (Bertozzo, Della Vecchia, et al., 2017). Anteriorly the parapophysis is set at the anterior end of a lateral ridge (that extends along the dorsoventral midpoint of the centrum), but migrates dorsally in posterior cervical vertebrae, e.g. *Bactrosaurus johnsoni* (Godefroit et al., 1998). Anteriorly the neural spine is a short ridge at the median junction of the postzygapophyses but becomes increasingly developed posteriorly into a prominent hook-shaped structure, e.g. *Mantellisaurus atherfieldensis*. The neural spine is virtually absent in the anterior cervical vertebrae of *Iguanodon bernissartensis*, being represented by paired thin ridges (Norman, 1980) that approach each other anteriorly. In some early diverging iguanodontians a small but more obvious neural spine is present in the anterior cervical vertebrae, e.g. *Tenontosaurus tilletti* (Forster, 1990), *Zalmoxes robustus* (Weishampel et al., 2003). A range of other characters change progressively posteriorly: the vertebrae become bigger, the transverse processes become longer and stouter, the diapophyses become larger and the prezygapophyses move further away from the neural

arch. Based on these trends the eight vertebrae were placed in presumed order and labelled A–H. The morphologies suggested that vertebrae A–C are from the anterior end of the cervical series, with D–F positioned more posteriorly. Vertebrae G and H are harder to place and appear to have some transitional features between cervical and dorsal vertebrae. The eight vertebrae do not appear to form an articulated series and several elements are probably missing.

Viewed laterally, the anterior vertebrae (A–C) have elongate centra with a ratio of length (excluding the convex anterior articular surface) to anterior height of 1.3–1.5. This contrasts with the more equidimensional posterior vertebrae, where the ratio was 0.9–1.0. This differs from *Mantellisaurus atherfieldensis*, *Iguanodon bernissartensis* (Norman, 1980) and *Ouranosaurus nigeriensis* (Bertozzo, Della Vecchia, et al., 2017), where all cervical centra are essentially square in lateral view. Centra that are anteroposteriorly longer than they are dorsoventrally tall are found throughout the series in *Camptosaurus dispar* (Carpenter & Wilson, 2008), while in *Tenontosaurus tilletti* (Forster, 1990) they are restricted to the most anterior vertebrae, as in *Comptonatus chasei*.

**Anterior cervical vertebrae.** Vertebra A is considered the most anterior of the preserved vertebrae, probably Cv3 based on the small dimensions of the articular surfaces, a parapophysis situated well below the neurocentral synchondrosis, prezygapophyses adjacent to the neurapophysis, a diminutive transverse process and diapophysis, and postzygapophyses separated for most of their length. The centrum is cylindrical in shape with a subcircular concave posterior articular surface and a convex anterior articular surface bearing a faint central notochordal pit. Opisthocoely in cervical vertebrae, with a pronounced hemispherical anterior articular surface, is also seen in other iguanodontians, for example *Iguanodon bernissartensis* (Norman, 1980), *Mantellisaurus atherfieldensis*, *Ouranosaurus nigeriensis* (Bertozzo, Della Vecchia, et al., 2017), *Equijubus normani* (McDonald et al., 2014), *Jeyawati rugoculus* (McDonald, Wolfe, et al., 2010), *Eolambia caroljonesa* (McDonald, Bird, et al., 2012) and *Gobihadros mongoliensis* (Tsogtbaatar et al., 2019), although the characteristic is usually more weakly represented in earlier diverging members of the clade such as *Zalmoxes robustus* (Weishampel et al., 2003), *Cumnoria prestwichii* (Maidment et al., 2022), *Uteodon aphanocetes* (Carpenter & Wilson, 2008), *Tenontosaurus tilletti* (Forster 1990) and *Camptosaurus dispar* (Gilmore, 1909). A notochordal pit is also recorded in the cervical vertebrae of *Iguanodon bernissartensis* (Norman, 1980), and *Mantellisaurus atherfieldensis*, but generally not reported in other iguanodontians. The anterior articular

surface has an everted margin that is more prominent dorsally. In lateral view the convexity is asymmetrical, being more marked dorsally where it protrudes further anteriorly, giving it a tilted upward orientation. This is also seen to varying degrees in the other cervical vertebrae and is a feature in other iguanodontians, for example *Iguanodon bernissartensis* (Norman, 1980), *Mantellisaurus atherfieldensis* and *Ouranosaurus nigeriensis* (Bertozzo, Della Vecchia, et al., 2017).

A robust ventral keel extends the length of the centrum, being a pronounced ridge anteriorly, while posteriorly it expands transversely, before becoming confluent with the posterior articular margin. Robust and broad longitudinal ventral keels are typical of iguanodontian postaxial cervical vertebrae and can be found for example in *Tenontosaurus tilletti* (Forster, 1990), *Camptosaurus dispar* (Gilmore, 1909), *Cumnoria prestwichii* (Maidment et al., 2022), *Iguanodon bernissartensis* (Norman, 1980), *Mantellisaurus atherfieldensis* (Bonsor et al., 2023), *Jinzhouosaurus yangi* (Wang et al., 2010), *Gobihadros mongoliensis* (Tsogtbaatar et al., 2019) and *Probactrosaurus gobiensis* (Norman, 2002). In the few examples that are figured or described in detail they also exhibit a posterior transverse expansion, e.g. *Camptosaurus dispar* (Gilmore, 1909), *Cumnoria prestwichii* (Maidment et al., 2022) and *Mantellisaurus atherfieldensis* (Bonsor et al., 2023). In lateral view the keel is slightly concave. The ventral aspect of the lateral wall on either side of the keel is depressed to form a shallow fossa. The fossa is bounded dorsally by a longitudinal ridge extending across the midline of the lateral wall, which anteriorly supports an oval (long axis anteroposterior) parapophysis which is slightly raised on a low pedestal. The parapophysis on vertebra A is notably smaller than the subsequent cervical vertebrae, suggesting possession of a much smaller cervical rib. Dorsally the lateral wall of the centrum curves convexly to meet the neurapophysis. The neural arch encloses a large neural canal and supports two sets of processes, the transverse and the postzygapophyseal processes. The right transverse process in vertebra A is completely preserved and is a weak structure extending laterally and slightly ventrally to support a small oval (long axis anteroposterior) diapophysis. Medially, the transverse process supports a large prezygapophysis adjacent to the neurapophysis, so that the bases of the transverse process and prezygapophysis are confluent. The facet of the prezygapophysis faces dorsomedially and is oval (long axis anteroposterior). Only the left postzygapophysis in vertebra A is complete but it is elongate and originates from the dorsoposterior aspect of the neural arch. The postzygapophysis considerably overhangs the posterior articular surface and diverges from its antimere at the

level of the posterior articular surface. It is slightly curved such that it is convex dorsally and medially. The oval facet is located distally and faces ventrolaterally. The neural spine is represented by a short thin ridge at the junction of the postzygapophyseal processes on the anterior arch. This divides posteriorly into two thin crests (spinopostzygapophyseal laminae), which extend along the mediodorsal surface of the postzygapophyseal process to the level of the facet.

Vertebrae B and C share several features with vertebra A. The centra are elongate, and vertebra B has a concave ventral margin in lateral view. Both have similar ventral keels and more obvious notochordal pits on their anterior articular surfaces. The parapophyses are larger than those of vertebra A, raised on short pedestals and situated anteriorly at the end of a midline lateral ridge. The transverse processes of vertebra B are much more robust than those of A, with larger diapophyses and prezygapophyseal facets located a short distance from the neurapophysis. Vertebra C has similarly placed prezygapophyses, but the transverse processes are damaged. In both vertebrae B and C, the postzygapophyses are incomplete but diverge at the level of the posterior articular surface of the centrum. The neural spines are present as tiny transversely compressed protuberances situated anterior to the junction of the postzygapophyseal processes. Posteriorly spinopostzygapophyseal laminae extend along the mediodorsal surface of the incomplete processes as far as they are preserved.

**Posterior cervical vertebrae.** Vertebrae D–F are more robust and bigger than vertebrae A–C and represent more posterior vertebrae. The three vertebrae are similar to each other, and it is difficult to place them in sequence. Vertebra D has lost the neural arch and postzygapophyses. The left transverse process is preserved and is more robust and supports a larger diapophysis than the anterior three vertebrae. The parapophysis is large and situated anteriorly but there is no pronounced lateral ridge. The ventral keel is similar to the earlier vertebrae and a notochordal pit is present. The centrum in lateral view is less elongate and more of an equidimensional shape than in vertebrae A–C.

Vertebrae E and F are like vertebra D in most respects, with vertebra E being almost complete. The postzygapophyses diverge just anterior to the margin of the posterior articular surface, creating a small shelf above the neural canal in vertebra E. Their neural spines are missing but the fractured bases show them to be small transversely compressed structures, although bigger than those found in vertebrae A–C.

**Transitional opisthocoelous vertebrae.** Vertebrae G and H exhibit a convex anterior articular surface,

albeit less pronounced than in preceding vertebrae. Most of the neural spine is missing in both specimens, but in vertebra G the fractured base shows a transversely compressed structure of considerably increased anteroposterior length compared to vertebra F. The parapophysis is situated dorsally on the centrum, and although the neurocentral synchondrosis is not visible, the parapophysis appears to extend onto the neurapophysis, although probably not entirely above the synchondrosis. Vertebra G has an even longer anteroposterior fractured base of the neural spine, which is separated from the posterior articular margin by a short posterior shelf. The anteroventral part of the neurapophyses and the parapophyses are not preserved. The posterior articular surface is less concave and more heart-shaped than in preceding vertebrae. There is a shallow fossa between the bases of the postzygapophyses, just dorsal to the neural canal.

The morphology of vertebrae G and H suggests they may be transitional elements, and vertebra H may have been the first dorsal, although it has not been modified sufficiently to articulate with the most anterior definite dorsal vertebra. This implies that there must have been at least one proximal dorsal that is not preserved and *Comptonatus chasei* possessed at least 16 or more dorsal vertebrae dependant on the status of vertebra H. Seventeen is a recurring number for the dorsal vertebra count in non-hadrosaurid iguanodontians, for example *Camptosaurus dispar* (Gilmore, 1909), *Bayannurosaurus perfectus* (Xu et al., 2018), *Iguanodon bernissartensis* (Norman, 1980), *Mantellisaurus atherfieldensis*, *Ouranosaurus nigeriensis* (Bertozzo, Della Vecchia, et al., 2017) and *Gobihadros mongoliensis* (Tsogtbaatar et al., 2019), or 16 in earlier diverging taxa such as *Tenontosaurus tilletti* (Forster, 1990) and *Uteodon aphanocetes* (Carpenter & Wilson, 2008).

**Comment on differentiating cervical and dorsal vertebrae.** The first dorsal vertebra has been defined as the first presacral vertebra to have the parapophysis positioned dorsal to the neurocentral synchondrosis (Forster, 1990; Norman, 1980, 1986). However, the position of the parapophysis relative to the neurocentral synchondrosis is often difficult to establish and even if visible may be a somewhat arbitrary discriminator between cervical and dorsal vertebrae in the presacral series. This may account for *Tenontosaurus tilletti* having the same number of presacral vertebrae as *Iguanodon bernissartensis* but one extra cervical and one less dorsal vertebra, and the different numbers allocated to the same specimen by different authors, e.g. *Cumnoria prestwichii* (Maidment et al., 2022) and the *Mantellisaurus atherfieldensis* holotype (Bonsor et al., 2023).

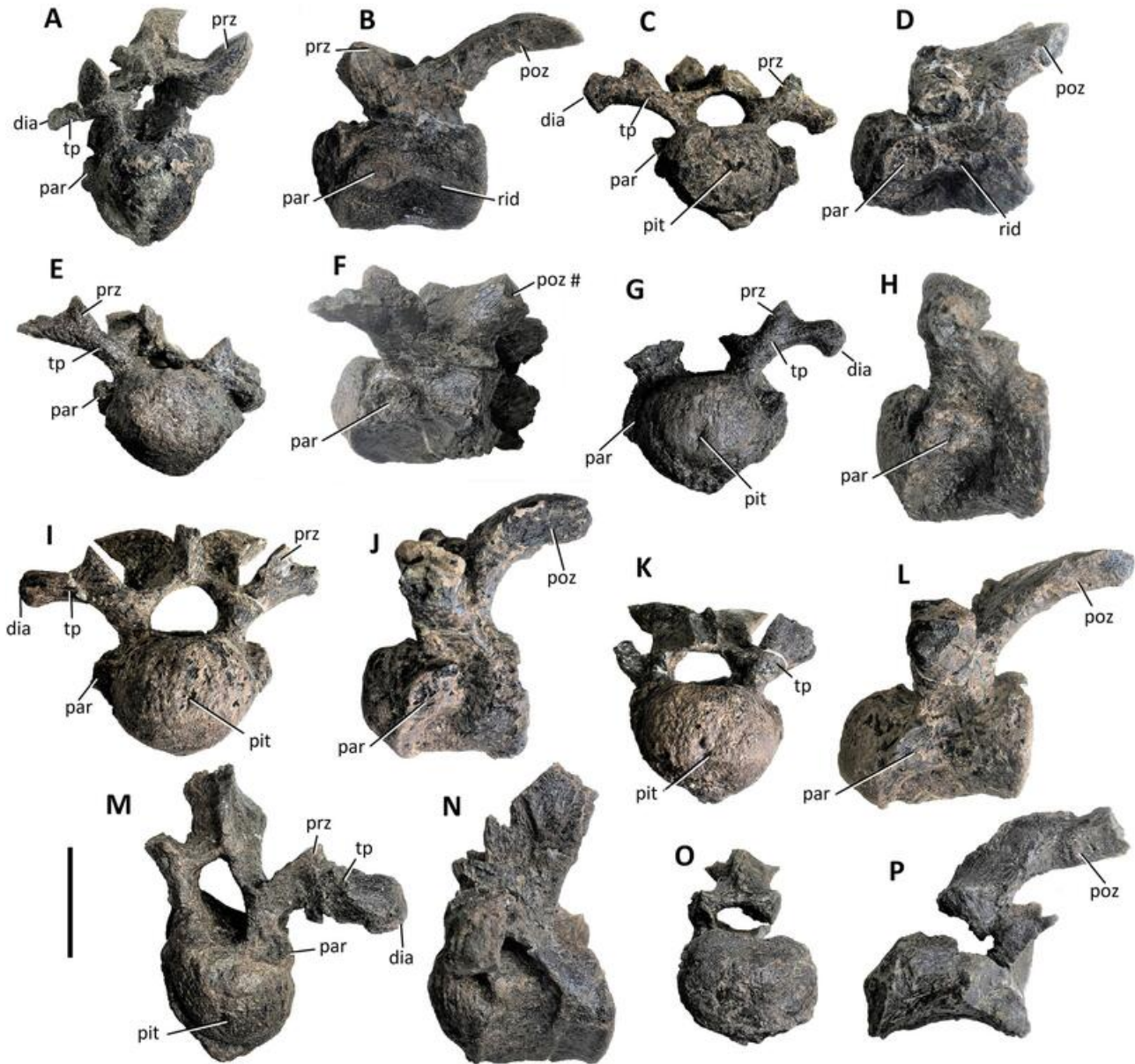


**Figure 14.** *Comptonatus chasei* gen. et sp. nov. (IWCMS 2014.80). Opisthocoelous presacral vertebrae. Vertebra A: **A**, anterior and **B**, left lateral; vertebra B: **C** anterior, **D**, left lateral; vertebra C: **E**, anterior, and **F**, left lateral; vertebra D: **G**, anterior, **H**, left lateral; vertebra E: **I**, anterior, **J**, left lateral; vertebra F: **K**, anterior and **L**, left lateral; vertebra G: **M**, anterior and **N**, left lateral; vertebra H: **O**, anterior and **P**, left lateral views. **Abbreviations:** **dia**, diaphysis; **par**, parapophysis; **pit**, notochordal pit; **rid**, lateral ridge; **poz**, postzygapophysis; **prz**, prezygapophysis; **tp**, transverse process; #, fracture. Scale bar represents 50 mm.

**Cervical rib.** A fragment of a dichocoelalic cervical rib is preserved (Fig. 15). The distal shaft and the tuberculum are both missing. There is only a very weakly developed ridge or spine (*sensu* Norman, 1980; Fig. 15B, spi) on the shaft, indicating that this was probably very early in the series.

**Dorsal vertebrae.** The vertebrae of *Comptonatus chasei* have all been subjected to varying degrees of transverse

compression and some longitudinal shearing forces. Some centra show evidence of crushing, especially ventrally between the articular surfaces. This may have exaggerated the heights and reduced the widths of some of the centra. Some of the vertebrae are attached to each other, as a result of post-depositional processes. Including the sacrodorsal the 15 definite dorsal vertebrae appear to form an articulated series. In most of these a neurocentral synchondrosis is visible. The most anterior

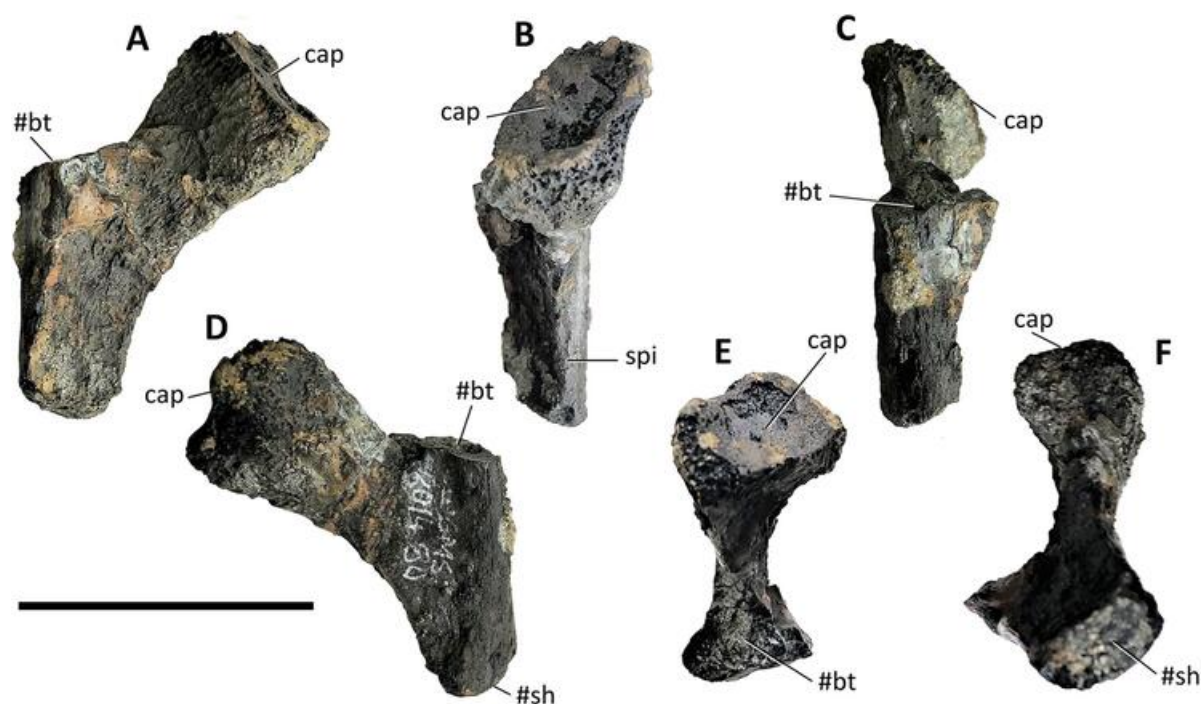


**Figure 15.** *Comptonatus chasei* gen. et sp. nov. (IWCMS 2014.80). Left cervical rib fragment in **A**, posterior, **B**, medial, **C**, lateral, **D**, anterior, **E**, dorsal and **F**, ventral views. **Abbreviations:** **cap**, capitulum; **#bt**, fractured base of tuberculum; **#sh**, fractured distal shaft; **spi**, spine. Scale bar represents 30 mm.

in the articulated series has a curved, short neural spine and represents a very proximal vertebra approximately in the D3 position. For the purposes of identification, preserved vertebrae will be referred to in their most likely life position of D3–17.

The dorsal vertebrae show many character changes between the anterior and the posterior series. The height of the centra increases posteriorly both in real terms and as a ratio of height to length. In *Comptonatus chasei* the centra of the early dorsal vertebrae (D3–D9) are longer anteroposteriorly than tall dorsoventrally, but D10–D16 are taller than long, the height to length ratio rapidly increasing in the most posterior vertebrae. In *Mantellisaurus atherfieldensis*, D7–D9 are longer than tall but the rest are taller than long, although the ratio is greatest in the most posterior dorsal vertebrae. In *Iguanodon bernissartensis* every dorsal vertebra is taller than long in the lectotype RBINS R51 and in RBINS R342 (Norman, 1980), although the ratio is greatest in the more posterior vertebrae. In ‘*Dollodon bampingi*’ the vertebrae are generally longer than tall except for the most posterior vertebra (Norman, 1986). Moving posteriorly along the dorsal vertebral column, the size of the parapophyses increases to a maximum in D4, and thereafter begins to gradually diminish in size. The position of the parapophysis also migrates up the neuropophysis and then along the transverse process. Its

likely position is obscured in D15 by a bone fragment, and it cannot be identified in D16. The transverse processes of the anterior dorsal vertebrae extend dorsolaterally in anterior view and posterolaterally in dorsal view. There is a gradual change towards the more posterior vertebrae where the transverse processes extend laterally in anterior and dorsal views. When viewed ventrally, all dorsal vertebrae in the series D3–16 are spool-shaped and possess a ventral keel, although the latter may be exaggerated by transverse compression. The majority of dorsal vertebrae also possess a ventral keel in *Iguanodon bernissartensis* (Norman, 1980), *Mantellisaurus atherfieldensis*, *Brighstoneus simmondsi* (MIWG 6344) and *Ouranosaurus nigeriensis* (Bertozzo, Della Vecchia, et al., 2017). The margins of the articular surfaces are everted, this being usually more pronounced in the posterior margin and becomes markedly more pronounced in D15 and D16. D17 the sacrodorsal is described with the sacrum.

**Osteological descriptions of selected dorsal vertebrae.** Dorsal vertebra 3 (Fig. 17A, B) is reasonably well preserved, although the anterior centrum has been transversely compressed, the right transverse process displaced anteriorly, and the distal end of the neural spine is missing. A section of the neural spine has been incorrectly placed. The anterior articular surface of the centrum has an oval outline (long axis dorsoventral,

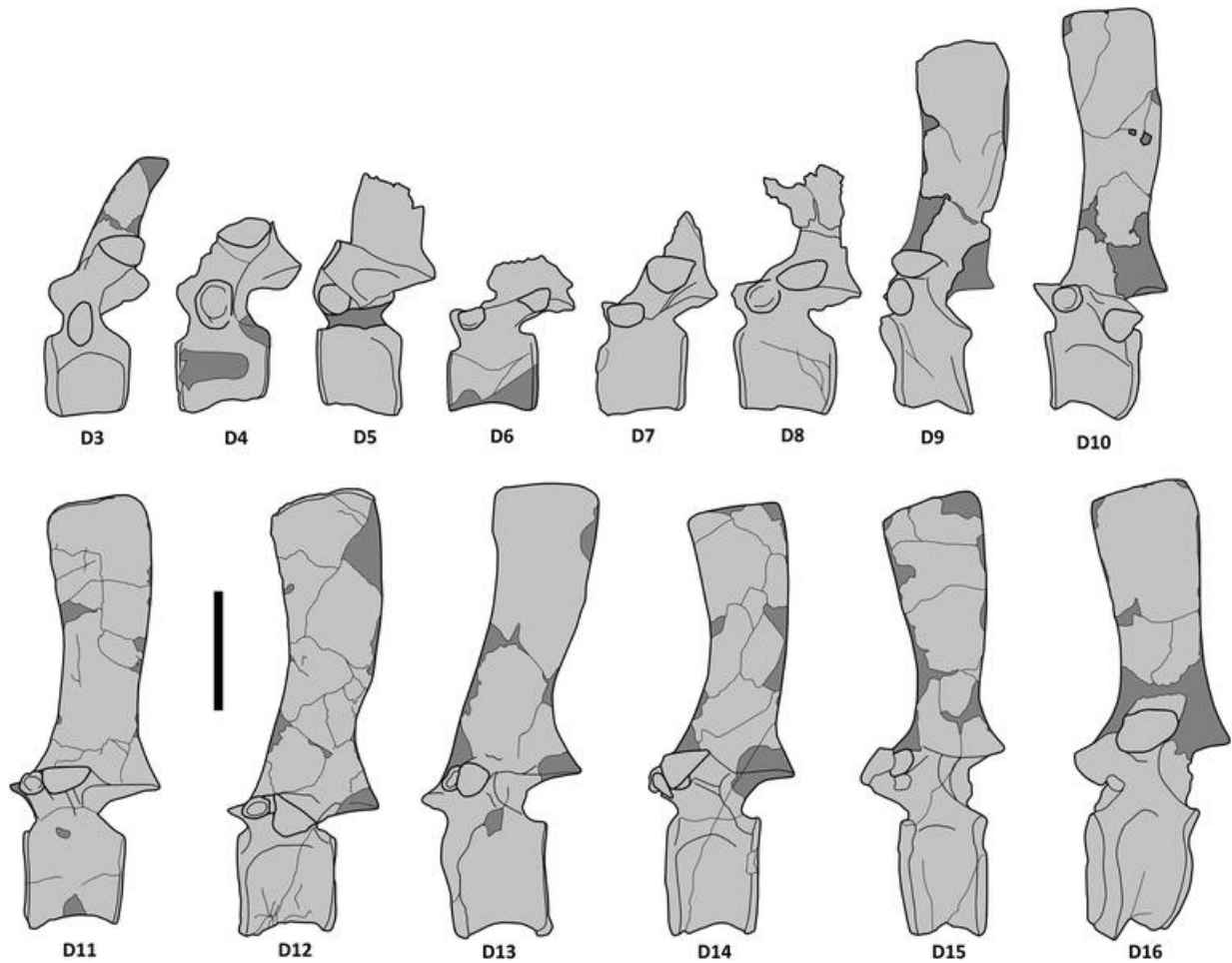


**Figure 16.** *Comptonatus chasei* gen. et sp. nov. (IWCMS 2014.80). Reconstructions of dorsal vertebrae in left lateral view. Light grey actual bone, dark grey unpreserved or obscured. Scale bar represents 100 mm.

although this has probably been accentuated by taphonomic transverse compression), with a flat surface and a slightly everted margin. The posterior articular surface is heart-shaped, gently concave, and also has a slightly everted margin. The lateral walls are almost flat dorsoventrally and concave anteroposteriorly giving it a spool-shape in ventral view. Ventrally there is a keel that has been distorted into a sigmoid shape. The neural arch bounds a large subcircular neural canal and has been fractured through what appears to be the neurocentral synchondrosis. The parapophysis lies 7 mm above the visible neurocentral synchondrosis and is large and ovoid with the long axis orientated dorsoventrally. The transverse processes extend dorsolaterally and a little posteriorly. They are slightly expanded distally in dorsal view and have a triangular cross-section with the apex directed ventrally. The ventral angle extends onto the centrum as a rounded ridge, the posterior centrodiapophyseal lamina, while the posterior margin extends towards the postzygapophyses as a more delicate ridge,

the postzygodiapophyseal lamina. These two laminae create a posterior recess between them. The prezygapophyses have facets which face steeply dorsomedially. These match the angles of the ventrolaterally facing facets of the postzygapophyses and are similarly orientated to the facets in D4 and D5. This contrasts with more posterior vertebrae where the prezygapophyseal facets, although still facing dorsomedially, are orientated more horizontally. Although the neural spine is incomplete dorsally, when correctly reconstructed (Figs 16, 17) it suggests a thin, short, and tapering spine that is convex anteriorly and forms a hook-like structure. This is very typical of transitional and early dorsal vertebrae and is seen in *Mantellisaurus atherfieldensis*; *Brighstoneus simmondsi* (Lockwood *et al.*, 2021); *Ouranosaurus nigeriensis* (Taquet, 1976) and *Iguanodon bernissartensis* (Norman, 1980).

Dorsal vertebra 4 is part of a block, mixed with fragments of a transverse process and the neural arch of D5. The right transverse process is missing. The anterior

articular surface is flat with a slightly transversely compressed heart-shape and slightly everted margin. The posterior articular surface has a similar outline and is gently concave, but with a more pronounced everted margin. Dorsal vertebra 3 and D4 are similarly platycocelian, but thereafter the middle series dorsal vertebrae are essentially amphiplatyan, although most surfaces are very slightly concave. The lateral walls of the centrum, presence of a keel, laminae and angles of the postzygapophyseal facets of D4 are similar to D3. The left transverse process is angled dorsolaterally and posteriorly.

The parapophysis is the largest of the dorsal series and is sited on the neuropophysis. The postzygapophyses are obscured.

Dorsal vertebra 11 has a well-preserved and complete neural spine. The right transverse process is missing. The centrum is taller than long, but only just. As with most of the dorsal vertebrae the centrum appears to have undergone some transverse compression. The neural spine in lateral view is widest dorsally and gently concave along its anterior margin. It is also slightly transversely expanded dorsally (thickness at midpoint of

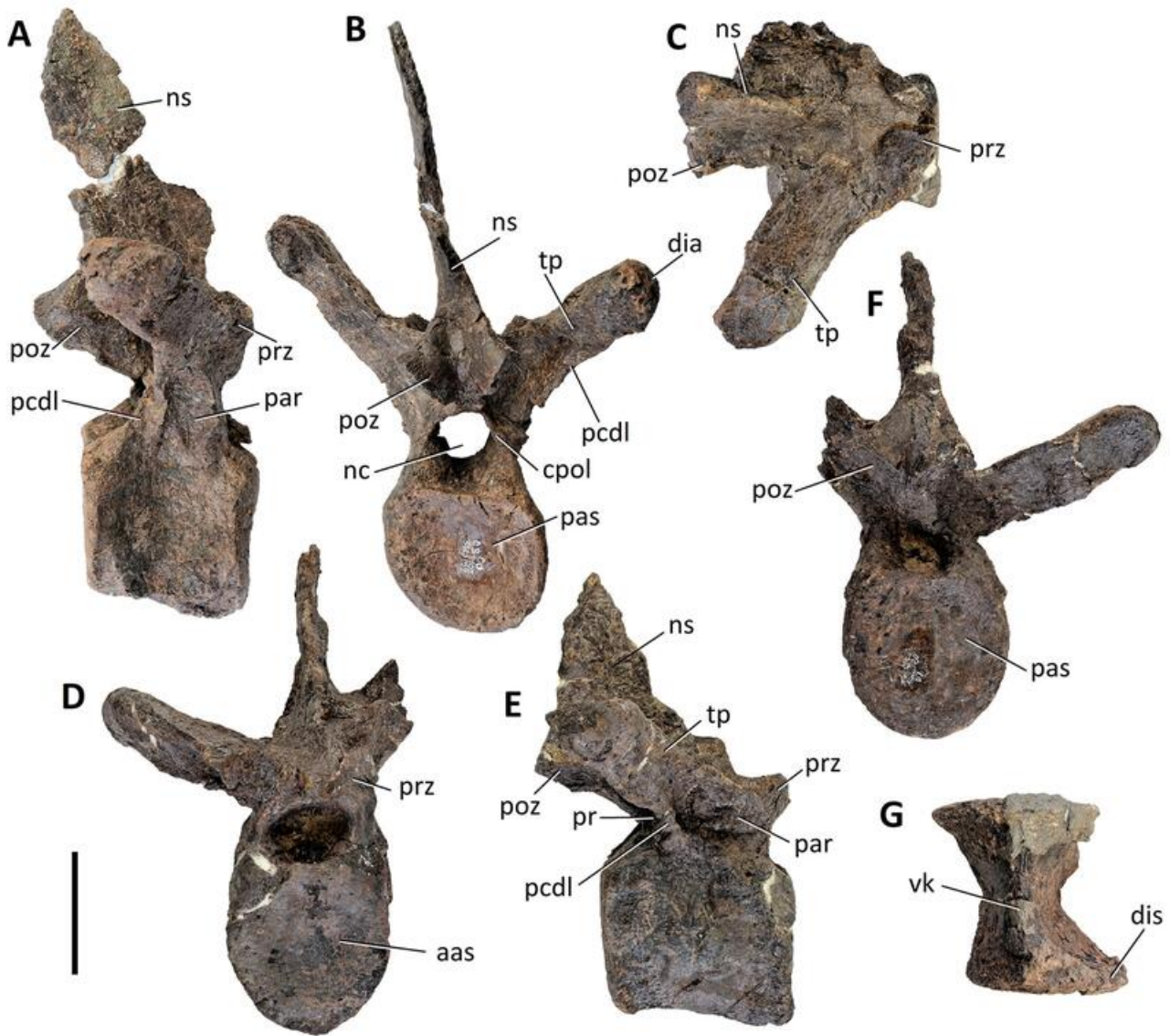


**Figure 17.** *Comptonatus chasei* gen. et sp. nov. (IWCMS 2014.80). Anterior series dorsal vertebrae. **D3** in **A**, right lateral, **B**, posterior. **D7** in **C**, dorsal, **D**, anterior, **E**, right lateral, **F**, posterior. **D6** in **G**, ventral views. **Abbreviations:** **aas**, anterior articular surface; **cpol**, centropostzygapophyseal lamina; **dia**, diapophysis; **dis**, taphonomic distortion; **nc**, neural canal; **ns**, neural spine; **par**, parapophysis; **pas**, posterior articular surface; **pcdl**, posterior centrodiapophyseal lamina; **poz**, postzygapophysis; **prz**, prezygapophysis; **tp**, transverse process; **vk**, ventral keel. Scale bar represents 50 mm.

dorsoventral height = 10 mm, and at dorsal margin = 16 mm). The anterior and posterior margins are thinner than the main body of the neural spine, although the anterior margin does not appear broader than the posterior margin. The left transverse process is well preserved. It projects horizontally and laterally at right angles to the sagittal plane. The cross-section is triangular with a flat dorsal surface, a slightly convex anterior surface and a convex ventroposterior facing surface. Distally the diapophysis is a convex articular surface. As with the more anterior vertebrae, a thick ridge extends from the ventral surface of the transverse process to the centrum (posterior centrodiaepophyseal lamina) and a thin lamina from the posterior margin to the anterior margin of the postzygapophyses (postzygodiaepophyseal lamina), which with the centropostzygapophyseal lamina, form a triangular recess, although less deep than in the more anterior vertebrae. The parapophysis has migrated onto

the anterior surface of the transverse process. The articular surfaces of the centrum have a transversely compressed oval outline, although this has almost certainly been exaggerated by post-depositional deformation. This also makes it difficult to interpret the ventral surface, although a keel is present, albeit less marked than in the other dorsal vertebrae. The anterior articular surface only preserves its left half. It has a slightly everted margin and is shallowly concave. The posterior articular surface has a slightly more pronounced everted margin and is shallowly opisthocelous. The prezygapophyses have not preserved. The postzygapophyses are large and overhang the posterior articular surface.

The more distal dorsal vertebrae are of similar morphology, although more robust. The centrum of D16 is particularly short anteroposteriorly and dorsoventrally tall and has markedly everted margins to both articular surfaces, as does the posterior margin in D15.



**Figure 18.** *Comptonatus chasei* gen. et sp. nov. (IWCMS 2014.80). Dorsal vertebrae D11–16 in left lateral view, with neural spines placed in approximate position. Scale bar represents 100 mm.

**Dorsal ribs and ossified tendons.** There are numerous small fragments of the rib shafts which are not particularly instructive and two articular end sections attached to blocks containing shaft fragments and dorsal vertebrae. The better-preserved articular end (Fig. 19B) has a rounded capitular surface and a tuberculum with a slightly everted margin. The size of the capitulum and the angle suggest a left rib that articulated with one of the middle series dorsal vertebrae. It is an otherwise typical iguanodontian rib head such as seen in *Iguanodon bernissartensis* (Norman, 1980) and *Mantellisaurus atherfieldensis* (Bonsor et al., 2023).

A block of pyritized matrix containing ossified tendons in transverse section was recovered with the dorsal vertebrae. It appears to show the tendons in two or possibly three layers, suggesting a lattice arrangement.

**Sacrum.** A block contains a sacrodorsal vertebra, five sacral vertebrae, and the left ilium (Figs 20, 21). However, the posterior articular surface of the centrum of S5 is a fracture surface and there is a fragment of the left transverse process/sacral rib complex attached to the medial surface of the postacetabular process of the ilium, indicating the presence of a sixth sacral vertebra. An unarticulated vertebra with no haemal facets, but otherwise having a typical early caudal morphology and lacking the distinctive robust and heavily striated posterior margin characteristic of the most posterior sacral is interpreted as a caudosacral. This unarticulated vertebra is discussed below as the first caudal vertebra. A sacrocaudal vertebra is common in hadrosaurids (Horner et al.,

2004) and is recorded in several non-hadrosaurid earlier diverging iguanodontians, including *Dysalotosaurus lettowvorbecki* (Janensch, 1955), *Valdosaurus canaliculatus* (Barrett, 2016), *Camptosaurus dispar* (Gilmore, 1909: *C. browni* therein), *Barilium dawsoni* (Norman, 2011b) and *Iguanodon bernissartensis* (Norman, 1980).

The single sacrodorsal vertebra has undergone some taphonomic transverse compression. The anterior articular surface is flat, oval, being taller dorsoventrally than wide transversely and has, as with D16, a strongly everted and rugose margin. The dorsoventral height is greater than the anteroposterior length, and the sides of the centrum are concave anteroposteriorly, generally expanding to produce a wider and taller posterior articular surface that is fused to the first true sacral vertebra. The ventral surface is quite strongly concave in lateral view and has a keel on its anterior half. The prezygapophyses are typical of the distal dorsal vertebrae, with flat, slightly dorsomedial facing articular facets, which are partially obscured, as a fractured fragment of the postzygapophyses of D16 has become attached by post-depositional processes. The neural spine is not preserved.

Apart from in ventral and ventrolateral views, most of the sacral vertebrae are obscured by a crushed, fused mass of the sacral ribs, sacricostal yoke, matrix, and the left ilium. The anterior articular surface of S1 is expanded and fused with the posterior articular surface of the SD. This forms the widest point of the preserved sacral rod. Sacral vertebra 2, S3 and S4 are spool-shaped and S5 is the most robust.

Two neural spine fragments and four almost complete neural spines are preserved (Fig. 21). The bases of the neural spines are attached to the neural arches, but this region of the vertebrae extending between SD and S5 is heavily fused and has been considerably deformed. A recent fracture has also occurred through this region and separated a bar of fused bone to which two neural spines are still attached. Two other neural spines are preserved separately, but the fracture lines are incomplete, and they cannot be placed accurately. The neural spines are dorsoventrally elongate, transversely compressed and anteroposteriorly expanded distally. If the curved deformation of the ventral section is corrected for, the neural spines are c. 290 mm tall (i.e. taller than the neural spines of the posterior dorsal vertebrae). They are slightly concave anteriorly and convex posteriorly so that they curve anterodorsally in lateral view. In the transverse plane the spines are thickest centrally and become thinner towards the anterior and posterior margins. The anterior margin is slightly thinner than the posterior, although this is somewhat variable due to crushing. The two neural spines attached to the bar of

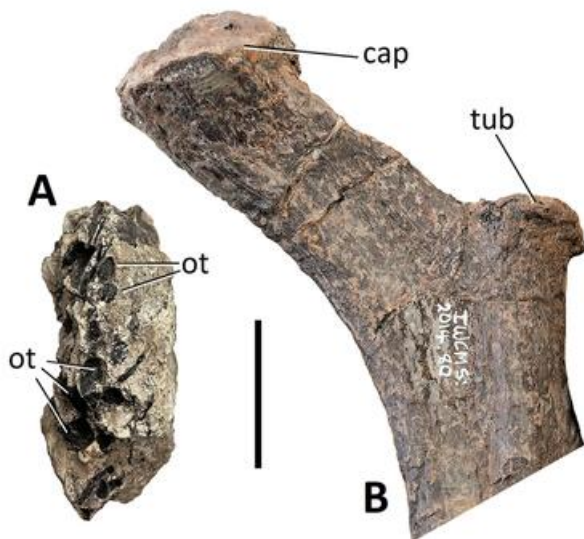


**Figure 19.** *Comptonatus chasei* gen. et sp. nov. (IWCMS 2014.80). **A**, block of pyritized matrix containing ossified tendons in transverse section. **B**, articular end of left dorsal rib in anterior view. **Abbreviation:** **cap**, capitulum; **ot**, ossified tendons; **tub**, tuberculum. Scale bar represents 30 mm.

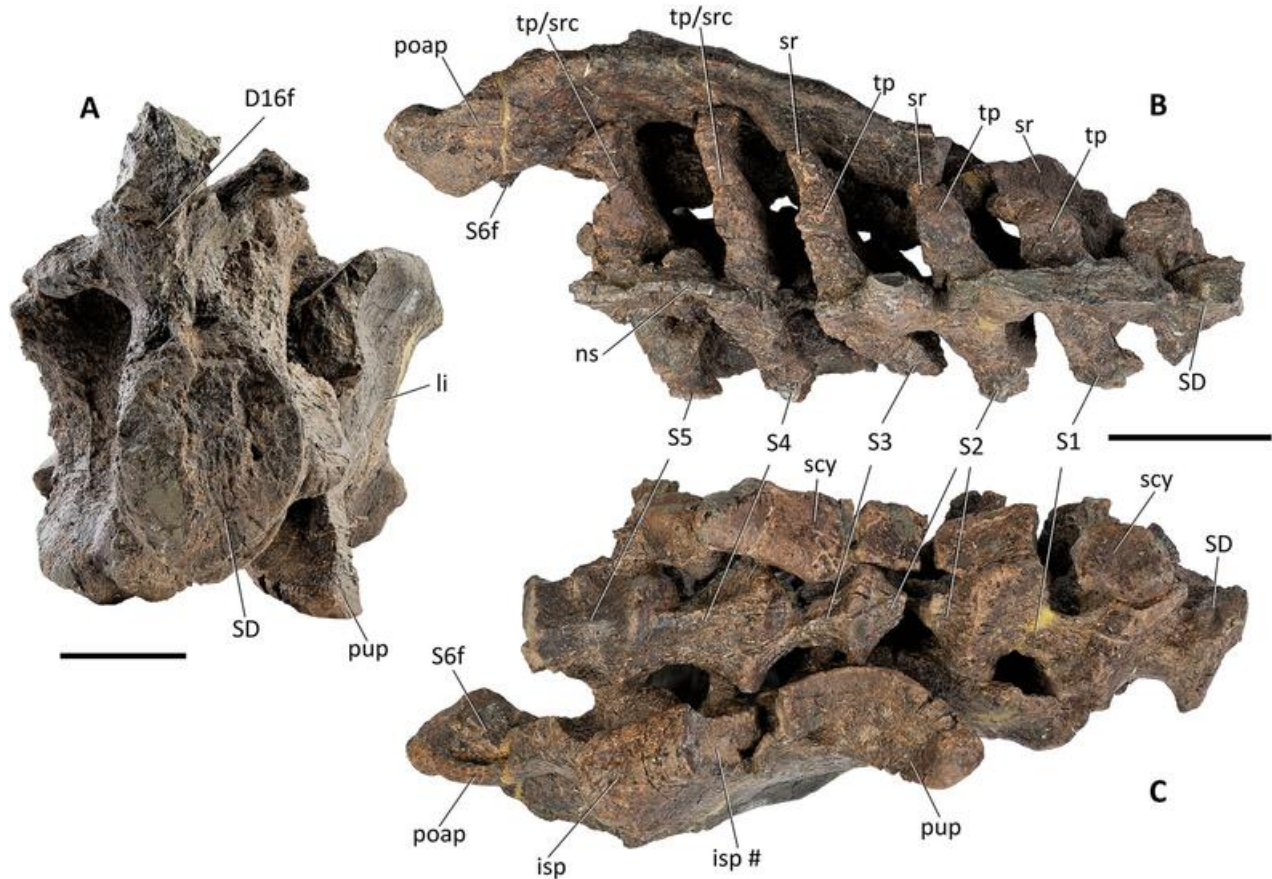


**Figure 20.** *Comptonatus chasei* gen. et sp. nov. (IWCMS 2014.80). Sacrum and left ilium in **A**, anterior, **B**, dorsal and **C**, ventral views. **Abbreviations:** **D16f**, fragment of dorsal vertebra 16; **isp**, ischiadic peduncle; **li**, left ilium; **ns**, neural spine; **poap**, postacetabular process; **pup**, pubic peduncle; **S**, true sacral vertebra; **S6f**, fragment of sacral vertebra 6; **scy**, sacriocostal yoke; **SD**, sacrodorsal vertebra; **sr**, sacral rib; **tp**, transverse process; **tp/src**, transverse process/sacral rib complex; **#**, fracture surface. Scale bar represents 50 mm in **A**, and 100 mm in **B** and **C**.

fused bone contact each other ventrally, although there is no evidence that they articulated in the same way as in *Brighstoneus simmondsi* (Lockwood *et al.*, 2021), where there is a groove in the anterior margin to lock with the posterior margin of the adjacent neural spine. A sketch made during the excavation shows five sacral neural spines forming a continuous plate as in *Bactrosaurus johnsoni* (Godefroit *et al.*, 1998). Metric values for sacral vertebrae are approximate due to fusion and distortion.

The centra of the true sacral vertebrae are distorted and damaged, making it difficult to interpret the morphology of the ventral surfaces accurately. Sacral vertebra 1 is too distorted and S2 too incomplete to describe the ventral surface. Sacral vertebra 3 possibly has a keel, S4 has a sulcus, while S5 is distorted but was probably flat.

The sacrum has been subjected to taphonomic transverse compression and a shearing force such that in dorsal view the transverse processes and sacral ribs extend

posterolaterally on the left and anterolaterally on the right. The transverse processes are fused to the underlying sacral ribs to form a complex. In S1 and S2 the transverse processes, although fused to their respective sacral ribs, remain distinct throughout their length. In S3 the transverse process is still reasonably distinct, but it is unclear how much it contributed to the articulation with the ilium. In S4 it is difficult to differentiate the transverse process and sacral rib and the two elements indistinguishably form a single complex in S5. The articulation sites for S2–5, on the medial surface of the left ilium, are visible and although the main body of S6 is missing, the distal section of its left transverse process/sacral rib complex is still articulated with the postacetabular process of the ilium. The left ilium is incomplete anteriorly, but the anterior section of the right ilium is preserved and has a facet for the transverse process of S1, confirming its status as a primordial sacral vertebra. The sacral ribs, which are fused dorsally

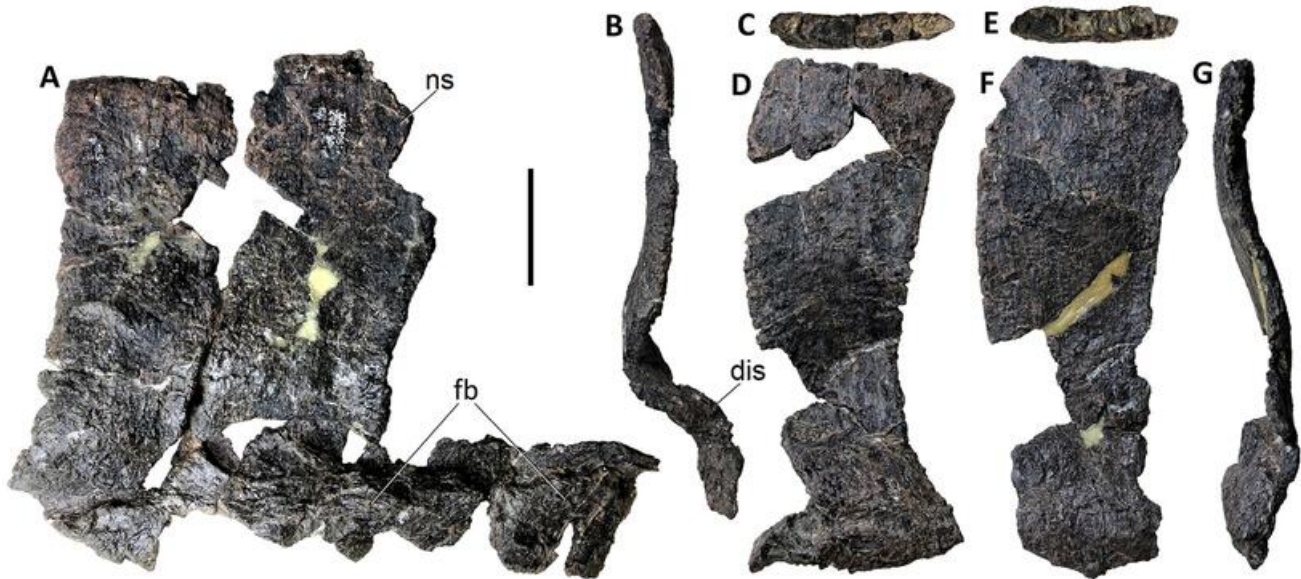


**Figure 21.** *Comptonatus chasei* gen. et sp. nov. (IWCMS 2014.80). Sacral neural spines. **A**, two spines attached to fused bony rod in left lateral view; **B–D** isolated neural spine 1 in **B**, posterior, **C**, dorsal and **D**, right lateral views; **E–G** isolated neural spine 2 in **E**, dorsal, **F**, right lateral and **G**, anterior views. **Abbreviation:** **dis**, taphonomic distortion; **fb**, fused bony rod; **ns**, neural spine. Scale bar represents 50 mm.

to the transverse processes, extend ventrally, and expand anteroposteriorly to fuse with their adjacent sacral ribs. This creates a robust bar of bone, the sacricostal yoke, which articulates with the ventromedial surface of the ilium.

**Caudal vertebrae.** Forty caudal vertebrae (Cd) are preserved (Figs 22, 23, 24), with most being found as part of several articulated (prior to excavation) sections, although some of the most distal vertebrae were separated due to a slight slump in the cliff. The first 21 are consecutive, although later ones may not be, and the latter are numbered in brackets. It is likely that only one or two vertebrae are missing from the first 35 and their numbers closely match their actual position. The gap between Cd(39) and Cd(40) may be bigger.

**General characteristics and trends.** Caudal vertebrae 1–15 form the proximal series, each possessing a caudal rib. The rest of the vertebrae lack caudal ribs but possess haemal facets. The anterior haemal facets disappear after *c.* Cd20, while the posterior facets continue through the series, although on some of the most posterior vertebrae they are barely visible, and it is not possible to accurately define a transition from middle series to distal series (*i.e.* no haemal facets). The proximal series in ‘*Dollodon bampingi*’ contains 16 vertebrae (Norman, 1986), in *Iguanodon bernissartensis* there are *c.* 14 (Norman, 1980) and in *Ouranosaurus nigeriensis* 15 in the holotype GDF 300 (Taquet, 1976), but 20 in

MSNVE 3714 (Bertozzo, Della Vecchia, et al., 2017), suggesting the possibility of considerable but perhaps unusual intraspecific variation.

The proximal series have centra that are taller dorsoventrally than long anteroposteriorly, the length remaining reasonably constant throughout the series but the height reducing moving distally. This ratio reverses in the middle series where the centra are longer than tall. This pattern of morphological change in the caudal vertebrae is commonly found in iguanodontians, for example *Uteodon aphanocetes* (Carpenter & Wilson, 2008), *Mantellisaurus atherfieldensis*, *Iguanodon bernissartensis* (Norman, 1980), *Brightstoneus simmondsi* (Lockwood et al., 2021) and *Brachylophosaurus canadensis* (Prieto-Marquez, 2001), although unusually the proximal series of *Tethyshadros insularis* (Chiarenza et al., 2021; Dalla Vecchia, 2009) are longer anteroposteriorly than tall dorsoventrally and the most proximal of *Barilium dawsoni* is dorsoventrally compressed (Norman, 2011b), and almost equidimensional in lateral view. The posterior articular surface is set ventrally relative to the anterior articular surface in the first seven vertebrae of *Comptonatus chasei*, this feature becoming gradually less marked moving posteriorly. This would have caused the proximal section of the tail to descend slightly.

Many of the caudal vertebrae are articulated and fused to each other (post-depositionally) in short sections, so that not all of the articular surfaces are visible.



**Figure 22.** *Comptonatus chasei* gen. et sp. nov. (IWCMS 2014.80). The seven anterior-most caudal vertebrae in left lateral view with neural spines placed in approximate position. Scale bar represents 100 mm.

The proximal series have oval articular surfaces (long axis dorsoventral), some of which is exaggerated by transverse compression. The anterior articular surfaces are all either flat or very slightly concave. The posterior articular surfaces in Cd1 and Cd2 and to a lesser extent Cd3 are concave but not smoothly, rather having a depressed central area surrounded by a broad torus-like margin. More distally, the posterior articular surfaces are either flat or slightly concave, this being the case up to the most distally preserved vertebra. At the transition to the middle series, a lateral ridge develops on the side of the centrum, dividing the lateral wall into dorsolateral and ventrolateral facing surfaces. This results in the articular surfaces having a hexagonal outline. Hexagonal middle series vertebrae are the norm for iguanodontians (Barrett & Bonsor, 2021), for example *Brighstoneus simmondsi* (Lockwood *et al.*, 2021) and *Iguanodon bernissartensis* (Norman, 1980).

The first two vertebrae have no haemal facets and an almost flat ventral surface with a slight keel, barely discernible in Cd1 but more pronounced in Cd2. In earlier diverging iguanodontians the first chevron most

commonly articulates with the posteroventral surface of the second caudal vertebra as in *Camptosaurus dispar* (Gilmore, 1909), *Dysalotosaurus lettowvorbecki* (Janensch, 1955), *Iguanodon bernissartensis* (Norman, 1980), ‘*Dollodon bampingi*’, (Norman, 1986), *Tenontosaurus tilletti* (Forster, 1990), *Uteodon aphanocetes* (Carpenter & Wilson, 2008), *Bolong yixianensis* (Wu & Godefroit, 2012), *Valdosaurus canaliculatus* (Barrett, 2016), possibly *Cumnorina prestwichii* (Maidment *et al.*, 2022), *Barilium dawsoni* (Norman, 2011b), *Gobihadros mongoliensis* (Tsogtbaatar *et al.*, 2019) and *Brighstoneus simmondsi* (Lockwood *et al.*, 2021). The first two caudal vertebrae in *Mantellisaurus atherfieldensis* are not preserved. *Ouranosaurus nigeriensis* has the first haemal facet on the third caudal vertebrae (Bertozzo, Della Vecchia, *et al.*, 2017; Taquet, 1976), as is probably the case with *Probaetriosaurus gobiensis* (Norman, 2002) and *Jinzhousaurus yangi* (Wang *et al.*, 2010), which also have two disarticulated caudal vertebrae without obvious haemal facets. In *Tethyshadros insularis* chevrons commence autapomorphically between caudal vertebrae seven and eight

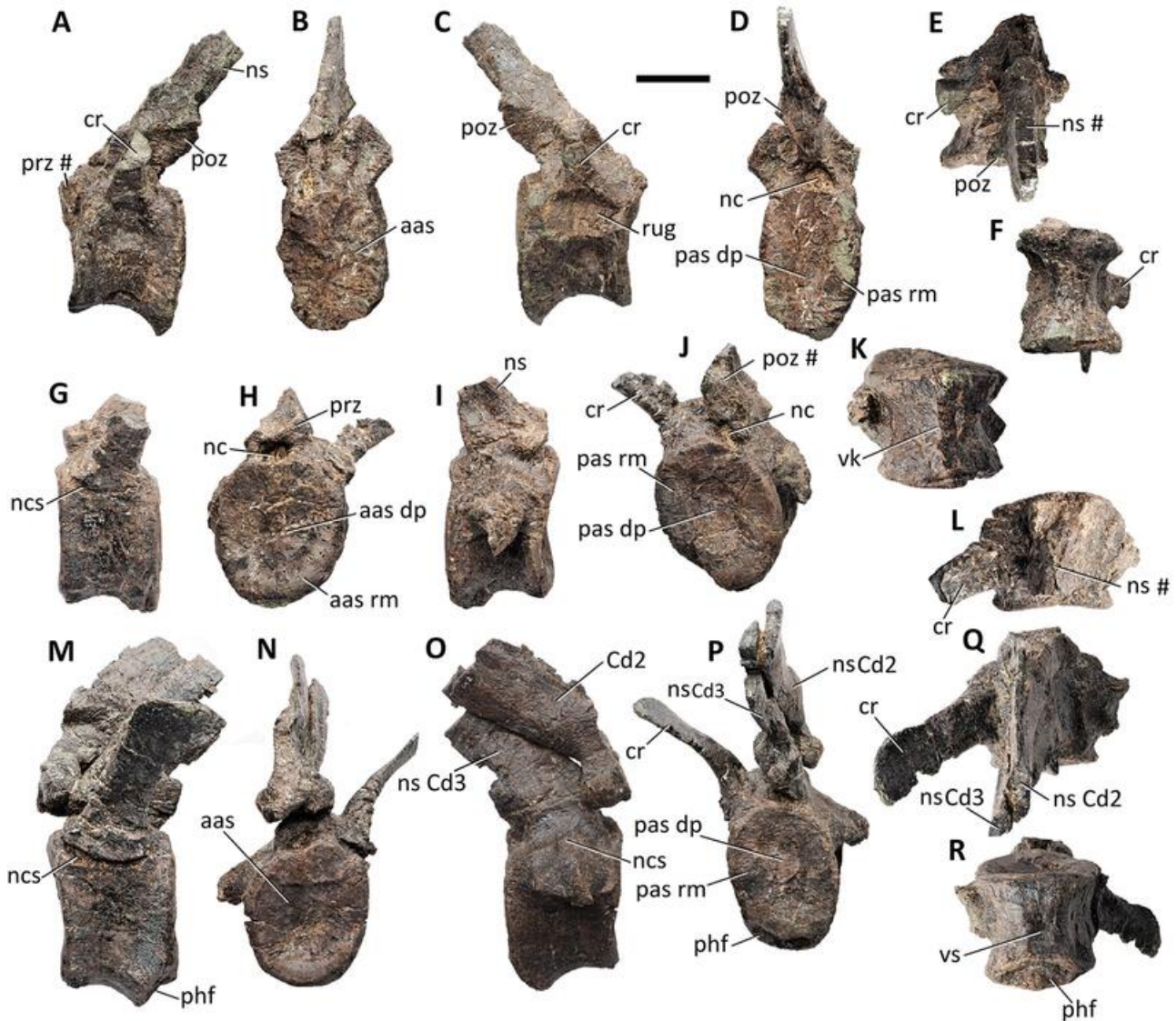


**Figure 23.** *Comptonatus chasei* gen. et sp. nov. (IWCMS 2014.80). Anterior three caudal vertebrae. Cd1 in **A**, left lateral, **B**, anterior, **C**, left lateral, **D**, posterior, **E**, dorsal and **F**, ventral views. Cd2 in **G**, left lateral, **H**, anterior, **I**, left lateral, **J**, posterior, **K**, dorsal and **L**, ventral views. Cd3 in **M**, left lateral, **N**, anterior, **O**, left lateral, **P**, posterior, **Q**, dorsal and **R**, ventral views. **Abbreviations:** aas, anterior articular surface; aas dp, anterior articular surface central depression; aas rm, anterior articular surface raised margin (torus); cr, caudal rib; nc, neural canal; ncs, neurocentral synchondrosis; ns, neural spine; pas dp, posterior articular surface central depression; pas rm, posterior articular surface raised margin (torus); phf, posterior haemal facet; poz, postzygapophysis; prz, prezygapophysis; rug, rugose surface of open neurocentral synchondrosis, vk, ventral keel; vs, ventral sulcus; #, fractured surface. Scale bar represents 50 mm.

(Chiarenza et al., 2021; Dalla Vecchia, 2009). In hadrosaurids the first chevron is posterior to caudal vertebra four or five in saurolophines, and vertebra two or three in lambeosaurines (Horner et al., 2004). Cd3 has a D-shaped posterior haemal facet and thereafter the proximal series have anterior and posterior haemal facets. Both anterior and posterior haemal facets from Cd3 to approximately Cd10 are D-shaped, the curved margins facing each other. Distal to this, as far as Cd(24), the posterior facets become B-shaped, the curves facing

anteriorly, while the anterior facets remain D-shaped but gradually disappear. The ventral surface is damaged or obscured by matrix in Cd5, Cd12, Cd18, Cd19 and Cd(20) but otherwise vertebrae Cd3 to Cd(24) possess two parasagittal ventral ridges connecting the haemal facets and producing a longitudinal sulcus between them. This ventral sulcus is seen most prominently between Cd4–Cd14, the latter corresponding approximately to the end of the proximal series. After Cd(24) the ventral surface is flat, a character that largely

corresponds to the loss of the anterior haemal facet and the separation of the posterior facet into two separate shallow tubers, possibly indicating a change in chevron morphology from a single head to two separate heads. This chevron morphology can be observed in *Iguanodon bernissartensis*, where the chevron articulation also changes from a single to a bifid pattern towards the end of the middle series (Norman, 1980). The sulcus may have been exaggerated by transverse compression in some vertebrae, but it represents a genuine anatomical feature. The tail of *Mantellisaurus atherfieldensis* is incomplete but a ventral sulcus is not a feature of Cd3–Cd12 in NHMUK PV R 5764. The ventral surfaces of the proximal and middle series of ‘*Dollodon bampingi*’ all lack sulci (Norman, 1986). A ventral sulcus in

middle series iguanodontian caudal vertebrae is common but more unusual in the proximal series. Iguanodontians with sulci in the middle series but not in the majority of the proximal series (the first caudal is more usually keeled or smooth) include *Tenontosaurus tilletti* (Forster, 1990); *Hypselospinus* cf. *fittoni* NHMUK PV R 1632 (Norman, 2015); *Ouranosaurus nigeriensis* (Bertozzo, Della Vecchia, et al., 2017); *Gobihadros mongoliensis* (Tsogtbaatar et al., 2019); *Tanius sinensis* (Borinder et al., 2021) and *Telmatosaurus transsylvanicus* (Weishampel et al., 1993). Sulci are described in the proximal series in some fragmentary examples of *Zalmoxes robustus* where the condition is variable (Weishampel et al., 2003), *Valdosaurus canaliculatus* (Barrett, 2016), *Magnamanus soriaensis* (Fuentes

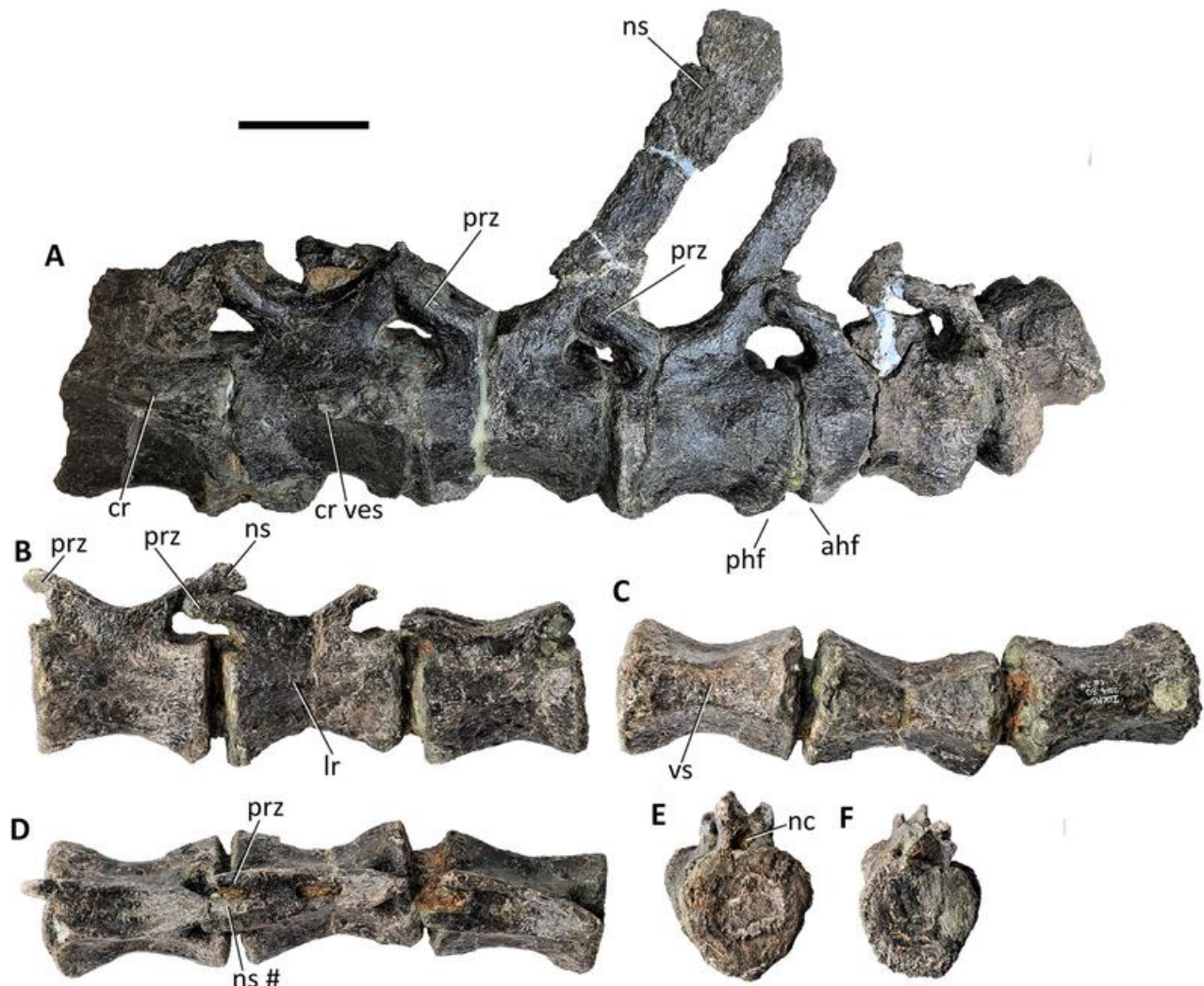


**Figure 24.** *Comptonatus chasei* gen. et sp. nov. (IWCMS 2014.80). Caudal vertebrae from the anterior to middle transition and middle series. Cd14–19 in A, left lateral view. Cd22–24 in B, left lateral, C, ventral, D, dorsal, E, anterior and F, posterior views. **Abbreviations:** ahf, anterior haemal facet; cr, caudal rib; cr ves, vestigial final caudal rib; lr, lateral ridge; nc, neural canal; ns, neural spine; phf, posterior haemal facet; prz, prezygapophysis; vs, ventral sulcus, #, fracture surface. Scale bar represents 50 mm.

Vidarte et al., 2016) and *Brighstoneus simmondsi* (Lockwood et al., 2021). Intraspecific variation has also been recorded in *Iguanodon bernissartensis*, where the majority of specimens have a flat ventral surface in the proximal and middle series, but some examples have a sulcus in the middle series (Verdu, Godefroit, et al., 2017).

Dorsally the wall of the centrum of the proximal series supports the base of the caudal rib. These are largely incomplete and pushed dorsally by postdepositional compression. It is likely that they extended horizontally, providing attachment ventrally for the caudofemoralis muscle and contributed to the separation of the epaxial and hypaxial musculature. The caudal rib is vestigial on Cd15, marking the end of the proximal series.

The neurocentral synchondroses appear to be physically opened on the left lateral side of the first 13 caudal vertebrae. On the right lateral side and on both sides distal to Cd13, the synchondrosis appears to be in position but is still visible, suggesting that postmortem the anterior neural arches were pushed over to the right. The right caudal rib is missing in Cd1, leaving a rugose pit that may be the surface of an open neurocentral synchondrosis.

The neuropophyses support pre- and postzygapophyses. These have flat oval articular facets that face dorso-medially in the prezygapophyses and ventrolaterally in the postzygapophyses. The angles are orientated much more vertically than in the dorsal vertebrae, and the prezygapophyses extend anteriorly beyond the margin of the anterior articular surface.

In lateral view the neural spines in the proximal series extend posterodorsally and are long, being nearly four times the height of the centrum in Cd1, dropping to *c.* 2.4 times the height in Cd8 and becoming quite short at 1.4 times the centrum height in Cd16, the first of the middle series. Compared to dorsal and sacral vertebrae the caudal neural spines are relatively narrow anteroposteriorly although a little expanded distally. No neural spines have preserved in the *Mantellisaurus atherfieldensis* holotype (NHMUK PV R 5764) and the early proximal series has been reconstructed from incomplete spines in '*Dollodon bampingi*' (RBINS R57) and may be inaccurate. The relative height of the neural spines in *Comptonatus chasei* is greater than in *Iguanodon bernissartensis* (RBINS R51) but Cd1 is estimated as being nearly equal to an anterior caudal from NHMUK PV R 604, referred to *Hypselospinus fittoni* (Norman, 2015), although this specimen also has relatively taller neural spines on the dorsal vertebrae. As the sacral neural spines are taller than the late dorsal spines, and the spines of the early caudal vertebrae are even taller, it is possible that this represents a degree of hyperelongation

that may have represented a sail-like structure over the haunches of *Comptonatus chasei*.

**Chevrons.** No complete chevrons are preserved, although proximal sections are present (Fig. 25) from 15 individual haemal arches which, from their size, suggest association with the proximal caudal series. A sketch in the field notes (held at Dinosaur Isle Museum) suggests many were articulated in the anterior series during the excavation and the numbers on the specimens may be accurate. There are no examples of a bifid chevron as suggested by the posterior haemal facets on the more posterior caudal vertebrae and as seen in *Iguanodon bernissartensis* (Norman, 1980). The best-preserved chevron is the dorsal section from an anterior caudal in the proximal series (Fig. 25), which fits neatly between Cd5 and Cd6 and is used in this description. In dorsal view the articular surface is divided transversely into two facets for articulation with the anterior and posterior haemal facets of adjacent caudal vertebrae. Both facets are similarly shaped, with a notch in the sagittal plane of the anterior and posterior margins, respectively. In lateral view the facets are angled at *c.* 90° to each other. Below the articular head in anterior and posterior views is the haemal canal, a dorsoventrally elongate oval opening, bounded laterally by the sides of the haemal arch. The sides of the arch coalesce ventrally to form a transversely compressed haemal spine. In lateral view, the anterior margin of the proximal section of the haemal spine is straight, and the posterior margin is gently concave. A more distal fragment from a different chevron (most likely from between Cd8 and Cd9) suggests that the haemal spine became increasingly transversely thin as it extended ventrally and also expanded a little anteroposteriorly. Although most of the chevrons are incomplete, it is likely that the neural spines of the most anterior caudal vertebrae were longer than the chevrons.

### Scapula

Both scapulae are preserved (Fig. 26). The following description assumes that in lateral view, the long axis of the scapula blade is orientated anteroposteriorly. The posterior margin of the blade of the right scapula is not preserved and there is a postmortem fracture that extends dorsoventrally across the mid-blade, which offsets the proximal and distal parts of the scapula. The left scapula is missing most of the proximal plate, although the blade is more complete, with a relatively thin posterior margin (*c.* 4 mm), suggesting minimal losses.

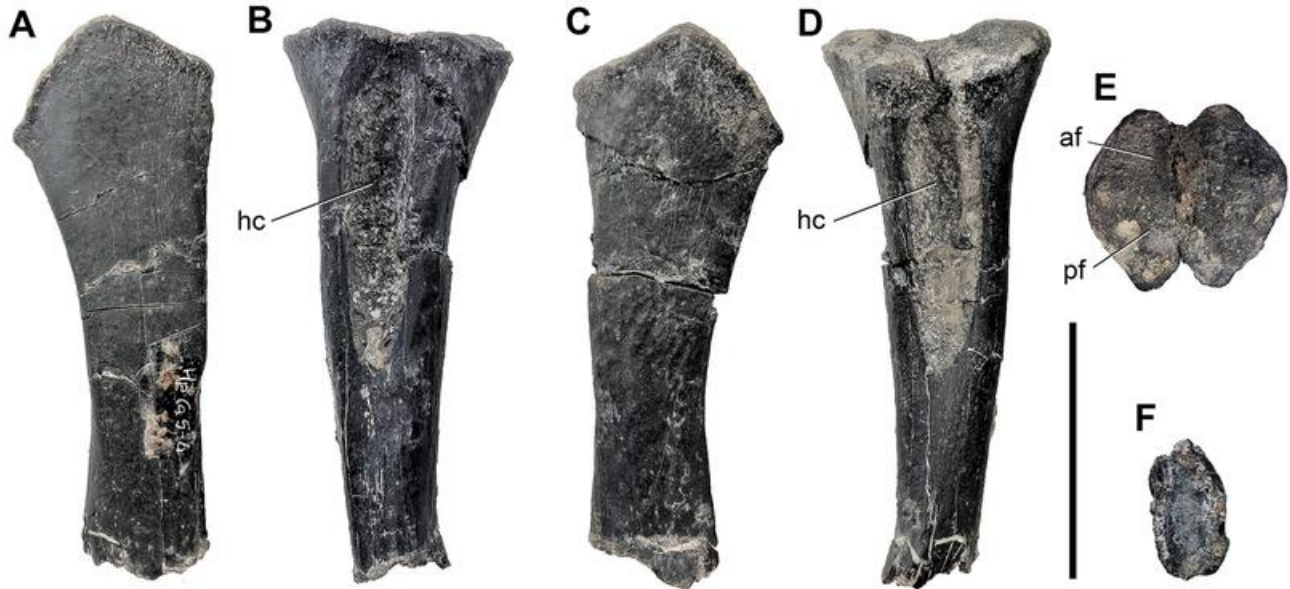


**Figure 25.** *Comptonatus chasei* gen. et sp. nov. (IWCMS 2014.80). Proximal section of chevron from Cd5/6, proximal caudal series (haemal canal unprepped) in **A**, right lateral, **B**, anterior, **C**, left lateral, **D**, posterior, **E**, proximal and **F**, distal views. **Abbreviations:** **af**, anterior facet; **hc**, haemal canal; **pf**, posterior facet. Scale bar represents 50 mm.

The scapula of *Comptonatus chasei* consists of a robust, square proximal plate, which extends posteriorly as a transversely compressed elongate blade.

The anterior two thirds of the scapula blade have a concave ventral margin and a gently convex dorsal margin. The margins of the posterior third have undergone some taphonomic damage but are straighter and diverge slightly. The medial surface of the blade is anteroposteriorly and dorsoventrally concave to accommodate the rib cage. The lateral surface is anteroposteriorly and dorsoventrally convex, the latter being most marked in the anterior section but becoming flatter as it extends posteriorly. The dorsoventral convexity in the anterior section is also more marked ventrally, where the margin is relatively robust, being about twice as thick transversely as the dorsal margin.

There is some posterior flaring of the blade of *Comptonatus chasei*, but as it is incomplete the full extent is uncertain, although the expansion is more pronounced posteroventrally. Based on the reconstruction of the scapula of *Comptonatus chasei* (Fig. 26C), the ratio of maximum depth distally to the minimum depth at the neck of the blade is *c.* 1.6. The degree of dorsoventral flaring of the distal blade is very variable amongst iguanodontians with the ratio ranging from 1.0 in *Iguanodon bernissartensis* (Norman, 1980; RBINS R51, but see above) where the sides are almost parallel, to 3.1 in *Dysalotosaurus lettowvorbecki* (Hübner, 2010), and an array of values in between, with *Mantellisaurus atherfieldensis* being 2.0, although possibly exaggerated

by transverse crushing. In those scapulae with more marked distal flaring, the expansion is asymmetrical, being more prominent posteroventrally. This is the case in *Mantellisaurus atherfieldensis* but is especially marked in *Dysalotosaurus lettowvorbecki* (Hübner, 2010) and *Camptosaurus dispar* (McDonald, 2011). In some hadrosaurids, significant intraspecific variation in the degree of flaring has been recorded (Brett-Surman & Wagner 2007, and references therein).

The proximal area of the iguanodontian scapular blade, in lateral view, is typically constricted to form the ‘neck’ of the scapula. The ratio of the minimum width of the neck to the maximum length of the scapula in *Comptonatus chasei* (based on the reconstruction) is 0.16, which is similar to other iguanodontians such as *Tenontosaurus tilletti* (Forster, 1990); *Barilium dawsoni* (Norman, 2011b); *Iguanodon bernissartensis* (Norman, 1980); ‘*Dollodon bampingi*’ (Norman, 1986); *Ouranosaurus nigeriensis* (Taquet, 1976) and *Gryposaurus latidens* (Prieto-Marquez, 2012).

In lateral view, anterior to the neck of the scapula, the robust acromial process projects dorsally from the proximal plate. The end of the process appears to be slightly crushed but has a broad and straight dorsal margin, similar to *Hippodraco scutodens* (McDonald, Kirkland, et al., 2010), ‘*Dollodon bampingi*’ (Norman, 1986), *Ouranosaurus nigeriensis* (Taquet, 1976), *Altirhinus kurzanovi* (Norman, 1998) and *Probactrosaurus gobiensis* (Norman, 2002). In most early diverging iguanodontians and hadrosauriforms, the acromial process extends either anterodorsally, e.g.

*Camptosaurus dispar* (McDonald, 2011), *Uteodon aphanoeetes* (Carpenter & Wilson, 2008), *Hippodraco scutodens* (McDonald, Kirkland, et al., 2010) and *Bolong yixianensis* (Wu & Godefroit, 2012), or dorsally, e.g. *Iguanodon bernissartensis* (Norman, 1980), ‘*Dollodon bampingi*’ (Norman, 1986), *Altirhinus kurzanovi* (Norman, 1998), *Probactrosaurus gobiensis* (Norman, 2002) and *Eolambia caroljonesa* (McDonald, Bird, et al., 2012), while in hadrosaurids it extends anteriorly in hadrosaurines and anterodorsally in lambeosaurines (Prieto-Marquez, 2008). As the acromial process extends ventrally onto the proximal plate, a dorsoventrally orientated groove separates its anterior margin from the anterior section of the proximal plate. About a third of the way across the plate, the anterior margin of the acromial process curves posteriorly to become the rounded deltoid ridge (Fig. 26D). The deltoid ridge continues to extend posteriorly, eventually blending in with the lateral surface before it reaches the neck of the scapula. Ventral to the deltoid ridge, the surface of the proximal plate (the deltoid fossa *sensu* Bertozzo, Della Vecchia, et al., 2017) is smooth, gently dorsoventrally concave, and anteroposteriorly flat. It extends from the deltoid ridge to the margin of the glenoid. The proximal plate is excavated ventrally, to form the scapular component of the glenoid fossa, which has a lateral margin with an everted edge (although not as prominently everted as in the coracoid component) and a medial margin which lacks an everted edge (although the most posterior part of this margin is incomplete). Posteriorly the glenoid fossa is extended and buttressed by the scapular labrum, a substantial ventral buttress. At the junction of the lateral and medial margins of the glenoid fossa, a prominent ridge (Fig. 26D, G, rid) forms, that extends posteriorly across the surface of the scapular labrum. The anterior surface of the scapular plate, which articulates with the coracoid, has been crushed slightly posteriorly into the plate, but there is no convincing evidence of a supraglenoid fossa. Although the supraglenoid fossa (*sensu* Carpenter & Wilson, 2008) appears to be absent in *Comptonatus chasei*, it is prominent in *Dysalotosaurus lettowvorbecki* (Hübner, 2010), *Cumnoria prestwichii* (Maidment et al., 2022), *Uteodon aphanoeetes* (Carpenter & Wilson, 2008; McDonald, 2011), and *Ouranosaurus nigeriensis* (Taquet, 1976) and less pronounced but present in *Camptosaurus dispar* (McDonald, 2011); *Hippodraco scutodens* (McDonald, Kirkland, et al., 2010); *Mantellisaurus atherfieldensis*, and *Hypselospinus fittoni*, where Norman (2015) considered it to act as a stop, to limit the excursion of the lateral tuberosity of the humerus. The supraglenoid fossa is absent in *Iguanodon bernissartensis* (RBINS R51) and ‘*Dollodon bampingi*’ (Norman, 1986) and in later-diverging hadrosauriforms such as *Probactrosaurus gobiensis* (Norman, 2002) and *Bactrosaurus johnsoni* (Godefroit et al., 1998). The medial

surface of the proximal plate has some crush damage, especially dorsally, but there is a raised central area, ventral to which is a depression separating it from the glenoid. This depressed area extends anteriorly as a groove (the coracoid gutter), which connects to a groove on the coracoid which links to the coracoid foramen. In anterior view, the anterior articular surface is quite rugose, tapering a little as it extends dorsally but transversely deep ventrally.

**Comment on the dorsal margin of the scapular blade.** The dorsal margin of the blade of iguanodontian scapulae is usually either straight or convex, a variation employed as a character state in some phylogenetic studies, including those by McDonald (2012b: character 99) and Xing et al. (2014: character 256), and was also used to differentiate *Uteodon aphanoeetes* from *Camptosaurus dispar* (Carpenter & Wilson 2008). In *Iguanodon bernissartensis* both character states were recorded by Verdu, Godefroit, et al. (2017), although the majority of scapulae were convex, and the scapular blade is particularly susceptible to taphonomic distortion (Brett-Surman & Wagner, 2007). Examples of markedly convex dorsal margins include *Uteodon aphanoeetes* (Carpenter & Wilson, 2008); *Telmatosaurus transsylvanicus* (Weishampel et al., 1993); *Magnapaulia laticaudus* (Prieto-Marquez et al., 2012) and *Gryposaurus latidens* (Prieto-Marquez, 2012), whereas straight examples include *Zalmoxes robustus* (Weishampel et al., 2003); *Camptosaurus dispar* (McDonald, 2011); *Hippodraco scutodens* (McDonald, Kirkland, et al., 2010); *Mantellisaurus atherfieldensis* and *Probactrosaurus gobiensis* (Norman, 2002). The majority of other non-hadrosaurid iguanodontians fall between these two morphological extremes and show gentle convexity. A concave dorsal margin is seen in *Dysalotosaurus lettowvorbecki* (Hübner, 2010), where the distal end is flared to over three times the dorsoventral width of the proximal constriction (neck) of the blade.

### Coracoid

The coracoid (Fig. 27) is a robust, transversely compressed bony plate, with a strongly convex lateral surface, and a concave medial surface. The posterior surface articulates dorsally with the scapula and ventrally expands transversely, to contribute to the glenoid fossa for articulation with the humerus. Both coracoids are preserved and are essentially mirror images of each other, with the right being the most complete and least abraded, although part of the dorsum is missing in both specimens.

Viewed laterally, the fractured ventral section of the base of a boss-like bicipital tubercle (*sensu* Prieto-Marquez, 2011; biceps tubercle, biceps tuber and coracoid tubercle of other authors) is situated anterodorsally,

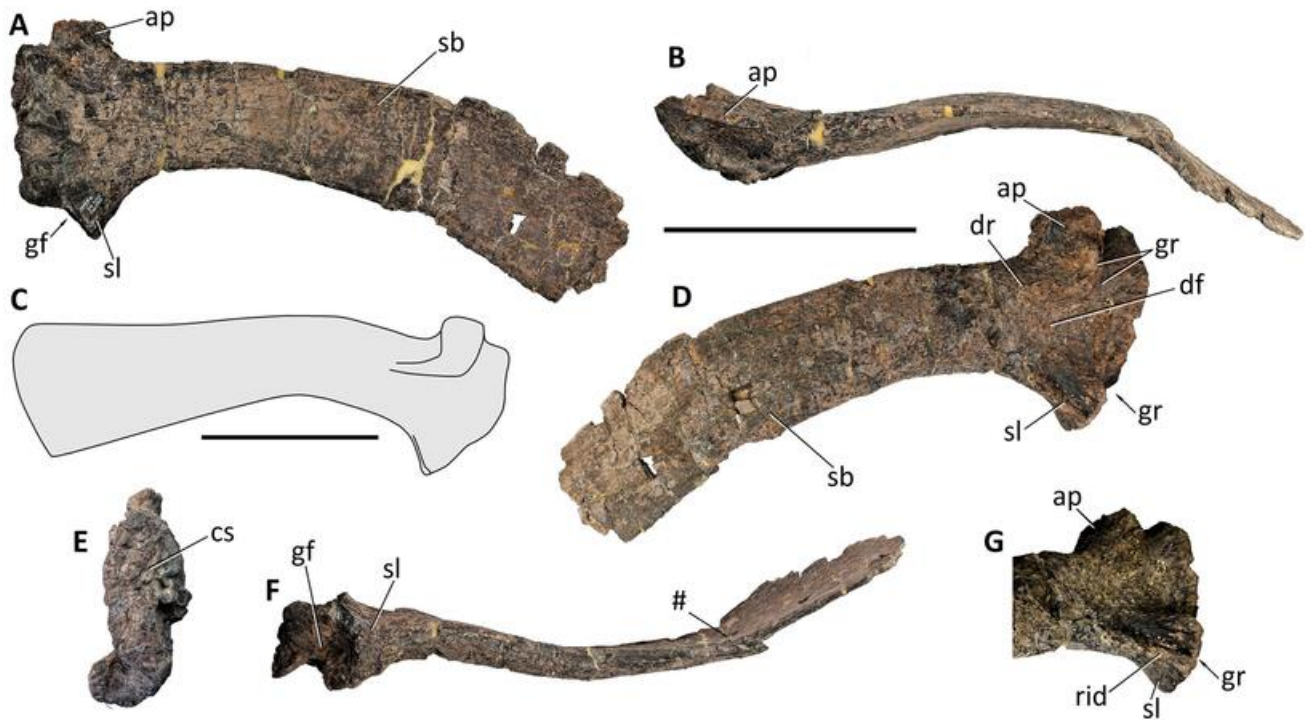


**Figure 26.** *Comptonatus chasei* gen. et sp. nov. (IWCMS 2014.80). Right scapula in **A**, medial, **B**, dorsal, **C**, reconstruction based on a composite of right and left scapulae, **D**, lateral, **E**, anterior, **F**, ventral and **G**, distal ventrolateral views. **Abbreviations:** ap, acromial process; cs, coracoid suture; df, deltoid fossa; dr, deltoid ridge; gf, glenoid fossa; gr, groove; rid, ridge; sb, scapular blade; sl, scapular labrum (ventral buttress); #, fracture. Scale bars represents 100 mm.

adjacent to the anterior margin, the remainder being lost with the rest of the dorsum (Fig. 27, bt #). A bicipital tubercle is found in *Dysalotosaurus lettowvorbecki* (Hübner, 2010, fig. 5.5), *Camptosaurus dispar* (Gilmore, 1909), *Iguanodon bernissartensis* (Norman, 1980), *Mantellisaurus atherfieldensis* (Bonsor et al., 2023), *Bactrosaurus johnsoni* (Prieto-Marquez, 2011), *Eolambia caroljonesa* (McDonald, Bird, et al., 2012) and *Gilmoresaurus mongoliensis* (Prieto-Marquez & Norell, 2010). A coracoid ridge, also positioned anterodorsally on the lateral surface, is found in *Altirhinus kurzanovi* (Norman, 1998), *Jinzhouosaurus yangi* (Wang et al., 2010) and *Probactrosaurus gobiensis* (Norman, 2002), and is probably homologous to the tubercle, while in some iguanodontians there is only muscle scarring, for example *Tenontosaurus tilletti* (Forster, 1990). A particularly well-developed bicipital tubercle is typical of hadrosaurid coracoids, for example *Edmontosaurus annectens* and *Parasaurolophus maximus* (Xing et al., 2014). In *Comptonatus chasei*, the anterior margin of the coracoid just ventral to the bicipital tubercle is expanded medially as part of an oval boss (26 mm by 15 mm, long axis dorso-ventral) on the medial surface (Fig. 27B, mtu), presumably indicative of an osteological correlate, although this is not described in other non-hadrosaurid iguanodontians.

The anterior margin of the coracoid forms a gently convex curve in lateral view, becoming thicker and more rugose ventrally. The anteroventral corner of the coracoid is drawn into a prominent triangular ventral (sternal) process for the attachment of sternal cartilage and gives the coracoid a hook-like appearance in lateral view. A sternal process with similar morphology and size, relative to the main coracoid plate, is seen across a range of ornithopods including *Hypsilophodon foxii* (Galton, 1974), *Cumnoria prestwichii* (Maidment et al., 2022), *Ouranosaurus nigeriensis* (Taquet, 1976), *Altirhinus kurzanovi* (Norman, 1998), *Probactrosaurus gobiensis* (Norman, 2002) and *Gilmoresaurus mongoliensis* (Prieto-Marquez & Norell, 2010). The process is larger relative to the main coracoid plate and more recurved in some hadrosaurids such as *Brachylophosaurus canadensis*, *Edmontosaurus* sp. and *Hypacrosaurus* sp. (Prieto-Marquez & Norell, 2010) and in some early diverging iguanodontians such as *Zalmoxes shqiperorum* (Godefroit et al., 2009) and *Tenontosaurus dossi* (Winkler et al., 1997), but weakly developed in *Dysalotosaurus lettowvorbecki* (Hübner, 2010) and absent in *Lesothosaurus diagnosticus* Galton, 1978 (Baron et al., 2016). In lateral view the posterior margin of the ventral process curves concavely as it extends posteriorly to produce an embayment. The posterior surface of the coracoid

is composed ventrally of a shallow, oval concavity which contributed to the glenoid. Its margins are everted to form a lip for the attachment of a cartilaginous labrum. Dorsal to this is a rugose area for articulation with the scapula via a synchondrosis (Carpenter & Wilson, 2008). This surface faces posteromedially compared to the glenoid surface but is incomplete dorsally. In lateral view, the coracoid foramen is oval with the long axis orientated antero-posteriorly (diameter 15 mm). The foramen is entirely enclosed by the coracoid, although at some stage in its development the posterior margin was formed by dorsal and ventral elements, that still show a clear line of fusion between them (Fig. 27A, C, lof). The posterior margin of the coracoid foramen is closed in most iguanodontians

but open in *Camptosaurus dispar* (Gilmore, 1909); *Magnamanus soriaensis* (Fuentes Vidarte et al., 2016); *Iguanodon bernissartensis* (Norman, 1980) and *Tethyshadros insularis* (Dalla Vecchia, 2009). The presence of a closed but visible line of fusion in *Comptonatus chasei* suggests a synchondrosis and presumably indicates that at least in some taxa an open or enclosed coracoid foramen could have been an ontogenetic variable, dependant on the degree of ossification. The foramen opens onto the medial surface, where there is a larger oval opening (26 mm diameter, axis anteroposterior). The posterior half of the internal opening produces an embayment in the proximal articular surface of the coracoid, forming a direct channel from the internal foramen to the coracoid

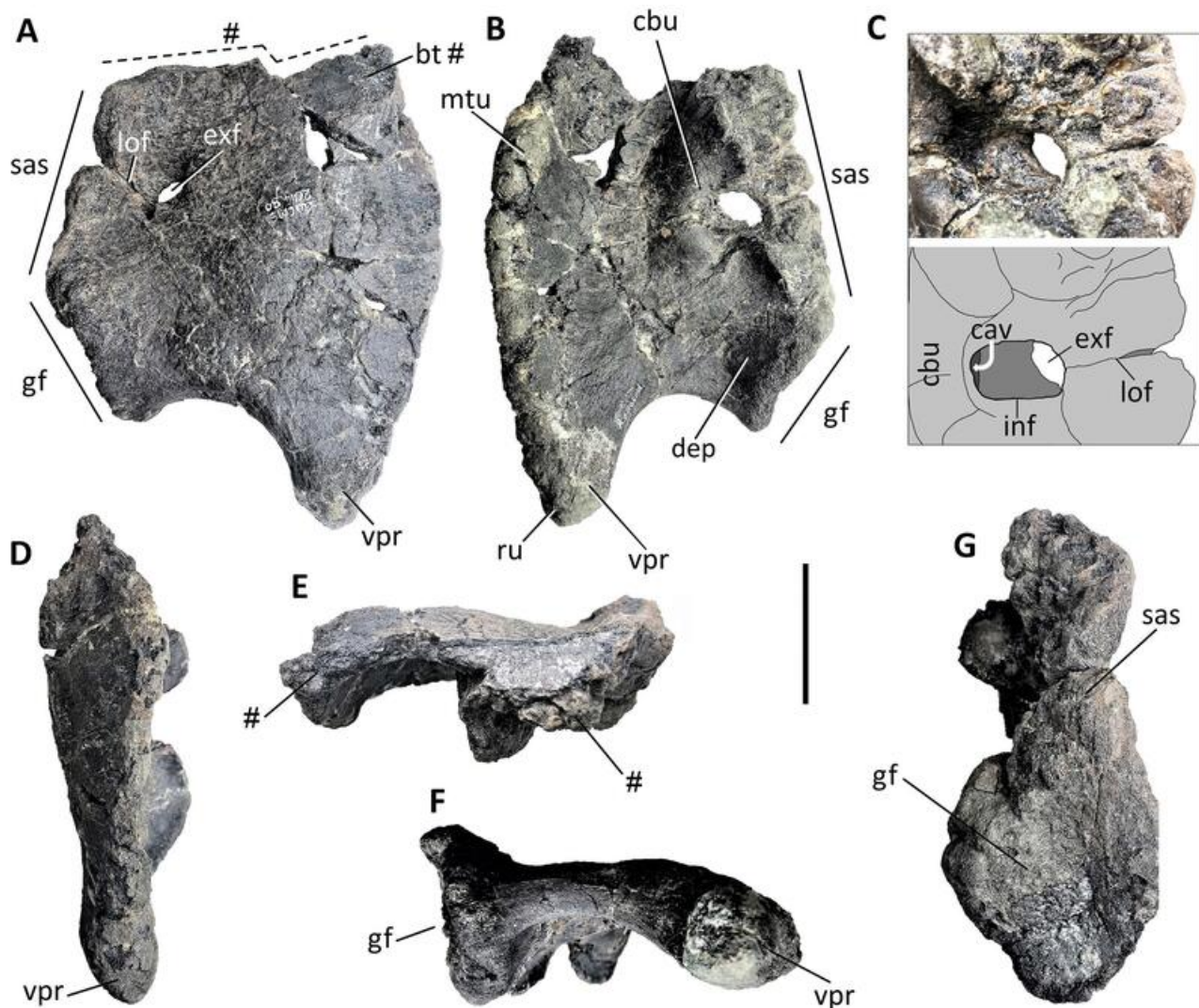


**Figure 27.** *Comptonatus chasei* gen. et sp. nov. (IWCMS 2014.80). Right coracoid in **A**, lateral, **B**, medial, **C**, close-up of coracoid foramen in medial view with drawing below, **D**, anterior, **E**, dorsal, **F**, ventral and **G**, posterior views. **Abbreviations:** **bt**, ventral end of bicipital tubercle; **cav**, entrance to cavity; **cbu**, cornuate buttress; **dep**, depressed area; **exf**, external foramen; **gf**, glenoid fossa; **inf**, internal foramen; **lof**, line of fusion; **mtu**, medial tubercle; **ru**, rugosity; **sas**, scapular articular surface; **vpr**, ventral process; #, fractured surface. Scale bar represents 50 mm.

gutter on the medial surface of the scapula, probably for the passage of the supracoracoid nerve and associated vessels (Romer, 1956). The margin of the anterior half of the internal opening is formed by part of a robust cornuate ridge of bone, the wide end of which buttresses the dorso-medial section of the articular surface for the scapula, while the body gradually tapers and curves around the coracoid foramen. The channel between the external and internal openings is also extended into a relatively large cavity, which also extends into the anterior wall (Fig. 27C, cav) under the cornuate buttress. This feature is present in both coracoids and appears to be autapomorphic to *Comptonatus chasei*.

### Sternal bone

Both sternal bones are preserved (Fig. 28). The left has been repaired, but they are otherwise in good condition and are almost complete. They are described as if their long axis was principally in the coronal plane as labelled in Fig. 28. Their overall form is hatchet-shaped, with a flattened anteromedial (sternal) plate dorsomedially and a rod-like, posterolateral process ventrolaterally. The posterolateral process is absent in the sternal bones of most early diverging iguanodontians such as

*Tenontosaurus tilletti* (Forster, 1990); *Dryosaurus altus*; *Dysalotosaurus lettowvorbecki* (Galton, 1981) and *Camptosaurus dispar* (Dodson & Madsen, 1981), while the hatchet shape was considered a synapomorphy of Styracosterna by Sereno (1986), but has recently been found to be present in the early-diverging ornithopods *Macrogyphosaurus gondwanicus* and *Iyuku raathi*, suggesting a more complicated distribution (Poole, 2022a, 2022b).

The anteromedial sternal plate is taller dorsoventrally than wide transversely and is anteroposteriorly compressed. It is anteroposteriorly thickest dorsally, presumably for the attachment of cartilage, but as seen in medial view (Fig. 28D), it tapers ventrally to become extremely thin (< 1 mm) along its fractured and incomplete ventromedial border. The dorsolateral margin forms a very gentle concave curve, which continues laterally as the dorsal margin of the posterolateral process. In anterior and posterior views the medial margin is irregular and damaged but broadly convex. Ventrally it curves laterally (Fig. 28E, dashed line), probably forming an obtuse angle, that then extends laterally as the ventral margin of the anteromedial plate, before curving concavely and continuing as the slightly expanded ventral margin of the posterolateral process. The overall

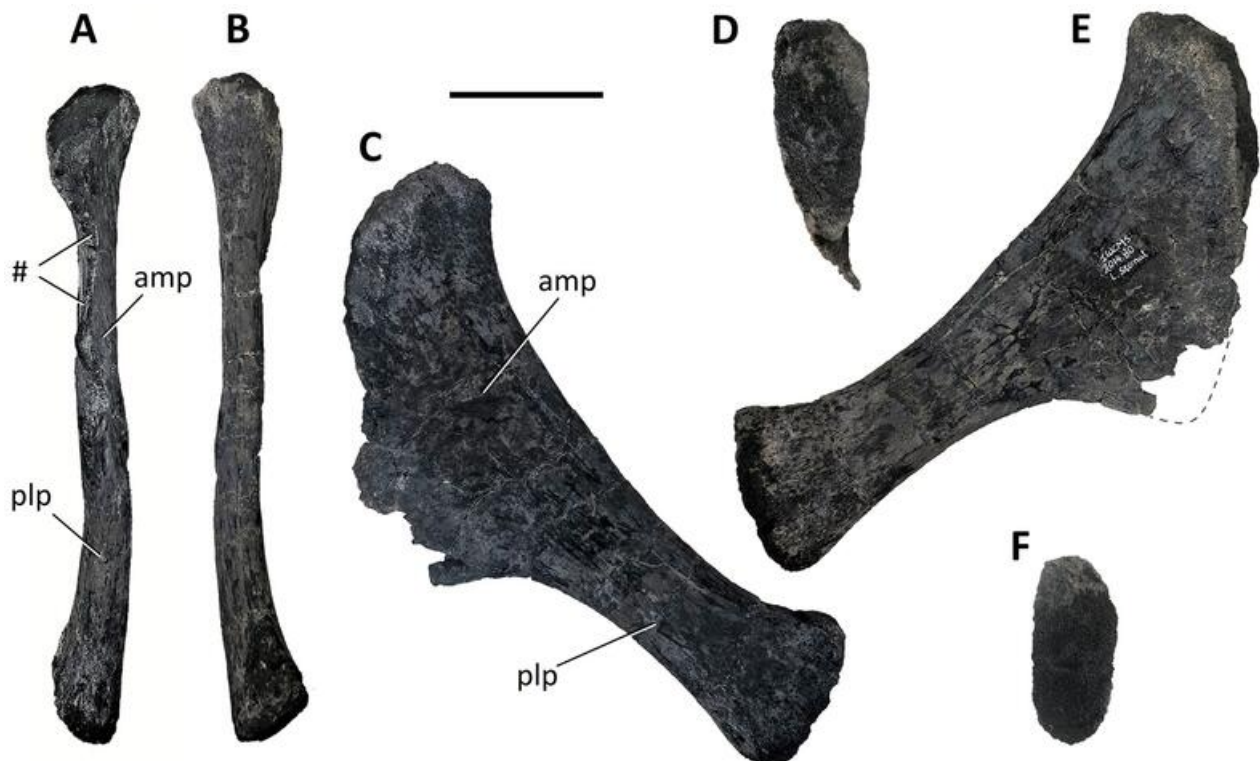


**Figure 28.** *Comptonatus chasei* gen. et sp. nov. (IWCMS 2014.80). Left sternal bone in **A**, ventral, **B**, dorsal, **C**, anterior, **D**, medial, **E**, posterior and **F**, lateral views. **Abbreviations:** amp, anteromedial plate; plp, posterolateral process; #, fractured surface. Scale bar represents 50 mm.

morphology most closely resembles *Fukuisaurus tetoriensis* (Kobayashi & Azuma, 2003); *Ouranosaurus nigeriensis* (Taquet, 1976) and *Probactrosaurus gobiensis* (Norman, 2002). In some hadrosauriforms the ventral border of the anteromedial plate forms a more deeply concave curve than in *Comptonatus chasei*, producing a more pronounced and slightly hook-shaped anteroventral process, as seen in *Jinzhousaurus yangi* where the process is more tab-like (Wang et al., 2010); *Equijubus normani* (McDonald et al., 2014); *Batyrosaurus rozhdestvenskyi* (Godefroit, Bolotsky, et al., 2012); and the hadrosaurids *Olorotitan arharensis* (Godefroit et al., 2011) and *Kundurosaurus nagorny* (Godefroit, Escuille, et al., 2012). The posterolateral process of *Comptonatus chasei* forms a stout rod, which flares slightly distally. It is compressed anteroposteriorly forming a stadium-shape in cross-section (Fig. 28F). The distally expanded articular surface is rugose. The posterolateral process is notably more robust than the more gracile sternal of *Mantellisaurus atherfieldensis* (ratio of length to minimum width in anterior view, *Comptonatus chasei* 2.9; *Mantellisaurus atherfieldensis* 5.6).

### Humerus

Only the right humerus is preserved (Fig. 29) and it is in good condition, although there are some losses and crushing to the articular surfaces of the condyles, especially the medial condyle.

Viewed anteriorly, the humerus is distinctly curved, the medial border of the diaphysis being concave, while the lateral border is sinusoidal, being principally convex proximally, where it incorporates the deltopectoral crest, but concave distally, before the diaphysis expands transversely, to form the lateral (radial) and medial (ulnar) condyles. The proximal half of the humerus is anteroposteriorly compressed, with the articular head, a large, rugose, and globular condyle, sited dorsally on its posterior surface, as in all quadrupedal ornithischians (Maidment & Barrett, 2012), for articulation with the scapulocoracoid. In anterior view, the articular head projects from the dorsal margin of the humerus, as a centrally placed convex curve. A straight tangential margin from this curve extends ventromedially to blend with the medial tuberosity, whereas laterally the margin takes a small downwards step (Fig. 29, 1st), before continuing horizontally to the lateral tuberosity. The lateral step is either absent or weakly present in early diverging iguanodontians such as *Zalmoxes robustus* (Weishampel et al., 2003); *Tenontosaurus tilletti* (Forster, 1990); *Dysalotosaurus lettowvorbecki* (Hübner, 2010) and *Camptosaurus dispar* (Gilmore, 1909), but a distinct lateral step is normally found in more deeply nested taxa, such as *Mantellisaurus atherfieldensis*, *Ouranosaurus*

*nigeriensis* (Taquet, 1976), *Gilmoreosaurus mongoliensis* (Prieto-Marquez & Norell, 2010), *Hadrosaurus foulkii* (Prieto-Marquez et al., 2006) and *Gryposaurus latidens* (Prieto-Marquez, 2012). In dorsal view the lateral tuberosity of *Comptonatus chasei* is expanded anteriorly (Fig. 29E, 1tu), whereas the medial tuberosity is not. The anterior expansion of the lateral tuberosity is similar to that seen in *Ouranosaurus nigeriensis* (Bertozzo, Della Vecchia, et al., 2017) and *Eolambia caroljonesa* (McDonald, Bird, et al., 2012), less marked than in *Mantellisaurus atherfieldensis* and *Nanyangosaurus zhugeii* (Xu et al., 2000), but more marked than in *Tenontosaurus tilletti* (Forster, 1990), *Dysalotosaurus lettowvorbecki* (Hübner, 2010) and *Uteodon aphanocetes* (Carpenter & Wilson, 2008). In proximal view, the lateral tuberosity also protrudes a little posteriorly and this is also observed in *Mantellisaurus atherfieldensis* (Bonsor et al. 2023). In anterior view the margin of the lateral tuberosity curves ventrally to form a convexity which continues seamlessly as the lateral border of the deltopectoral crest. The deltopectoral crest expands slightly anteriorly as it extends distally, before merging smoothly with the diaphysis. There is no definitive ventral angle or apex marking the distal margin of the crest, as is also the case in *Iguanodon bernissartensis* (Norman, 1980), *Mantellisaurus atherfieldensis*, *Ouranosaurus nigeriensis* (Bertozzo, Della Vecchia, et al., 2017), *Eolambia caroljonesa* (McDonald, Bird, et al., 2012), *Telmatosaurus transsylvanicus* (Weishampel et al., 1993) and *Tanais sinensis* (Borinder, 2015). The lateral margin of the distal humerus curves concavely towards the lateral border of the lateral condyle.

The anteroposteriorly compressed proximal end of the humerus flares transversely as it extends dorsally. The degree of flaring (ratio of maximum length of humerus to maximum width of the proximal end) in *Comptonatus chasei* is 3.1 which is very typical of many iguanodontians, for example *Mantellisaurus atherfieldensis* 3.3 and *Iguanodon bernissartensis* 3.3 (Norman, 1980). Hadrosaurids tend to have less flaring and therefore higher ratios, for example *Hadrosaurus foulkii* 3.7 (Prieto-Marquez et al., 2006), *Gryposaurus latidens* 4.1 (Prieto-Marquez, 2012) and *Brachylophosaurus canadensis* 5.0 (Prieto-Marquez, 2001). Transversely the anterior surface of the proximal humeral diaphysis is shallowly concave, forming a wide bicapital gutter which extends ventrally for approximately two thirds of the way down the humerus. The surface is then flat for a short distance before becoming transversely concave again, dorsal to the distal condyles. Posteriorly, the proximal surface is transversely convex and supports the articular head of humerus. This is reinforced ventrally by a sturdy buttress

and on both sides by the stout, anteroposteriorly thick ‘shoulders’ connecting it to the tuberosities (see above).

Distally the lateral condyle has been damaged by crushing, and there are losses to the medial margin of the medial condyle, making interpretation difficult. Posteriorly, the distal condyles are separated by a wide but shallow intercondylar groove. The medial condyle extends further ventrally than the lateral condyle. The anterior intercondylar groove is hardly discernible partly due to crushing but must have been considerably narrower than the posterior groove. The lateral condyle in *Eolambia caroljonesa* (McDonald, Bird, *et al.*, 2012); *Mantellisaurus atherfieldensis* and *Ouranosaurus nigeriensis* (Bertozzo, Della Vecchia, *et al.*, 2017) has a prominent anterolateral epicondylar flange or supinator ridge, which in the latter two is separated from the main condyle by a second anterior groove. A supinator ridge may have been present in *Comptonatus chasei* but has been lost, leaving only a short, fractured base. However, although badly crushed there is the suggestion of a secondary groove.

### Antebrachium

The left ulna and radius (Fig. 30) are both preserved and attached to each other by matrix. Some carpals (see

below) are also attached to the distal radius. The antebrachium is described with the bones aligned horizontally, and the radius placed dorsal to the ulna.

**Ulna.** Posteriorly the ulna flares dorsoventrally. It gives rise to three processes arranged approximately at right angles to each other; a medial and lateral flange projecting dorsomedially and dorsolaterally, connected to each other by a gently curved, transversely concave surface, which cradles the head of the radius, and an olecranon process for the attachment of the triceps musculature (Maidment & Barrett, 2011), extending posteriorly from the posteroventral edge of the ulna. The medial process is considerably larger than the lateral process, extending further dorsally and in medial view presenting a triangular shape, which significantly overlaps the medial surface of the radial head. The lateral process by contrast is little more than a stout ridge which abuts against the ventral radial head. A prominent medial process and smaller lateral process are seen widely across iguanodontians, for example *Uteodon aphanoeetes* (Carpenter & Wilson, 2008); *Tenontosaurus tilletti* (Forster, 1990); *Mantellisaurus atherfieldensis*; *Ouranosaurus nigeriensis* (Bertozzo, Della Vecchia, *et al.*, 2017); *Eolambia caroljonesa* (McDonald, Bird, *et al.*, 2012) and *Brachylophosaurus canadensis* (Prieto-Marquez, 2001),

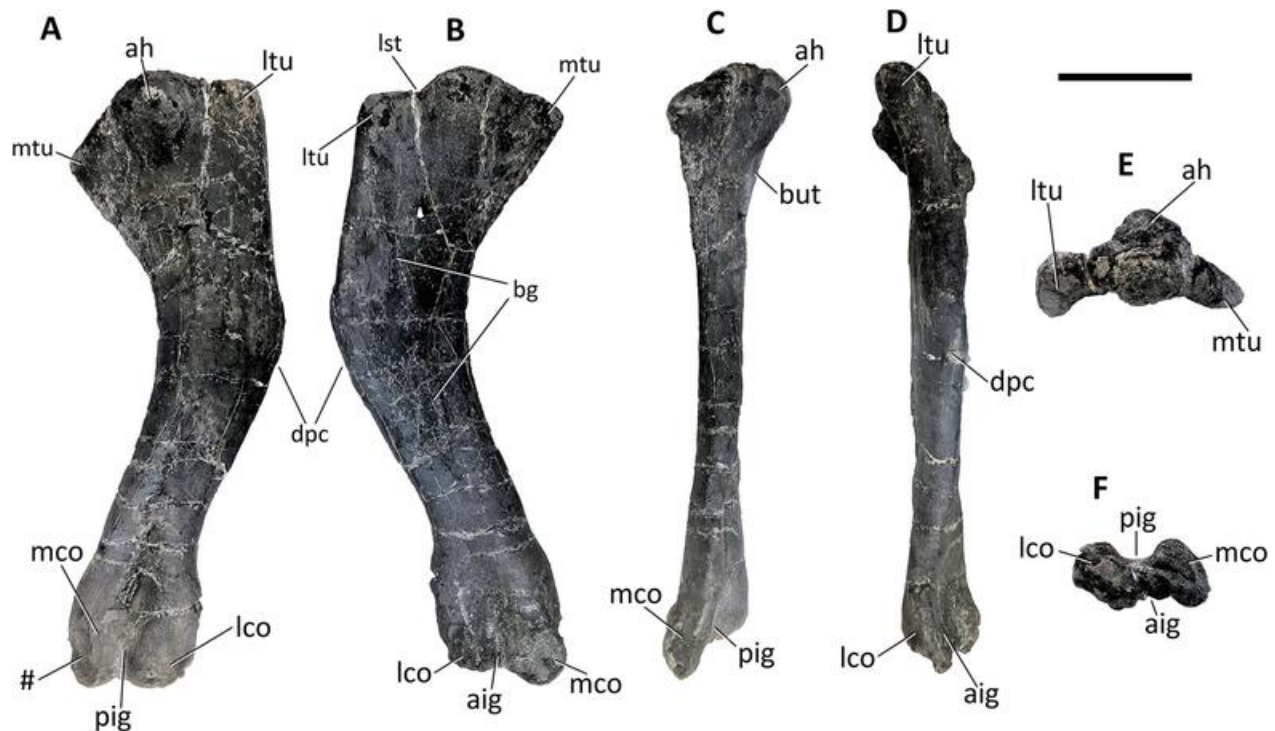


**Figure 29.** *Comptonatus chasei* gen. et sp. nov. (IWCMS 2014.80). Right humerus in **A**, posterior, **B**, anterior, **C**, medial, **D**, lateral, **E**, proximal and **F**, distal views. **Abbreviations:** **ah**, articular head; **aig**, anterior intercondylar groove; **bg**, bicipital groove; **but**, buttress; **dpc**, deltopectoral crest; **lst**, lateral step; **lco**, lateral condyle; **ltu**, lateral tuberosity; **mco**, medial condyle; **mtu**, medial tuberosity; **pig**, posterior intercondylar groove; **#**, fractured surface. Scale bar represents 100 mm.

although in the first two taxa, the concavity for the radial head is less pronounced.

The olecranon process is well developed with a rugose surface. It is more pronounced and extends relatively further posteriorly than in early diverging iguanodontians such as *Tenontosaurus tilletti* (Forster, 1990) and *Dysalotosaurus lettowvorbecki* (Hübner, 2010) but is similar to *Barilium dawsoni* (Norman, 2011b), *Mantellisaurus atherfieldensis*, *Ouranosaurus nigeriensis* (Bertozzo, Della Vecchia, et al., 2017), *Eolambia caroljonesa* (McDonald, Bird, et al., 2012) and *Gobihadros mongoliensis* (Tsogtbaatar et al., 2019). The cross-section of the olecranon process in the transverse plane is oval with a dorsoventral long axis.

In ventral view the surface of the ulna is transversely convex with a straight shaft, although it is slightly

narrowed posteriorly, due to a shallow depression post-eromedially, at the base of the medial process. In medial and lateral views, the dorsal margin describes a gently concave arc (slightly exaggerated by a midshaft fracture), while the ventral margin is shallowly concave anteriorly and straight posteriorly.

The dorsal surface of the ulna, facing the radius, is transversely flat in its middle section but anterior to the posterior articular surface with the radius, is a longitudinal groove, bordered by extensions of the medial and lateral processes. This groove has probably been exaggerated by transverse crushing. The lateral margin of the dorsal surface is transversely rounded but is more angular medially. Anteriorly the medial margin divides to form a pronounced medial ridge and a weaker lateral ridge, which crosses the ventral surface anterolaterally.



**Figure 30.** *Comptonatus chasei* gen. et sp. nov. (IWCMS 2014.80). Left radius and ulna in **A**, posterior, **B**, medial, **C**, dorsal, **D**, anterior, **E**, lateral and **F**, ventral views. **Abbreviations:** cp, carpus; ios, interosseus space; lpr, lateral process; mpr, medial process; opr, olecranon process; pur, prominent ulnar ridge; rad, radius; uln, ulna. Scale bar represents 50 mm.

These ridges bound a flat elongate triangular surface on the distal ulna for articulation with the radius. The distal end is expanded, again principally in the dorsoventral axis and viewed distally has a convex, rugose, subrectangular surface whose margins are straight dorsally, convex laterally and ventrally, while the dorsal aspect of the medial edge protrudes due to the medial ridge (Fig. 30D, *pur*). This ridge is considerably more pronounced than in *Tenontosaurus tilletti* (Forster, 1990), *Uteodon aphanocetes* (Carpenter & Wilson, 2008) and *Mantellisaurus atherfieldensis* but shows similarities with *Eolambia caroljonesa* (McDonald, Bird, et al., 2012) and *Ouranosaurus nigeriensis* (Bertozzo, Della Vecchia, et al., 2017). The distal articular surface is gently convex, and is extended a short distance ventromedially onto the medial surface of the ulna, presumably as part of its articulation with carpal V.

**Radius.** The radius is an elongate and slender bone, in which the proximal head is expanded transversely and the distal end dorsoventrally. In proximal view the posterior articular surface of the head is sub-oval in shape, being convex dorsally, but with slightly flattened edges ventromedially and ventrolaterally. The ventrolateral edge forms the base of a facet that extends onto the radial head for articulation with the lateral process of the ulna. The head of the radius has an everted rim, which is most prominent dorsomedially. The shaft of the radius is 'D'-shaped in its midsection with the flat surface facing ventrally. In dorsal view the shaft is slightly bowed, convex medially, and in lateral and medial views it is bowed with a concave ventral margin. The concave ventral surface faces the concave dorsal shaft of the ulna, creating an elongate elliptical interosseous space between the proximal and distal articulations of the two bones. The distal articular surface is obscured by bones of the carpus, although does extend slightly onto the dorsolateral aspect of the distal radius, possibly for articulation with metacarpal I of the pollex. The lateral surface of the distal radius is slightly convex, the medial surface slightly concave and the ventral surface flat for articulation with a facet on the ulna.

### Carpus

The carpus (Fig. 31) and manus are described with the manus held horizontal and the flexor surface facing downwards. Detailed photographs of all elements are figured in the [Supplemental material \(S1, figs S79–88\)](#).

The left carpus of *Comptonatus chasei* is preserved in two blocks but is incomplete. The larger block is fused to the distal radius, while the smaller block, although not fused to the distal ulna, articulates closely with it. In early diverging ankylopollexians such as *Camptosaurus*

*dispar* (Gilmore, 1909), the carpus has a proximal row of three bones, the radiale, intermedium and ulnare, and a distal row of five carpal bones. Within Ankylopollexia there is usually partial fusion of the carpals into two blocks (Sereno, 1986), one containing the radiale, intermedium, plus distal carpals 1–3 and metacarpal I, and the other block containing the ulnare and distal carpals 4 and 5 (Sereno, 1986). This appears to be the arrangement in *Comptonatus chasei* (see below). Two such blocks are also found in *Iguanodon bernissartensis*, although there is some suture between the intermedium and the ulnare (Norman, 1980) and they functioned as a single unit (Bertozzo, Della Vecchia, et al., 2017). In the *Ouranosaurus nigeriensis* holotype there are also two blocks, but Taquet (1976) describes the intermedium being fused to the ulnare, while the radiale, intermedium and ulnare are distinct in MSNVE 3714 (Bertozzo, Della Vecchia, et al., 2017). The carpus is possibly fused or sutured into one solid mass in *Barilium* cf. *dawsoni* NHMUK PV R 2357, although the surface is obscured by extensive ossified tendons (Norman, 2011b), making this unclear. The carpals may be incompletely fused in *Mantellisaurus atherfieldensis* but held together in a single block by matrix (Hooley 1925). More deeply nested taxa can differ, for example *Bolong yixianensis* (Wu & Godefroit, 2012) has an unfused carpus and *Gobihadros mongoliensis* (Tsogtbaatar et al., 2019) only has two ossified carpals, the ulnare and intermedium. Hadrosaurids typically have only one or two ossified carpals (Horner et al., 2004). In the majority of iguanodontian taxa the carpus is not preserved or has not been described.

**Proximal carpal row.** The medial carpal block in ventral view (Fig. 31A) is divided into three sections, a medial section formed by the first metacarpal and possibly first carpal, and middle and lateral sections formed by the radiale and intermedium respectively. The radiale is a dorsoventrally elongate block that articulates with the carpal 1-metacarpal I complex medially and the intermedium laterally. Its ventral surface is rectangular, being slightly longer transversely than anteroposteriorly. Its anterior surface is excavated to produce a possible socket for articulation with the base of metacarpal II. This has revealed an area of cancellous bone, a feature also seen in *Iguanodon bernissartensis* (Norman, 1980), which may indicate that the socket contained cartilage antemortem. An area of cancellous bone is also reported on the radiale of *Magnamanus soriaensis* (Fuentes Vidarte et al., 2016), but on the proximal surface. Dorsally the fusion of the radiale to the carpal 1/metacarpal I complex, and intermedium is complete, and definite lines of articulation are difficult to identify.

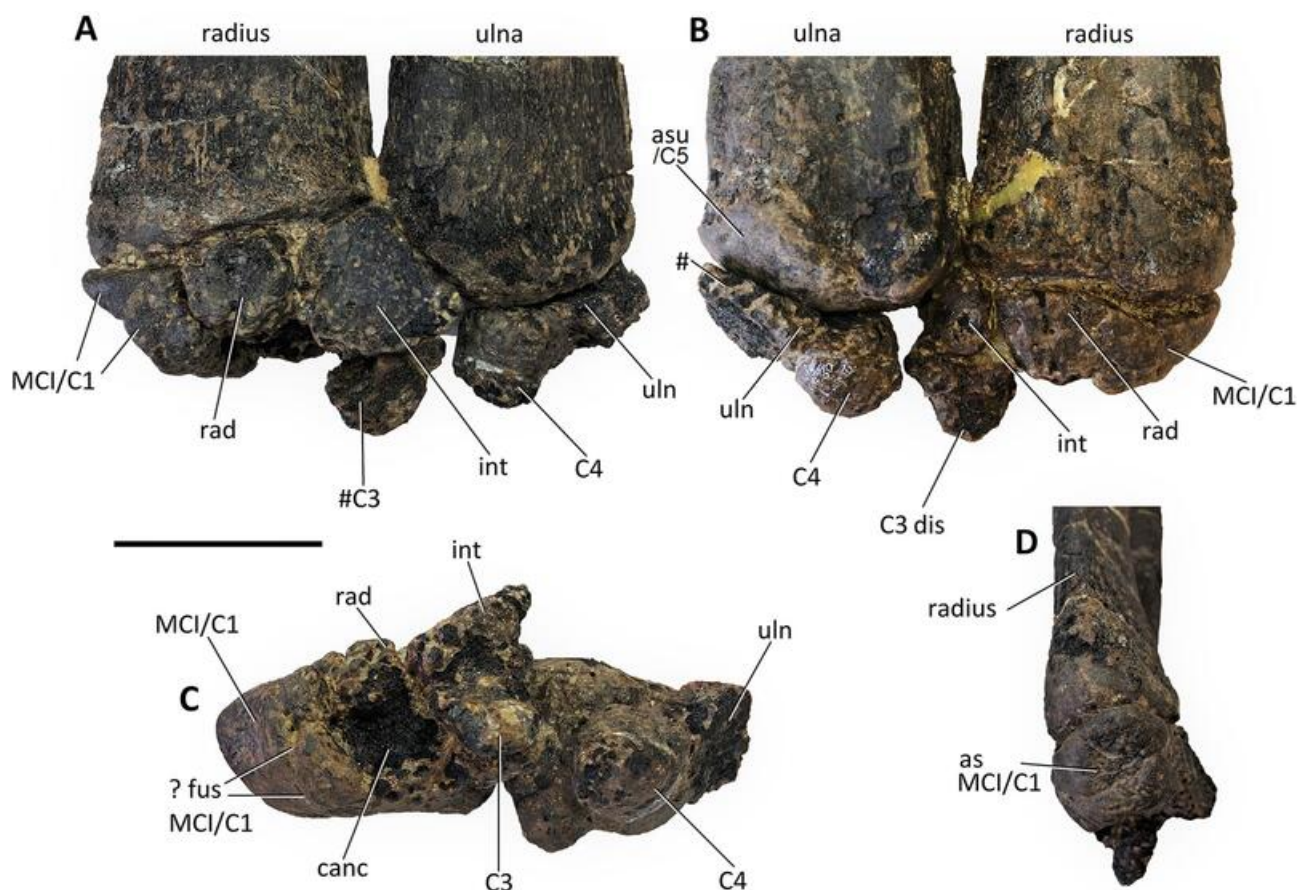


**Figure 31.** *Comptonatus chasei* gen. et sp. nov. (IWCMS 2014.80). Left carpalia in **A**, dorsal, **B**, ventral, **C**, distal and **D**, medial views. **Abbreviations:** **as** MCI/C1, articular surface of metacarpal I/carpal 1 complex; **asu/C5**, articular surface for unpreserved lateral section of ulnare and probably carpal 5; **canc**, cancellous bone; **C**, carpal; **dis**, displaced; **MC**, metacarpal; **int**, intermedium; **rad**, radiale; **uln**, ulnare; **? fus**, possible line of fusion; **#**, fracture surface. Scale bar represents 50 mm.

The intermedium is larger than the radiale. Its ventral surface is quadrilateral and gently concave. Posteriorly it has two articular surfaces facing posteromedially and posterolaterally, for articulation with the radius and ulna respectively. Medially it articulates with the radiale and anteriorly the surface is convex, although the dorsal and anterior surfaces are fractured and distorted making interpretation difficult.

The lateral block of *Comptonatus chasei* contains an incomplete ulnare and distal carpal 4. The incomplete ulnare has a shallowly concave posterior surface for articulation with the distal ulna.

**Distal carpal row.** The medial surface, of the medial section, of the medial block, faces anteromedially and is subcircular, slightly concave and irregularly grooved. Laterally it is fused to the radiale although ventrally there is a break that could be a recent fracture or the line of articulation, and posteriorly it articulates with the distal radius. The medial section probably represents

metacarpal I but could equally be a fused complex of distal carpal 1 and metacarpal I as is seen in *Iguanodon bernissartensis* (Norman, 1980).

Distal carpal 2 is absent but may never have ossified as is proposed for *Iguanodon bernissartensis* (Norman, 1980) and *Mantellisaurus atherfieldensis* (Norman, 1986).

Distal carpal 3 appears to have broken from the anterior surface of the intermedium, and is held in place by matrix, with its fractured surface facing ventrally. If this is correct, distal carpal 3 is an anteriorly convex circular bone of *c.* 20 mm diameter.

Distal carpal 4 is a circular and gently anteriorly convex nubbins of bone much like distal carpal 3 and is *c.* 22 mm in diameter. It is articulated with the anteromedial surface of the ulnare.

Distal carpal 5 is missing, but its presence can be inferred by a dorsolateral extension of the articular surface onto the distal ulna.

## Metacarpus

**Metacarpal II (right).** Metacarpal II (Fig. 31A, B) is transversely compressed and is shorter than metacarpals III and IV. The shaft is convex medially and flat laterally, where it would have been appressed against metacarpal III. The proximal end is expanded, principally dorsoventrally, with a 'D'-shaped articular surface in proximal view and a convex shape in lateral view. A metacarpal II that is shorter than metacarpals III and IV and which may also have been articulated in a more proximal position within the wrist, is commonly seen in iguanodontians, such as *Iguanodon bernissartensis* (Norman, 1980), *Altirhinus kurzanovi* (Norman, 1998), *Bolong yixianensis* (Wu & Godefroit, 2012) and *Gobihadros mongoliensis* (Tsogtbaatar *et al.*, 2019). The distal end of metacarpal II is expanded dorsally, producing a broadly 'D'-shaped articular surface that ventrally slightly tapers and extends a little onto the surface of the shaft.

**Metacarpal III (left).** Metacarpal III (Fig. 31C, D) is the longest of the metacarpals and extends further distally than the rest when articulated. Proximally the shaft is expanded dorsoventrally to produce a quadrilateral articular surface that is convex in both lateral and dorsal views. The shaft is also broadly quadrilateral in cross-section. The proximal halves of the medial and lateral sides are slightly depressed for articulation with metacarpals II and IV. Viewed dorsally, the lateral margin of the shaft is almost straight until it expands for the lateral condyle, but medially it curves concavely throughout the distal half. This characteristic is also apparent in *Uteodon aphanocetes* (Carpenter & Wilson, 2008), *Magnamanus soriaensis* (Fuentes Vidarte, *et al.* 2016), *Mantellisaurus atherfieldensis* and *Altirhinus kurzanovi* (Norman, 1998). Distally, the shaft is expanded transversely and ventrally to form medial and lateral condyles. They have a dorsoventrally convex articular surface and are divided by an intercondylar groove. The lateral condyle is slightly bigger than the medial condyle and protrudes further distally.

**Metacarpal IV (left).** Metacarpal IV (Fig. 31E, F) is slightly shorter than metacarpal III but similarly robust in its proximal half. Proximally the cross-section of the shaft and the articular surface are rectangular, although the long axis is mediolateral rather than dorsoventral as in metacarpal III. The articular surface is also only minimally convex in lateral and dorsal views, essentially being flat. Viewed dorsally the lateral margin is only very slightly concave, whereas medially it is straight proximally, but distally it curves laterally and concavely, almost halving the transverse width. This is commonly seen in metacarpal IV of iguanodontians, although it is

not usually so pronounced. Examples include *Mantellisaurus atherfieldensis*, *Altirhinus kurzanovi* (Norman, 1998), *Jinzhousaurus yangi* (Wang *et al.*, 2010), *Eolambia caroljonesa* (McDonald, Bird, *et al.*, 2012), *Gobihadros mongoliensis* (Tsogtbaatar *et al.*, 2019), *Plesihadros djadokhtaensis* (Tsogtbaatar *et al.*, 2014) and *Hypacrosaurus altispinus* (Brown, 1913a). It is less marked in *Iguanodon bernissartensis* but absent in *Uteodon aphanocetes* (Carpenter & Wilson, 2018), *Tenontosaurus tilletti* (Forster, 1990), *Magnamanus soriaensis* (Fuentes Vidarte *et al.*, 2016), *Ouranosaurus nigeriensis* (Taquet, 1976) and *Tethyshadros insularis* (Dalla Vecchia, 2009). In dorsal view, the medial and lateral borders of metacarpal IV of *Comptonatus chasei* are almost straight and parallel proximally, while in *Mantellisaurus atherfieldensis* the lateral border is concave. The distal articular surface is a dorsoventrally expanded quadrilateral shape, slightly wider ventrally than dorsally and gently convex in lateral view.

**Metacarpal V (right).** Metacarpal V (Fig. 31G, H) is a moderately robust bone (ratio of proximodistal length to minimum shaft diameter 4.2), and is much shorter than metacarpals II–IV, being less than half their length. The proximal articular surface is gently concave and somewhat oval in outline (long axis dorsoventral), but with a straight margin ventrally. This margin forms the proximal side of a triangular flattened area situated ventrally on the proximal third of the shaft. The shaft twists slightly so that the bisecting line of symmetry of the proximal articular surface is angled at approximately 45° to that of the distal articular surface, the proximal ventral surface facing ventromedially distally. The proximal articular surface in *Comptonatus chasei* is taller dorsoventrally than wide transversely, whereas in *Mantellisaurus atherfieldensis* it is wider than tall. In both, the ratio between the proximodistal length and the mediolateral width of the proximal end is less than 2. Ratios below 2 are commonly found in non-hadrosaurid iguanodontians such as *Iguanodon bernissartensis*, *Ouranosaurus nigeriensis* and *Bactrosaurus johnsoni*, whereas more gracile metacarpals with ratios above 2 are found in hadrosaurids such as *Brachylophosaurus canadensis*, *Corythosaurus casuarius* and *Hypacrosaurus altispinus* (Prieto-Marquez & Wagner, 2009). The distal articular surface is oval in outline but flattened ventromedially. A ventromedial ridge extends posteriorly along the shaft for a short distance.

## Manual phalanges

Unless stated otherwise, the position and side of the manual phalanges assumes a similar arrangement to NHMUK PV R 5764 (Bonsor *et al.*, 2023).

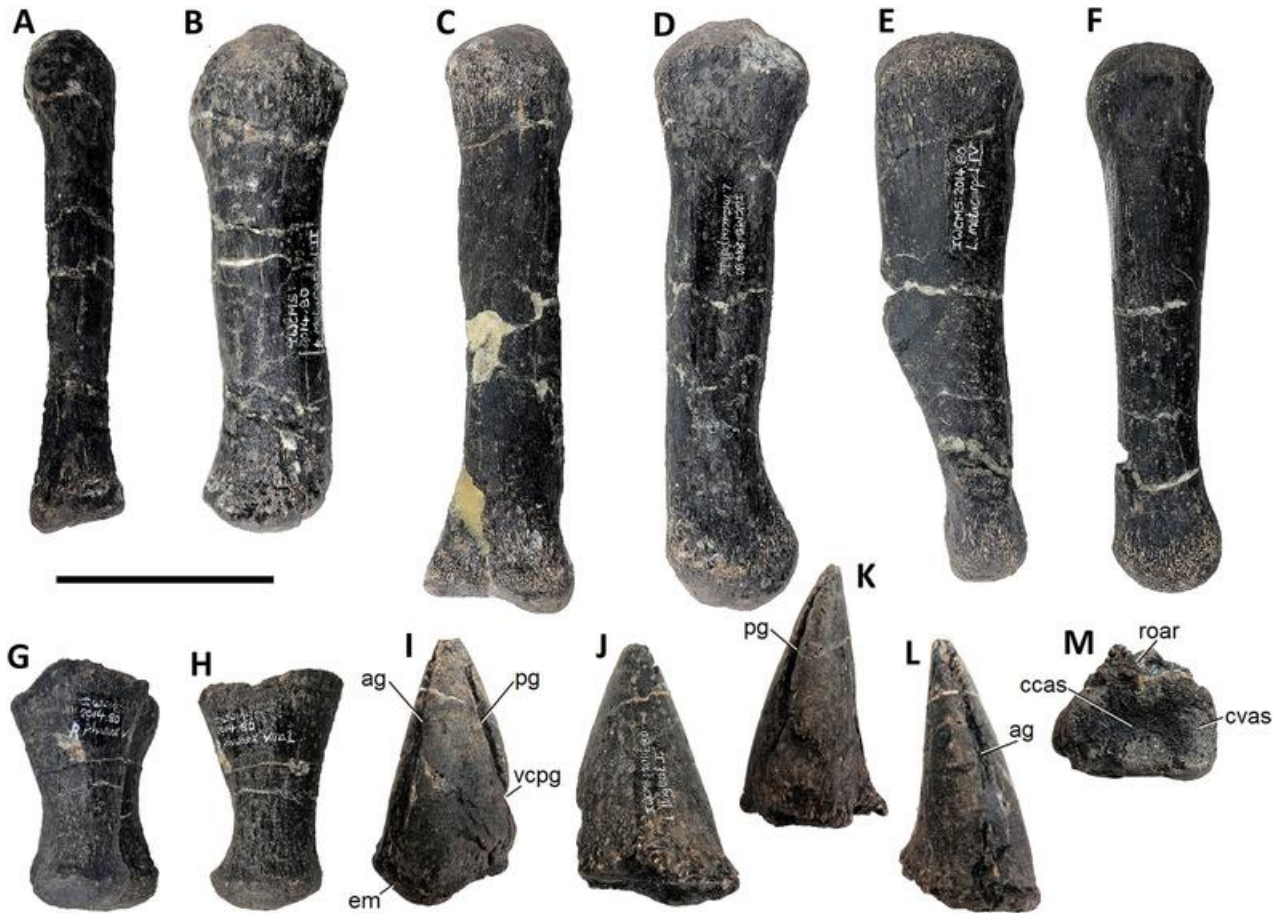


**Figure 32.** *Comptonatus chasei* gen. et sp. nov. (IWCMS 2014.80). Metacarpals (MC) and left pollex. MCII (R) **A**, dorsal, **B**, lateral; MCIII (L) **C**, dorsal, **D**, lateral; MCIV (L) **E**, dorsal, **F**, lateral; MCV (R) **G**, dorsal, **H**, lateral; Pollex (L) **I**, dorsal, **J**, ventral, **K**, posterior, **L**, anterior, **M**, lateral. **Abbreviations:** **ag**, anterior nail groove; **ccas**, concave articular surface; **cvas**, convex articular surface; **em**, everted margin; **pg**, posterior nail groove; **roar**, roughened area; **vcpg**, ventral curvature in posterior nail groove. Scale bar represents 50 mm.

**Ungual phalanges of the pollex.** Both unguinal phalanges of the pollex (Fig. 31I–M) are preserved and are almost mirror images of each other. The exact life orientation of the pollices is difficult to determine in disarticulated specimens, but based on the angle of the distal articular surface of metacarpal I they extended anteromedially at approximately 45° to digits II–IV (as is usually the case in ankylopollexians, in the rare instances where the manus is complete and articulated, such as in *Magnamanus soriaensis* (Fuentes Vidarte et al., 2016); *Iguanodon bernissartensis* (Norman, 1980) and *Bolong yixianensis* (Wu & Godefroit, 2012)). For the purposes of the description, it is assumed that the unguinal grooves are situated on the dorsal (extensor) surface, with the deeper groove sited posteriorly as in *Hypselospinus fittoni* (Norman, 2015, fig. 40), and the raised, roughened area on the articular margin (Fig. 32M, roar), located on the proximal ventral (flexor) surface.

The pollex is subconical but dorsoventrally compressed so that at the midpoint of length the width is 32 mm and the depth 22 mm. This degree of compression contrasts with the more uniform conical shape found in *Iguanodon bernissartensis* (Norman, 1980), although this may be variable (Verdu, Godefroit, et al., 2017, fig. 8). It is similar, however, to that found in *Mantellisaurus atherfieldensis* but is not as pronounced as in *Hypselospinus fittoni* (Norman, 2015). Viewed dorsally, the slightly convex posterior and anterior margins taper distally to a point. There are unguinal grooves positioned close to the margins, with the posterior groove being more pronounced than the anterior. From the distal end, the deeper posterior groove extends laterally but curves ventrally before reaching the proximal articular surface, whereas the anterior groove extends laterally but gradually fades out. Also, in dorsal view the dorsal margin of the articular surface is sinusoidal, being

convex in the anterior half. In anterior and posterior views, the pollex is curved, being convex dorsally and concave ventrally. The articular surface is oval (long axis anteroposterior). It has a concave surface in its posterior two-thirds and an anteroposteriorly convex anterior surface, similar to that shown in Norman's (2015, fig. 40) reconstruction of the manus of *Hypselospinus cf. fittoni*. The roughened area on the flexor surface of the medial margin was presumably a tendinous osteological correlate (Norman, 1980).

**Manual phalanx 1 of digit II (left).** This is a relatively long phalanx, being over half the length of metacarpal II. The proximal end is generally expanded, principally dorsoventrally. The articular surface is very slightly concave. Its ventral, medial and lateral margins are straight and at right-angles to each other, but dorsally the margin is convex and extends dorsolaterally, forming a dorsolateral apex. This raised area extends as a straight ridge along the shaft to the dorsal apex of the distal articular surface. The lateral wall below the ridge is markedly concave proximodistally, especially in ventral view, and slopes ventromedially so that the dorsal ridge overhangs it. The medial wall is dorsoventrally convex and much straighter proximodistally. There is a depressed area situated ventrally on the medial wall just behind the distal articular margin. The distal articular surface is slightly skewed, being arch shaped with two weakly developed prominences ventrally, more so medially. The articular surface is convex dorsoventrally and flat transversely.

**Manual phalanx 2 of digit II (side unknown).** This is a short phalanx, being as long as it is wide, and is slightly dorsoventrally compressed. The proximal articular surface is oval but flattened ventrally and shallowly concave. The shaft is 'D'-shaped in cross-section with the straight surface facing ventrally. The distal articular surface is slightly convex dorsoventrally and concave transversely. The phalanx has near longitudinal symmetry, and its side of origin cannot be determined with certainty.

**Manual phalanx 1 of digit IV (right).** This phalanx is shorter and smaller than phalanx 1 of digit II. The proximal articular surface has a convexly curved dorsolateral margin and slightly concave medial and ventral margins. The distal articular surface is dorsoventrally convex and slightly concave transversely, almost forming medial and lateral condyles. There is a slightly everted margin to both articular surfaces.

### Pelvic girdle

**Ilium.** Both ilia are preserved (Figs 20, 33). The left is in articulation with the sacrum and is missing the

preacetabular process and the anterior section of the ischiadic peduncle. The postacetabular process has been crushed, such that a gutter has formed extending anteroventrally between the dorsal and ventral margins. The right ilium preserves the preacetabular process, pubic peduncle and acetabulum, but the posterior section is incomplete, heavily crushed, and almost brecciated. There is a post-depositional fracture at the midpoint of the preacetabular process, so that in lateral view the distal section slightly underlaps the proximal section. The tip of the process is incomplete, but the losses appear slight.

The preacetabular process is transversely compressed along its length, forming a deep strap-like structure in its proximal half, which lacks the distinctive narrowing of the middle section seen in some iguanodontians such as *Mantellisaurus atherfieldensis*, *Probactrosaurus gobiensis* (Norman, 2002) and *Eolambia caroljonesa* (McDonald, Bird, et al., 2012). Also in lateral view, the process is slightly decurved and extends anteroventrally, the dorsal margin being gently convex and the ventral margin concave. Distally, the concave ventral margin curves convexly, then becomes straighter (Fig. 33B, C), extending more horizontally to form a long, tapering terminal boot-like structure (preacetabular boot *sensu* McDonald, Bird, et al., 2012, ventral flange of others). The length of the boot can be taken as the distance from the inflection point on the ventral margin to the distal tip. The length of the preacetabular boot compared to the overall length of the preacetabular process is c. 43%, which is greater than in *Mantellisaurus atherfieldensis* (28%) and *Brighstoneus simmondsi* (c. 30%) (Lockwood et al., 2021). The angle of inflection in *Comptonatus chasei* is also more obtuse. A boot-shaped distal preacetabular process is commonly found in iguanodontians, being very evident in *Iguanacolossus fortis* (McDonald, Kirkland, et al., 2010), *Eolambia caroljonesa* (McDonald, Bird, et al., 2012), *Ouranosaurus nigeriensis* (Bertoazzo, Della Vecchia, et al., 2017), *Proa valdearinnensis* (McDonald, Espilez, et al., 2012) and *Mantellisaurus atherfieldensis*. Some have more tabulate endings, such as *Tenontosaurus tilletti* (Forster, 1990), *Camptosaurus dispar* (McDonald, 2011), *Bactrosaurus johnsoni* (Godefroit et al., 1998) and *Edmontosaurus annectens* (Brett-Surman & Wagner, 2007), although even when the ending is tabulate, there is often a slight inflection point on the ventral margin. In some, the preacetabular boot exceeds the length of the proximal section, such as in *Tanius sinensis* (Borinder, 2015) and *Hypacrosaurus altispinus* (Brown, 1913a). Viewed dorsally, the preacetabular process also curves anterolaterally as it extends anteroventrally, although the overall degree has been exaggerated by a taphonomic fracture

at the base. At the base of the process, on the medial surface, there is a facet for the transverse process of the first true sacral vertebra, which is deepened dorsally by a buttress. The buttress extends anteriorly along the preacetabular process as a ridge, that in its proximal course divides the medial surface into ventromedial and dorso-medial facing surfaces. At its base, just anterior to the facet, the ventromedial surface forms an angle of *c.* 30° with the transverse plane and occupies 25% of the dorsoventral height of the process. Extending anteriorly, the ridge gradually migrates dorsally, while the ventromedial surface increasingly faces medially. Eventually, near the dorsal margin, the ridge fades out, leaving a nearly flat, medially facing surface, which continues distally as the preacetabular boot. The preacetabular process shows some gentle axial rotation, which commences in the middle section and results in the lateral surface of the preacetabular boot facing slightly dorsolaterally. Axial twisting, when present, typically is in this direction and is seen for example in *Mantellisaurus atherfieldensis*, *Barilium dawsoni* (Norman, 2011b), *Iguanodon bernissartensis* (Norman, 1980), *Ouranosaurus nigeriensis* (Bertozzo, Della Vecchia, et al., 2017), *Bactrosaurus johnsoni* (Godefroit et al., 1998), MPZ 2022/735 an unnamed styracosternan from the Iberian Peninsula (Medrano-Aguado et al., 2023) and *Delapparentia turolensis* (Ruiz-Omeñaca, 2011), but is absent in some iguanodontians, such as *Camptosaurus dispar* (McDonald, 2011), *Hypselospinus fittoni* (Norman, 2015), *Brighstoneus simmondsi* (Lockwood et al., 2021), *Iguanodon galvensis* (Verdu et al., 2015) and *Magnapaulia laticaudus* (Prieto-Marquez et al., 2012). The ridge dividing the medial surface contrasts with *Iguanodon bernissartensis* (Norman, 1980) and *Mantellisaurus atherfieldensis*, where the proximal end of the process is subtriangular in cross-section with an almost horizontal ventral shelf (i.e. the ridge is the ventromedial margin and the angle with the transverse plane is 0°). *Brighstoneus simmondsi* (Lockwood et al., 2021) also lacks a horizontal shelf, the ventromedial surface forming an angle of *c.* 40° with the transverse plane. In dorsal view, the thickness of the dorsal surface of the preacetabular process tapers very slightly as it extends distally. It is transversely rounded but unequally, as the dorsolateral surface is slightly flatter, although it does not form the distinct bevelled edge seen in *Brighstoneus simmondsi* (Lockwood et al., 2021).

The body of the ilium in *Comptonatus chasei* (delineated following the methodology in Prieto-Marquez & Norell [2010], character 234) is slightly longer anteroposteriorly than dorsoventrally. This is similar to *Iguanodon bernissartensis* (Norman, 1980), *Mantellisaurus atherfieldensis*,

*Gilmoreosaurus mongoliensis* (Prieto-Marquez & Norell, 2010) and *Dryosaurus altus* (Gilmore, 1925). Examples where the body is taller than long include *Hypsilophodon foxii* (Galton, 1974), *Zalmoxes shqiperorum* (Godefroit et al., 2009), *Tenontosaurus tilletti* (Ostrom, 1970), *Brighstoneus simmondsi* (Lockwood et al., 2021) and *Jinzhouosaurus yangi* (Wang et al., 2010). The dorsal margin of the body of the ilium is slightly convex in lateral view. In dorsal view it is transversely rounded, moderately rugose and expands in thickness as it extends posteriorly, reaching a maximum at the junction with the postacetabular process (15 mm at the base of the preacetabular process, 43 mm at its maximum). In lateral view, a very gently everted dorsal rim begins at the posterior end of the preacetabular process. This continues posteriorly, eventually expanding dorsoventrally and also becoming maximally deep at the level of the junction between the ischiadic peduncle and the postacetabular process, where it forms a relatively pronounced lateral (supraacetabular) process. The process occupies 29% of the dorsoventral height of the ilium (measured from the dorsal margin to the most ventral part of the ischiadic peduncle). This is considerably more prominent than the more modest lateral processes in *Mantellisaurus atherfieldensis* (16%), and *Brighstoneus simmondsi* (21%). Extending posteriorly beyond the lateral process there is a short upwards step, so that in lateral view the gently convex margin of the postacetabular process is slightly raised above the level of the dorsal margin of the main iliac plate. This is also seen in *Tenontosaurus tilletti* (Forster, 1990), *Hypselospinus fittoni* (Norman, 2015), *Zuoyunlong huangi* (Wang et al., 2015), *Mantellisaurus atherfieldensis*, *Brighstoneus simmondsi* (Lockwood et al., 2021), *Ouranosaurus nigeriensis* (Bertozzo, Della Vecchia, et al., 2017) and *Eolambia caroljonesa* (McDonald, Bird, et al., 2012). In dorsal view, the dorsal surface of the postacetabular process is relatively wide and curves medially. Distally it becomes transversely expanded to a maximum of 77 mm, although this has probably been exaggerated by taphonomic distortion, which has reflected the distal section laterally, creating an anteroventrally orientated furrow distorting the brevis shelf, in what was probably a gently anteroposteriorly concave lateral surface.

The lateral wall of the iliac body is almost flat dorsoventrally, although there is a depressed area anterodorsally, at the base of the preacetabular process. In lateral view the anterior margin of the iliac body is deeply concave, producing an embayment extending from the base of the preacetabular process as a thin ridge of bone, that continues as the anterolateral angle of the pubic peduncle. The pubic peduncle extends anteroventrally and forms an elongate triangle in cross-section with the vertex of the

longest altitude orientated medially. It has a narrow lateral facing surface, a deep anteromedial facing surface which is smooth distally but obscured by the sacrum proximally, and a deep ventroposterolateral facing surface, which is slightly dorsoventrally concave and contributes to the acetabulum. The articular surface of the pubic peduncle is slightly rugose, presumably for attachment of cartilage. The acetabular surface curves to meet the ischiadic peduncle, although the anterior part of this peduncle is not preserved due to recent fracture. In ventral view, the posterior section of the ischiadic peduncle broadens slightly as it extends posteriorly and is also orientated slightly posterolaterally, so that between its posterior margin and the postacetabular process there is a distinct step. Viewed laterally the step continues as a ridge, extending anterodorsally across the lateral surface, before fading out on the body of the ilium. However, the lateral wall of the ischiadic peduncle is essentially flat and lacks a distinct posterolateral boss ('posteroventral protuberance' and 'ischial tuberosity' of some authors). A boss is also absent in *Morelladon beltrani* (Gasulla *et al.*, 2015), *Proa valdearinnensis* (McDonald, Espilez, *et al.*, 2012), *Iguanodon bernissartensis* (Norman, 1980), *Brighstoneus simmondsi* (Lockwood *et al.*, 2021) and *Ouranosaurus nigeriensis* (Taquet, 1976), but present in *Hypselospinus fittoni* (Norman, 2015), *Mantellisaurus atherfieldensis*, *Altirhinus kurzanovi* (Norman, 1998, fig. 32), *Choyrodon barsboldi* (Gates *et al.*, 2018) and *Gilmoresaurus mongoliensis* (Prieto-Marquez & Norell, 2010). Hadrosaurids possess a boss, although the articular surface is also divided by a groove into anterior and posterior segments (Prieto-Marquez & Norell, 2010). The ventral articular surface of the ischiadic peduncle is rugose, and in lateral view, inclined very slightly posterodorsally compared to the dorsal margin of the iliac blade, rather than parallel to the dorsal margin as in *Mantellisaurus atherfieldensis*, and not in line with the postacetabular process, as in *Brighstoneus simmondsi* (Lockwood *et al.*, 2021).

Much of the medial surface of the ilium is obscured by the sacrum, but in dorsal view the medial surface can be seen sloping in a ventromedial direction, to join an anteroposteriorly orientated ridge that is continuous with the buttress over the facet for the transverse process of the first true sacral vertebra. This ridge is further indented by the robust, concave dorsal margins of the facets for the subsequent three transverse process/sacral rib complexes, while the fifth and sixth articulate with the postacetabular process.

**Pubis.** Both pubes (Fig. 34) are preserved but incomplete. The left pubis has undergone some post-depositional transverse compression, but preserves the iliac peduncle, acetabular component, ischial peduncle, obturator canal and the proximal part of the postpubic rod.

The prepubic process is incomplete, although the overall shape of the blade can be deduced (Fig. 34D) with reasonable certainty. The prepubic process and postpubic rod are missing from the right pubis but the acetabular component and peduncles are not distorted.

Posteriorly, the pubis consists of a transversely compressed robust body. In lateral view the posterior surface is concavely curved and contributes to the acetabulum. The acetabular surface principally faces posteriorly but is slightly tilted laterally and has everted margins. Dorsally, the acetabular surface expands transversely to form the posterior surface of the stout iliac peduncle. This projects posterodorsally to support a triangular, rugose dorsal surface for articulation with the pubic peduncle of the ilium. The apex of the triangle continues anteriorly as the dorsal margin of the prepubic process. Ventrally the acetabular surface provides the posterior surface of the smaller ischial peduncle. Anteriorly the ischial peduncle forms the posterior margin of an oval (long axis dorsoventral) obturator foramen. The anterior margin of the obturator foramen is provided by the base of the postpubic rod, from which a small process extends posteriorly forming the ventral margin. This process does not contact the ischial peduncle, although there is little more than a millimetre between them. Anteriorly, the base of the postpubic rod continues as the ventral margin of the prepubic process.

The prepubic process forms a deep, transversely compressed, paddle-shaped blade. The dorsal border of the process is transversely rounded and uniform in thickness until it reaches the anterior third when it rapidly thins to *c.* 4–6 mm (due to fragility, removal of matrix in this section is incomplete). In dorsal view, this border is slightly warped, although overall was probably gently laterally concave. The prepubic process differs in several ways from *Mantellisaurus atherfieldensis*. The posterior constriction or 'neck' of the blade has a similar depth in both specimens but anteriorly the blade is much more expanded dorsoventrally in *Comptonatus chasei*. The dorsoventral expansion of the blade has a more pronounced ventral component in *Comptonatus chasei* and is relatively more pronounced dorsally in *Mantellisaurus atherfieldensis*. The ratio of the maximum estimated depth of the blade (albeit based on reconstruction) to the minimum depth at the posterior constriction of the process in *Comptonatus chasei* is *c.* 2.5, which is greater than in any other non-hadrosaurid iguanodontian of which we are aware. By comparison *Mantellisaurus atherfieldensis* is 1.5. The expansion of the blade of the prepubis also has a pronounced ventral component in *Altirhinus kurzanovi* (Norman, 1998); *Choyrodon barsboldi* (Gates *et al.*, 2018); *Huehucanauhtlus tiquichensis* (Ramirez-Velasco *et al.*,

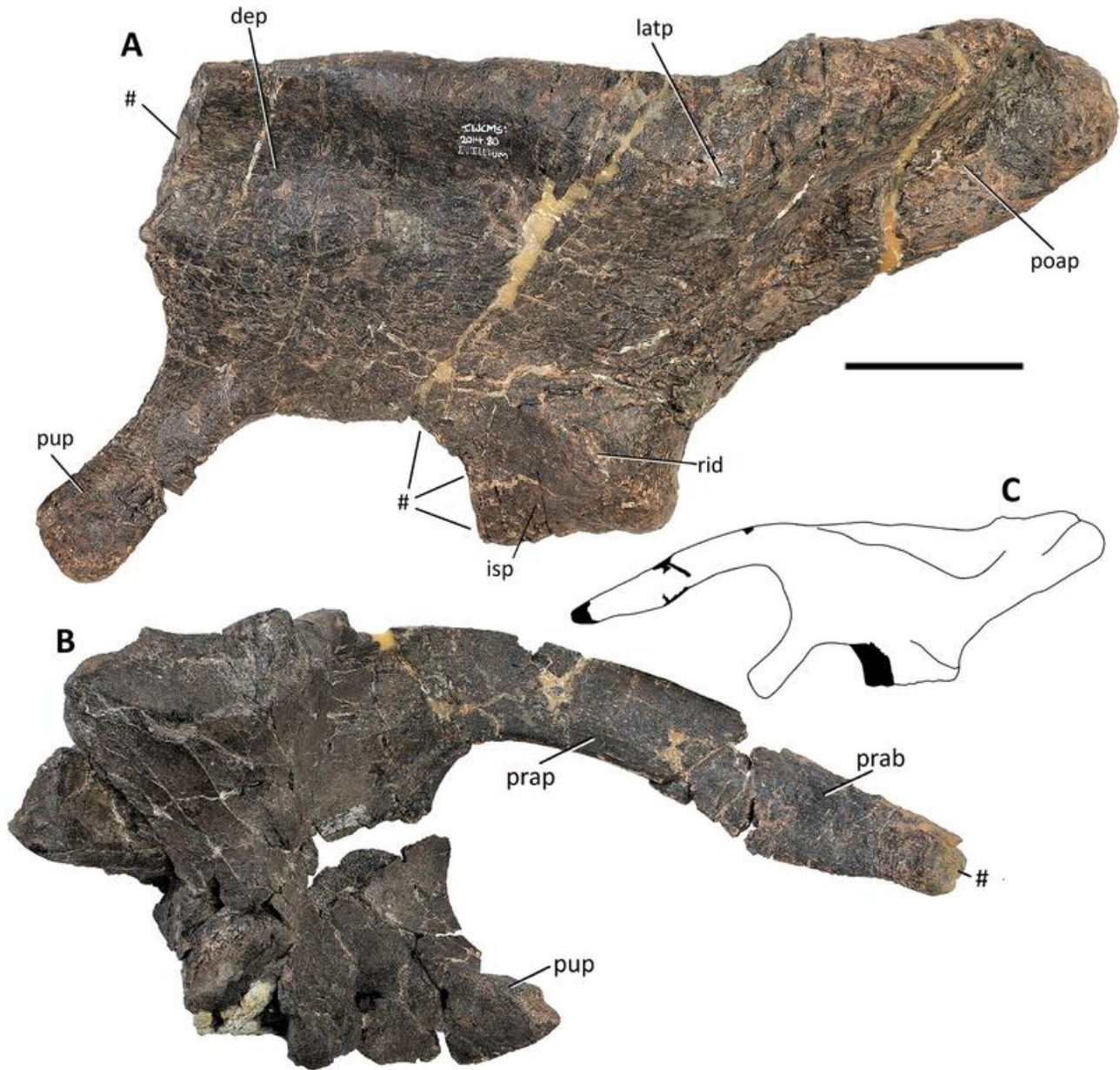


**Figure 33.** *Comptonatus chasei* gen. et sp. nov. (IWCMS 2014.80). Ilium. **A**, left ilium in lateral view, **B**, right ilium in lateral view, **C**, preliminary reconstruction based on right and left ilia. Black areas in reconstruction are unpreserved. **Abbreviations:** **dep**, depressed area; **isp**, ischiadic peduncle; **latp**, lateral process; **poap**, postacetabular process; **prab**, preacetabular boot; **prap**, preacetabular process; **pup**, pubic peduncle; **rid**, ridge; #, fracture surface. Scale bar represents 100 mm.

2012) and some hadrosaurids, for example *Brachylophosaurus canadensis* (Prieto-Marquez, 2001).

**Comment on terminology of the obturator foramen.** The term ‘obturator foramen’ is usually used to refer to the foramen between the postpubic rod and the ischial peduncle of the pubis (e.g. Norman, 1980, 1986, 2015; Taquet, 1976). However, it is also used by some authors for the foramen created by the embayment between the pubic peduncle and obturator process of the

ischium (e.g. Prieto-Marquez, 2001; Prieto-Marquez et al., 2016; Tsogtbaatar et al., 2019). Obturator ‘gutter’ is used for both foramina in *Bactrosaurus johnsoni* (Godefroit et al., 1998) and for the pubic canal by Prieto-Marquez (2010). Notch has also been used for the embayment between the pubic peduncle of the ischium and the obturator process (Wu & Godefroit, 2012; Bertozzo, Dal Sasso, et al., 2017). We use the term obturator foramen for the pubic canal as is usual in avian anatomy and ischiopubic

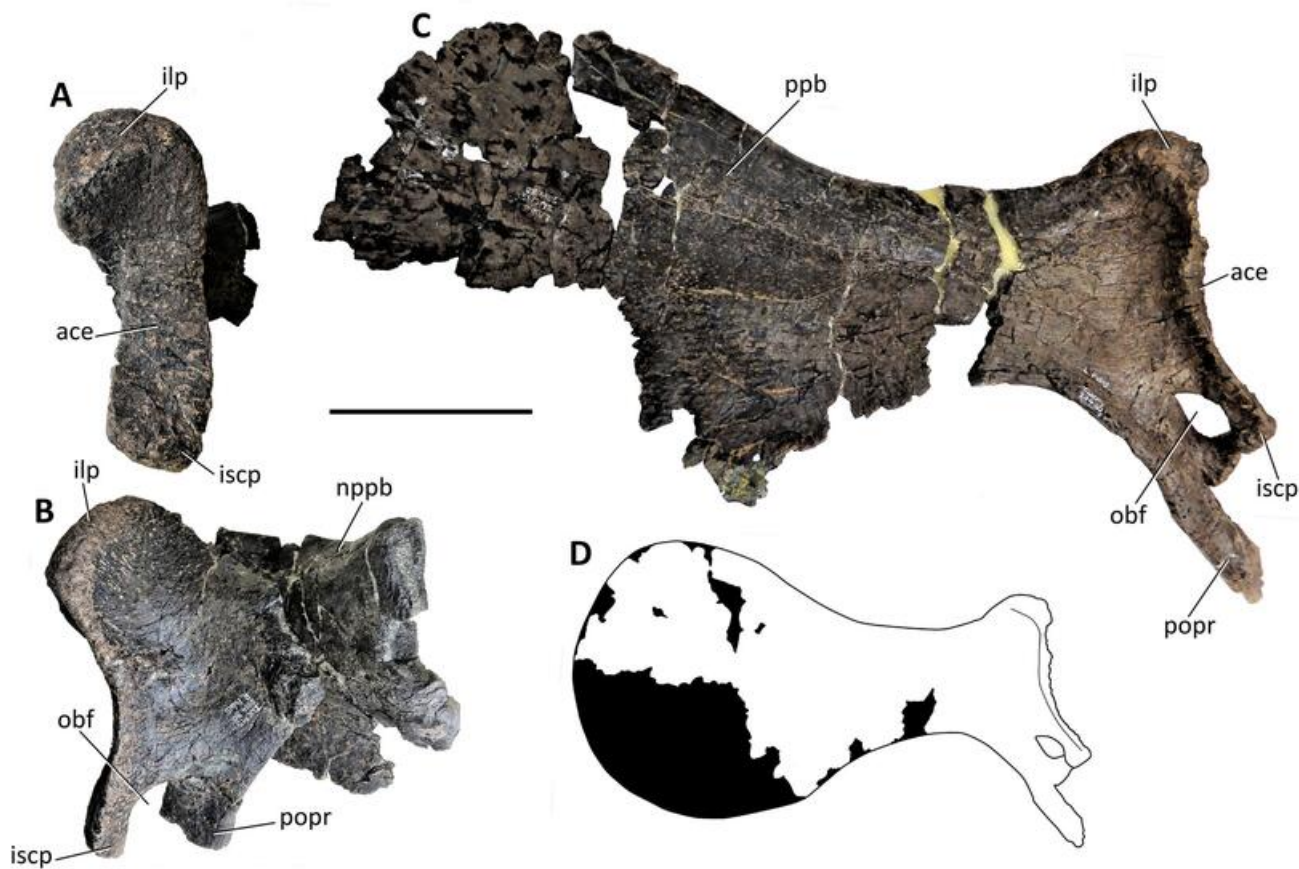


**Figure 34.** *Comptonatus chasei* gen. et sp. nov. (IWCMS 2014.80). Left and right pubes. Right pubis in **A**, posterior and **B**, lateral views, left pubis in **C**, lateral view. **D**, reconstruction of left pubis in lateral view. **Abbreviations:** **ace**, acetabular surface; **ilp**, iliac peduncle; **iscp**, ischial peduncle; **nppb**, neck of prepubic blade; **obf**, obturator foramen; **popr**, postpubic rod; **ppb**, prepubic blade. Scale bar represents 100 mm.

foramen (*sensu* Kinne, 2016), where the obturator process of the ischium contributes to the margin.

**Ischium.** Both ischia (Fig. 35) are preserved. They are described with the long axis of the shaft orientated vertically.

The iliac peduncle extends posterodorsally and is considerably larger and more robust than the pubic peduncle. The articular surface is rugose, faces posterodorsally and is anteroposteriorly elongate, with a rounded posterior margin and a pointed anterior margin. In lateral view the posterodorsal section of the iliac peduncle is further extended posteriorly, to produce a short overhang. This feature is particularly well-developed in lambeosaurines (Brett-Surman & Wagner, 2007; Wagner, 2001), but is also seen in some non-hadrosaurid iguanodontians such as *Tenontosaurus tilletti* (Ostrom, 1970), *Delapparentia turolensis* MPZ 2014/328 (Gasca *et al.*, 2014), *Morelladon beltrani* (Gasulla *et al.*, 2015); *Eolambia caroljonesa* (McDonald, Bird, *et al.*, 2012) and *Gilmoreosaurus mongoliensis* (Prieto-Marquez & Norell, 2010). In lateral view, a transversely thin concave ridge of

bone extends from the pointed anterior end of the iliac peduncle to the pubic peduncle. The lateral surface below this margin provides the ischial contribution to the acetabulum. Anteriorly, the pubic peduncle has a much smaller antero-dorsally facing triangular articular surface, with the apex directed anteroventrally. On the left ischium, a thin, broken process located on the distal end of the pubic peduncle points ventrally towards the obturator process (Fig. 35B, *vee*). The pubic peduncle also has an anteroventral facing surface, which forms an obtuse angle with the articular surface and continues as a thin-walled ‘C’-shaped embayment, which ventrally forms the dorsal margin of the obturator process. The obturator process extends anteriorly, while curving gently laterally to form a cradle for the postpubic rod. In lateral view, the obturator process is deepest at its base and tapers as it extends anteriorly. However, the anterior end is expanded dorsally towards the pubic peduncle (Fig. 35B, *doe*), although this extension is fractured and incomplete (see below).

In lateral view the shaft is essentially straight, although the anterior margin is slightly concave. In the

left ischium the distal section of the shaft has been crushed and distorted, accounting for the degree to which the distal boot curves anteriorly. A straight ischial shaft is commonly seen in iguanodontians, for example in *Morelladon beltrani* (Gasulla et al., 2015), ‘*Dollodon bampingi*’ (Norman, 1986), *Altirhinus kurzanovi* (Norman, 1998), *Choyrodon barsboldi* (Gates et al., 2018), *Eolambia caroljonesa* (McDonald, Bird, et al., 2012) and *Eotrachodon orientalis* (Prieto-Marquez et al., 2016). Anteriorly curved ischial shafts are seen in *Dysalotosaurus lettowvorbecki* (Hübner, 2010) and *Hypselospinus cf. fittoni* (Norman, 2015). In its proximal part the shaft is triangular in cross-section. In lateral view there is a lateral ridge (Fig. 35A, lar) that extends down the shaft of the ischium forming the apex of the triangle and dividing an anterolateral face from a posterolateral face. As this ridge extends ventrally, it migrates increasingly anteriorly, until it forms the anterior margin approximately halfway down the shaft. Distal to this, the surface is gently anteroposteriorly convex and faces laterally, while in cross-section there is also a posteromedial and an anteromedial surface. Viewed medially, the ventral margin of the blade of the obturator process extends as a medial ridge across the shaft (Fig. 35B, mer), angled posteroventrally, to become the posterior margin of the shaft. The combined effect of these ridges is to give the shaft a twisted appearance.

Distally, the ischium expands predominantly anteriorly and is transversely compressed to form the ischial boot. This is over two and half times the width of the shaft. There is a short nubbin of bone at the anterior end of the boot that extends anterodorsally. The ischial boot in *Mantellisaurus atherfieldensis* is preserved, although damaged, but is less developed than in *Comptonatus chasei* and was described by Norman (1998) as being ‘slightly booted’. Other relatively weakly booted taxa include *Dysalotosaurus lettowvorbecki* (Galton, 1980b); *Iguanodon bernissartensis* (Norman, 1980) and *Morelladon beltrani* (Gasulla et al., 2015). Ischial boots more closely resembling *Comptonatus chasei* are found in *Eolambia caroljonesa* (McDonald, Bird, et al., 2012); *Hypselospinus fittoni* (Norman, 2015) and *Ouranosaurus nigeriensis* (Taquet, 1976), although the last two are slightly less well developed. The distal ischium has not preserved in the majority of non-hadrosaurid iguanodontians.

**Comment on dorsoventral extensions of the pubic peduncle and obturator process.** In non-hadrosaurids dorsal extension of the obturator process is not commonly seen, the obturator process usually being a simple tab with a rounded distal margin (although many are damaged and incomplete). Exceptions are *Ouranosaurus nigeriensis* (Taquet, 1976) and especially *Bactrosaurus*

*johnsoni* (Gilmore, 1933), where the obturator process also has a dorsal extension. Gilmore (1933, p. 70) attributed this to intraspecific variation, suggesting that taxa probably had varying degrees of ossification between the obturator process and pubic peduncle and reported that open and closed examples of ischiopubic foramina can be observed in *Camptosaurus*. This suggests that the gap was probably occupied by cartilage in at least some taxa. In hadrosaurids fusion of the obturator process and pubic peduncle, forming an ischiopubic foramen surrounded by bone, may occur in mature individuals (Horner et al., 2004), and is seen in *Eotrachodon orientalis* (Prieto-Marquez et al., 2016); *Brachylophosaurus canadensis* (Prieto-Marquez, 2001) and *Saurolophus osborni* (Brown, 1913b).

### Femur

Only the left femur is preserved (Fig. 36). There is some erosion to the medial surface of the femoral head, the anterior and fourth trochanters are incomplete and there has been some anteroposterior compression of the mid-diaphysis resulting in a gutter where the cortex has collapsed into the medullary cavity.

Proximally, the femur is transversely expanded, with a globular articular head medially and a robust greater trochanter laterally, connected by a narrower waist, giving the whole a saddle-shape. In anterior and posterior views, the femoral shaft is essentially straight except distally, where it curves slightly medially to create a concave medial margin. In lateral and medial views, the dorsal two thirds of the diaphysis are also straight but the ventral third curves posteroventrally towards the massive distal condyles, such that the anterior margin is convex and the posterior margin concave. A very similar curvature is present in ‘*Dollodon bampingi*’ (Norman, 1986) but is absent in *Ouranosaurus nigeriensis* (Bertozzo, Della Vecchia, et al., 2017); *Iguanodon bernissartensis* (Norman, 1980); *Brighstoneus simmondsi* (Lockwood et al., 2021) and *Mantellisaurus atherfieldensis* (Bonsor et al., 2023). The diaphysis is anteroposteriorly compressed, and broadest in anterior and posterior views.

The greater trochanter extends slightly more dorsally than the femoral head. In posterior view there is a groove extending ventrolaterally from the medial margin of the femoral head towards the diaphysis, that is initially narrow and deep, but rapidly becomes shallow and fades out after 45 mm. This has been suggested as a channel for the ligament of the head of femur (Forster, 1990). Only the base of the anterior (lesser) trochanter has survived. It is transversely compressed and is thinner posteriorly than anteriorly. There is a cleft separating the anterior trochanter from the greater trochanter. The anterior margin of the anterior trochanter continues

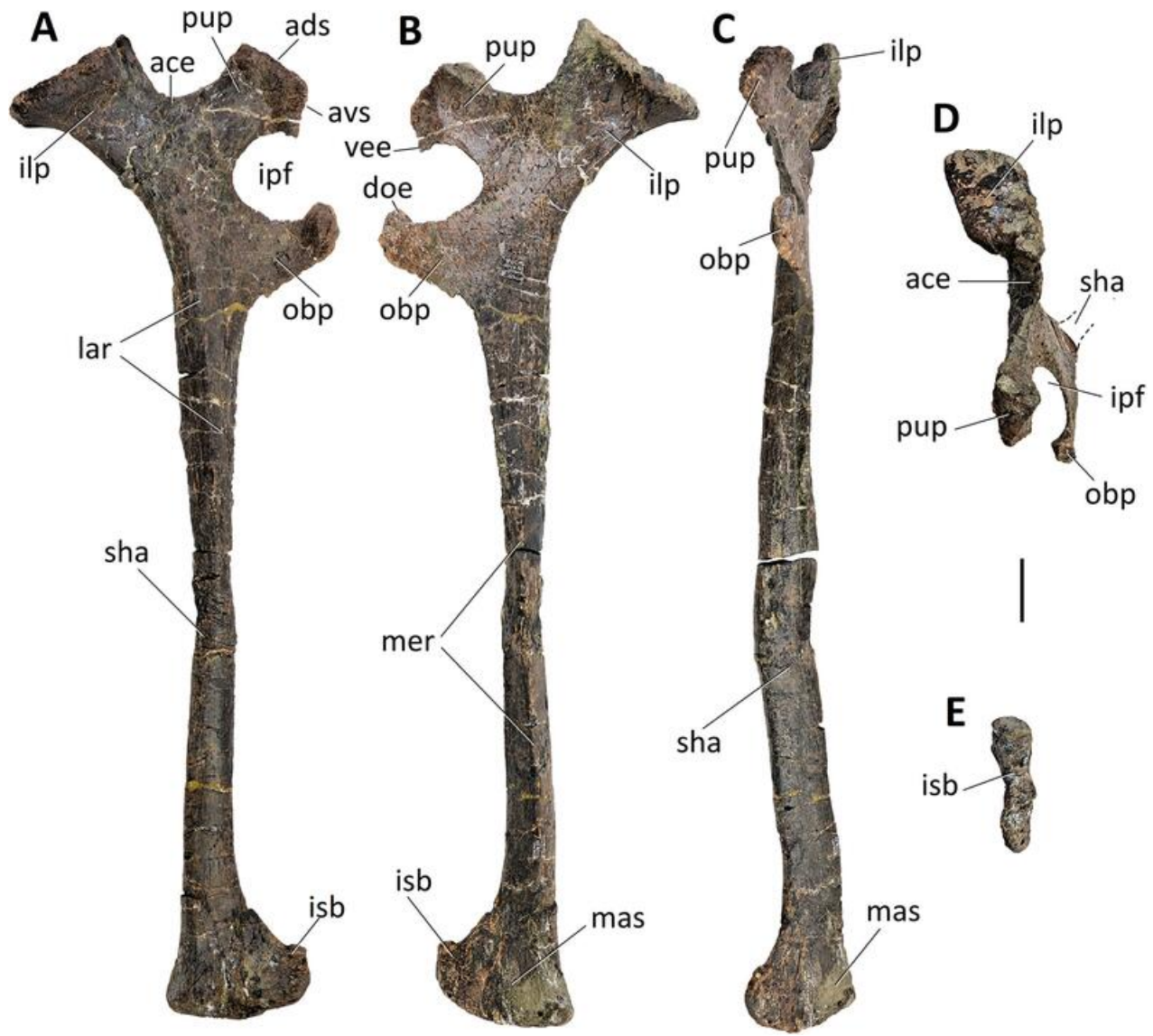


**Figure 35.** *Comptonatus chasei* gen. et sp. nov. IWCMS 2014.80. Right ischium in **A**, lateral, **B**, medial, **C**, anterior, **D**, dorsal and **E**, ventral views. **Abbreviations:** **ace**, acetabular surface; **ads**, anterodorsal surface of pubic peduncle; **avs**, anteroventral surface of pubic peduncle; **doe**, dorsal extension of obturator process; **ilp**, iliac peduncle; **ipf**, ischiopubic foramen; **isb**, ischial boot; **lar**, lateral ridge; **mas**, medial articular surface; **mer**, medial ridge; **obp**, obturator process; **pup**, pubic peduncle; **sha**, shaft; **vee**, ventral extension of pubic peduncle. Scale bar represents 50 mm.

ventrally as a pronounced rounded ridge that extends diagonally across the shaft of the femur towards the medial condyle, gradually becoming less prominent. The fourth trochanter is situated posteriorly, predominantly but not exclusively on the dorsal half of the femoral mid-shaft. It is transversely compressed and forms an elongate triangle (Fig. 36B, C) with the apex dorsally, although the distal section is broken, so it is unknown if the trochanter was pendent. Anterior to the medial side of the fourth trochanter is a slight depression on the diaphysis that extends onto the trochanter and provided the area of attachment for the caudifemoralis longus

muscle (Norman, 1986). Anterior to the fourth trochanter on the lateral side is a deep gutter, extending dorsally and ventrally, which represents a taphonomic area of collapse. The distal femur is expanded both transversely and anteroposteriorly, being most marked posteriorly, to form an articular surface composed of medial and lateral condyles. Anteriorly these two condyles are separated by the extensor intercondylar groove, which essentially forms a tube, being very nearly enclosed anteriorly by the curved margins of the condyles, which are barely separated by *c.* 2 mm. Ventrally, the two condyles are separated by a narrow waisted region with

rugose ridges orientated anterolaterally, while the rugosities on the condylar articular surfaces are predominantly orientated transversely but fade laterally on the medial condyle. Posteriorly, the condyles extend posteriorly, forming massive heel-like buttresses, which are separated by the deep flexor intercondylar groove. The groove is slightly narrower than the extensor groove but apart from a slight bulge on the lateral wall of the medial condyle, it is open posteriorly. The medial condyle is much larger than the lateral condyle, the latter being transversely compressed posteriorly to form a condylid (Fig. 36A, cd). Lateral to the condylid is a wide groove to accommodate the insertion tendon of the iliofibularis muscle (Madzia et al., 2020).

**Comments on the extensor intercondylar groove.** This tube enclosed the insertion tendon of the iliotibialis muscle, which attached to the cnemial crest of the tibia (Godefroit et al. 1998). Early diverging iguanodontian taxa tend to have widely open extensor grooves, such as *Cumnoria prestwichii* (Maidment et al., 2022); *Dysalotosaurus lettowvorbecki* (Hübner, 2010); *Uteodon aphanocetes* (Carpenter & Wilson, 2008); *Valdosaurus canaliculatus* (Barrett et al., 2011) and *Tenontosaurus till-etti* (Forster, 1990), while still substantially open grooves

but with curved margins are present in *Barilium dawsoni* (Norman, 2011b); *Mantellisaurus atherfieldensis* and *Ouranosaurus nigeriensis* (Bertozzo, Della Vecchia, et al., 2017; Taquet, 1976). The extensor intercondylar groove is closed or almost closed in *Gobihadros mongoliensis* (Tsogtbaatar et al., 2019); *Telmatosaurus transsylvanicus* (Weishampel et al., 1993) and *Orthomerus dolloi* (Madzia et al., 2020). The taxonomic utility of this character has yet to be fully established in iguanodontians. It is always closed in *Telmatosaurus transsylvanicus* and *Bactrosaurus johnsoni*, even in immature animals (Brett-Surman & Wagner, 2007; Godefroit et al., 1998) and Weishampel & Horner (1990) considered it species specific and not ontogenetic in hadrosaurids. In *Maiasaura peeblesorum* increased closure may have developed during ontogeny (Brett-Surman & Wagner, 2007; Dilkes, 1993).

### Tibia

Both tibiae are preserved (Fig. 37). The left has undergone some taphonomic crushing and distortion. The right tibia is better preserved but has lost the majority of the cnemial crest and the lateral (fibular) condyle.

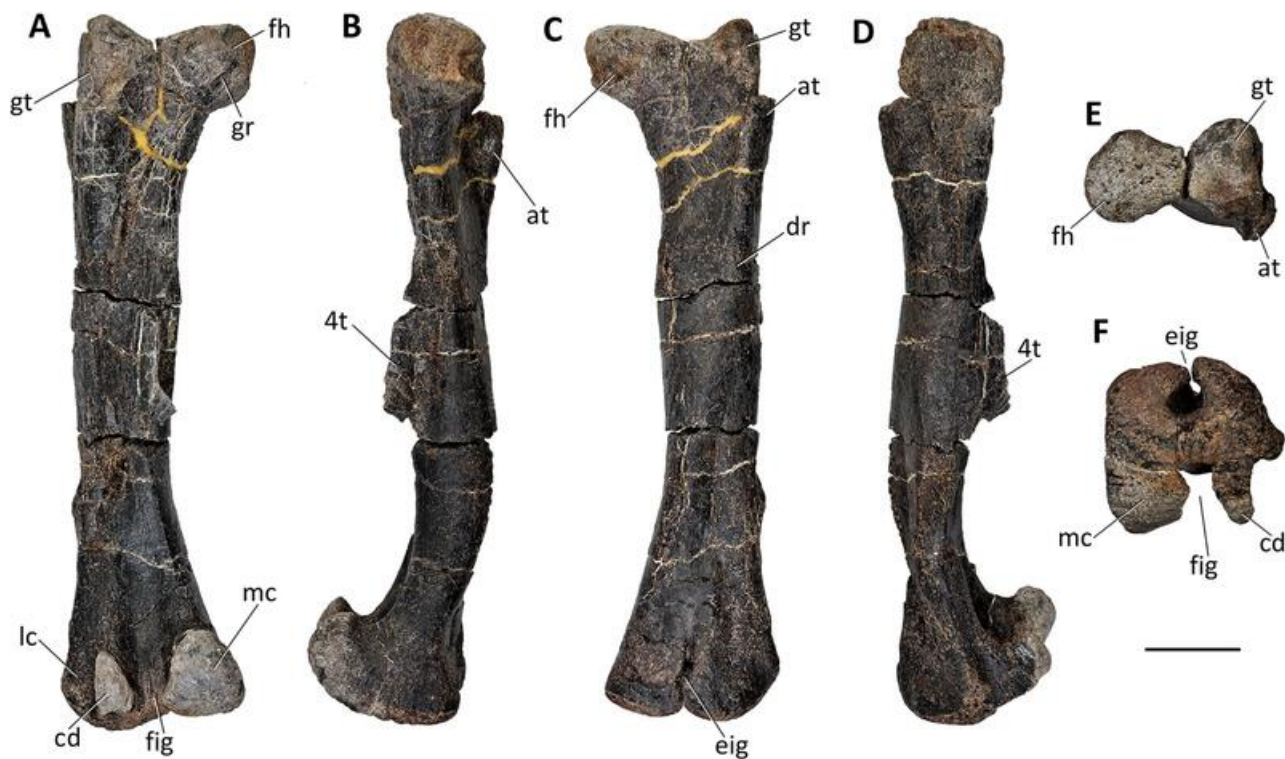


**Figure 36.** *Comptonatus chasei* gen. et sp. nov. (IWCMS 2014.80). Left femur in **A**, posterior, **B**, medial, **C**, anterior, **D**, lateral, **E**, proximal and **F**, distal views. **Abbreviations:** at, anterior trochanter; cd, condylid; dr, diagonal ridge; eig, extensor intercondylar groove; fh, femoral head; fig, flexor intercondylar groove; gr, groove; gt, greater trochanter; lc, lateral condyle; mc, medial condyle; 4t, fourth trochanter. Scale bar represents 100 mm.

The tibia appears to be axially twisted, being transversely compressed and anteroposteriorly expanded at its proximal end and anteroposteriorly compressed and transversely expanded at the distal end. The proximal articular surface is deeply rugose and slightly convex in lateral view, but almost flat transversely. In proximal view the medial margin of the articular surface is convex (it is slightly concave in the left tibia, but this appears to be secondary to taphonomic crushing). There is a boss situated centrally on the medial surface (Fig. 37E, mb), where it abuts the dorsal margin, that is more prominent in the better-preserved right tibia, but partially abraded on the left, although a feature of both. Such a boss, as far as we are aware, is not described in other non-hadrosaurid iguanodontian tibiae so appears autapomorphic and may represent a pronounced osteological correlate for the site of attachment of the medial collateral ligament. The lateral surface has two condyles separated by a cleft-like groove; a centrally placed lateral condyle which extends posterolaterally and has a convex anterolateral surface for articulation with the fibula and an internal condyle that also extends posterolaterally but is larger than the lateral condyle and in lateral view projects well beyond the posterior surface of the

shaft. Anteriorly, the expanded proximal end of the tibia curves laterally and becomes transversely compressed, forming the cnemial crest. The cnemial crest is relatively short, only extending a small distance down the anterior surface of the tibia before continuing as a ridge which extends down the shaft towards the medial malleolus, fading before it reaches it. This morphology is typical of early diverging iguanodontians such as *Camptosaurus dispar* (Gilmore, 1909), *Dysalotosaurus lettowvorbecki* (Hübner, 2010), *Tenontosaurus tilletti* (Forster, 1990), *Barilium dawsoni* (Norman, 2011b), *Mantellisaurus atherfieldensis* (Bonsor *et al.*, 2023), *Iguanodon bernissartensis* (Norman, 1980), *Ouranosaurus nigeriensis* (Taquet, 1976), *Oblitosaurus bunnueli* (Sanchez-Fenollosa *et al.*, 2023) and *Draconyx loureiroi* (Rotatori *et al.*, 2022). In more deeply nested taxa such as *Gilmoreosaurus mongoliensis* (Prieto-Marquez & Norell, 2010) the crest often extends further distally down the tibial shaft and in *Gobihadros mongoliensis* (Tsogtbaatar *et al.*, 2019) and the hadrosaurids it frequently extends onto the distal half of the tibial shaft (Prieto-Marquez & Norell, 2010). In its distal half, the shaft of the tibia has a 'D'-shaped cross-section with the flat surface facing anteriorly.

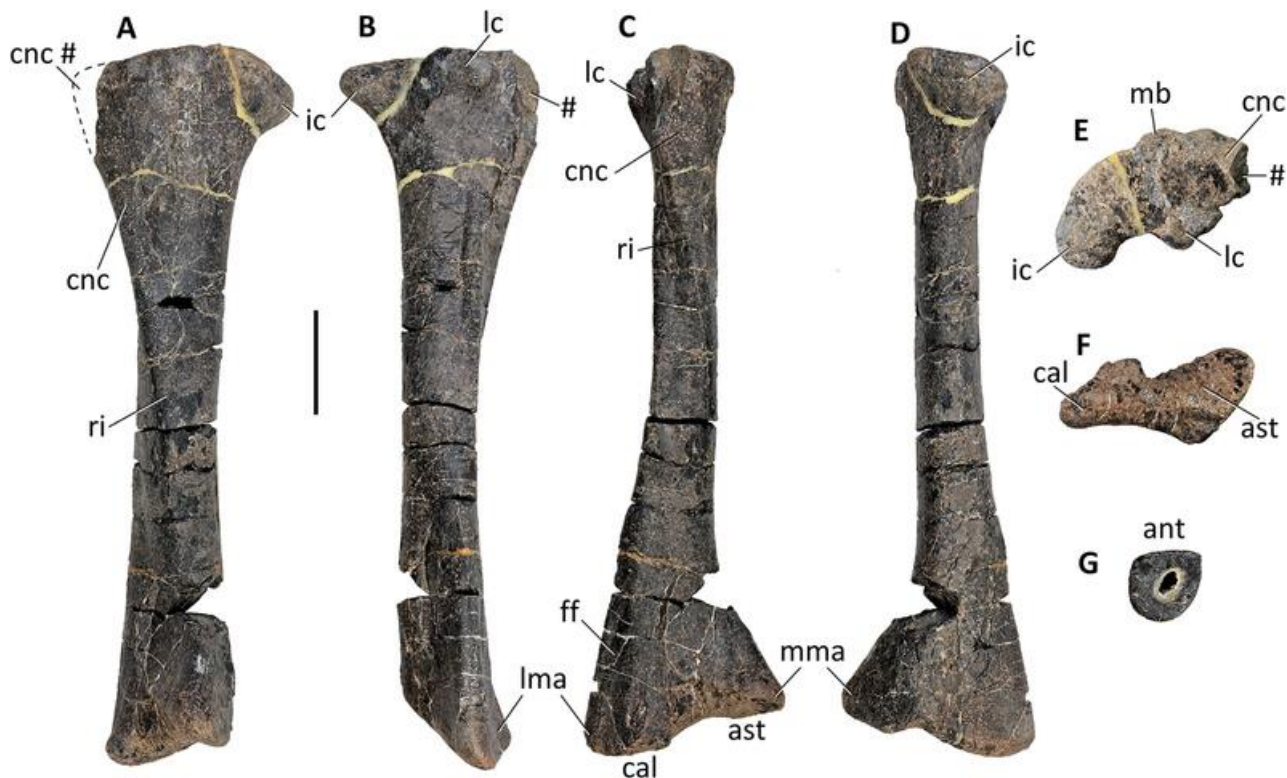


**Figure 37.** *Comptonatus chasei* gen. et sp. nov. (IWCMS 2014.80). Right tibia in **A**, medial, **B**, lateral, **C**, anterior, **D**, posterior, **E**, proximal, **F**, distal views and **G**, transverse section mid-shaft. **Abbreviations:** ant, anterior; ast, articular surface for astragalus; cal, articular surface for calcaneum; cnc, cnemial crest; ff, fibular facet; ic, internal (medial) condyle; lc, lateral condyle; lma, lateral malleolus; mb, medial boss; mma, medial malleolus; ri, ridge of cnemial crest; #, fracture surface. Scale bar represents 100 mm.

The distal end of the tibia is divided into medial and lateral malleoli which articulate with the astragalus and calcaneum respectively. The lateral malleolus extends further ventrally than the medial malleolus. The anterolateral aspect of the lateral malleolus has a long, dorsoventrally extending, rectangular facet for articulation with the distal fibula. This facet is essentially flat but has minimal transverse concavity. It is positioned more anteriorly than the anterior surface of the medial malleolus, producing a step between the two, and distally between the two malleoli is a depressed area, extending onto the distal articular surface, that receives the anterior ascending process of the astragalus. In ventral view, there is a flat oval-shaped surface medially which extends laterally, developing a waist due to the wide but shallow depressed area anteriorly for the ascending process of the astragalus, and a smaller but deeper excavation posteriorly, also for the astragalus. Laterally is a subtriangular area for articulation with the tibial surface of the calcaneum.

### Fibula

Both fibulae are preserved and are complete (Fig. 38). There is slight taphonomic crushing and fracturing along the diaphyses of both specimens. The fibula is an elongate, transversely compressed bone that is expanded at both ends although this is considerably more pronounced proximally. In dorsal view, the articular surface is crescent-shaped and rugose. The lateral margin of the articular surface is convex and the medial margin concave for articulation with the lateral condyle of the tibia. In lateral view, although the whole proximal third of the fibula is expanded, this is most marked at the anterodorsal corner, which projects anteriorly as the ‘anterior wing’ of the fibula. The diaphysis of the fibula is transversely compressed and is convex on its lateral surface and essentially flat on its medial surface. In lateral view it gradually tapers as it extends distally, reaching its narrowest anteroposterior diameter at the junction between the dorsal two thirds and the ventral third where it is 30% of the maximal proximal diameter. The distal end

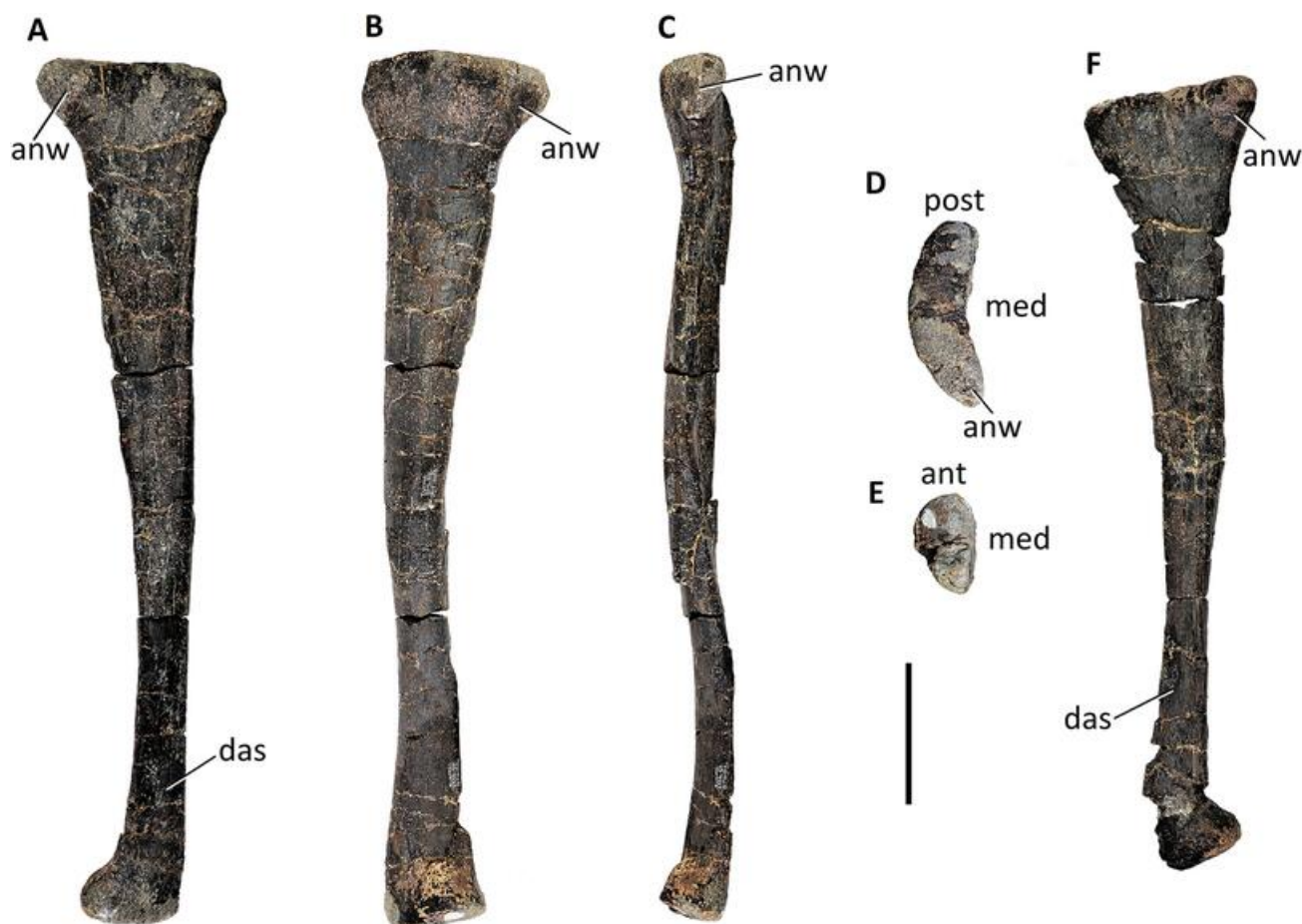


**Figure 38.** *Comptonatus chasei* gen. et sp. nov. (IWCMS 2014.80). Both fibulae. Right fibula in **A**, medial, **B**, lateral, **C**, anterior, **D**, proximal and **E**, distal views; left fibula in **F**, medial view. **Abbreviations:** **ant**, anterior; **anw**, anterior fibular wing; **das**, distal articular surface for tibia; **med**, medial; **post**, posterior. Scale bar represents 100 mm.

of the fibula is also expanded, especially anteriorly, but to a lesser degree than the proximal end. There is a prominence on the distal anterolateral surface, so that in ventral view the articular surface is somewhat teardrop-shaped, being transversely deeper anteriorly. The distal medial surface of the fibula is flat with dorsoventrally orientated striations, where it articulates with the tibia.

### The tarsus

**The proximal tarsus.** Both astragali are preserved (Fig. 39) but the calcaneal elements are missing. The lateral part of both astragali are fractured surfaces, so the calcanei may have been fused to them, but both are disarticulated and show no evidence that they were fused to the tibiae. The astragalus is the larger element of the proximal tarsus and articulates with the medial and much of the lateral malleoli of the tibia. Medially, the distal articular surface forms an anteroposteriorly convex, subcircular surface with a flattened medial margin. Laterally the astragalus narrows to produce a waist before expanding a little, where it articulates with the lateral malleolus of the tibia. The proximal articular surface has a large flat area for articulation with the medial malleolus of the tibia, although the posteromedial margin extends dorsally to form a robust process which articulates with a triangular depression on the posterior surface of the tibia (Fig. 39K). Anteriorly the proximal margin gradually ascends dorsally as it extends laterally, to form the ascending process of the astragalus, which is less robust than the posterior process, and articulates with a relatively shallow, but broad depression on the distal anterior tibial surface (Fig. 39H). Laterally the proximal surface of the astragalus is deeply excavated, producing a step to accommodate the lateral malleolus of the tibia, which extends further distally than the medial malleolus.

**The distal tarsus.** Distal tarsals II, III and IV, which normally articulate with the proximal articular surfaces of the metatarsals have not preserved as they have in *Iguanodon bernissartensis* (Norman, 1980), and distal tarsal III in *Mantellisaurus atherfieldensis*. However, there are subcircular concavities (Fig. 40G, H) on the articular surfaces of metatarsals II, III and IV, which suggest they were originally either present or failed to ossify.

### Pedes

Several bones from both pedes are preserved (Fig. 40). The metatarsalia are described with their long axes orientated dorsoventrally and the phalanges with the pes orientated horizontally with the flexor surface facing

ventrally. Detailed photographs of all elements are figured in the [Supplemental material \(S1, figs S104–120\)](#).

**Metatarsal II (left and right).** The proximal end of metatarsal II is transversely compressed and anteroposteriorly expanded. The articular surface in dorsal view forms an elongate rectangle, but with slightly sinusoidal medial and lateral margins, being gently convex in the anterior half and concave in the posterior half on both sides. The anterior part of the articular surface is depressed by a slight concavity, possibly for articulation with distal tarsal II. In medial view the expansion is more prominent anteriorly, producing a beak-like process that overhangs the shaft, making the anterior margin more concave than the posterior margin. Proximally the medial and anterior surfaces are strongly striated for ligamentous attachment. There is a shard of fractured bone attached to the medial surface of the proximal end of metatarsal II by a thin layer of probable calcite. This possibly represents a fragment of metatarsal I, although is indeterminate. A metatarsal I is present in *Camptosaurus dispar* (Galton & Powell, 1980; Gilmore, 1909); *Tenontosaurus dossi* (Winkler *et al.*, 1997) and *Tenontosaurus tilletti* (Forster, 1990), with a more vestigial form found in *Iguanodon bernissartensis* (Norman, 1980); *Draconyx loureiroi* (Rotatori *et al.*, 2022); *Cumnoria prestwichii* (Maidment *et al.*, 2022) and *Dysalotosaurus lettowvorbecki* (Janensch, 1955). Proximally the lateral surface is appressed against the surface of metatarsal III. The shaft is contracted and transversely compressed but develops a flange on its anterolateral border slightly ventral to the midpoint, which overlaps the anteromedial shaft of metatarsal III. Distal to the flange the shaft extends ventromedially (presumably to accommodate a transversely widening metatarsal III, although this has not preserved), before expanding to form a smooth, convex articular surface. In distal view the anterior margin is slightly convex and posteriorly are two poorly defined condyles. Distally the medial surface is flat but laterally, there is a well-developed concavity, which probably articulated with metatarsal III.

**Metatarsal III (left).** In dorsal view the articular surface of the proximal end of metatarsal III is roughly quadrilateral. The medial margin is slightly sinusoidal, being gently concave anteriorly and convex posteriorly and articulates with metatarsal II. The lateral margin is also sinusoidal, being convex over the middle and anterior sections but concave posteriorly. The posterior concavity extends a short distance ventrally onto the shaft and is bounded posteriorly by a low dorsoventrally orientated ridge of bone. This depression accepts the convexly curved posterior medial surface of metatarsal IV, the curvature and bony ridge presumably bracing

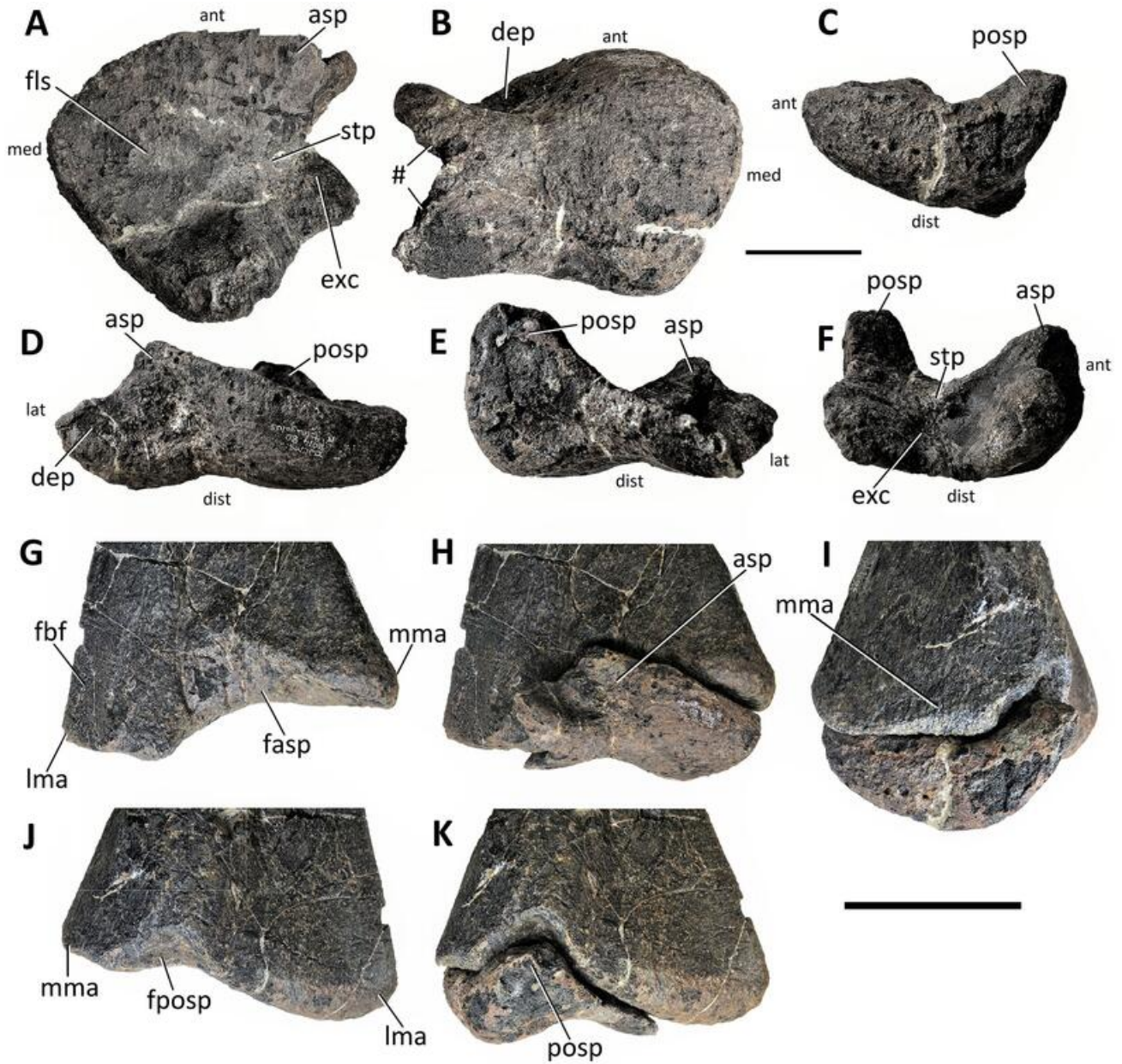


**Figure 39.** *Comptonatus chasei* gen. et sp. nov. (IWCMS 2014.80). Right astragalus isolated (A–F) and showing articulation with distal right tibia (G–K). Right astragalus in A, proximal, B, distal, C, medial, D, anterior, E, posterior, and F, lateral. Distal tibia in G, anterior, H, anterior with astragalus, I, medial with astragalus, J, posterior and K, posterior with astragalus. **Abbreviations:** asp, ascending process; dep, depression; exc, excavation; fasp, facet for ascending process; fbf, fibular facet; fls, flat surface; fposp, facet for posterior process; lma, lateral malleolus; mma, medial malleolus; postp, posterior process; stp, step; #, fractured surface. Small lettering ant, anterior; med, medial; lat, lateral; dist, distal. Scale bar (A–F) represents 50 mm, (G–K) 100 mm.

metatarsal IV against anteroposterior movement. The proximal articular surface is shallowly concave centrally, possibly for articulation with a distal tarsal III. Extending distally the shaft becomes anteroposteriorly compressed, forming an oval cross-section (long axis transverse). The distal half of the metatarsal is missing.

**Metatarsal IV (left).** The proximal articular surface of metatarsal IV is broadly ‘D’-shaped but smaller than metatarsal III. The straighter edge of the ‘D’ faces medially and is quite strongly sinusoidal, being concave anteriorly and convex posteriorly. There is a relatively deep central concavity on the articular surface, possibly for articulation with the fourth distal tarsal. Some of the mid-shaft is missing

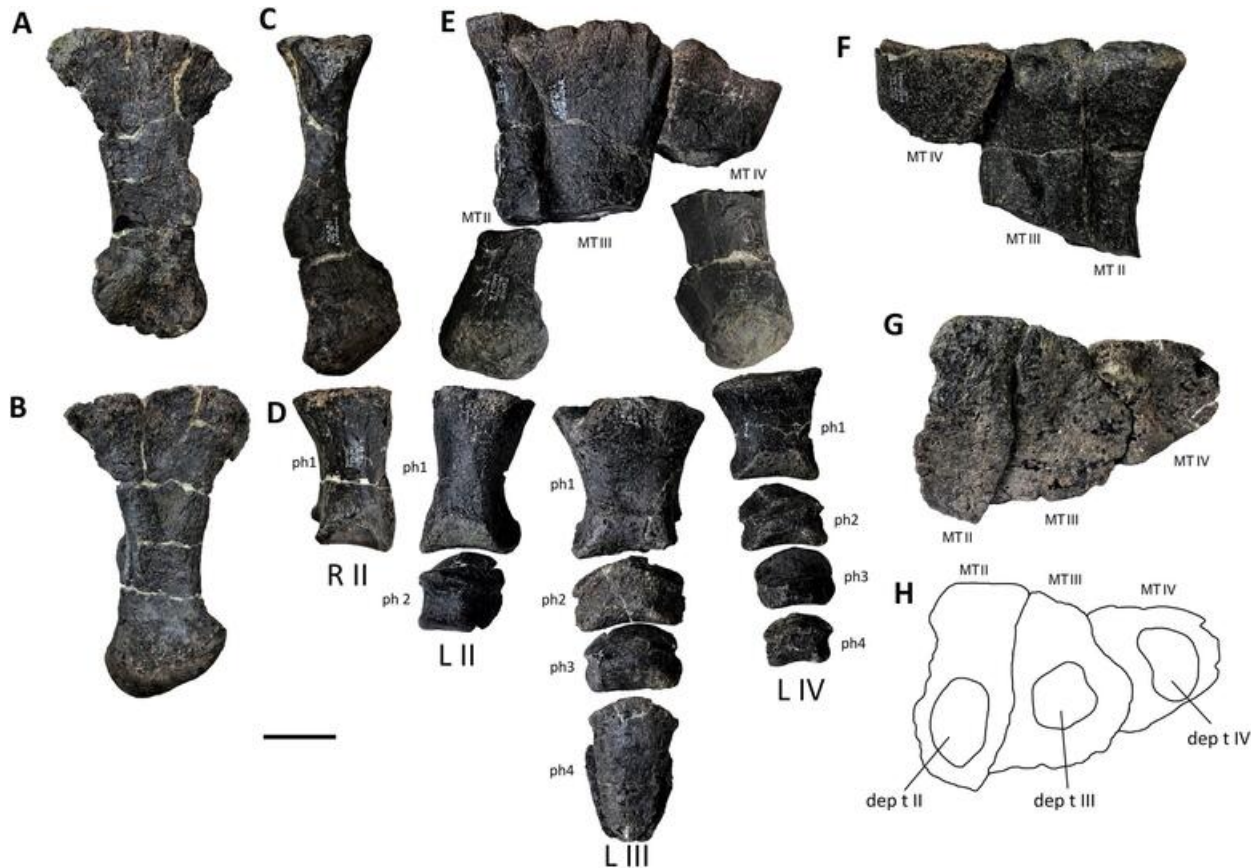


**Figure 40.** *Comptonatus chasei* gen. et sp. nov. Metatarsals and pes. Right MT II in **A**, medial, **B**, lateral and **C**, anterior views; **D**, phalanx 1 digit IV R in dorsal view; **E**, left pes in dorsal view; Left MT 2–4 in **F**, posterior view and **G**, dorsal view; **H**, drawing of **G** to show depressed areas presumably for distal tarsals I–III, **Abbreviations:** **dep**, depressed area; **MT**, metatarsal; **ph**, phalanx; **t**, distal tarsal. Scale bar represents 50 mm.

but it probably extended ventrolaterally and lost contact with metatarsal III for some of its length as in *Camptosaurus dispar* (Gilmore, 1909); *Proactrosaurus gobiensis* (Norman, 2002), *Mantellisaurus atherfieldensis*, *Gobihadros mongoliensis* (Tsogtbaatar et al., 2019); *Bactrosaurus johnsoni* (Gilmore, 1933) and *Hypacrosaurus altispinus* (Brown, 1913a). The distal end of metatarsal IV has an anteroposteriorly convex articular surface, which extends onto the anterior surface and is grooved posteriorly to form two condyles. The lateral condyle is larger than the medial, although the medial is incomplete. Distally, the medial surface like the lateral surface of metatarsal II is concave and presumably articulated with metatarsal III. The lateral surface has a pronounced circular depression, reminiscent of the insertion pit for collateral ligaments found in theropod pedal phalanges.

**Pedal digits.** It is difficult to identify the side of some of the more distal phalanges with certainty although most fit well together as part of the left pes, and the remaining two bones, phalanx II-1 and ungual phalanx III-4 have a

slightly different preservation. The pedes are incomplete but consistent with the iguanodontian phalangeal formula of 0, 3, 4, 5, 0 (Moreno et al., 2007).

**Digit II, pedal phalanx 1 (left and right).** Phalanx 1 of digit II is longer and more gracile than the robust first phalanges of digits III and IV, being almost twice as long as wide in dorsal view, whereas the latter two are more equidimensional. The proximal articular surface is approximately ‘D’-shaped with the straight margin situated laterally, adjoining the phalanx 1 of digit III, and the convex margin forming the medial outer border, while the ventral margin is slightly concave. The proximal articular surface is gently concave. The shaft is waisted, so that in dorsal view the margins are concave, more so laterally. The dorsal surface is transversely convex and the ventral surface almost flat. Distally is a trochlear, the articular surface extending onto the dorsal and ventral surfaces and being transversely wider ventrally. Distally the medial and lateral surfaces are depressed to form shallow pits for ligament or tendon insertion.

**Digit II, pedal phalanx 2 (left).** Phalanx 2 is quite a stout bone, that is almost square in dorsal view and relatively longer than the second phalanx in digits III and IV which are rectangular with a transverse long axis. The proximal articular surface is dorsoventrally concave and almost flat transversely. Distally the articular surface is trochlea-shaped and dorsoventrally convex. The distal lateral and medial walls have circular depressions for ligament or tendon attachment.

**Digit III, pedal phalanx 1 (probably left).** Phalanx I of digit III is the most robust and transversely wide of the first row of phalanges. This phalanx is almost bilaterally symmetrical so the side cannot be determined with certainty, although the distal articular surface extends further onto the dorsal surface on one side, which in the first phalanges of digit II and IV is medial, therefore making this probably a left-sided specimen. The proximal articular surface is sub-oval in shape (long axis transverse) with a flattened ventral margin, which extends as a flattened area on the proximal ventral surface of the shaft, presumably for the attachment of a strong flexor tendon. The articular surface is slightly concave. The shaft is contracted dorsoventrally and transversely. Distally is a trochlea, which is transversely slightly wider ventrally than dorsally. Slight depressions are present on the distal medial and lateral surfaces.

**Digit III, pedal phalanges 2 and 3 (left).** Phalanges 2 and 3 of digit III are short bones, approximately twice as wide as long. The proximal articular surfaces are dorsoventrally concave and slightly transversely convex. The distal articular surfaces are somewhat trochlea shaped, dorsoventrally convex and slightly transversely concave. Phalanx 3 is smaller than phalanx 2.

**Digit III, Ungual phalanx 4 (left and right).** The unguinal phalanges are preserved on both sides. They are dorsoventrally compressed so that the proximal articular surface is oval, the surface being almost flat transversely but deeply concave dorsoventrally. The dorsal surface is both convex transversely and proximodistally, while the ventral surface is flat transversely and concave proximodistally, giving a claw shape in lateral view. There is a narrow shelf along the lateral and medial margins, which does not extend as far as the proximal articular surface. The nail groove runs proximodistally along this shelf being much the same on both sides. The tips of the unguinals are missing but appear to have ended bluntly.

**Digit IV, pedal phalanx 1 (left).** Phalanx 1 of digit IV is considerably shorter than the first phalanges of digits II and III but is still a robust bone. The proximal

articular surface is essentially flat and 'D'-shaped, the straight margin facing medially and the convex margin forming the outer or lateral surface. The shaft is slightly contracted dorsoventrally and transversely. There is a shallow trochlea distally, transversely widest ventrally and almost straight in dorsal view.

**Digit IV, pedal phalanges 2–4 (left).** The following three phalanges are short bones, which are smaller but have similar morphology to phalanges 2 and 3 in digit III. Moving distally the phalanges become progressively smaller.

A robust phalanx III-1, with a more elongate and gracile phalanx II-1 and a smaller, shorter phalanx IV-1 is also seen in *Camptosaurus dispar* (Gilmore, 1909), *Bactrosaurus johnsoni* (Gilmore, 1933), *Iguanodon bernissartensis* (Norman, 1980) and *Mantellisaurus atherfieldensis*.

## Phylogenetic analysis

The phylogenetic analysis (Fig. 41) resulted in two most parsimonious trees (MPTs) with a tree length of 344 steps. The consistency index = 0.573, rescaled consistency index = 0.497 and the retention index = 0.869.

This cladistic analysis produced a strict consensus tree that showed no significant differences with the results obtained by Xu et al. (2018), regarding the relationships between the major clades of Iguanodontia. *Comptonatus chasei* was recovered as a hadrosauriform nested within Iguanodontidae, with *Iguanodon bernissartensis*, *Barilium dawsoni* and *Mantellisaurus atherfieldensis*. The sympatric *Brighstoneus simmondsi* was recovered outside Hadrosauriformes and Iguanodontidae, as the earliest diverging hadrosauroid (Hadrosauroidea: all Hadrosauriformes closer to *Parasaurolophus walkeri* than to *Iguanodon bernissartensis*, Wu & Godefroit, 2012) and *Ouranosaurus nigeriensis* as the sister taxon to Hadrosauriformes). In this study, the Iguanodontidae node was supported by three synapomorphies: Character 56 (1), a surangular with a horizontal ventrolateral suture with the angular; Character 100 (1), a preacetabular process with an axial twist; and Character 124 (0), the lack of an anteroventral nasal process.

## Histological results

The ontogenetic stage of *Comptonatus chasei* was principally assessed using bone histology in dorsal rib shaft sections.

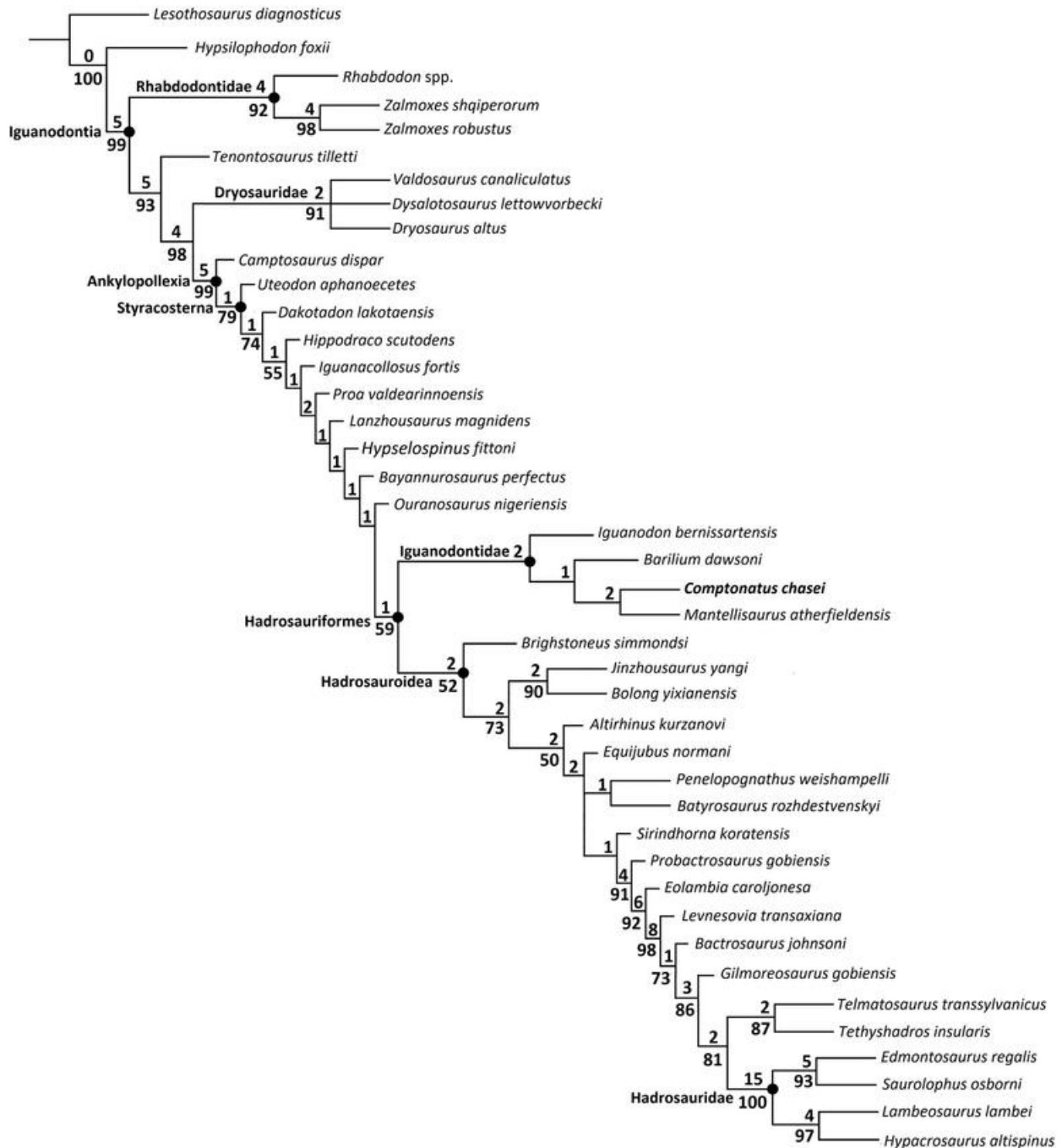


**Figure 41.** Strict consensus of two MPTs depicting the phylogenetic relationships of *Comptonatus chasei* gen. et sp. nov. (IWCMS 2014.80). Tree length = 344 steps, consistency index = 0.573, rescaled consistency index = 0.497, retention index = 0.869. Bremer support numbers are given above and TNT bootstrap values >50% below the line.

One section showed a deep and uniform layer affecting the outer cortical bone, which was pale with loss of detailed histological structure. This is suggestive of either aqueous or subaerial weathering in an oxic environment (Clarke, 1994) and the specimen was not used. The other section was well preserved apart from some taphonomic crushing. Microscopic examination showed

no evidence of an external fundamental system (EFS). At least five circumferential growth marks (lines of arrested growth/annuli) could be identified (Fig. 42), although due to taphonomic crushing these were not easily traced around the whole specimen. The inner growth mark showed evidence of partial erosion by the remodelling activity of secondary osteons. Haversian

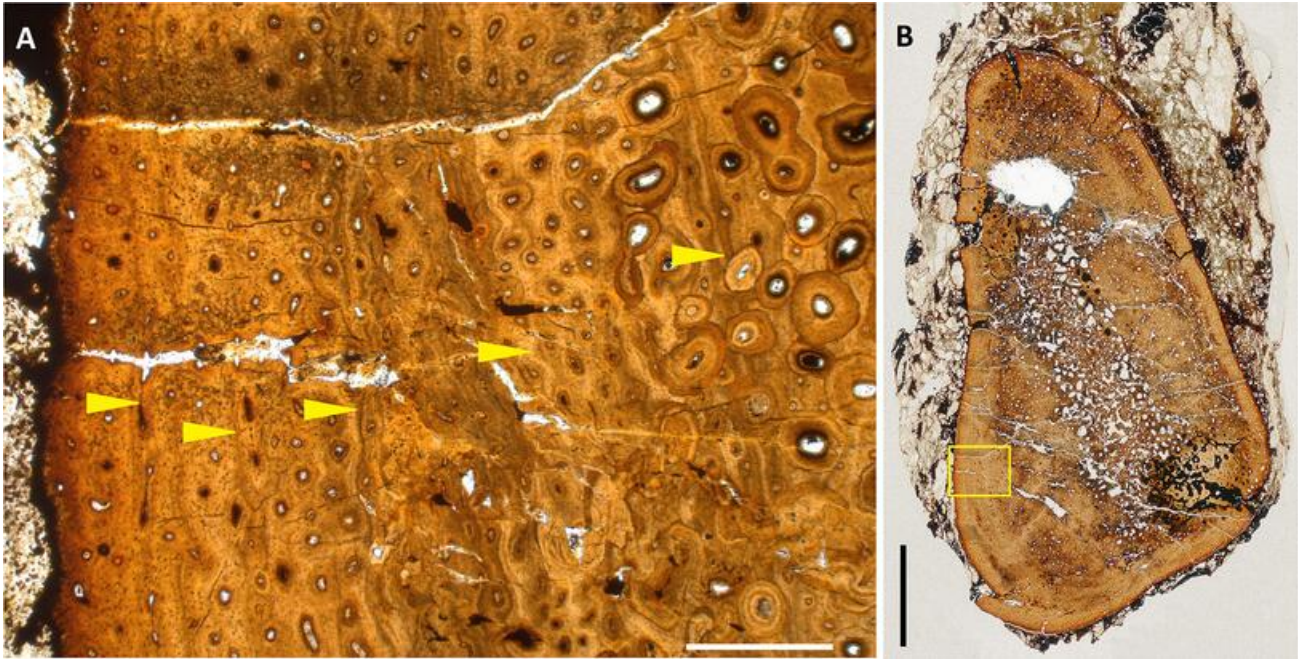


**Figure 42.** *Comptonatus chasei* gen. et sp. nov. (IWCMS 2014.80). Thin transverse section of dorsal rib shaft. **A**, yellow arrows indicate growth lines. Scale bar represents 500  $\mu\text{m}$ . **B**, scan of complete section with area in **A** marked in yellow. Scale bar represents 5 mm.

remodelling was generally well established and extensive in this specimen, suggesting that earlier growth marks may have been lost. Extending radially, the zones between the growth marks decrease in depth, this being most pronounced in the final three zones. These findings indicate a minimum age for *Comptonatus chasei* of five or six years.

## Discussion

Finds of large and moderately large iguanodontian dinosaurs throughout the Wealden Group of the Isle of Wight have led to the paradigm that *Mantellisaurus atherfieldensis* and *Iguanodon bernissartensis* lived from the late Hauterivian through to the early Aptian, a time period that could be as long as 10 million years. However, evidence has been emerging in North America, from the Dinosaur Park Formation (Late Cretaceous, Campanian) in Canada and the Hell Creek Formation (Late Cretaceous, Maastrichtian) in the United States, suggesting that diversity, and evolutionary and speciation rates in the Late Cretaceous may have been underestimated. The Dinosaur Park Formation represents a flood plain, probably with comparable depositional rates to the Wealden Group, that was also subjected to increasing transgressive events (Eberth, 1996, 2005), in which Mallon et al. (2012)

documented a relatively rapid turnover of megaherbivore taxa, with novel species appearing during intervals of less than a million years. The Hell Creek Formation represents a subtropical, near coastal floodplain (Fowler, 2020), in which Scannella et al. (2014) demonstrated a greater ceratopsian diversity, due to both anagenesis and cladogenesis, than had previously been appreciated. Paul (2008, 2012) and Carpenter & Ishida (2010) have also suggested a possible incongruity between the apparent endurance of Wealden Group iguanodontian taxa and expected dinosaurian species longevity.

Evidence of a wider iguanodontian diversity in Early Cretaceous ecosystems is being recovered from late Hauterivian–Barremian deposits in Spain, from which *Iguanodon galvensis* (Camarillas Formation, lower Barremian [Verdu et al., 2015]), *Magnamanus soriaensis* (Golmayo Formation, upper Hauterivian–lower Barremian [Fuentes Vidarte et al., 2016]), *Morelladon beltrani* (Arcillas de Morella Formation, Barremian [Gasulla et al., 2015]), *Portellsaurus sosbaynati* (Mirambell Formation, early Barremian–early late Barremian [Santos-Cubedo et al., 2021]) and *Delapparentia turolensis* (Camarillas Formation, Barremian, [Gasca et al., 2015; Ruiz-Omeñaca, 2011]) are known, although the latter has been considered a *nomen dubium* (Norman, 2015; Verdu, Royo-Torres, et al., 2017). Other specimens, for example those described by Verdu et al. (2019) and Medrano-Aguado

*et al.* (2023), appear to show significant differences indicative of diversity but with insufficient material to justify being named. Furthermore, evidence from fragmentary specimens from the Iberian Peninsula suggests a wider diversity in early diverging ankylopollexians from the late Kimmeridgian and Tithonian of the Jurassic (Rotatori *et al.*, 2022; Sanchez-Fenollosa *et al.*, 2021, 2022). Iguanodontian diversity in the Iberian Peninsula has also been supported ichnologically by track evidence (Castanera *et al.*, 2022). The Yellow Cat Member of the Cedar Mountain Formation in Utah, North America, has recently been dated to the earliest Early Cretaceous, with deposition probably occurring in the Berriasian and Valanginian (Joeckel *et al.*, 2023). This has also yielded several iguanodontian taxa such as *Cedrorestes crichtoni* (Gilpin *et al.*, 2007), *Hippodraco scutodens* (McDonald, Kirkland, *et al.*, 2010), and *Iguanacolossus fortis* (McDonald, Kirkland, *et al.*, 2010), and probably other taxa that have yet to be formally described (Scheetz *et al.*, 2010).

In the context of this high iguanodontian diversity elsewhere in the Early Cretaceous, and the evidence for rapid faunal turnover in iguanodontian-dominated ecosystems, it seems unwise to presuppose that *Mantellisaurus atherfieldensis* and *Iguanodon bernissartensis* persisted in the Wealden across three stages as the sole iguanodontians. It should also not be assumed that the Wessex sub-basin characterizes an ecosystem in stasis. The early Barremian may have represented a wetter environment with the onset of a more arid climate during the middle to late Barremian (Ruffell & Batten, 1990). Rising sea-levels in the late Barremian and early Aptian led to freshwater and brackish lagoonal formation followed by a marine transgression, a known

evolutionary driver for anagenesis (Horner *et al.*, 1992), as well as a cause of forced dispersal.

Three well-preserved specimens of medium large iguanodontians have been collected from the Barremian–Aptian Wealden Group deposits of the Isle of Wight, probably separated from each other by 2–3 Ma intervals. NHMUK PV R 5764 is the holotype of *Mantellisaurus atherfieldensis* and traditionally all medium large iguanodontians from these deposits were referred to this taxon. However, detailed anatomical information clearly separates these specimens into three distinct taxa. The numerous character differences are summarized in Table 1.

The taxonomic utility of some of the characters in Table 1, particularly when viewed in isolation, is difficult to quantify. *Comptonatus chasei* has a well-preserved neurocranium showing details around the supraoccipital that are usually absent or poorly preserved in the majority of iguanodontians, including *Mantellisaurus atherfieldensis* and *Brighstoneus simmondsi*. This affords them little practical function, even if autapomorphic, in helping to differentiate taxa. Some of the differences might be explained in terms of intraspecific variation, ontogeny, or even sexual dimorphism but in the vast majority of iguanodontians nested between hadrosaurids and the earliest diverging taxa, there are so few good specimens that it is difficult to draw statistically valid conclusions. For example, the differences in the number of anterior caudal vertebrae lacking chevrons (Table 1, character 24) has been considered an interspecific characteristic (Dalla Vecchia, 2009; Poole, 2015, 2022a) but has also been postulated as being sexually dimorphic (Erickson *et al.* 2005; Larson, 1994; Romer, 1956) using a neontological

**Table 1.** Principal differences between *Comptonatus chasei* gen. et sp. nov. and the sympatric *Mantellisaurus atherfieldensis* and *Brighstoneus simmondsi*. Autapomorphies relate to non-hadrosaurid iguanodontians.

	Character	<i>Comptonatus chasei</i> IWCMS 2014.80	<i>Brighstoneus simmondsi</i> MIWG 6344	<i>Mantellisaurus atherfieldensis</i> NHMUK PV R 5764
1	Frontals	Anteroposteriorly longer than transversely wide.	Not preserved.	Not preserved.
2	Parietal	Tuberosity and step in posterior parietal margin. *	Not preserved.	Not preserved.
3	Exoccipital	Overhang and cavity between exoccipital bridge and exoccipital pillar. *	Not preserved.	Not preserved.
4	Dentary	Straight ventral margin lacking anteroventral deflection and posterior ventral expansion.	Concave ventral margin with anteroventral deflection and posterior ventral expansion.	Concave ventral margin with anteroventral deflection and posterior ventral expansion.

(Continued)

Table 1. (Continued).

Character	<i>Comptonatus chasei</i> IWCMS 2014.80	<i>Brighstoneus simmondsi</i> MIWG 6344	<i>Mantellisaurus</i> <i>atherfieldensis</i> NHMUK PV R 5764
5	Ratio of midpoint depth to length = 0.18	Ratio of midpoint depth to length = 0.15	Ratio of midpoint depth to length = 0.19
6	Amplitude of sigmoid curve along medial edge in dorsal view. Low	Amplitude of sigmoid curve along medial edge in dorsal view. Low	Amplitude of sigmoid curve along medial edge in dorsal view. High
7	Maximum width of posterior dentary in dorsal view / dentary length = 0.13	Maximum width of posterior dentary in dorsal view / dentary length = 0.14	Maximum width of posterior dentary in dorsal view / dentary length = 2.0
8	Angle of anteroventral deflection = 0°	Angle of anteroventral deflection = 16°	Angle of anteroventral deflection = 22°
9	Dentary alveolar positions	c. 24	28
10	Maxilla	Flat dorsal surface of medial shelf. Margin not everted.	Medial shelf slightly transversely concave with everted margin.
11	Ratio of length of maxilla anterior to the midpoint of the ascending process, to overall length = 0.56	Ratio of length of maxilla anterior to the midpoint of the ascending process, to overall length = 0.76	Ratio of length of maxilla anterior to the midpoint of the ascending process, to overall length = 0.61
12	'Special foramina' circular but elliptical at extremities.	'Special foramina' circular.	'Special foramina' mainly letterbox shaped some elliptical.
13	Oval depression lateral to premaxillary groove in anterior maxilla.	No depression.	No depression.
14	Maxillary alveolar positions	c. 27	29
15	Maxillary crowns	Primary ridge set very distally.	Primary ridge set slightly distally.
16	Primary ridge has fine apicobasal groove extending along its full length. *	Primary ridge lacks apicobasal groove.	Not preserved.
17	Dentary crowns	Primary ridge has fine apicobasal groove extending along its full length. *	Primary ridge lacks apicobasal groove.
18	Quadrate	Weakly developed posterior quadratic buttress.	Not preserved.
19	Relatively short quadrate. Quadrate length / dentary length = 0.557	Not preserved.	Strongly developed posterior quadratic buttress.
20	Cervical vertebrae	Anterior vertebrae in lateral view are elongate with concave ventral margin.	Not preserved.
21	Dorsal vertebrae	At least 2 opisthocoelous transitional vertebrae.	Relatively tall quadrate. Quadrate length / dentary length = 0.645
		At least 1 opisthocoelous transitional vertebra.	Anterior vertebrae in lateral view equidimensional with straight ventral margin.
			1 opisthocoelous transitional vertebra.

(Continued)

**Table 1.** (Continued).

Character	<i>Comptonatus chasei</i> IWCMS 2014.80	<i>Brighstoneus simmondsi</i> MIWG 6344	<i>Mantellisaurus</i> <i>atherfieldensis</i> NHMUK PV R 5764
22	Centra of anterior dorsal vertebrae anteroposteriorly longer than tall.	Centra of probable middle series dorsal vertebrae mostly taller than long.	Centra of anterior dorsal vertebrae taller than long.
23	SD + 6 + sacrocaudal	SD + 6	SD + 6
24	Ventral surfaces. S1 ?, S2 ?, S3 keel, S4 sulcus, S5 flat.	Ventral surfaces S1 keel, S4–S6 flat.	Ventral surface after Hooley (1925). S1 flat, S2 ?, S3–5 sulcus, S6 flat.
25	Caudal vertebrae	Marked ventral sulcus on proximal series (except Ca1 and Ca2) and middle series to Ca24.	Sulcus in later proximal and middle series caudal vertebrae.
26	First chevron appears posteriorly on Ca3.	First chevron appears posteriorly on Ca2.	First chevron appears posteriorly on Ca2.
27	Scapula	Dorsally orientated acromial process.	Not preserved.
28	Supraglenoid fossa absent.	Supraglenoid fossa present.	Supraglenoid fossa present.
29	Ratio of depth at neck to overall length = 0.16	Ratio of depth at neck to overall length = 0.11	Ratio of depth at neck to overall length = 0.11
30	Coracoid	Enlarged internal coracoid foramen with excavation of anterior surface. *	No enlargement and excavation of internal foramen opening.
31	Small boss on anterodorsal internal surface adjacent to thickened area on anterior margin. *	Small boss on anterodorsal internal surface adjacent to thickened area on anterior margin. *	Small boss on anterodorsal internal surface adjacent to thickened area on anterior margin. *
32	Large cornuate ridge on internal surface, that forms buttress for articular surface for scapula.	Large cornuate ridge on internal surface, that forms buttress for articular surface for scapula.	Large cornuate ridge absent.
33	Sternal	Robust posterolateral process. Length/minimum width in lateral view = 2.9	Gracile posterolateral process. Length/minimum width in lateral view = 5.6
34	Ulna	Pronounced ridge on distal ulna.	Very subtle ridge on distal ulna.
35	Metacarpal IV	In dorsal view, the lateral border is straight.	In dorsal view, the lateral border is concave.
36	Metacarpal V	The proximal articular surface is taller than wide.	The proximal articular surface is wider than tall.
37	Ilium	In lateral view the preacetabular process is strap-like with parallel margins.	In lateral view the preacetabular process becomes less deep (waisted) in its middle section.
38	Preacetabular boot is <i>c.</i> 43% of length of preacetabular process.	Preacetabular boot is <i>c.</i> 30% of length of preacetabular process.	Preacetabular boot is 28% of length of preacetabular process.

(Continued)

Table 1. (Continued).

Character	<i>Comptonatus chasei</i> IWCMS 2014.80	<i>Brighstoneus simmondsi</i> MIWG 6344	<i>Mantellisaurus atherfieldensis</i> NHMUK PV R 5764	
39	Angle of the surface below the medial ridge at the base of the preacetabular process to the transverse plane <i>c.</i> 30°	Angle of the surface below the medial ridge at the base of the preacetabular process to the transverse plane <i>c.</i> 40°	Angle of the surface below the medial ridge at the base of the preacetabular process and the transverse plane 0°	
40	Axial twisting of preacetabular process present.	Axial twisting of preacetabular process absent.	Axial twisting of preacetabular process present.	
41	In lateral profile, the angle between the articular surface of the ischiadic peduncle and dorsal margin of the ilium is small.	In lateral profile, the angle between the articular surface of the ischiadic peduncle and dorsal margin of the ilium is large.	In lateral profile, the articular surface of the ischiadic peduncle and the dorsal margin of ilium are parallel.	
42	A lateral boss on the ischiadic peduncle is absent.	A lateral boss on the ischiadic peduncle is absent.	A lateral boss on the ischiadic peduncle is present.	
43	In lateral view the lateral process occupies 28% of the depth of the iliac body.	In lateral view the lateral process occupies 21% of the depth of the iliac body.	In lateral view the lateral process occupies 16% of the depth of the iliac body.	
44	Pubis	Very deep and expanded prepubic blade. Ratio maximum to minimum depth <i>c.</i> 2.5.	Possibly modestly deep and expanded prepubic blade. Ratio unknown.	Moderately deep and expanded prepubic blade. Ratio <i>c.</i> 1.7
45	Ischium	Strongly booted.	Unpreserved.	Weakly booted.
46	Femur	Extensor intercondylar groove almost closed.	Extensor intercondylar groove probably open.	Extensor intercondylar groove open.
47		In lateral view distal third curves markedly posteroventrally.	In lateral view distal third nearly straight.	In lateral view distal third nearly straight.
48	Tibia	Boss on medial surface of tibia near dorsal margin.*	Not preserved.	Boss absent.
49	Length of humerus to length of radius	1.33	Not preserved.	1.41
50	Length of femur to length of tibia	1.07	Not preserved.	1.20

model based on 36 *Alligator mississippiensis* individuals considered intraspecific variation to be a more likely explanation. Despite this, there are character suites that appear unique, and the large number of differences, when combined, distinguish *Comptonatus chasei* as a new taxon. The dentary and pelvis display two of the more important characters in this respect and are discussed in detail below.

#### Ventral deflection of the anterior dentary in iguanodontians

A dentary that has a straight ventral margin extending across the entire lateral profile distinguishes *Comptonatus chasei* from other Barremian–Aptian iguanodontians found on the Isle of Wight (*Mantellisaurus atherfieldensis*, *Brighstoneus simmondsi* and *Iguanodon cf. bernissartensis*). The ventral margin of the dentary is

usually concave to some degree in iguanodontians, with the concavity sometimes extending along the whole length of the dentary and sometimes restricted to the anterior half or middle region. The whole anterior section may be deflected ventrally or become increasingly deep ventrally as it extends anteriorly. Completely straight dentaries are unusual, although a few taxa have almost straight dentaries, such as *Jinzhousaurus yangi* from the early Aptian of China (Wang & Xu, 2001) and *Sirindhorna khoratensis* from the Aptian of Thailand (Shibata *et al.*, 2015), where the deflection is limited to a slight deepening of the anterior section of the dentary.

NHMUK PV OR 28660 is an isolated dentary that forms the holotype of *Kukufeldia tilgatensis* (McDonald, Barrett, *et al.*, 2010) and, like *Comptonatus chasei*, was also recovered from the Wealden Group, albeit from *c.* 10 Ma older (Cohen *et al.*, 2013, updated 2022), Valanginian strata in the Wealden Sub-basin. The taxon was based on an autapomorphic arrangement of vascular foramina, although it has subsequently been referred to *Barilium dawsoni* by Norman (2011b). It is unusual in that it is straight along its ventral margin in lateral view and has parallel ventral and dorsal margins. McDonald, Barrett, *et al.* (2010) considered the lack of ventral deflection to be sufficient to distinguish it from NHMUK PV R 1831, a dentary also from the Valanginian of the Wealden Sub-basin (subsequently referred to *Hypselospinus fittoni* by Norman, 2015) but with a very gently concave ventral margin, especially posteriorly. Their decision was based on observations that dentaries from several sites, which yielded multiple mature specimens (representing *Camptosaurus dispar*, *Iguanodon bernissartensis* and *Eolambia caroljonesa*), showed no significant intraspecific variation in the morphology of the anterior ramus. *Comptonatus chasei* lacks the autapomorphic arrangement of foramina found in NHMUK PV OR 28660, and also exhibits many other differences that distinguish it from *Barilium dawsoni*: relatively taller neural spines on the dorsal vertebrae; anteroposteriorly compressed anterior caudal vertebrae; distal caudal vertebrae not deeply amphicoelous; the ventral margin of the postacetabular process is not parallel with the ventral margin of the ischiadic peduncle of the ilium; the preacetabular process is not axially rotated to the same degree; and the iliac facet for the transverse process of the first sacral vertebra is not visible laterally.

The few reasonably complete dentaries from late Hauterivian–early Aptian iguanodontians, sympatric with *Comptonatus chasei*, are all ventrally deflected. The angle of the ventral margin of the anterior section to the middle section of the dentary is 22° in NHMUK PV R 5764 (*Mantellisaurus atherfieldensis* holotype),

16° in MIWG 6344 (*Brighstoneus simmondsi* holotype), 10° in IWCMS 1997.55 (referred to *Iguanodon cf. bernissartensis* [McDonald, 2012a]), 19° in NHMUK PV R 11521 (referred to *Mantellisaurus atherfieldensis* [Barrett, Butler, *et al.*, 2009; McDonald, 2012a; Norman, 2013]) and 9° in IWCMS 1996.4 (referred to *Mantellisaurus atherfieldensis* [McDonald, 2012a]). The range of deflection angles in iguanodontians varies, but this range of values is in the typical range, for example *Proa valdearinnensis* 18° (McDonald, Espilez, *et al.*, 2012), *Batyrosaurus rozhdestvenskyi* 15° (Godefroit, Bolotsky, *et al.*, 2012), *Choyrodon barsboldi* 19° (Gates *et al.*, 2018), *Ouranosaurus nigeriensis* 10°, *Equijubus normani* 13°, *Eolambia caroljonesa* 14°, *Bactrosaurus johnsoni* 23°, *Telmatosaurus transsylvanicus* 16° (Prieto-Marquez, 2010) and many more. The range is greater in hadrosaurids, varying from 10° to over 40° in some taxa such as *Kritosaurus navajovius* (Prieto-Marquez, 2014a). Within this clade there can also be wide intraspecific variation, with differences ranging up to 10°, for example *Corythosaurus casuarius* 22–32°, *Brachylophosaurus canadensis* 17.5–26° and *Gryposaurus notabilis* 23–29° (Fondevilla *et al.*, 2018). Amongst hadrosaurids there is no consistent change in the angle of deflection with ontogeny, the angle increasing in *Amurosaurus riabinini* (Godefroit *et al.* 2004) but decreasing in *Edmontosaurus* spp. (Mori *et al.*, 2012, 2013). Prieto-Marquez (2014b) described a juvenile *Edmontosaurus annectens* with a ventral deflection of 18° as opposed to the normal adult range of 10–14°, while Gates *et al.* (2018) figured a juvenile dentary of *Gryposaurus* sp. with a nearly straight ventral border (albeit damaged and partially restored) while the ventral border is considerably deflected in adults. There is little information on the ontogeny of ventral deflection in non-hadrosaurid hadrosauriforms. Poole (2015) found in *Eolambia caroljonesa* the angle was greater in immature dentaries than in the mature adult. However, Garrison *et al.* (2007) figured a number of dentaries from *Eolambia caroljonesa*, covering a wide range of sizes from very immature to mature adult, which showed a consistent morphology within the juveniles, except for specimen CEUM 34447, a marked outlier that is highly deflected, to a degree that makes it questionable that it is the same taxon (McDonald, Bird, *et al.*, 2012).

Apart from the ventral deflection of the anterior section there are differences in the curvature of the whole ventral border of the dentaries when viewed laterally. In *Mantellisaurus atherfieldensis* NHMUK R 5764, the entire ventral border forms a concave curve blending with the deflection anteriorly and producing a ventral bulge posteriorly. This general curve is also seen in *Brighstoneus simmondsi* MIWG 6344, despite losses to

the posteroventral section of both of its dentaries. Specimen NHMUK R 11521 is almost straight throughout, apart from the anterior ventral deflection and IWCMS 1996.4, an isolated dentary (see below), only has a very shallow concavity.

We conclude that although there is evidence of intra-specific variation, especially in hadrosaurids, the degree of difference between *Comptonatus chasei* and the sympatric *Mantellisaurus atherfieldensis* and *Brighstoneus simmondsi* is too great to accept this as the likely cause.

### Some observations on potential skull shape variation in Isle of Wight iguanodontians

While appreciating that trying to reconstruct the skull of an animal when key elements are missing can lead to error, the amplitude of the sigmoid curve along the medial edge of the dentary in dorsal view (Table 1, Character 6), the maximum width of the posterior dentary in dorsal view relative to the dentary length (Table 1, Character 7), and differences in the size ratio between the quadrate and dentary (Table 1, Character 19) merit some discussion.

Although the dentary of *Comptonatus chasei* differs from *Mantellisaurus atherfieldensis* and *Brighstoneus simmondsi* in having a straight ventral margin in lateral view, there are also differences in dorsal view. Four Isle of Wight iguanodontian dentaries are shown in Fig. 43,

where the dentary image has been flipped horizontally and the two images placed so that the line of the mandibular symphysis is orientated sagittally. This also results in the mid tooth rows being approximately parallel. The resulting images have then been scaled to the same length. A further dentary (IWCMS 1996.4) discovered by Mr Stephen Hutt near Grange Chine in the Wessex Formation, at a different level but in the same plant debris bed (Fig. 1C; bed L9) that yielded *Brighstoneus simmondsi* and which was previously figured by McDonald (2012a), is also included (see Supplemental material [S3, p. 151] for an osteological description).

In dorsal view the medial wall of the iguanodontian dentary has a characteristic sigmoid outline, the posterior tooth row curving laterally and the anterior edentulous section curving medially to meet its antimeres at the mandibular symphysis. It can be seen that the amplitude of this sigmoid curve is more marked in *Mantellisaurus atherfieldensis* and IWCMS 2016.4 than in *Comptonatus chasei* and the well-preserved dentary of *Brighstoneus simmondsi*, making the coronoid processes relatively further apart in the former two. The relative anteroposterior length of the mandibular symphysis and the transverse width of the buccal shelf are also greater in *Mantellisaurus atherfieldensis* and IWCMS 1996.4 than in *Comptonatus* and *Brighstoneus*, making them more robust (ratio of the maximum transverse width of posterior dentary to dentary length measured from the anterior

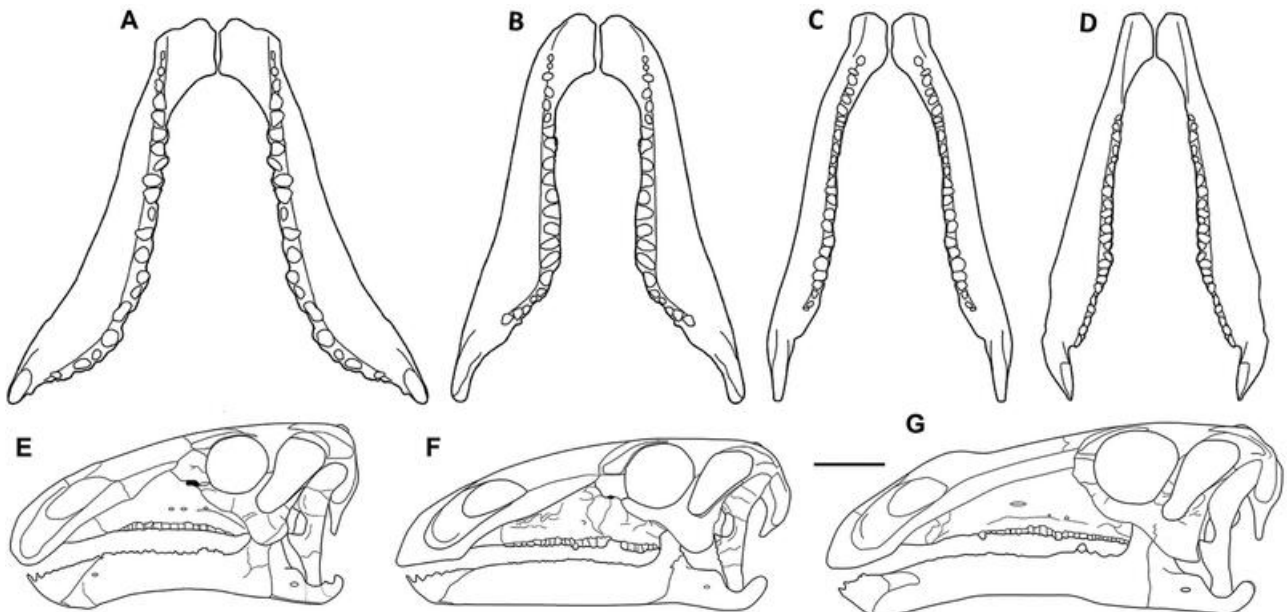


**Figure 43.** Reconstruction of iguanodontian dentaries and skulls from the Isle of Wight. **A–D:** Dentaries in dorsal view from **A**, IWCMS 1996.4, **B**, *Mantellisaurus atherfieldensis* (NHMUK PV R 5764), **C**, *Comptonatus chasei* and **D**, *Brighstoneus simmondsi* (MIWG 6344). All scaled to approximately the same length. **E–G:** Preliminary skull reconstructions of **E**, *Mantellisaurus atherfieldensis*, **F**, *Comptonatus chasei* and **G**, *Brighstoneus simmondsi*. Scale bar E–G represents 100 mm.

margin of the coronoid process: *Comptonatus chasei* 0.13, *Brighstoneus simmondsi* 0.14, *Mantellisaurus atherfieldensis* 0.20, and IWCMS 1996.4 0.19). The dental row also extends further anteriorly in *Mantellisaurus atherfieldensis* and IWCMS 1996.4. The transverse diameter between the coronoid processes is critical to the width of the skull, and the inference is that *Mantellisaurus atherfieldensis* and IWCMS 1996.4 had relatively wider and rounder skulls in dorsal view with more robust dentaries than the more elongate skulls of *Comptonatus chasei* and *Brighstoneus simmondsi*. It is also interesting that IWCMS 2016.4 was found in the same plant debris bed as *Brighstoneus simmondsi*, showing that these two morphologies were contemporary.

The quadrate of *Comptonatus chasei* is 3% shorter anteroposteriorly than in the *Mantellisaurus atherfieldensis* holotype, whereas its dentary is 14% longer, suggesting a relatively lower profile for the skull in lateral view (Fig. 43), although this is more speculative.

### The prepubic blade

The pelves of Isle of Wight iguanodontians show considerable differences (Fig. 44), especially in the prepubic blade. In iguanodontians the prepubic blade is usually a thin, transversely compressed, and fragile structure, which is rarely preserved in its entirety, without damage or deformation (Brett-Surman & Wagner, 2007).

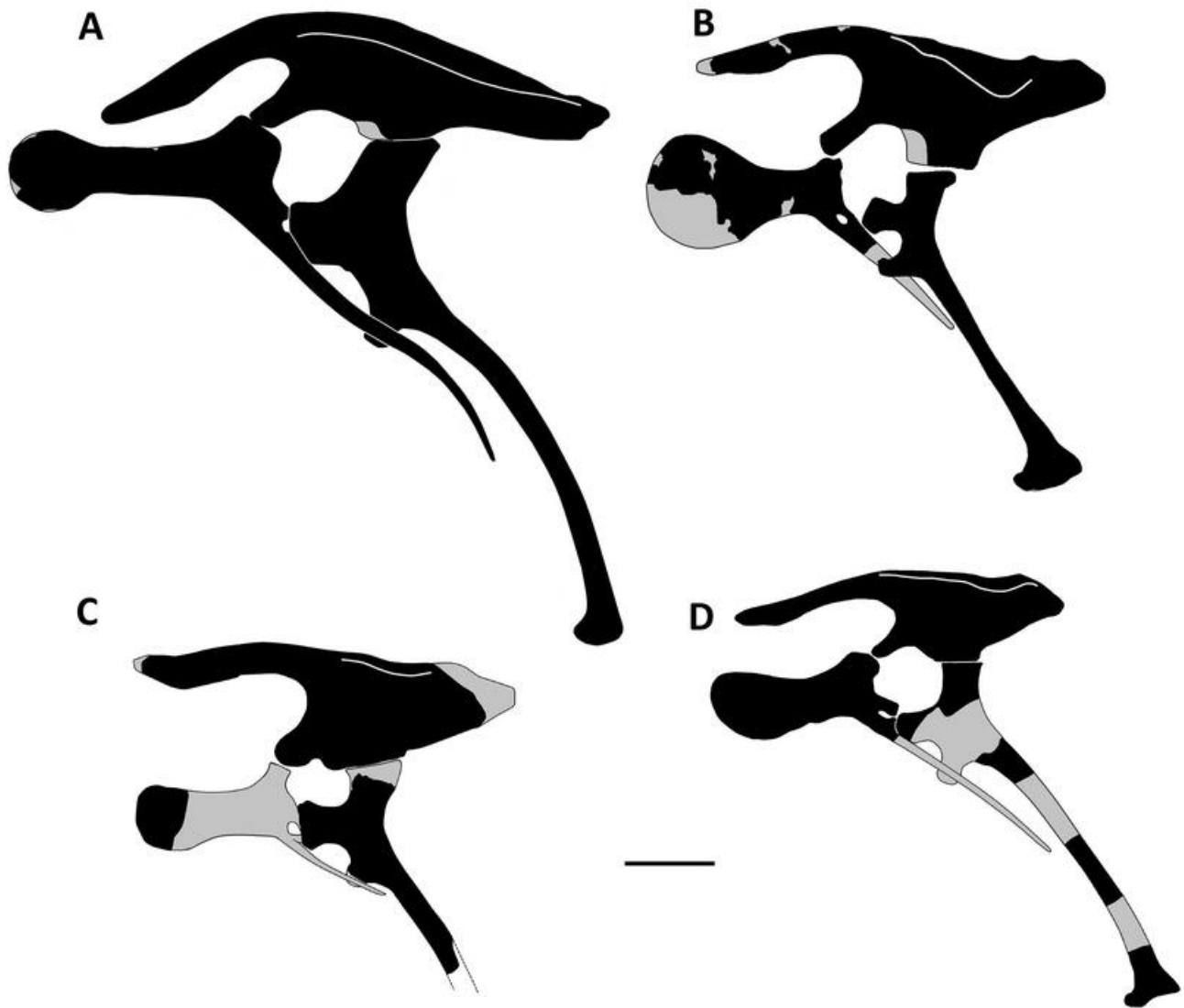


**Figure 44.** Pelvic girdle reconstructions of Isle of Wight iguanodontian holotypes and the Belgian *Iguanodon bernissartensis* lectotype, with some restoration. Black areas represent actual material, grey restoration. **A**, *Iguanodon bernissartensis* RBINS R51 redrawn after Norman (1980; fig. 64), **B**, *Comptonatus chasei* IWCMS 2014.80, **C**, *Brighstoneus simmondsi* MIWG 6344 (fragment of assumed prepubis) and **D**, *Mantellisaurus atherfieldensis*, ilium and pubis from NHMUK PV R 5764, ischium based on Hooley (1925; fig. 10). Scale bar represents 200 mm.

The *Iguanodon bernissartensis* specimens collected from the Fosse Sainte Barbe mine at Bernissart in southern Belgium, although frequently subjected to significant taphonomic distortion (Lauters et al., 2012; McDonald, 2011; Norman, 1980; Verdu, Godefroit, et al., 2017), nevertheless provide a rare opportunity to study intraspecific variation of this structure in non-hadrosaurid ankylopollexians. One of the better-preserved prepubic blades, from the left side of the lectotype, RBINS R51 (Fig. 45A), shows the typical spatulate morphology associated with this clade.

Verdu, Godefroit, et al. (2017) noted variation in the ratios between the deepness at the distal end to the minimum deepness of the prepubic blade, and the minimum deepness of the prepubic blade to its length, as well as different degrees of abruptness in the transition from the neck to the distal prepubic expansion. However, maximum depth of the distal expansion to the overall length of the prepubic blade was reasonably constant in those specimens with complete data: RBINS R51 = 0.30, RBINS R52 = 0.32, RBINS Vert-05144-05162 = 0.34, and RBINS R341 = 0.36. Some of this variation may have been exaggerated by diagenetic distortion, but overall, the general morphology of a relatively long narrow neck and a subcircular distal expansion remains apparent (Fig. 45A–J). *Iguanodon galvensis* also has a pubic blade with a similar morphology to *Iguanodon bernissartensis*, and this morphology was preserved in the remains of perinates (Verdu et al., 2015). A similar finding was made by Prieto-Marquez (2014b), in the hadrosaurid *Edmontosaurus annectens*, comparing immature pubes (Fig. 45M, N) with adults (Fig. 45K, L). Again, this was complicated by incomplete and distorted specimens, but showed a prepubic blade that was morphologically consistent during ontogeny within the clade. This seems to be the case in hadrosaurids generally (Brett-Surman & Wagner, 2007; Horner & Currie, 1994), although in *Brachylophosaurus canadensis* (Prieto-Marquez, 2001), the dorsoventral height of the blade and neck relative to length were greater in the more robust adult, although the morphology between the immature example (Fig. 45O) and the adult (Fig. 45P) was broadly similar. McDonald et al. (2017) have described an adult (Fig. 45Q) and juvenile (Fig. 45R) pubis from *Eolambia caroljonesa*, showing the juvenile has a deeper distal expansion relative to its length than the adult (although it is unclear if the anterodorsal margin of the adult specimen has been damaged). The morphology of the prepubic blade is therefore subject to some variation, but the overall shape appears fairly constant within a taxon. This strongly suggests that the large morphological differences between the prepubic blades in *Comptonatus chasei* and *Mantellisaurus atherfieldensis* are indicative of interspecific variation.

### The phylogenetic position of *Comptonatus chasei*

The small clade Iguanodontidae, which in this study contained *Comptonatus chasei*, has also been resolved in several other phylogenies (Godefroit, Escuille, et al., 2012; Norman, 2015; Wu & Godefroit, 2012; Xu et al., 2018). Wu & Godefroit (2012) in their analysis of *Bolong yixianensis* recovered a monophyletic clade, which included *Iguanodon bernissartensis*, *Mantellisaurus atherfieldensis* and *Ouranosaurus nigeriensis*, with the latter two as sister taxa. They subdivided Hadrosauriformes into the Iguanodontidae and the Hadrosoidea. An autapomorphy for Iguanodontidae was the presence of ossified epaxial tendons extending posteriorly from the 10th cervical vertebra, and within Iguanodontidae, *Mantellisaurus* and *Ouranosaurus* were united by the presence of elongate neural spines on the posterior dorsal and sacral vertebrae, which were more than 2.5 times the centrum height. It should be noted that no complete neural spines have survived on vertebrae posterior to the transitional dorsal and ossified epaxial tendons are only preserved on dorsal vertebrae posterior to the 11th in the *Mantellisaurus atherfieldensis* holotype. Wu and Godefroit (2012) defined Iguanodontidae as the most inclusive clade containing *Iguanodon bernissartensis* but not *Parasaurolophus walkeri*. However, Iguanodontidae is only weakly supported with low bootstrap percentages and Bremer support values in these studies.

More generally, phylogenies of ankylopollexians (Bertozzo, Della Vecchia, et al., 2017; Della Vecchia, et al., 2017; Godefroit, Escuille, et al., 2012; Lockwood et al. 2021; McDonald, 2011; Norman, 2015; Poole, 2022a; Wu & Godefroit 2012; Xu et al. 2018) have shown poor support and instability, with inconsistent relationships between *Iguanodon bernissartensis*, *Barilium dawsoni*, *Ouranosaurus nigeriensis*, *Brighstoneus simmondsi*, *Mantellisaurus atherfieldensis* and now *Comptonatus chasei*. Further work, which includes additional taxonomic reassessment and the discovery of new characters, is probably required to improve resolution in this group.

### Assessing the ontogenetic stage of *Comptonatus chasei*

This study showed that, extending radially, the zones between the growth marks reduced in depth, especially between the final three. However, care needs to be taken with regard to relative depths between growth marks as without an EFS these can be misleading and do not necessarily indicate a slowing of growth or that a high percentage of maximum mass had been obtained (Cullen et al., 2021). Several studies have looked at ontogenetic osteohistology in iguanodontians, including the lambeosaurine hadrosaurid *Hypacrosaurus stebingeri*

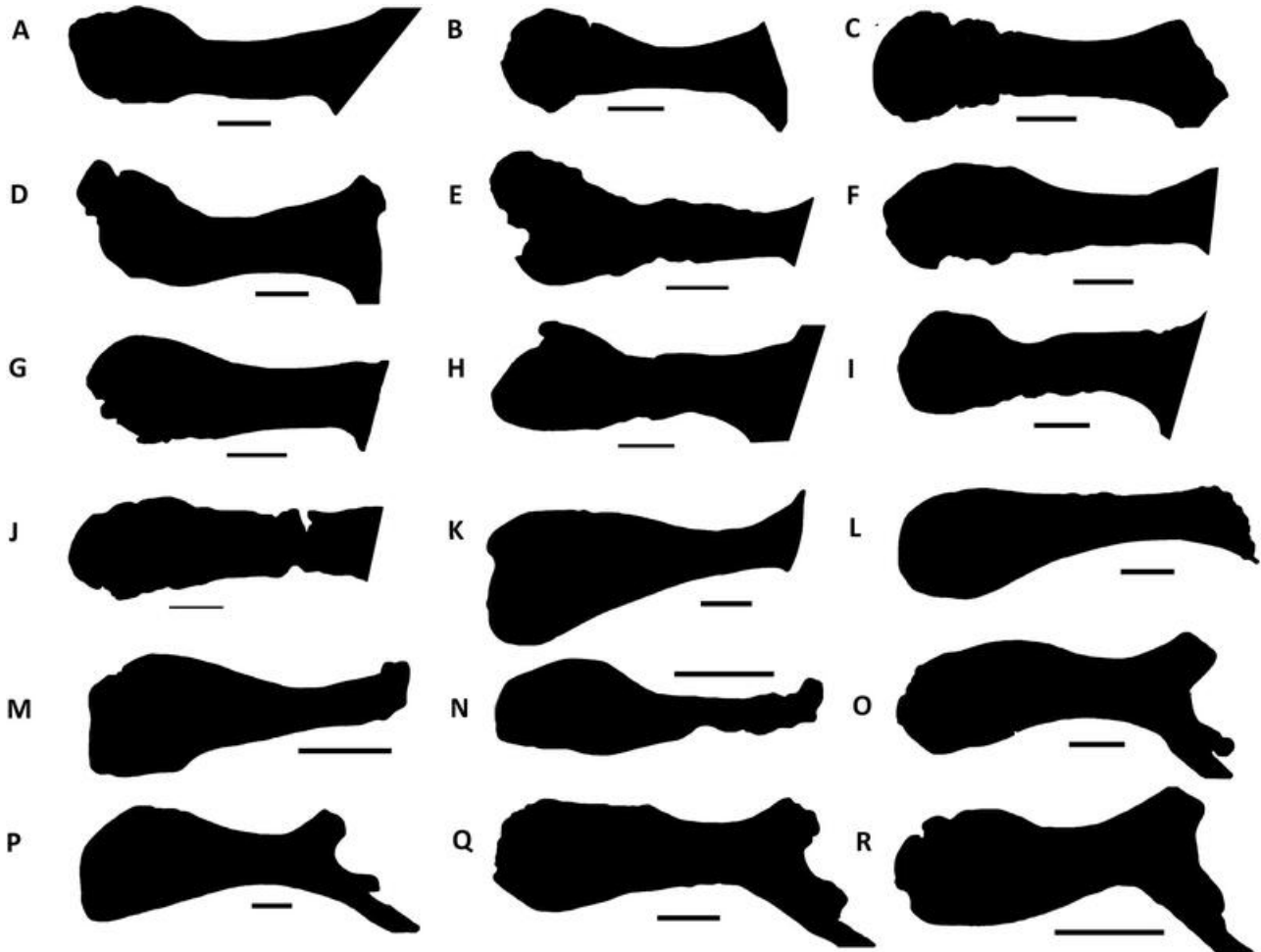


**Figure 45.** Silhouettes of the prepubic blades (scaled to approximately the same anteroposterior length) in left lateral view. **A–I**, adult *Iguanodon bernissartensis* specimens from the Bernissart collection. **A**, RBINS R51 (lectotype); **B**, RBINS R51 (lectotype) right reversed; **C**, RBINS R52 (paratype); **D**, RBINS R55 (paratype); **E**, RBINS 56 (paratype); **F**, RBINS R343; **G**, RBINS R344; **H**, RBINS VERT-5147-1562; **I**, RBINS VERT-1547-1562 right reversed; **J**, RBINS VERT-5144-1657; **K–N**, *Edmontosaurus annectens* redrawn from Prieto-Marquez (2014a): **K**, SM R4036; **L**, LACM 23502 right reversed; **M**, LACM 23504 juvenile; **N**, LACM 23504 right reversed, juvenile; **O, P**, *Brachylophosaurus canadensis* redrawn from Prieto-Marquez (2001): **O**, MOR 1071-7-16-98-243 juvenile; **P**, MOR 794; **Q, R**, *Eolambia caroljonesa* redrawn from McDonald *et al.* 2017. **Q**, FMNH PR 3847; **R**, CEUM 52152 juvenile. Scale bars represent 100 mm.

(Horner *et al.*, 1999), the saurolophine hadrosaurid *Maiasaura peeblesorum* (Erickson *et al.*, 2001; Horner *et al.*, 2000; Woodward *et al.*, 2015), an indet. hadrosaurid (Cullen *et al.*, 2021), and the early diverging *Tenontosaurus tilletti* (Werning, 2012) and *Dysalotosaurus lettowvorbecki* (Hübner, 2012). The growth curves showed that the earlier diverging taxa took much longer to reach a body mass asymptote, in the order of 15 + years (Hübner, 2012), whereas *Maiasaura peeblesorum* was estimated to take as little as four years by Woodward *et al.* (2015), with sexual maturity being reached between two and three years. Horner *et al.* (1999) showed that rib sections had reasonable utility in *Hypacrosaurus* but recorded fewer

lines of arrested growth than in the femur, so may underestimate age.

The osteohistological results for *Comptonatus chasei* if compared to *Maiasaura peeblesorum* would suggest a likely sexually mature animal that had achieved a substantial amount of its body mass but was not yet fully skeletally mature. This would fit with the open neurocentral synchondroses (*sensu* Brochu 1996) in the dorsal and caudal vertebrae and possibly partially fused cervical vertebrae, although these are increasingly being seen as unreliable indicators of maturity in dinosaurs without histological confirmation (Griffin *et al.*, 2020; Heinrich *et al.*, 2021).

## Conclusions

The recent increase in known dinosaur taxa from the Isle of Wight, including the ornithischians *Vectidromeus insularis*, *Brighstoneus simmondsi* and *Vectipelta barretti*, and the theropods *Vectiraptor greeni*, *Ceratosuchops inferodios*, *Riparovenator milnerae* and a gigantic spinosaurid suggest that either the Wessex Formation supported a greater diversity than previously realized, or that evolutionary and/or migratory pressures resulted in faunal change between the latest Hauterivian and the early Aptian. *Comptonatus chasei* provides further evidence for a greater iguanodontian

diversity and now makes it unclear which iguanodontian taxon or taxa dominated in the Wessex sub-basin during the Barremian. At the present time there is no direct evidence to support *Mantellisaurus atherfieldensis* being present in the early Barremian. Phylogenetic analyses in this and previous studies show that traditional characters are failing to bring consensus and resolution to this important group of iguanodontians. A reappraisal of existing material with a greater awareness of autapomorphies and character differences, such as the variation recorded in this study, are probably necessary to broaden our understanding of these questions.

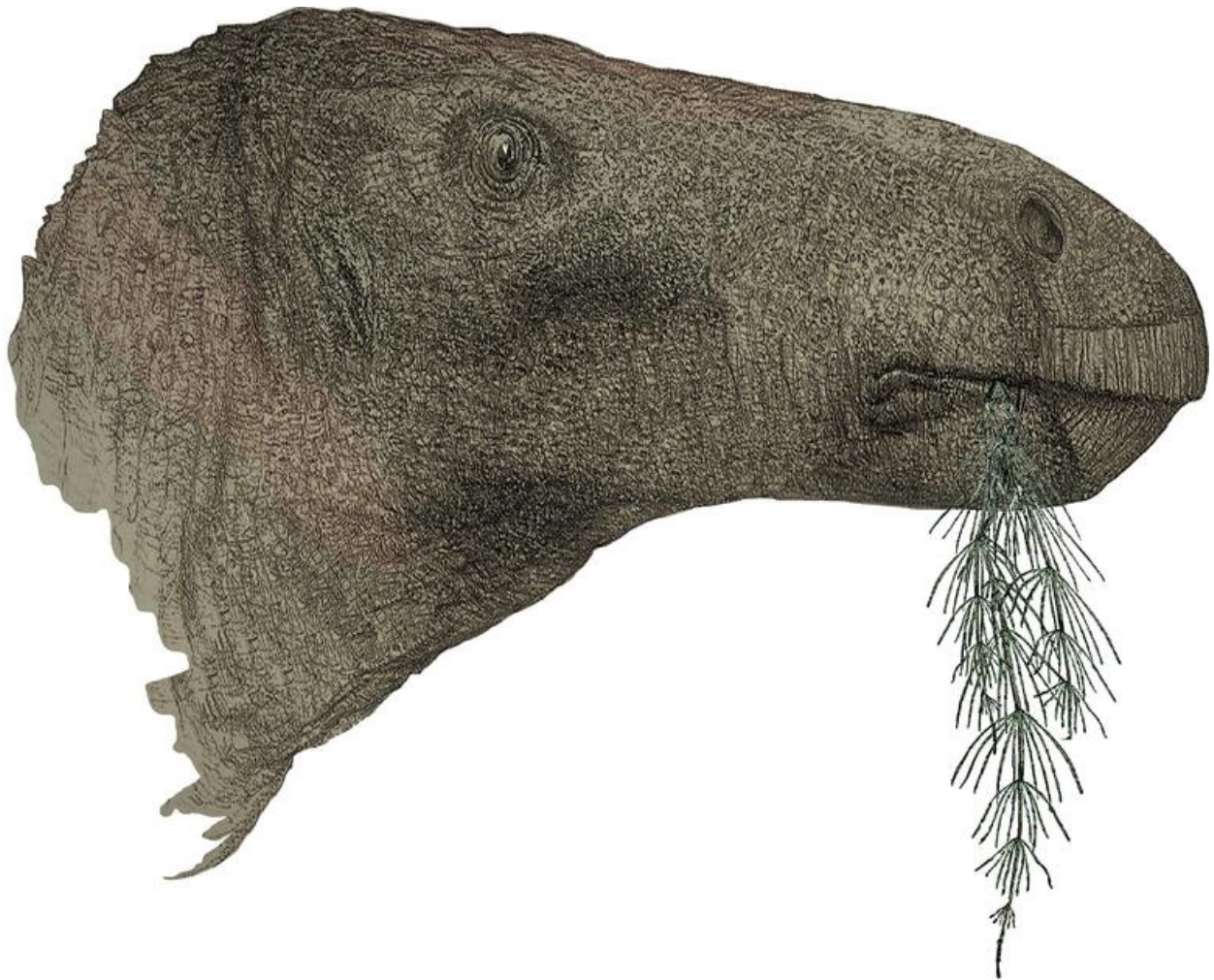


**Figure 46.** *Comptonatus chasei* gen. et sp. nov. (IWCMS 2014.80). Life restoration. Original artwork by John Sibbick.

## Acknowledgements

We are indebted to Dr Martin Munt and the staff at Dinosaur Isle Museum, Isle of Wight, especially Simon Penn and Alex Peaker, for the enormous amount of time and effort afforded to this project, and also earlier staff including Gary Blackwell for preparing the material and Peter Pusey for agreeing to the project. We thank Barbara Close for her invaluable expertise in photographing the skeleton of *Comptonatus*. We are grateful to the National Trust for kindly allowing the excavation on their property and to John Sibbick for generously providing the artwork. We also thank volunteers Martyn Hornett and Sandra Garbett for their help and assistance, the late, great Nick Chase, and Stephen Hutt for useful discussions on the excavation, local collectors Mick Green, Mark Penn, Fiona Wight, Shaun Smith, Andrew Cocks, Martin Simpson, Megan Jacobs and Keith Simmonds for supporting the Isle of Wight iguanodontian project, and Geoff Long and Richard Hing of the University of Portsmouth for preparing thin sections and providing photographs and scans of the slides. We also thank our anonymous reviewers for their detailed comments, which improved this paper considerably. The programme TNT is made freely available courtesy of the Willi Hennig Society.

## Disclosure statement

The authors report there are no competing interests to declare.

## Supplemental material

Supplemental material for this article can be accessed here: <http://dx.doi.org/10.1080/14772019.2024.2346573>.

## ORCID

Jeremy A. F. Lockwood  <http://orcid.org/0000-0002-3233-0819>

David M. Martill  <http://orcid.org/0000-0002-3208-5702>

Susannah C. R. Maidment  <http://orcid.org/0000-0002-7741-2500>

## References

Allen, P., & Wimbledon, W. A. (1991). Correlation of NW European Purbeck-Wealden (non-marine Lower

Cretaceous) as seen from the English type-areas. *Cretaceous Research*, 12, 511–526. [https://doi.org/10.1016/0195-6671\(91\)90005-W](https://doi.org/10.1016/0195-6671(91)90005-W)

- Austen, P. A., & Batten, D. J. (2018). English Wealden fossils: an update. *Proceedings of the Geologists' Association*, 129, 171–201. <https://doi.org/10.1016/j.pgeola.2018.02.007>
- Averianov, A. O., Leshchinskiy, S. V., Kudryavtsev, V. I., & Zabelin, V. I. (2007). Braincase of a Late Jurassic stegosaurian dinosaur from Tuva, Russia (Central Asia). *Journal of Vertebrate Paleontology*, 27, 727–733. [https://doi.org/10.1671/0272-4634\(2007\)27\[727:BOALJS\]2.0.CO;2](https://doi.org/10.1671/0272-4634(2007)27[727:BOALJS]2.0.CO;2)
- Bailleul, A. M., & Holliday, C. M. (2017). Joint histology in *Alligator mississippiensis* challenges the identification of synovial joints in fossil archosaurs and inferences of cranial kinesis. *Proceedings of the Royal Society B*, 284, 20170038. <https://doi.org/10.1098/rspb.2017.0038>
- Barker, C. T., Hone, D. W. E., Naish, D., Cau, A., Lockwood, J. A. F., Foster, B., Clarkin, C. E., Schneider, P., & Gostling, N. J. (2021). New spinosaurids from the Wessex Formation (Early Cretaceous, UK) and the European origins of Spinosauridae. *Scientific Reports*, 11, 1–15. <https://doi.org/10.1038/s41598-020-79139-8>
- Barker, C. T., Lockwood, J. A. F., Naish, D., Brown, S., Hart, A., Tulloch, E., & Gostling, N. J. (2022). A European giant: a large spinosaurid (Dinosauria: Theropoda) from the Vectis Formation (Wealden Group, Early Cretaceous), UK. *PeerJ* 10:e13543 <https://doi.org/10.7717/peerj.13543>
- Baron, M. G., Norman, D. B., & Barrett, P. M. (2016). Postcranial anatomy of *Lesothosaurus diagnosticus* (Dinosauria: Ornithischia) from the Lower Jurassic of southern Africa: implications for basal ornithischian taxonomy and systematics. *Zoological Journal of the Linnean Society*, 179, 125–168. <https://doi.org/10.1111/zoj.12434>
- Barrett, P. M. (2016). A new specimen of *Valdosaurus canaliculatus* (Ornithopoda: Dryosauridae) from the Lower Cretaceous of the Isle of Wight, England. *Memoirs of Museum Victoria*, 74, 29–48. <https://doi.org/10.24199/j.mmv.2016.74.04>
- Barrett, P. M., & Bonsor, J. A. (2021). A revision of the non-avian dinosaurs *Eucercosaurus tanyspondylus* and *Syngonosaurus macrocerus* from the Cambridge Greensand, UK. *Cretaceous Research*, 118, 1–13. <https://doi.org/10.1016/j.cretres.2020.104638>
- Barrett, P. M., Butler, R. J., Twitchett, R. J., & Hutt, S. (2011). New material of *Valdosaurus canaliculatus* (Ornithischia: Ornithopoda) from the Lower Cretaceous of Southern England. *Special Papers in Palaeontology*, 86, 131–163.
- Barrett, P. M., Butler, R. J., Wang, X.-L., & Xu, X. (2009). Cranial anatomy of the iguanodontoid ornithopod *Jinzhouosaurus yangi* from the Lower Cretaceous Yixian Formation of China. *Acta Palaeontologica Polonica*, 54, 35–48. <https://doi.org/10.4202/app.2009.0105>
- Barrett, P. M., McGowan, A. J., & Page, V. (2009). Dinosaur diversity and the rock record. *Proceedings of the Royal Society B*, 276, 2667–2674. <https://doi.org/10.1098/rspb.2009.0352>
- Batten, D. J. (2011). Wealden Geology. In D. J. Batten (Ed.), *Palaeontological Association Field Guide to Fossils*, 14.

- English Wealden fossils* (pp. 7–14). The Palaeontological Association.
- Batten, D. J. & Austen, P. A. (2011).** The Wealden of Southeast England. In D. J. Batten (Ed.), *Palaeontological Association Field Guide to Fossils, 14. English Wealden fossils* (pp. 15–51). The Palaeontological Association.
- Baur, G. (1891).** Remarks on the reptiles generally called Dinosauria. *American Naturalist*, 25, 434–454.
- Bertozzo, F., Dal Sasso, C., Fabbri, M., Manucci, F., & Maganuco, S. (2017).** Redescription of a remarkably large *Gryposaurus notabilis* (Dinosauria: Hadrosauridae) from Alberta, Canada. *Memorie della Societa Italiana di Scienze Naturali e del Museo Civico di Storia Naturale di Milano*, 153, 1–56.
- Bertozzo, F., Della Vecchia, F. M., & Fabbri, M. (2017).** The Venice specimen of *Ouranosaurus nigeriensis* (Dinosauria, Ornithopoda). *PeerJ*, 5, 1–70. e3403; <https://doi.org/10.7717/peerj.3403>
- Bertozzo, F., Manucci, F., Dempsey, M., Tanke, D. H., Evans, D. C., Ruffell, A., & Murphy, E. (2021).** Description and etiology of paleopathological lesions in the type specimen of *Parasaurolophus walkeri* (Dinosauria: Hadrosauridae), with proposed reconstructions of the nuchal ligament. *Journal of Anatomy*, 238, 1055–1069. <https://doi.org/10.1111/joa.13363>
- Bonsor, J. A., Lockwood, J. A. F., Vasco Leite, J., Scott-Murray, A., & Maidment, S. C. R. (2023).** The osteology of the holotype of the British iguanodontian dinosaur *Mantellisaurus atherfieldensis*. *Monographs of the Palaeontographical Society*, 177 (665), 1–63. <https://doi.org/10.1080/02693445.2023.2234156>
- Borinder, N. H. (2015).** *Postcranial anatomy of Tanius sinensis Wiman, 1929 (Dinosauria: Hadrosauoidea)* [PhD thesis]. Uppsala University.
- Borinder, N. H., Poropat, S. F., Campione, N. E., Wigren, T., & Kear, B. P. (2021).** Postcranial osteology of the basally branching hadrosauroid dinosaur *Tanuis sinensis* from the Upper Cretaceous Wangshi Group of Shandong, China. *Journal of Vertebrate Paleontology*, 41(1), 1–20. <https://doi.org/10.1080/02724634.2021.1914642>
- Boyd, C. A., & Pagnac, D. C. (2015).** Insight on the anatomy, systematic relationships, and age of the Early Cretaceous ankylopollexian dinosaur *Dakotadon lakotaensis*. *PeerJ* 3: e1263; <https://doi.org/10.7717/peerj.1263>
- Brett-Surman, M. K., & Wagner, J. R. (2007).** Discussion of character analysis of the appendicular anatomy in Campanian and Maastrichtian North American hadrosaurids – variation and ontogeny. In K. Carpenter (Ed.), *Horns and beaks: Ceratopsian and ornithopod dinosaurs* (pp. 135–169). Indiana University Press, Bloomington and Indianapolis, USA.
- Brochu, C. A. (1996).** Closure of neurocentral sutures during crocodylian ontogeny: Implications for maturity assessment in fossil archosaurs. *Journal of Vertebrate Paleontology*, 16, 49–62. <https://doi.org/10.1080/02724634.1996.10011283>
- Brown, B. (1913a).** A new trachodont dinosaur, *Hypacrosaurus*, from the Edmonton Cretaceous of Alberta. *Bulletin of the American Museum of Natural History*, 32, 395–406.
- Brown, B. (1913b).** The skeleton of *Saurolophus*, a crested duck-billed dinosaur from the Edmonton Cretaceous. *Bulletin of the American Museum of Natural History*, 32, 387–393.
- Carpenter, K., & Ishida, Y. (2010).** Early and "Middle" Cretaceous iguanodonts in time and space. *Journal of Iberian Geology*, 36, 145–164. [https://doi.org/10.5209/rev\\_JIGE.2010.v36.n2.3](https://doi.org/10.5209/rev_JIGE.2010.v36.n2.3)
- Carpenter, K., & Wilson, Y. (2008).** A new species of *Camptosaurus* (Ornithopoda: Dinosauria) from the Morrison Formation (Upper Jurassic) of Dinosaur National Monument, Utah, and a biomechanical analysis of its forelimb. *Annals of Carnegie Museum*, 76, 227–263. [https://doi.org/10.2992/0097-4463\(2008\)76\[227:ANSOCO\]2.0.CO;2](https://doi.org/10.2992/0097-4463(2008)76[227:ANSOCO]2.0.CO;2)
- Castanera, D., Badenas, B., Aurell, M., Canudo, J. I., & Gasca, J. M. (2022).** New ornithopod tracks from the Lower Cretaceous El Castellar Formation (Spain): Implications for track preservation and evolution of ornithopod footprints. *Palaeogeography, Palaeoclimatology, Palaeoecology*, 591, 1–12. <https://doi.org/10.1016/j.palaeo.2022.110866>
- Chiarenza, A. A., Fabbri, M., Consorti, L., Muscioni, M., Evans, D. C., Cantalapiedra, J. L., & Fanti, F. (2021).** An Italian dinosaur lagerstätte reveals the tempo and mode of hadrosauriform body size evolution. *Scientific Reports*, 11(1), 23295. <https://doi.org/10.1038/s41598-021-02490-x>
- Clarke, J. B. (1994).** Authigenic minerals in vertebrate fossils from the Wealden Group (Lower Cretaceous) of the Isle of Wight. *Geological Curator*, 6, 11–15. <https://doi.org/10.55468/GC174>
- Cohen, K. M., Finney, S. C., Gibbard, P. L., & Fan, J.-X. (2013; updated 2022).** The ICS International Chronostratigraphic Chart. *Episodes*, 36, 199–204. <https://doi.org/10.18814/epiugs/2013/v36i3/002>
- Cullen, T. M., Brown, C. M., Chiba, K., Brink, K. S., Makovicky, P. J., & Evans, D. C. (2021).** Growth variability, dimensional scaling, and the interpretation of osteohistological growth data. *Biology Letters*, 17, 20210383. <https://doi.org/10.1098/rsbl.2021.0383>
- Dalla Vecchia, F. M. (2009).** *Tethyshadros insularis*, a new hadrosauroid dinosaur (Ornithischia) from the Upper Cretaceous of Italy. *Journal of Vertebrate Paleontology*, 29, 1100–1116. <https://doi.org/10.1671/039.029.0428>
- Dilkes, D. W. (1993).** *Growth and locomotion in the hadrosaurian dinosaur Maiasaura from the Upper Cretaceous of Montana*. [PhD thesis]. University of Toronto.
- Dodson, P., & Madsen, J. H. (1981).** On the sternum of *Camptosaurus*. *Journal of Paleontology*, 55, 109–112.
- Eberth, D. A. (1996).** Origin and significance of mud-filled incised valleys (Upper Cretaceous) in southern Alberta, Canada. *Sedimentology*, 43, 459–477. <https://doi.org/10.1046/j.1365-3091.1996.d01-15.x>
- Eberth, D. A. (2005).** The geology. In P. J. Currie & E. B. Koppelhus (Eds.), *Dinosaur Provincial Park: A spectacular ancient ecosystem revealed* (pp. 54–82). Indiana University Press.
- Edmund, A. G. (1957).** On the special foramina in the jaws of many ornithischian dinosaurs. *Contributions of the Royal Ontario Museum*, 48, 3–14.
- Erickson, G. M., Lappin, A. K., & Larson, P. (2005).** Androgynous rex - the utility of chevrons for determining the sex of crocodylians and non-avian dinosaurs. *Zoology (Jena)*, 108, 277–286. <https://doi.org/10.1016/j.zool.2005.08.001>

- Erickson, G. M., Rodgers, K. C., & Yerby, S. A. (2001).** Dinosaurian growth patterns and rapid avian growth rates. *Nature*, 412, 429–433. <https://doi.org/10.1038/35086558>
- Falcon, N. L., & Kent, P. E. (1960).** Geological results of petroleum exploration in Britain. 1945–1957. *Memoir of the Geological Society of London*, 2, 66.
- Fondevilla, V., Dalla Vecchia, F. M., Gaete, R., Galobart, À., Moncunill-Sole, B., & Kohler, M. (2018).** Ontogeny and taxonomy of the hadrosaur (Dinosauria, Ornithopoda) remains from Basturs Poble bonebed (late early Maastrichtian, Tremp Syncline, Spain). *PLoS ONE* 13, e0206287. <https://doi.org/10.1371/journal.pone.0206287>
- Forster, C. A. (1990).** The postcranial skeleton of the ornithopod dinosaur *Tenontosaurus tilletti*. *Journal of Vertebrate Paleontology*, 10, 273–294. <https://doi.org/10.1080/02724634.1990.10011815>
- Fowler, D. (2020).** The Hell Creek Formation, Montana: A stratigraphic review and revision based on a sequence stratigraphic approach. *Geosciences*, 10, 1–59. <https://doi.org/10.3390/geosciences10110435>
- Francis, J. E. (1987).** The palaeoclimatic significance of growth rings in the Late Jurassic/Early Cretaceous fossil wood from southern England. In R. G. W. Ward (Ed.), *Applications of tree ring studies. Current research in dendrochronology and related subjects, BAR International Series*, 333 (pp. 21–36). University of Virginia, Charlottesville.
- Fuentes Vidarte, C., Meijide Calvo, M., Meijide Fuentes, F., & Meijide Fuentes, M. (2016).** Un nuevo dinosaurio estiracosterno (Ornithopoda: Ankylopollexia) del Cretácico Inferior de España. *Spanish Journal of Palaeontology*, 31, 407–446. <https://doi.org/10.7203/sjp.31.2.17163>
- Gale, A. S. (2019).** *The Isle of Wight. Geologists' Association Guide No. 6*, The Geologists' Association.
- Gale, A. S., Mutterlose, J., & Batenburg, S.** with contributions by Gradstein, F. M., Agterberg, F. P., Ogg, J. G., & Petrizzo, M. R. (2020). The Cretaceous Period. In F. M. Gradstein, J. G. Ogg, M. D. Schmitz, & G. M. Ogg. (Eds.), *Geologic time scale 2020*, 2 (pp. 1–63). Elsevier.
- Galton, P. M. (1974).** The ornithischian dinosaur *Hypsilophodon* from the Wealden of the Isle of Wight. *Bulletin of the British Museum (Natural History), Geology*, 25, 1–152. <https://doi.org/10.5962/p.313819>
- Galton, P. M. (1977).** The Upper Jurassic dinosaur *Dryosaurus* and a Laurasia-Gondwana connection in the Upper Jurassic. *Nature*, 268, 230–232. <https://doi.org/10.1038/268230a0>
- Galton, P. M. (1978).** Fabrosauridae, the basal family of ornithischian dinosaurs (Reptilia: Ornithischia). *Paläontologische Zeitschrift*, 52, 138–159. <https://doi.org/10.1007/BF03006735>
- Galton, P. M. (1980a).** European Jurassic ornithopod dinosaurs of the families Hypsilophodontidae and Camptosauridae. *Neues Jahrbuch für Geologie und Paläontologie, Abhandlungen*, 160, 73–95.
- Galton, P. M. (1980b).** *Dryosaurus* and *Camptosaurus*, intercontinental genera of Upper Jurassic ornithopod dinosaurs. *Memoires de la Societe geologique de France*, 139, 103–108.
- Galton, P. M. (1981).** *Dryosaurus*, a hypsilophodontid dinosaur from the Upper Jurassic of North America and Africa. *Paläontologische Zeitschrift*, 55, 271–312.
- Galton, P. M. (1983).** The cranial anatomy of *Dryosaurus*, a hypsilophodontid dinosaur from the Upper Jurassic of North America and East Africa, with a review of hypsilophodontids from the Upper Jurassic of North America. *Geologica et Palaeontologica*, 17, 207–243.
- Galton, P. M. (2009).** Notes on Neocomian (Lower Cretaceous) ornithopod dinosaurs from England – *Hypsilophodon*, *Valdosaurus*, “*Camptosaurus*”, “*Iguanodon*” – and referred specimens from Romania and elsewhere. *Revue de Paleobiologie, Geneve*, 28, 211–273.
- Galton, P. M., & Powell, H. P. (1980).** The ornithischian dinosaur *Camptosaurus prestwichii* from the Upper Jurassic of England. *Palaeontology*, 23, 411–443.
- Garrison, J. R., Brinkman, D., Nichols, D. J., Layer, P., Burge, D., & Thayne, D. (2007).** A multidisciplinary study of the Lower Cretaceous Cedar Mountain Formation, Mussentuchit Wash, Utah: a determination of the paleoenvironment and paleoecology of the *Eolambia caroljonesa* dinosaur quarry. *Cretaceous Research*, 28, 461–494. <https://doi.org/10.1016/j.cretres.2006.07.007>
- Gasca, J. M., Canudo, J. I., & Moreno-Azanza, M. (2014).** On the diversity of Iberian iguanodont dinosaurs: new fossils from the lower Barremian, Teruel province, Spain. *Cretaceous Research*, 50, 264–272. <https://doi.org/10.1016/j.cretres.2014.05.009>
- Gasca, J. M., Moreno-Azanza, M., Ruiz-Omeñaca, J. I., & Canudo, J. I. (2015).** New material and phylogenetic position of the basal iguanodont dinosaur *Delapparentia turolensis* from the Barremian (Early Cretaceous) of Spain. *Journal of Iberian Geology*, 41, 57–70. [https://doi.org/10.5209/rev\\_JIGE.2015.v41.n1.48655](https://doi.org/10.5209/rev_JIGE.2015.v41.n1.48655)
- Gasulla, J. M., Escaso, F., Narvaez, I., Otega, F., & Sanz, J. L. (2015).** A new sail-backed styracosternan (Dinosauria: Ornithopoda) from the Early Cretaceous of Morella, Spain. *PLoS ONE*, 10, e0144167. <https://doi.org/10.1371/journal.pone.0144167>
- Gates, T. A., & Lamb, J. P. (2021).** A redescription of *Lophorhynchon atopus* (Ornithopoda: Dinosauria) from the Late Cretaceous of Alabama based on new material. *Canadian Journal of Earth Sciences*, 58, 918–935. <https://doi.org/10.1139/cjes-2020-0173>
- Gates, T. A., Tsogtbaatar, K., Zanno, L. E., Chinzorig, T., & Watabe, M. (2018).** A new iguanodontian (Dinosauria: Ornithopoda) from the Early Cretaceous of Mongolia. *PeerJ*, 6, e5300; <https://doi.org/10.7717/peerj.5300>
- Gilmore, C. W. (1909).** Osteology of the Jurassic reptile *Camptosaurus*, with a revision of the species of the genus, and descriptions of two new species. *Proceedings of the United States National Museum*, 36, 197–332. <https://doi.org/10.5479/si.00963801.36-1666.197>
- Gilmore, C. W. (1925).** Osteology of ornithopodous dinosaurs from the Dinosaur National Monument, Utah. *Memoirs of the Carnegie Museum*, 10(4), 385–411. <https://doi.org/10.5962/p.234845>
- Gilmore, C. W. (1933).** On the dinosaurian fauna of the Iren Dabasu Formation. *Bulletin of the American Museum of Natural History*, 67, 23–78.
- Gilmore, C. W. (1937).** On the detailed skull structure of a crested hadrosaurian dinosaur. *Proceedings of the United States National Museum*, 84, 481–491. <https://doi.org/10.5479/si.00963801.84-3023.481>
- Gilpin, D., DiCroce, T., & Carpenter, K. (2007).** A possible new basal hadrosaur from the Lower Cretaceous Cedar Mountain Formation of eastern Utah. In K. Carpenter (Ed.), *Horns and beaks: Ceratopsian and ornithopod dinosaurs* (pp. 79–89). Indiana University Press.

- Godefroit, P., Bolotsky, Y. L., & Bolotsky, I. Y. (2011).** Osteology and relationships of *Olorotitan arharensis*, a hollow crested hadrosaurid dinosaur from the latest Cretaceous of Far Eastern Russia. *Acta Palaeontologica Polonica*, 57, 527–560. <https://doi.org/10.4202/app.2011.0051>
- Godefroit, P., Bolotsky, Y. L., & Lauters, P. (2012).** A new saurolophine dinosaur from the latest Cretaceous of far eastern Russia. *PLOS ONE*, 7, <https://doi.org/10.1371/journal.pone.0036849>
- Godefroit, P., Bolotsky, Y. L., & Van Itterbeeck, J. (2004).** The lambeosaurine dinosaur *Amurosaurus riabinini*, from the Maastrichtian of Far Eastern Russia. *Acta Palaeontologica Polonica*, 49, 585–618.
- Godefroit, P., Codrea, V., & Weishampel, D. B. (2009).** Osteology of *Zalmoxes shqiperorum* (Dinosauria, Ornithopoda), based on new specimens from the Upper Cretaceous of Nalat-Vad (Romania). *Geodiversitas*, 31, 525–553. <https://doi.org/10.5252/g2009n3a3>
- Godefroit, P., Dong, Z.-M., Bultynck, P., Li, H., & Feng, L. (1998).** Sino-Belgian Cooperative Program. Cretaceous dinosaurs and mammals from Inner Mongolia: 1) New *Bactrosaurus* (Dinosauria: Hadrosauridae) material from Iren Dabasu (Inner Mongolia, P.R. China). *Bulletin de l'Institut Royal des Sciences Naturelles du Belgique*, 68, 1–70.
- Godefroit, P., Escuille, F., Bolotsky, Y. L., & Lauters, P. (2012).** A new basal hadrosauroid dinosaur from the Upper Cretaceous of Kazakhstan. In P. Godefroit (Ed.), *Bernissart dinosaurs and Early Cretaceous terrestrial ecosystems* (pp. 335–362). Indiana University Press.
- Godefroit, P., Li, H., & Shang, C.-Y. (2005).** A new primitive hadrosauroid dinosaur from the Early Cretaceous of Inner Mongolia (P.R. China). *Comptes Rendus Palevol*, 4, 697–705. <https://doi.org/10.1016/j.crpv.2005.07.004>
- Goloboff, P. A., & Morales, M. (2023).** TNT version 1.6, with graphical interface for MacOs and Linux, including new routines in parallel [Computer software]. *Cladistics*. <https://doi.org/10.1111/cla.12524>
- Griffin, C. T., Stocker, M. R., Colleary, C., Stefanic, C. M., Lessner, E. J., Riegler, M., Formosal, K., Koeller, K., & Nesbitt, S. J. (2020).** Assessing ontogenetic maturity in extinct saurian reptiles. *Biological Reviews*, 96, 470–525. <https://doi.org/10.1111/brv.12666>
- Head, J. J. (1998).** A new species of basal hadrosaurid (Dinosauria, Ornithopoda) from the Cenomanian of Texas. *Journal of Vertebrate Paleontology*, 18, 718–738. <https://doi.org/10.1080/02724634.1998.10011101>
- Heaton, M. J. (1972).** The palatal structure of some Canadian Hadrosauridae (Reptilia: Ornithischia). *Canadian Journal of Earth Sciences*, 9, 185–205. <https://doi.org/10.1139/e72-015>
- Heinrich, C., Paes Nato, V. D., Lacerda, M. B., Martinelli, A. G., Fiedler, M. S., & Schultz, C. L. (2021).** The ontogenetic pattern of neurocentral suture closure in the axial skeleton of Hyperodapedontinae (Archosauromorpha, Rhynchosauria) and its evolutionary implications. *Palaeontology*, 64, 409–427. <https://doi.org/10.1111/pala.12528>
- Hooley, R. W. (1917).** On the integument of *Iguanodon bernissartensis*, Boulenger, and of *Morosaurus becklesii*, Mantell. *The Geological Magazine*, 64, 140–150. <https://doi.org/10.1017/S0016756800192386>
- Hooley, R. W. (1925).** On the skeleton of *Iguanodon atherfieldensis* sp. nov., from the Wealden Shales of Atherfield (Isle of Wight). *Quarterly Journal of the Geological Society of London*, 81, 1–61. <https://doi.org/10.1144/GSL.JGS.1925.081.01-04.02>
- Horner, J. R., Currie, P. J. (1994).** Embryonic and neonatal morphology and ontogeny of a new species of *Hypacrosaurus* (Ornithischia, Lambeosauridae) from Montana and Alberta. In K. Carpenter, K. F. Hirsch & J. R. Horner (Eds.), *Dinosaur eggs and babies* (pp. 312–336). Cambridge University Press.
- Horner, J. R., Ricqles, A. & de Padian, K. (1999).** Variation in dinosaur skeletochronology indicators: implications for age assessment and physiology. *Paleobiology*, 25(3), 295–304. <https://doi.org/10.1017/S0094837300021308>
- Horner, J. R., Ricqles, A. & de Padian, K. (2000).** Long bone histology of the hadrosaurid dinosaur *Maiasaura peeblesorum*: growth dynamics and physiology based on an ontogenetic series of skeletal elements. *Journal of Vertebrate Paleontology*, 20, 115–129. [https://doi.org/10.1671/0272-4634\(2000\)020\[0115:LBHOTH\]2.0.CO;2](https://doi.org/10.1671/0272-4634(2000)020[0115:LBHOTH]2.0.CO;2)
- Horner, J. R., Varricchio, D. J., & Goodwin, M. B. (1992).** Marine transgressions and the evolution of Cretaceous dinosaurs. *Nature*, 358, 59–61. <https://doi.org/10.1038/358059a0>
- Horner, J. R., Weishampel, D. B., & Forster, C. A. (2004).** Hadrosauridae. In D. B. Weishampel, P. Dodson, & H. Osmolska (Eds.) *The Dinosauria* (2nd ed., pp. 436–463). University of California Press.
- Hübner, T. R. (2010).** Ontogeny in *Dysalotosaurus lettowvorbecki* [PhD thesis]. Ludwig Maximilians Universität.
- Hübner, T. R. (2012).** Bone histology in *Dysalotosaurus lettowvorbecki* (Ornithischia: Iguanodontia) – variation, growth, and implications. *PLoS ONE*, 7(1), e29958. <https://doi.org/10.1371/journal.pone.0029958>
- Hughes, N. F., & McDougall, A. D. (1990).** New Wealden correlation for the Wessex Basin. *Proceedings of the Geologists' Association*, 101, 85–90.
- Hulke, J. W. (1871).** Note on a large reptilian skull from Brook, Isle of Wight, probably dinosaurian and referable to the genus *Iguanodon*. *The Quarterly Journal of the Geological Society of London*, 27, 199–206. <https://doi.org/10.1144/GSL.JGS.1871.027.01-02.27>
- Hulke, J. W. (1879).** *Vectisaurus valdensis*, a new Wealden Dinosaur. *Quarterly Journal of the Geological Society of London*, 35, 421–424. <https://doi.org/10.1144/GSL.JGS.1879.035.01-04.27>
- Hulke, J. W. (1880).** *Iguanodon prestwichii*, a new species from the Kimmeridge Clay, founded on numerous fossil remains lately discovered at Cumnor, near Oxford. *Quarterly Journal of the Geological Society of London*, 36, 433–456. <https://doi.org/10.1144/GSL.JGS.1880.036.01-04.36>
- Hulke, J. W. (1882).** Description of some *Iguanodon* remains indicating a new species *I. seelyi*. *Quarterly Journal of the Geological Society*, 150, 135–144. <https://doi.org/10.1144/GSL.JGS.1882.038.01-04.16>
- Jacobs, M. L., Perez-Garcia, A., Martín-Jimenez, M., Mottram, C. M., Martill, D. M., Gale, A. S., Mattsson, O., & Wood, C. (2023).** A well preserved pan-pleurodiran (Dortokidae) turtle from the English Lower Cretaceous and the first radiometric date for the Wessex Formation (Hauterivian-Barremian) of the Isle of Wight, United

- Kingdom. *Cretaceous Research*, 150, 1–15. <https://doi.org/10.1016/j.cretres.2023.105590>
- Janensch, W.** (1955). Der Ornithopode *Dysalotosaurus* der Tendaguruschichten. *Palaeontographica (Supplementbände 7)*, 3, 105–176.
- Joeckel, R. M., Suarez, C. A., McLean, N. M., Möller, A., Ludvigson, G. A., Suarez, M. B., Kirkland, J. I., Andrew, J., Kiessling, S., & Hatzell, G. A.** (2023). Berriasian–Valanginian geochronology and carbon-isotope stratigraphy of the Yellow Cat Member, Cedar Mountain Formation, Eastern Utah, USA. *Geosciences*, 13 (32), 18. <https://doi.org/10.3390/geosciences13020032>
- Kerth, M., & Hailwood, E. A.** (1988). Magnetostratigraphy of the Lower Cretaceous Vectis Formation (Wealden Group) on the Isle of Wight, southern England. *Journal of the Geological Society, London*, 145, 351–360. <https://doi.org/10.1144/gsjgs.145.2.0351>
- Kinne, J.** (2016). Postmortem examination. In Samour, J. (Ed.), *Avian Medicine* (3rd ed., pp. 567–581). Elsevier.
- Kobayashi, Y., & Azuma, Y.** (2003). A new iguanodontian (Dinosauria: Ornithopoda) from the Lower Cretaceous Kitadani Formation of Fukui Prefecture, Japan. *Journal of Vertebrate Paleontology*, 23, 392–396. [https://doi.org/10.1671/0272-4634\(2003\)23\[166:ANIDOF\]2.0.CO;2](https://doi.org/10.1671/0272-4634(2003)23[166:ANIDOF]2.0.CO;2)
- Langer, M. C.** (2004). Basal Saurischia. In D. B. Weishampel, P. Dodson, & H. Osmolska (Eds.), *The Dinosauria* (2nd ed., pp. 25–46). University of California Press.
- Langstone, W.** (1960). The vertebrate fauna of the Selma Formation of Alabama, Part VI: The dinosaurs. *Fieldiana Geology Memoirs*, 3 (pp. 316–363). Chicago Natural History Museum.
- Larson, P. L.** (1994). *Tyrannosaurus* sex. In G. D. Rosenberg & D. L. Wolberg (Eds.), *Dino Fest. The Paleontological Society Special Publication*, 7 (pp. 139–155). The Paleontological Society.
- Lauters, P., Coudyzer, W., Vercauteren, M., & Godefroit, P.** (2012). The brain of *Iguanodon* and *Mantellisaurus*: Perspectives on ornithopod evolution. In P. Godefroit (Ed.), *Bernissart Dinosaurs and early Cretaceous Terrestrial Ecosystems* (pp. 213–224). Indiana University Press.
- Lauters, P., Vercauteren, M., Bolotsky, Y. L., & Godefroit, P.** (2013). Cranial endocast of the lambeosaurine hadrosaurid *Amurosaurus riabinini* from the Amur Region, Russia. *PLoS ONE* 8, e78899. <https://doi.org/10.1371/journal.pone.0078899>
- Lockwood, J. A. F., Larkin, N., & Lomax, D.** (2019). *The palaeontological contributions of Nick Chase: A 20th century fox* [SVPCA Conference Abstracts 2019]. The 67<sup>th</sup> Symposium on Vertebrate Palaeontology and Comparative Anatomy, Isle of Wight, UK.
- Lockwood, J. A. F., Martill, D. M., & Maidment, S. R. M.** (2021). A new hadrosauriform dinosaur from the Wessex Formation, Wealden Group (Early Cretaceous), of the Isle of Wight, southern England. *Journal of Systematic Palaeontology*, 19, 847–888. <https://doi.org/10.1080/14772019.2021.1978005>
- Longrich, N. R., Martill, D. M., & Jacobs, M. L.** (2022). A new dromaeosaurid dinosaur from the Wessex Formation (Lower Cretaceous, Barremian) of the Isle of Wight, and implications for European palaeobiogeography. *Cretaceous Research*, 134, 105–123. <https://doi.org/10.1016/j.cretres.2021.105123>
- Longrich, N. R., Martill, D. M., Munt, M., Green, M., Penn, M., & Smith, S.** (2023). *Vectidromeus insularis*, a new hypsilophodontid dinosaur from the Lower Cretaceous Wessex Formation of the Isle of Wight, England. *Cretaceous Research*, 105707. <https://doi.org/10.1016/j.cretres.2023.105707>
- Lydekker, R.** (1888). Note on a new Wealden iguanodont and other dinosaurs. *Quarterly Journal of the Geological Society of London*, 44, 46–61. <https://doi.org/10.1144/GSL.JGS.1888.044.01-04.08>
- Lydekker, R.** (1889). On the remains and affinities of five genera of Mesozoic reptiles. *Quarterly Journal of the Geological Society of London*, 45, 41–59. <https://doi.org/10.1144/GSL.JGS.1889.045.01-04.04>
- Lull, R. S., & Wright, N. E.** (1942). Hadrosaurian dinosaurs of North America. *Special Paper of the Geological Society of America*. 40, 1–242 pp.
- Maddison, W. P., & Maddison, D. R.** (2015). *Mesquite: A modular system for evolutionary analysis* (Version 3.61) [Computer software]. [www.mesquiteproject.org](http://www.mesquiteproject.org)
- Madzia, D., Jagt, J. W. M., & Mulder, E. W. A.** (2020). Osteology, phylogenetic affinities and taxonomic status of the enigmatic late Maastrichtian ornithopod taxon *Orthomerus dolloi* (Dinosauria, Ornithischia). *Cretaceous Research*, 108, 1–19. <https://doi.org/10.1016/j.cretres.2019.104334>
- Maidment, S. C. R., & Barrett, P. M.** (2011). The locomotor musculature of basal ornithischian dinosaurs. *Journal of Vertebrate Paleontology*, 31, 1265–1291. <https://doi.org/10.1080/02724634.2011.606857>
- Maidment, S. C. R., & Barrett, P. M.** (2012). Does morphological convergence imply functional similarity? A test using the evolution of quadrupedalism in ornithischian dinosaurs. *Proceedings of the Royal Society B*, 279, 3765–3771. <https://doi.org/10.1098/rspb.2012.1040>
- Maidment, S. C. R., Chapelle, K. E. J., Bonsor, J. A., Button, D., & Barrett, P. M.** (2022). Osteology and relationships of *Cumnoria prestwichii* (Ornithischia: Ornithopoda) from the late Jurassic of Oxfordshire, UK. *Monograph of the Palaeontological Society*, 1–55, pl. 1–12.
- Mallon, J. C., Evans, D. C., Ryan, M. J., & Anderson, J. S.** (2012). Megaherbivorous dinosaur turnover in the Dinosaur Park Formation (upper Campanian) of Alberta, Canada. *Palaeogeography, Palaeoclimatology, Palaeoecology*, 350–352, 124–138. <https://doi.org/10.1016/j.palaeo.2012.06.024>
- Mantell, G. A.** (1825). Notice on the *Iguanodon*, a newly discovered fossil reptile, from the sandstone of Tilgate Forest, in Sussex. *Philosophical Transactions of the Royal Society*, 115, 179–186.
- Marsh, O. C.** (1881). Principal characters of American Jurassic dinosaurs. Part IV. Spinal cord, pelvis, and limbs of *Stegosaurus*. *American Journal of Science, Series 3*, 21, 167–170. <https://doi.org/10.2475/ajs.s3-21.122.167>
- Martill, D. M., & Naish, D.** (2001). *Dinosaurs of the Isle of Wight. Field guide to fossils, No. 10. The Palaeontological Association*. Wiley-Blackwell.
- McDonald, A. T.** (2011). The taxonomy of species assigned to *Camptosaurus* (Dinosauria: Ornithopoda). *Zootaxa*, 2783, 52–68. <https://doi.org/10.11646/zootaxa.2783.1.4>
- McDonald, A. T.** (2012a). The status of *Dollodon* and other basal iguanodonts (Dinosauria: Ornithischia) from the upper Wealden beds (Lower Cretaceous) of Europe.

- Cretaceous Research*, 33, 1–6. <https://doi.org/10.1016/j.cretres.2011.03.002>
- McDonald, A. T.** (2012b). Phylogeny of basal iguanodonts (Dinosauria: Ornithischia): an update. *PLoS ONE*, 7, e36745. <https://doi.org/10.1371/journal.pone.0036745>
- McDonald, A. T., Barrett, P. M., & Chapman, S. D.** (2010). A new basal iguanodont (Dinosauria: Ornithischia) from the Wealden (Lower Cretaceous) of England. *Zootaxa*, 2569, 1–43. <https://doi.org/10.11646/zootaxa.2569.1.1>
- McDonald, A. T., Bird, J., Kirkland, J. I., & Dodson, P.** (2012). Osteology of the basal hadrosauroid *Eolambia caroljonesa* (Dinosauria: Ornithopoda) from the Cedar Mountain Formation of Utah. *PLoS ONE*, 7, e45712. <https://doi.org/10.1371/journal.pone.0045712>
- McDonald, A. T., Espilez, E., Mampel, L., Kirkland, J. I., & Alcalá, L.** (2012). An unusual new basal iguanodont (Dinosauria: Ornithopoda) from the Lower Cretaceous of Teruel, Spain. *Zootaxa*, 3595, 61–76. <https://doi.org/10.11646/zootaxa.3595.1.3>
- McDonald, A. T., Gates, T. A., Zanno, L. E., & Makovicky, P. J.** (2017). Anatomy, taphonomy, and phylogenetic implications of a new specimen of *Eolambia caroljonesa* (Dinosauria: Ornithopoda) from the Cedar Mountain Formation, Utah, USA. *PLoS ONE*, 12, 1–32. <https://doi.org/10.1371/journal.pone.0176896>
- McDonald, A. T., Kirkland, J. I., DeBlieux, D. D., Madsen, S. K., Cavin, J., Milner, A. R. C., & Panzarin, I.** (2010). New basal iguanodonts from the Cedar Mountain Formation of Utah and the evolution of thumb-spiked dinosaurs. *PLoS ONE*, 5, e14075. <https://doi.org/10.1371/journal.pone.0014075>
- McDonald, A. T., Maidment, S. C. R., Barrett, P. M., You, H.-L., & Dodson, P.** (2014). Osteology of the basal Hadrosauroid *Equijubus normani* (Dinosauria, Ornithopoda) from the Early Cretaceous of China. In D. A. Eberth & D. C. Evans (Eds.), *Hadrosaurs* (pp. 44–72). Indiana University Press.
- McDonald, A. T., Wolfe, D. G., & Kirkland, J. I.** (2010). A new basal hadrosauroid (Dinosauria: Ornithopoda) from the Turonian of New Mexico. *Journal of Vertebrate Paleontology*, 30, 799–812. <https://doi.org/10.1080/02724631003763516>
- Medrano-Aguado, E., Parrilla-Bel, J., Gasca, J. M., Alonso, A., & Canudo, J. I.** (2023). Ornithopod diversity in the Lower Cretaceous of Spain: new styracosternan remains from the Barremian of the Maestrazgo Basin (Teruel province, Spain). *Cretaceous Research*, 144. <https://doi.org/10.1016/j.cretres.2022.105458>
- Moreno, K., Carrano, M. T., & Snyder, R.** (2007). Morphological changes in pedal phalanges through ornithopod dinosaur evolution: A biomechanical approach. *Journal of Morphology*, 268, 50–63. <https://doi.org/10.1002/jmor.10498>
- Mori, H., Druckenmiller, P., Erickson, G., & Prieto-Marquez, A.** (2013). Cranial ontogeny of *Edmontosaurus*: implications for the taxonomic status of the Prince Creek Formation species (lower Maastrichtian, northern Alaska). 73rd Annual Meeting of the Society of Vertebrate Paleontology, Los Angeles, California, USA. *Journal of Vertebrate Paleontology*, 33 (Supplement to 3), 180.
- Mori, H., Druckenmiller, P., Prieto-Marquez, A., & Joshi, S.** (2012). Reconstruction and morphometric analysis of juvenile *Edmontosaurus* sp. from the lower Maastrichtian (Cretaceous) Prince Creek Formation of northern Alaska. 72nd Annual Meeting of the Society of Vertebrate Paleontology, Raleigh, North Carolina, USA. *Journal of Vertebrate Paleontology*, 32 (Supplement to 3), 145.
- Norman, D. B.** (1980). On the ornithischian dinosaur *Iguanodon bernissartensis* of Bernissart (Belgium). *Memoires de l'Institut Royal des Sciences Naturelles de Belgique*, 178, 1–105.
- Norman, D. B.** (1986). On the anatomy of *Iguanodon atherfieldensis* (Ornithischia: Ornithopoda). *Bulletin de l'Institut Royal des Sciences Naturelles de Belgique Sciences de la Terre*, 56, 281–372.
- Norman, D. B.** (1990). A review of *Vectisaurus valdensis*, with comments on the family Iguanodontidae. In K. Carpenter & P. J. Currie (Eds.), *Dinosaur systematics: Approaches and perspectives* (pp. 147–162). Cambridge University Press.
- Norman, D. B.** (1998). On Asian ornithopods (Dinosauria, Ornithischia). 3. A new species of iguanodontid dinosaur. *Zoological Journal of the Linnean Society*, 122, 291–348. <https://doi.org/10.1111/j.1096-3642.1998.tb02533.x>
- Norman, D. B.** (2002). On Asian ornithopods (Dinosauria: Ornithischia). 4. *Probaetosauros Rozhdvestvensky*, 1966. *Zoological Journal of the Linnean Society*, 136, 113–144. <https://doi.org/10.1046/j.1096-3642.2002.00027.x>
- Norman, D. B.** (2011a). Ornithopod dinosaurs. In D. J. Batten (Ed.), *Field Guide to the Wealden of England* (pp. 407–475). The Palaeontological Association.
- Norman, D. B.** (2011b). On the osteology of the lower Wealden (Valanginian) ornithopod *Barilium dawsoni* (Iguanodontia: Styracosterna). *Special papers in Palaeontology*, 86, 165–194.
- Norman, D. B.** (2012). Iguanodontian taxa (Dinosauria: Ornithischia) from the Lower Cretaceous of England and Belgium. In P. Godefroit (Ed.), *Bernissart dinosaurs and Early Cretaceous terrestrial ecosystems* (pp. 175–212). Indiana University Press.
- Norman, D. B.** (2013). On the taxonomy and diversity of Wealden iguanodontian dinosaurs (Ornithischia: Ornithopoda). *Revue de Paleobiologie*, 32, 385–404.
- Norman, D. B.** (2015). On the history, osteology, and systematic position of the Wealden (Hastings Group) dinosaur *Hypselospinus fittoni* (Iguanodontia: Styracosterna). *Zoological Journal of the Linnean Society*, 173, 92–189. <https://doi.org/10.1111/zoj.12193>
- Norman, D. B.** (2021). *Scelidosaurus harrisonii* (Dinosauria: Ornithischia) from the Early Jurassic of Dorset, England: biology and phylogenetic relationships. *Zoological Journal of the Linnean Society*, 191, 1–86. <https://doi.org/10.1093/zoolinnean/zlaa061>
- Ogg, J. G.** (2020). Geomagnetic polarity time scale. In F. M. Gradstein, J. G. Ogg, M. D. Schmitz & G. M. Ogg (Eds.), *Geologic Time Scale 2020* (pp. 159–189). Elsevier.
- Oldham, T. C. B.** (1976). The plant debris beds of the English Wealden. *Palaeontology*, 19, 437–502.
- Ostrom, J. H.** (1961). Cranial morphology of the hadrosaurian dinosaurs of North America. *Bulletin of the American Museum of Natural History*, 122, 33–186.
- Ostrom, J. H.** (1970). Stratigraphy and paleontology of the Cloverly Formation (Lower Cretaceous) of the Bighorn Basin area, Wyoming and Montana. *Peabody Museum Bulletin*, 35, 1–205.
- Owen, R.** (1842). Report on British fossil reptiles. Part II. *Report of the eleventh meeting of the British Association*

- for the Advancement of Science, held at Plymouth in July 1841 (pp. 60–204). John Murray.
- Parks, W. A.** (1922). *Parasaurolophus walkeri*, a new genus and species of trachodont dinosaur. *University of Toronto Studies: Geological Series*, 13, 5–32.
- Paul, G. S.** (2008). A revised taxonomy of the iguanodont dinosaur genera and species. *Cretaceous Research*, 29, 192–216. <https://doi.org/10.1016/j.cretres.2007.04.009>
- Paul, G. S.** (2012). Notes on the rising diversity of iguanodont taxa, and iguanodonts named after Darwin, Huxley, and evolutionary science. *Actas de V Jornadas Internacionales sobre Paleontología de Dinosaurios y su Entorno* (pp. 123–133), Salas de los Infantes, Burgos.
- Penn, S. J., & Sweetman, S. C.** (2023). Microvertebrate-rich gutter casts from the basal Wessex Formation (Wealden Group, Lower Cretaceous) of Dungey Head, Dorset: insights into the palaeoecology and palaeoenvironment of a non-marine wetland. *Cretaceous Research*, 143, 1–19. <https://doi.org/10.1016/j.cretres.2022.105397>
- Pond, S., Strachan, S., Raven, T. J., Simpson, M. I., Morgan, K., & Maidment, S. C. R.** (2023). *Vectipelta barretti*, a new ankylosaurian dinosaur from the Lower Cretaceous Wessex Formation of the Isle of Wight, UK. *Journal of Systematic Palaeontology*, 21 (1), 2210577, <https://doi.org/10.1080/14772019.2023.2210577>
- Poole, K. E.** (2015). *Phylogeny and biogeography of iguanodontian dinosaurs, with implications from ontogeny and an examination of the function of the fused carpal-digit I complex* [PhD thesis]. The Faculty of Columbian College of Arts and Sciences of The George Washington University.
- Poole, K. E.** (2022a). Phylogeny of iguanodontian dinosaurs and the evolution of quadrupedality. *Palaeontologia Electronica*, 25(3), 1–19. <https://doi.org/10.26879/702>
- Poole, K. E.** (2022b). Placing juvenile specimens in phylogenies: An ontogenetically sensitive phylogenetic assessment of a new genus of iguanodontian dinosaur from the Early Cretaceous Kirkwood Formation, South Africa. *The Anatomical Record*, Special issue article, 1–12. <https://doi.org/10.1002/ar.250951>
- Prieto-Marquez, A.** (2001). *Osteology and variation of Brachylophosaurus canadensis (Dinosauria, Hadrosauridae) from the Upper Cretaceous Judith River Formation of Montana* [Master's thesis]. Montana State University.
- Prieto-Marquez, A.** (2005). New information on the cranium of *Brachylophosaurus canadensis* (Dinosauria, Hadrosauridae), with a revision of its phylogenetic position. *Journal of Vertebrate Paleontology*, 25, 144–156.
- Prieto-Marquez, A.** (2008). *Phylogeny and historical biogeography of hadrosaurid dinosaurs* [PhD thesis]. Florida State University.
- Prieto-Marquez, A.** (2010). Global phylogeny of Hadrosauridae (Dinosauria: Ornithomorph) using parsimony and Bayesian methods. *Zoological Journal of the Linnean Society*, 159, 435–502. <https://doi.org/10.1111/j.1096-3642.2009.00617.x>
- Prieto-Marquez, A.** (2011). Cranial and appendicular ontogeny of *Bactrosaurus johnsoni*, a hadrosaurid dinosaur from the Late Cretaceous of northern China. *Palaeontology*, 54, 773–792. <https://doi.org/10.1111/j.1475-4983.2011.01053.x>
- Prieto-Marquez, A.** (2012). The skull and appendicular skeleton of *Gryposaurus latidens*, a saurolophine hadrosaurid (Dinosauria: Ornithomorph) from the early Campanian (Cretaceous) of Montana, USA. *Canadian Journal of Earth Sciences*, 49, 510–532. <https://doi.org/10.1139/e11-069>
- Prieto-Marquez, A.** (2014a). Skeletal morphology of *Kritosaurus navajovius* (Dinosauria: Hadrosauridae) from the Late Cretaceous of the North American south-west, with an evaluation of the phylogenetic systematics and biogeography of Kritosaurini. *Journal of Systematic Palaeontology*, 12, 133–175. <https://doi.org/10.1080/14772019.2013.770417>
- Prieto-Marquez, A.** (2014b). A juvenile *Edmontosaurus* from the late Maastrichtian (Cretaceous) of North America: Implications for ontogeny and phylogenetic inference in saurolophine dinosaurs. *Cretaceous Research*, 50, 282–303. <https://doi.org/10.1016/j.cretres.2014.05.003>
- Prieto-Marquez, A., Chiappe, L. M., & Joshi, S. H.** (2012). The lambeosaurine dinosaur *Magnapaulia laticaudus* from the Late Cretaceous of Baja, California, Northwestern Mexico. *PLoS ONE*, 7, e38207. <https://doi.org/10.1371/journal.pone.0038207>
- Prieto-Marquez, A., Erickson, G. M., & Ebersole, J. A.** (2016). Anatomy and osteohistology of the basal hadrosaurid dinosaur *Eotrachodon* from the uppermost Santonian (Cretaceous) of southern Appalachia. *PeerJ*, 4, e1872; <https://doi.org/10.7717/peerj.1872>
- Prieto-Marquez, A., & Norell, M. A.** (2010). Anatomy and relationships of *Gilmoresaurus mongoliensis* (Dinosauria: Hadrosauridae) from the Late Cretaceous of Central Asia. *American Museum Novitates*, 3694, 1–52.
- Prieto-Marquez, A., & Wagner, J. R.** (2009). *Pararhabdodon isonensis* and *Tsintaosaurus spinorhinus*: a new clade of lambeosaurine hadrosaurids from Eurasia. *Cretaceous Research*, 30, 1238–1246. <https://doi.org/10.1016/j.cretres.2009.06.005>
- Prieto-Marquez, A., Weishampel, D. B., & Horner, J. R.** (2006). The dinosaur *Hadrosaurus foulkii*, from the Campanian of the east coast of North America, with a reevaluation of the genus. *Acta Palaeontologica Polonica*, 51, 77–98.
- Radley, J. D.** (1994). Stratigraphy, palaeontology and palaeoenvironment of the Wessex Formation (Wealden Group, Lower Cretaceous) at Yaverland, Isle of Wight, Southern England. *Proceedings of the Geologists' Association*, 105, 199–208. [https://doi.org/10.1016/S0016-7878\(08\)80119-8](https://doi.org/10.1016/S0016-7878(08)80119-8)
- Radley, J. D.** (2006). A Wealden guide I: The Weald Sub-basin. *Geology Today*, 22, 109–118. <https://doi.org/10.1111/j.1365-2451.2006.00563.x>
- Radley, J. D., & Barker, M. J.** (1998). Stratigraphy, palaeontology and correlation of the Vectis Formation (Wealden Group, Lower Cretaceous) at Compton Bay, Isle of Wight, southern England. *Proceedings of the Geologists' Association*, 109, 187–195. [https://doi.org/10.1016/S0016-7878\(98\)80065-5](https://doi.org/10.1016/S0016-7878(98)80065-5)
- Radley, J. D., & Barker, M. J.** (2000). Palaeoenvironmental significance of storm coquinas in a Lower Cretaceous coastal lagoonal succession (Vectis Formation, Isle of Wight, southern England). *Geological Magazine*, 137, 193–205. <https://doi.org/10.1017/S0016756800003782>
- Radley, J. D., Barker, M. J., & Harding, I.** (1998). Palaeoenvironment and taphonomy of dinosaur tracks in the Vectis Formation (Lower Cretaceous) of the Wessex

- Sub-basin, southern England. *Cretaceous Research*, 19, 471–487. <https://doi.org/10.1006/cres.1997.0107>
- Ramirez-Velasco, A. A., Benammi, M., Prieto-Marquez, A., Ortega, J. A., & Hernandez-Rivera, R. (2012).** *Huehucanauhtlus tiquichensis*, a new hadrosauroid dinosaur (Ornithischia: Ornithopoda) from the Santonian (Late Cretaceous) of Michoacan, Mexico. *Canadian Journal of Earth Sciences*, 49, 379–395. <https://doi.org/10.1139/e11-062>
- Robinson, S. A., & Hesselbo, S. P. (2004).** Fossil-wood carbon-isotope stratigraphy of the non-marine Wealden Group (Lower Cretaceous, southern England). *Journal of the Geological Society, London*, 161, 133–145. <https://doi.org/10.1144/0016-764903-004>
- Romer, A. S. (1956).** The skull – general structure. Chapter 3, *Osteology of the reptiles*, University of Chicago Press, Chicago, USA.
- Rotatori, F. M., Moreno-Azanza, M., & Mateus, O. (2022).** Reappraisal and new material of the holotype of *Draconyx loureiroi* (Ornithischia: Iguanodontia) provide insights on the tempo and modo of evolution of thumb-spiked dinosaurs. *Zoological Journal of the Linnean Society*, 195, 125–156. <https://doi.org/10.1093/zoolinnean/zlab113>
- Ruffell, A. H., & Batten, D. J. (1990).** The Barremian–Aptian arid phase in western Europe. *Palaeogeography, Palaeoclimatology, Palaeoecology*, 80, 197–212. [https://doi.org/10.1016/0031-0182\(90\)90132-Q](https://doi.org/10.1016/0031-0182(90)90132-Q)
- Ruiz-Omeñaca, J. I. (2011).** *Delapparentia turolensis* nov. gen et sp., un nuevo dinosaurio iguanodontoideo (Ornithischia: Ornithopoda) en el Cretacico Inferior de Galve. *Estudios Geologicos*, 67, 83–110. <https://doi.org/10.3989/egeol.40276.124>
- Ruiz-Omeñaca, J. I. Pereda Suberbiola, X., & Galton, P. M. (2007).** *Callososaurus leedsi*, the earliest dryosaurid dinosaur (Ornithischia: Euornithopoda) from the Middle Jurassic of England. In K. Carpenter (Ed.), *Horns and beaks: Ceratopsian and ornithopod dinosaurs* (pp. 3–16). Indiana University Press.
- Sanchez-Fenollosa, S., Verdu, F. J. & Cobos, A. (2023).** The largest ornithopod (Dinosauria: Ornithischia) from the Upper Jurassic of Europe sheds light on the evolutionary history of basal ankylopollexians. *Zoological Journal of the Linnean Society*, 119, 1–21. <https://doi.org/10.1093/zoolinnean/zlad076>
- Sanchez-Fenollosa, S., Verdu, F. J., & Suñer, M. (2021).** Current knowledge of Late Jurassic ornithopod dinosaurs from Europe. *Ciències da Terra/Earth Sciences Journal Procedia*, 1, 54–57.
- Sanchez-Fenollosa, S., Verdu, F. J., Suñer, M., & Santisteban, C. (2022).** Tracing Late Jurassic ornithopod diversity in the eastern Iberian Peninsula: *Camptosaurus*-like postcranial remains from Alpuente (Valencia, Spain). *Journal of Iberian Geology*, 48, 65–78. <https://doi.org/10.1007/s41513-021-00182-z>
- Santos-Cubedo, A., de Santisteban, C., Poza, B., & Meseguer, S. (2021).** A new styracosternan hadrosauroid (Dinosauria: Ornithischia) from the Early Cretaceous of Portell, Spain. *PLoS ONE*, 16, e0253599. <https://doi.org/10.1371/journal.pone.0253599>
- Scannella, J. B., Fowler, D. W., Goodwin, M. B., & Horner, J. R. (2014).** Evolutionary trends in *Triceratops* from the Hell Creek Formation, Montana. *PNAS*, 111, 10245–10250. <https://doi.org/10.1073/pnas.1313334111>
- Scheetz, R., Britt, B., & Higginson, J. (2010).** A large, tall-spined iguanodontid dinosaur from the Early Cretaceous (Early Albian) basal Cedar Mountain Formation of Utah. Society of Vertebrate Paleontology, 2010 *Program and abstracts. 70th Anniversary meeting.* <https://vertpaleo.org/wp-content/uploads/2021/03/2010AnnualMeetingAbstracts.pdf>
- Seeley, H. G. (1887).** On the classification of the fossil animals commonly named Dinosauria. *Proceedings of the Royal Society of London*, 43, 165–171.
- Sereno, P. C. (1986).** Phylogeny of the bird-hipped dinosaurs (Order Ornithischia). *National Geographic Research*, 2, 234–256.
- Sereno, P. C. (1997).** The origin and evolution of dinosaurs. *Annual Review of Earth and Planetary Sciences*, 25, 435–489. <https://doi.org/10.1146/annurev.earth.25.1.435>
- Shibata, M., Jintasakul, P., Azuma, Y., & You, H.-L. (2015).** A new basal hadrosauroid dinosaur from the Lower Cretaceous Khok Kruat Formation in Nakhon Ratchasima province, northeastern Thailand. *PLoS ONE*, 10, e0145904. doi: journal.pone.0145904. <https://doi.org/10.1371/journal.pone.0145904>
- Sobral, G., Hipsley, C. A., & Müller, J. (2012).** Braincase redescription of *Dysalotosaurus lettowvorbecki* (Dinosauria, Ornithopoda) based on computed tomography. *Journal of Vertebrate Paleontology*, 32, 1090–1102. <https://doi.org/10.1080/02724634.2012.693554>
- Sues, H. D., & Averianov, A. (2009).** A new basal hadrosauroid dinosaur from the Late Cretaceous of Uzbekistan and the early radiation of duck-billed dinosaurs. *Proceedings of the Royal Society B*, 276, 2549–2555. <https://doi.org/10.1098/rspb.2009.0229>
- Sweetman, S. C. (2007).** Aspects of the microvertebrate fauna of the Early Cretaceous (Barremian) Wessex Formation of the Isle of Wight, Southern England [Unpublished PhD thesis]. University of Portsmouth.
- Sweetman, S. C. (2011).** The Wealden of the Isle of Wight. In D. J. Batten (Ed.), *Palaeontological Association Field Guide to Fossils, 14. English Wealden fossils* (pp. 52–78). The Palaeontological Association.
- Sweetman, S. C. (2016).** A comparison of Barremian–early Aptian vertebrate assemblages from the Jehol Group, north-east China and the Wealden Group, southern Britain: the value microvertebrate studies in adverse preservational settings. *Palaeobiodiversity and Palaeoenvironments*, 96, 149–167. <https://doi.org/10.1007/s12549-015-0217-9>
- Sweetman, S. C., Goedert, J., & Martill, D. M. (2014).** A preliminary account of the fishes of the Lower Cretaceous Wessex Formation (Wealden Group, Barremian) of the Isle of Wight, southern England. *Biological Journal of the Linnean Society*, 113, 872–896. <https://doi.org/10.1111/bij.12369>
- Sweetman, S. C., & Insole, A. N. (2010).** The plant debris beds of the Early Cretaceous (Barremian) Wessex Formation of the Isle of Wight, southern England: their genesis and palaeontological significance. *Palaeogeography, Palaeoclimatology, Palaeoecology*, 292, 409–424. <https://doi.org/10.1016/j.palaeo.2010.03.055>
- Taquet, P. (1976).** Geologie et paleontologie du Gisement de Gadoufaoua (Aptien du Niger). *Cahiers de paleontologie.* Éditions du Centre National de la Recherche Scientifique.
- Thomas, D. A. (2015).** The cranial anatomy of *Tenontosaurus tilletti* Ostrom, 1970 (Dinosauria, Ornithopoda).

- Palaeontologia Electronica*. **18**.2.37A. <https://doi.org/10.26879/450>
- Torrens, H.** (2014). The English Isle of Wight and its crucial role in the invention of dinosaurs. *Biological Journal of the Linnean Society*, *113*, 664–676. <https://doi.org/10.1111/bij.12341>
- Tsogtbaatar, K., Weishampel, D. B., Evans, D. C., & Watabe, M.** (2014). A new hadrosauroid (*Plesiohadros djadokhtensis*) from the Late Cretaceous Djadokhtan fauna of southern Mongolia. In D. A. Eberth & D. C. Evans (Eds.), *Hadrosaurs* (pp. 108–135). Indiana University Press.
- Tsogtbaatar, K., Weishampel, D. B., Evans, D. C., & Watabe, M.** (2019). A new hadrosauroid (Dinosauria: Ornithopoda) from the Late Cretaceous Baynshire Formation of the Gobi Desert (Mongolia). *PLoS ONE*, *14*, e0208480. <https://doi.org/10.1371/journal.pone.0208480>
- Tsuihiji, T.** (2010). Reconstructions of the axial muscle insertions in the occipital region of dinosaurs: evaluations of past hypotheses on Marginocephalia and Tyrannosauridae using the extant phylogenetic bracket approach. *The Anatomical Record*, *293*, 1360–1386. <https://doi.org/10.1002/ar.21191>
- Van Beneden, P. J.** (1881). Sur l'arc pelvien chez les dinosauriens de Bernissart. *Bulletins de l'Academie royale des sciences, des lettres et des beaux-arts de Belgique*, *3*, 600–608.
- Verdu, F. J., Godefroit, P., Royo-Torres, R., Cobos, A., & Alcalá, L.** (2017). Individual variation in the postcranial skeleton of the Early Cretaceous *Iguanodon bernissartensis* (Dinosauria: Ornithopoda). *Cretaceous Research*, *74*, 65–86. <https://doi.org/10.1016/j.cretres.2017.02.006>
- Verdu, F. J., Royo-Torres, A., Cobos, A. & L. Alcalá.** (2015). Perinates of a new species of *Iguanodon* (Ornithischia: Ornithopoda) from the lower Barremian of Galve (Teruel, Spain). *Cretaceous Research*, *56*, 250–264. <https://doi.org/10.1016/j.cretres.2015.05.010>
- Verdu, F. J., Royo-Torres, R., Cobos, A., & Alcalá, L.** (2017). New systematic and phylogenetic data about the early Barremian *Iguanodon galvensis* (Ornithopoda: Iguanodontoida) from Spain. *Historical Biology*, *30*, 437–474. <https://doi.org/10.1080/08912963.2017.1287179>
- Verdu, F. J., Cobos, A., Royo-Torres, R., & Alcalá, L.** (2019). Diversity of large ornithopod dinosaurs in the upper Hauterivian–lower Barremian (Lower Cretaceous) of Teruel (Spain): a morphometric approach. *Spanish Journal of Palaeontology*, *34*(2), 269–288. <https://doi.org/10.7203/sjp.34.2.16116>
- Wagner, J. R.** (2001). *The hadrosaurian dinosaurs (Ornithischia: Hadrosauria) of Big Bend National Park, Brewster County, Texas, with implications for Late Cretaceous paleogeography* [M.Sc. thesis]. Texas Tech University.
- Wang, X., Pan, R., Butler, R. J., & Barrett, P. M.** (2010). The postcranial skeleton of the iguanodontian ornithopod *Jinzhousaurus yangi* from the Lower Cretaceous Yixian Formation of western Liaoning, China. *Earth and Environmental Science Transactions of the Royal Society of Edinburgh*, *101*, 135–159. <https://doi.org/10.1017/S1755691010009266>
- Wang, X., & Xu, X.** (2001). A new iguanodontid (*Jinzhousaurus yangi* gen. et sp. nov.) from the Yixian Formation of western Liaoning, China. *Chinese Science Bulletin*, *46*, 1669–1672. <https://doi.org/10.1007/BF02900633>
- Wang, R.-F., You, H.-L., Wang, S.-Z., Xua, S.-C., Yia, J., Xiea, L.-J., Jiaa, L., & Xing, H.** (2015). A second hadrosauroid dinosaur from the early Late Cretaceous of Zuoyun, Shanxi Province, China. *Historical Biology*, *29*, 17–24. <https://doi.org/10.1080/08912963.2015.1118688>
- Watson, J.** (1977). Some lower Cretaceous conifers of the Cheirolepidiaceae from the U.S.A. and England. *Palaeontology*, *20*, 715–749.
- Weishampel, D. B.** (1984). Evolution of jaw mechanisms in ornithopod dinosaurs. *Advances in anatomy, embryology and cell biology*, **87**. Springer-Verlag.
- Weishampel, D. B., Barrett, P. M., Coria, R. A., Le Loeuff, J., Xu, X., Zhao, X.-J., Sahni, A., Gomani, E. M. P., & Noto, C. R.** (2004). Dinosaur distribution. In D. B. Weishampel, P. Dodson & H. Osmolska (Eds.), *The Dinosauria* (2nd ed., pp. 517–606), University of California Press.
- Weishampel, D. B., & Bjork, P.** (1989). The first indisputable remains of *Iguanodon* (Ornithischia: Ornithopoda) from North America: *Iguanodon lakotaensis*, sp. nov. *Journal of Vertebrate Paleontology*, *9*, 56–66. <https://doi.org/10.1080/02724634.1989.10011738>
- Weishampel, D. B., & Horner, J. R.** (1990). Hadrosauridae. In D. B. Weishampel, P. Dodson & H. Osmolska (Eds.), *The Dinosauria* (pp. 534–561), University of California Press.
- Weishampel, D. B., Jianu, C.-M., Csiki, Z., & Norman, D. B.** (2003). Osteology and phylogeny of *Zalmoxes* (n. g.), an unusual euornithopod dinosaur from the latest Cretaceous of Romania. *Journal of Systematic Palaeontology*, *1*, 65–123. <https://doi.org/10.1017/S1477201903001032>
- Weishampel, D. B., Norman, D. B., & Grigorescu, D.** (1993). *Telmatosaurus transylvanicus* from the Late Cretaceous of Romania: the most basal hadrosaurid dinosaur. *Palaeontology*, *36*, 361–385.
- Werning, S.** (2012). The ontogenetic osteohistology of *Tenontosaurus tilletti*. *PLoS ONE*, *7*(3). e33539. <https://doi.org/10.1371/journal.pone.0033539>
- Winkler, D. A., Murry, P. A., & Jacobs, L. L.** (1997). A new species of *Tenontosaurus* (Dinosauria: Ornithopoda) from the Early Cretaceous of Texas. *Journal of Vertebrate Paleontology*, *17*, 330–348. <https://doi.org/10.1080/02724634.1997.10010978>
- Woodward, H. N., Freedman Fowler, E. A., Farlow, J. O., & Horner, J. R.** (2015). *Maiasaura*, a model organism for extinct vertebrate population biology: a large sample statistical assessment of growth dynamics and survivorship. *Paleobiology*, *41*(4), 503–527. <https://doi.org/10.1017/pab.2015.19>
- Wu, W., & Godefroit, P.** (2012). Anatomy and relationships of *Bolong yixianensis*, an Early Cretaceous iguanodontoid dinosaur from Western Liaoning, China. In P. Godefroit (Ed.), *Bernissart dinosaurs and Early Cretaceous terrestrial ecosystems* (pp. 292–333), Indiana University Press.
- Xing, H., Mallon, J. C., & Currie, M. L.** (2017). Supplementary cranial description of the types of *Edmontosaurus regalis* (Ornithischia: Hadrosauridae), with comments on the phylogenetics and biogeography of Hadrosaurinae. *PLoS ONE*, *12*, e0175253. <https://doi.org/10.1371/journal.pone.0175253>

- Xing, H., Wang, D., Han, F., Sullivan, C., Ma, Q., He, Y., Hone, D. W. E., Yan, R., Du, F., & Xu, X. (2014). A new basal hadrosauroid dinosaur (Dinosauria: Ornithopoda) with transitional features from the Late Cretaceous of Henan Province, China. *PLoS ONE*, *9*, e98821. <https://doi.org/10.1371/journal.pone.0098821>
- Xu, X., Tan, Q., Gao, Y., Bao, Z., Yin, Z., Guo, B., Wang, J., Tan, L., Zhang, Y., & Xing, H. (2018). A large-sized basal ankylopollexian from East Asia, shedding light on early biogeographic history of Iguanodontia. *Science Bulletin*, *63*, 556–563. <https://doi.org/10.1016/j.scib.2018.03.016>
- Xu, X., Zhao, X., Lu, J., Huang, W., Li, Z., & Dong, Z. (2000). A new iguanodontian from Sangping Formation of Neixiang, Henan and its stratigraphical implication. *Vertebrata Palasiatica*, *7*, 176–191.
- You, H., Ji, Q., & Li, D. (2005). *Lanzhousaurus magnidens* gen. et sp. nov. from Gansu Province, China: the largest-toothed herbivorous dinosaur in the world. *Geological Bulletin of China*, *24*, 785–794.
- You, H., Ji, Q., Li, J., & Li, Y. (2003). A new hadrosauroid dinosaur from the Mid-Cretaceous of Liaoning, China. *Acta Geologica Sinica*, *77*, 148–154.
- You, H., & Li, D. (2009). A new basal hadrosauriform dinosaur (Ornithischia: Iguanodontia) from the Early Cretaceous of northwestern China. *Canadian Journal of Earth Sciences*, *46*, 949–957. <https://doi.org/10.1139/E09-067>
- You, H., Li, D., & Lui, W. (2011). A new hadrosauriform Dinosaur from the Early Cretaceous of Gansu Province, China. *Acta Geologica Sinica*, *85*, 51–57.

**Associate Editor: Victoria Arbour**